COLD WEATHER ADMIXTURE SYSTEMS FOR CEMENT-BASED MATERIALS APPLIED TO MASONRY MORTAR BINDER

A Thesis Submitted to the College of

Graduate and Postdoctoral Studies

In Partial Fulfillment of the Requirements

For the Degree of Doctor of Philosophy

In the Department of Civil, Geological and Environmental Engineering

University of Saskatchewan

Saskatoon

By

OUAFI SAHA

© Copyright Ouafi Saha, August, 2019. All rights reserved.

PERMISSION TO USE

In presenting this thesis in partial fulfilment of the requirements for a Postgraduate degree from the University of Saskatchewan, I agree that the Libraries of this University may make it freely available for inspection. I further agree that permission for copying of this thesis/dissertation in any manner, in whole or in part, for scholarly purposes may be granted by the professor or professors who supervised my thesis/dissertation work or, in their absence, by the Head of the Department or the Dean of the College in which my thesis/dissertation work was done. It is understood that any copying or publication or use of this thesis/dissertation or parts thereof for financial gain shall not be allowed without my written permission. It is also understood that due recognition shall be given to me and to the University of Saskatchewan in any scholarly use which may be made of any material in my thesis/dissertation.

Requests for permission to copy or to make other use of material in this thesis/dissertation in whole or part should be addressed to:

Head of the Department of Civil, Geological and Environmental Engineering

University of Saskatchewan

Engineering Building, 57 Campus Drive

Saskatoon, Saskatchewan S7N 5A9 Canada

OR

Dean

College of Graduate and Postdoctoral Studies

University of Saskatchewan

116 Thorvaldson Building, 110 Science Place

Saskatoon, Saskatchewan S7N 5C9 Canada

ABSTRACT

Masonry construction in cold weather is a challenge due to the slow or even non-existent hydration reaction of the cementitious material at low and subfreezing temperatures. The construction industry's need for an alternative to providing thermal protection has motivated the exploration of using antifreeze admixtures. The main objectives of this project were to develop and evaluate an effective antifreeze admixture for masonry mortars from available products, and to identify the active components responsible for promoting the strength gain and the mechanisms by which they act.

In the first stage of the experimental program, an incomplete response surface design approach was used to develop an antifreeze admixture. The approach consisted of combining a total of six off-the-shelf concrete admixtures, up to five at a time at three dosage levels each. The target optimization function of the system was the minimization of the freezing point of the mortar, which was measured using an embedded thermocouple in the center of the mortar cylinders. Several combinations of admixtures were effective at lowering the freezing point of the mortar mix; however, the compressive strength was found not to be systematically correlated to the freezing temperature. The compressive strengths of mortar samples prepared with the best candidates, when cured at -10°C and -15°C, reached acceptable levels. However, a pre-curing (heat protection) period of between 6 and 12 hours was necessary for the mortar to reach these strength levels.

The best performing candidate from the previous stage was selected to undergo further investigation to identify the active compound and to study its effect on the hydration process. Elemental and mineral characterization of the admixture, using mainly X-ray fluorescence (XRF) and X-ray diffraction (XRD), revealed a high concentration of sodium nitrite with some mullite, in addition to an unidentified amorphous phase. The characterization of the hydration products did not reveal any uncommon phases, suggesting the presence of a certain amount of unfrozen water in the pore structure that allowed the hydration reaction to proceed and the C-S-H phase to develop. The suspected active ingredient (sodium nitrite) was tested as a stand-alone admixture to confirm its action as an antifreeze agent, and produced masonry mortar with an acceptable 28-day compressive strength when cured at -10°C. No pre-curing period was required in this phase of testing. The dosage of sodium nitrite was also optimized and found to be approximately 5% by cement weight to maximize the strength gain.

Given that no hard evidence of any unusual ongoing chemical reactions was found using the characterization techniques, the physical action of the antifreeze was investigated. The working hypothesis was that a certain amount of liquid water was present at subfreezing temperatures, which allowed the hydration reaction to proceed. As an indirect way of confirming the hypothesis, the non-destructive time domain reflectometry (TDR) technique was used to measure the bulk dielectric constant of the plain and treated cement pastes during the curing process up to an age of three weeks. A mixing model was formulated to quantitatively track the individual constituents of the cement paste, with a particular interest in the available liquid water at temperatures below the normal freezing temperature. The results showed clear evidence of the existence of liquid water in the antifreeze treated samples, as well as evidence of the consumption of water and unreacted cement at subfreezing temperatures.

CO-AUTHORSHIP

All of the experimental and analytical work presented in this thesis was performed by O. Saha. M. Boulfiza and L.D. Wegner reviewed and contributed to the analytical work. All manuscripts included in this thesis are co-authored.

The authors would like to express their gratitude to the Saskatchewan Masonry Institute (SMI), the Saskatchewan Centre for Masonry Design (SCMD), the Canada Masonry Design Centre (CMDC), the Natural Sciences and Engineering Research Council of Canada (NSERC), MITACS, and the Department of Civil, Geological, and Environmental Engineering of the University of Saskatchewan for their financial support to this project.

The manuscript corresponding to Chapter 3 was published in the proceedings of the 12th North American Masonry Conference. The manuscript was reformatted for inclusion in the thesis, and the copyright permission provided in Appendix M. It is cited as "Saha, O., Boulfiza, M., and Wegner, L.D. 2015a. Developing antifreeze admixtures for mortar from available off-the-shelf admixtures. In 12NAMC. Denver, CO. USA."

The manuscript corresponding to Chapter 4 (Behavior of masonry mortar containing a non-harmful antifreeze admixture) was accepted in 2019 by the TMS Journal.

The manuscript corresponding to Chapter 5 (Antifreeze admixture for masonry mortar – identification and dosage optimization of active ingredient) was submitted in April 2019 to the ACI Materials Journal.

The manuscript corresponding to Chapter 6 (Tracking the hydration of antifreeze treated cement paste at subfreezing temperatures using the TDR technique) has been submitted in July 2019 to Construction and Building Materials.

Note: The authors declare no competing financial interest and no conflict of interest.

ACKNOWLEDGMENTS

I want to start by thanking God the almighty for giving me the force and courage to start and finish this work.

I would like to express my gratitude to my supervisors, Dr. Moh Boulfiza and Dr. Leon Wegner for their continuous support, encouragement and their valuable advices throughout my Ph.D. program, more particularly in the difficult moments before the finish line. They were and will remain a valuable source of inspiration for me.

I want to thank all my Advisory committee members Dr. Bruce Sparling, Dr. Lisa Feldman, and Dr. Ike Oguocha for their valuable comments and orientations during my study and research.

I would like to address a special thank-you to our Structural Laboratory Technician Brennan Pokoyoway, and the other Laboratory technicians including Yin Helen, Heli Eunike, Dale Pavier, Adam Hammerlindl, and all the fellow grad students who assisted and discussed this work.

I want to thank Bob Afseth, Kathy Beznoska and Sasha Kisin from the Saskatchewan Masonry Institute for accommodating the completion of the experience requirement of the IPS and the MITACS scholarship in their facility.

I am very grateful to the Saskatchewan Masonry Institute (SMI), the Saskatchewan Centre for Masonry Design (SCMD), the Canada Masonry Design Centre (CMDC), the Natural Sciences and Engineering Research Council of Canada (NSERC), the MITACS, and the Department of Civil, Geological, and Environmental Engineering of the University of Saskatchewan for their financial support to this project. Without missing to thank my company (MOSAIC) for consenting the time and providing resources to help with finalizing the thesis writing.

I will never forget the precious and pleasant memories with my friends and colleagues at the University of Saskatchewan.

DEDICATION

To my Mother and Father who indefectibly encouraged me to be here

To my beloved wife Fatiha

To my children Lina and Raouf

To all my big family

TABLE OF CONTENTS

LIST OF TABLES

LIST OF FIGURES

LIST OF ABBREVIATIONS AND SYMBOLS

ACI	American Concrete Institute
ASCE	American Society of Civil Engineers
ASTM	American Standard for Testing and Materials
CCDC	Cambridge Crystallographic Data Centre
CEM	Concrete Equivalent Mortar
CHNS	Carbon Hydrogen Nitrogen Sulfur
CIF	Crystallographic Information File
CMDC	Canada Masonry Design Centre
COD	Crystallography Open Database
CRIM	Complex Refractive Index Model
CRREL	Cold Region Research and Engineering Laboratory
CSA	Canadian Standard Association
CWAS	Cold Weather Admixture System
FP	Freezing Point
HRWR	High Range Water Reducer
ICDD	International Centre for Diffraction Data
ICP-MS	Inductively Coupled Plasma Mass Spectrometry
IRA	Initial Rate of Absorption of masonry units
MSJC	Masonry Standard Join Committee
NMR	Nuclear Magnetic Resonance
RH	Relative Humidity
SEM	Scanning Electron Microscopy
TDR	Time Domain Reflectometry
TMS	The Masonry Society
XRD	X-ray Diffraction
XRF	X-ray Fluorescence
a/c	Aggregate to Cement ratio
f_i	Volume Fraction of an individual constituents
K_{app}	Apparent Dielectric Constant (measured)

K_i	Dielectric Constant of an individual constituents
L_{app}	Apparent Length of probe
L_p	Probe Length
v_p	Relative Velocity of electromagnetic wave
w/c	Water to Cement ratio
α	Geometric Arrangement factor
γ_i	Specific Gravity of an individual constituent
λ	Coper K_α wavelength

1 INTRODUCTION

1.1 Background

Cement-based materials (masonry, concrete, mortar, and grout) are composite materials made of aggregates and paste. The paste itself is made of water and, in most cases, portland cement. People have long known how to make concrete and masonry. The ancient Romans were masters of the craft. It is at least 2,000 years since the ancient "engineers" first heated limestone (calcium carbonate) and minerals to make a substance which when powdered and mixed with water set into a material of remarkable strength. Complex chemical reactions start when these two materials, the powder (either cement or calcium carbonate) and the water, are mixed together. They are called hydration reactions or, more commonly, "the hydration reaction" as a meta-reaction. Unfortunately, when the temperature drops below the freezing point, these reactions slow down and eventually stop completely when there is no water left in liquid form. When this happens, strength gain becomes very slow and irreversible damage to the cement paste, due to water-to-ice expansion, can occur. These are two of the major problems for concrete and masonry construction in cold weather.

Two approaches can be seen in the literature to address these problems. The first is to plan, prepare, and protect the cementitious material under controlled thermal conditions, which can range from heating the mixing water and aggregates to a complete heated enclosure; this approach is the one adopted by the majority of the current codes and standards (e.g., ACI 1990, CSA 2004a, MSJC 2011). One problem with this method is the extra thermal protection cost. The second approach is to reduce the effect of low-temperature by using chemical admixtures, which act usually as accelerators, freezing depressants and, in some cases, as water reducers. The exploration of this second path is the main topic of this research project.

Despite the observed successes of using cold-weather admixture systems (CWAS) in concrete over the last two decades, and the similarities between concrete and masonry mortar, since both are based on cementitious materials, codes and standards are still too restrictive regarding their use in masonry. The main reasons are: 1) the historical practice of using calcium chloride and alcohols as antifreeze compounds, knowing their adverse effect on promoting steel corrosion and lowering material strength; and 2) the lack of reliable experimental data associated with their usage in

masonry, knowing that masonry mortar differs from concrete in its initial water content, the initial rate of absorption by the masonry units, the aggregate sizes, and the presence of lime. This restrictive approach has led to a safe response to uncertainty, and at the same time to a significant cost increase.

To sum-up, the problem of the slow hydration reaction associated with masonry mortar in cold weather construction must be addressed. Practically, combinations of chemicals from commercially available admixtures must be tested for their effect on allowing strength development in masonry mortar at temperatures lower than that allowed by the current regulations. Scientifically, the active ingredients responsible for the promotion of hydration at cold temperatures should be identified, and the evolution of the pore water over time under freezing conditions should be tracked.

1.2 Objectives

The first objective of this project was to develop a CWAS from commercially available chemical admixtures for masonry mortar and to produce experimental data that can justify a safe reduction in thermal protection (i.e. without compromising the material's performance in terms of strength), re-establishing the fact that a non-harmful antifreeze admixture for masonry exists and may be used in field construction, using conventional materials, techniques, and equipment, for temperatures as low as -10°C to -15°C. It is expected that adoption of this technology could extend the typical unprotected construction season and reduce the costs compared to conventional cold-weather techniques. All guides and codes specify three main phases of protection in masonry construction: preparation and material protection, protection while construction is in progress, and protection of the finished work. Achieving this first objective would relax the protection requirement during the last two phases.

The mechanism of hydration is of particular interest when cementitious materials are used in cold weather conditions. An antifreeze admixture may attenuate the adverse effects of cold weather by a physical and/or a chemical mechanism, and at the same time increase the complexity of the hydration reactions. Identifying the active ingredients in an effective antifreeze admixture and the mechanisms by which they act is the second main objective of this project.

The objectives are summarized as follows:

1. To develop and evaluate a CWAS for masonry mortars from commercially available admixtures. Specific sub-objectives include:
    a. to evaluate the ability of the CWAS to reduce the freezing point to between -10°C and -15°C;
    b. to evaluate the ability of the CWAS mortars to develop acceptable compressive strengths, and to determine the initial protection time required to achieve those strengths; and
    c. to assess whether the findings support relaxing current protection requirements.
2. To identify the active ingredients responsible for promoting the strength development and the mechanisms by which they act at subfreezing temperatures. Specific sub-objectives are:
    a. to qualitatively identify the major phases present in the cement paste before and during the hydration;
    b. to identify the key components responsible for the strength development and validate their individual effect and their optimal dosage; and
    c. to quantify the presence and consumption of liquid water in the treated cement pastes at below freezing temperatures.

1.3 Methodology and Scope

To a certain extent, cold-weather admixture systems have been successfully used in concrete over the last two decades. Since masonry mortars are also portland cement-based, it seems reasonable to investigate the application of CWAS to masonry mortar as well, and to understand how they work. Two main goals have been stated previously; they consist in finding a good chemical to allow strength development at below freezing temperatures (the practical goal), and identifying the active compounds and how they affect the hydration process (the scientific goal).

The objectives were addressed by means of a laboratory based experimental program.

The first phase of the laboratory experiments was preceded by the identification of some commercially available admixture candidates to combine in an attempt to depress the freezing

point of the masonry mortar to an acceptable level. This was based on the assumption that a lower freezing point would result in the development of a higher compressive strength. A statistical design and optimization approach was used in this step. The best candidates from this step were selected for the following step, which involved testing treated mortar samples for acceptable compressive strength. The results produced in this phase were used to develop recommendations about the minimum thermal protection requirements for cold weather masonry construction and to help justify the relaxation of the current protection times in the existing regulations.

The second phase of the experimental program focused on the identification of the chemical composition of the admixture and the hydration products of the best candidate tested in the previous phase. This was undertaken in three main steps. First, several characterization techniques were used, including combustion (CHNS), inductively coupled plasma mass spectrometry (ICP-MS), and X-ray fluorescence (XRF) X-ray diffraction (XRD), to identify the initial products before the hydration and, more particularly, to isolate the active ingredient. A semi quantitative XRF-XRD approach was used to detect any uncommon phases potentially responsible for the strength development. Next, the active ingredient was isolated and used as the main antifreeze ingredient in preparing additional mortar specimens to confirm its effect on the strength development, and to optimize its dosage. Finally, since the results from step one showed no major chemical reaction of the antifreeze, the physical action of depressing the freezing point of the cement pore solution was explored using the TDR technique to infer the amount of liquid water available for hydration at subfreezing temperatures.

The scope of this project was limited to developing antifreeze admixtures from commercially available products. The focus was on masonry mortar using Type S mortar cement, and cement paste using Type GU cement. No concrete or grout were addressed in this work. The durability aspect and freezing/thawing resistance were out of the scope of this project. For practicality, two temperatures of -10 and -15°C were considered for the masonry mortar curing in cold conditions.

1.4 Organization

Chapter 1 presents the background and problem statement related to cold weather masonry construction, along with conventional and innovative solutions. The global and specific objectives and the methodology to achieve the objectives are stated.

Chapter 2 covers a wide review of the literature pertaining to cold weather concrete and masonry construction. A more detailed review of masonry and concrete problems associated with cold weather is given, along with the current code regulations and practices in North America. A historical review of cold weather admixture systems and their potential effects on cementitious materials is provided. Finally, a description of some preliminary tests, undertaken in an attempt to replicate some of the experiments described in the literature, is given.

Chapter 3 presents the methods and results of a combinatorial approach used to identify an effective antifreeze admixture from a selection of off-the-shelf admixtures. The freezing point was the optimization target of the statistical design, which is hypothetically related to the compressive strength development of the masonry mortar tested.

Chapter 4 discusses the preparation and compressive strength testing of the mortar samples prepared using the antifreeze admixture identified in Chapter 3. The pre-curing time necessary to reach the minimum standard strength requirements is presented. Also, a comparison with the compressive strength of control mortar specimens cured under identical conditions is presented to show the beneficial effect of the antifreeze.

Chapter 5 describes the characterization techniques used in this phase of the experimental program, as well as the procedure used for sample preparation, curing, and stopping the hydration at specified ages. In this chapter, the identification of the major crystalline phases of the antifreeze agent is presented and the main ingredient is tested to confirm its action. Finally, the results of the dosage optimization are discussed.

The use of the time domain reflectometry (TDR) technique in quantifying water content in porous media is summarized in Chapter 6. It then describes the TDR experimental program and presents the results of the investigation of liquid water content available for the cement hydration at subfreezing temperature using the TDR technique.

Finally, Chapter 7 provides general conclusions regarding the main objectives of this work and recommendations for future work.

2 LITERATURE REVIEW

2.1 Introduction

In many northern regions of the world, the use of cementitious materials for construction in cold seasons requires special procedures. Canada, the USA, the Scandinavian region, Russia, China, and Japan are the main countries affected by the problem of cold weather concreting, each of them having its own regulations and practices, some of which are more restrictive than others.

Concrete, mortar and grout are composite materials made of aggregate and paste. In most cases, the paste is made of water and portland cement. In normal conditions, a chemical reaction starts when these two materials (water and cement) are mixed together, known as hydration reaction. When the air temperature drops, this reaction slows down. The hydration may stop completely if the temperature is low enough to convert the available liquid water into ice. When this happens, strength gain becomes very slow and irreversible damage to cement paste may occur, due to water-to-ice volume increase. This is the major problem of concrete and masonry construction in cold weather.

The solutions given for this problem by several guidance documents (e.g., IMIAWC 1988, Kurtz 1997, ACI 2010a) start by heating the ingredients; the easiest one to heat is usually water, but heating may extend to sand and aggregate if heating the water is insufficient. Some standards recommend increasing the cement dosage, using Type HE cement (aka Type III), or using accelerating admixtures (e.g., ACI 2010a, MSJC 2011). In extreme cases, it is required to heat the whole construction area by using heated enclosures. This solution is found to be costly, and for small projects the cost may not be justified.

Antifreeze admixtures seem to be an attractive alternative solution to classic cold weather concreting practices, and their usage started in the early 1950's in the former USSR (Korhonen 1990); their use in North America, though, is still very limited and restricted by design codes. The main reason for this restrictive approach is that the popular compounds known for their antifreeze effects are calcium chloride and alcohols; unfortunately, they are also known for their detrimental effect on promoting steel corrosion and lowering concrete strength.

Many research projects have been conducted in North America since the late 1980's, particularly by the U.S. Army Cold Region Research and Engineering Laboratory (CRREL), with the aim of developing new admixtures, testing them in the laboratory and in the field, disseminating the results, and participating in updating construction standards (Korhonen 1990, 1999, 2002a, 2006, Korhonen et al. 1994a, 1997a, Korhonen and Brook 1996, Barna et al. 2010).

The initial purpose of this literature review was to summarize the use of antifreeze admixtures as applied to masonry construction; however, after an extensive search of the literature, not much work was found to have been done explicitly on the topic. Two main reasons may explain this: the great similarities between concrete and masonry, and the strict regulation on the use of admixtures in masonry. A third reason may be the relatively short curing period required by masonry compared to concrete.

Despite the fact that concrete and masonry are both composite materials based on cement, there are many differences between them, justifying why research should be conducted specifically for antifreeze admixtures applied to masonry construction. Initial water content, initial rate of absorption of masonry units, aggregate size and the possible presence of lime are the main differences between concrete and masonry binders.

This chapter reviews the main problems in masonry and concrete construction caused by low temperatures, as well as the current regulations and practices applied in North America. A brief historical background on antifreeze admixtures and their various effects on concrete properties is then presented. The major part of this chapter is a review of the use of antifreeze admixtures in concrete, since there is abundant literature on concrete rather than masonry. Nevertheless, some sections are dedicated to masonry.

2.2 Problems Associated with Masonry and Concrete Construction in Cold Weather

Concrete and mortar are essentially a blend of water, cement, and aggregates. This composite material evolves from a plastic state to a solid state under the effect of a chemical reaction between water and cement, commonly called "the hydration reaction". Like any chemical reaction, the rate of a hydration reaction is proportional to temperature according to the Arrhenius equation. As the temperature decreases, the hydration reaction slows down, leading to a reduction in strength gain. If the temperature continues to decrease, it will eventually reach the freezing point, approximately

−3°C, where more than 90% of the liquid water in the pore structure will turn into ice (Korhonen 1990), and the hydration reaction will practically come to a halt. Theoretically, cement continues hydrating down to -20°C provided the water is prevented from freezing (Brook et al. 1988) but this does not typically occur in practice. The transformation of water from liquid to ice increases its volume by 9%. This volume expansion may disrupt the weak structure of the fresh mix by forcing apart the bond of the pore structure itself and the bond between the cement paste and the aggregate particles, causing permanent damage to the hardened concrete or mortar.

In a comprehensive work related to cold weather construction, Davison (1970), and more recently Woodham and Schuller (2005), pointed out two similar problems for masonry construction. First, as the temperature drops the hydration reactions become slow and ultimately stop, resulting in lower strength gain. Second, if mortar or grout is permitted to freeze, ice formation may disrupt internal bonds and cause permanent damage to the masonry. However, a noticeable difference exists between mortars and concrete, which relates to the water content before and after placement. Mortar has a higher water content for higher workability, but is in contact with a porous material, which absorb the excess water. On the other hand, concrete has a lower initial water content, but is in contact with a water repellent surface, which keeps all the water within the concrete volume. Thus, concrete is more vulnerable to freezing at early ages.

The rate at which the temperature drops has an effect on the type of ice that forms (Korhonen 1990, Suprenant 1992). For rapid cooling, water does not have enough time to migrate to colder areas, which leads to a uniform distribution of small ice crystals. For slow cooling, however, water can move to colder regions and freezes there. This creates layers of ice or lenses which are known as crow’s feet, illustrated in Figure 2.1. Both rapid and slow freezing have a detrimental effect on the fresh material, which can result in a loss of up to 50% of its final compressive strength.

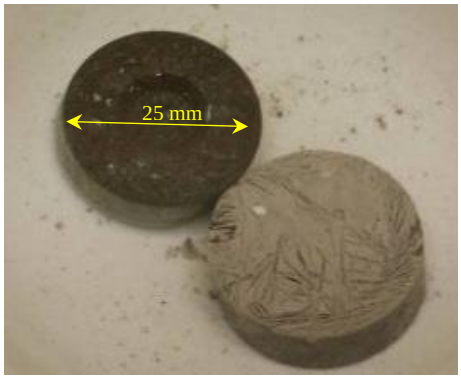

Figure 2.1 Effect of frost on fresh cement paste: ice formation imprint known as Crow's feet, apparent on the right disk

The high evaporative property of water is commonly associated with high temperatures. In fact, evaporation is controlled by the difference between vapor pressure at the moist surface and its surrounding air. Evaporation therefore reaches its highest level when the evaporating water is warm and the air is cold and dry, which is a typical situation on cold windy days (Hover 2002). Plastic shrinkage is highly influenced by this phenomenon, where the rate of evaporation is higher than the rate of bleeding (Senbetta and Bury 1991). The combination of evaporation and freezing problems leads to a conflict between the need of having a wet surface to prevent plastic shrinkage and the need of having a dry surface before exposing the material to freezing temperatures. Evaporation also leads to efflorescence, which happens when a water solution containing salts is driven by a cold temperature to the surface; when the solution contacts the dry air, the water evaporates leaving behind salts in the form of efflorescence.

The use of fossil fuel and gas heaters in cold weather generates high carbon dioxide emissions (CO_2), especially in enclosed spaces without exhaust systems. This can be a risk for the workers' health and for the fresh concrete where CO_2 can provoke surface dusting. In addition, metals have a high thermal conductivity. Steel in winter construction can be very cold; when in contact with warm concrete or grout, this can generate a thin layer of ice on the steel reinforcing bars, preventing a good bond between the concrete and steel (Basham 2005).

Durability is another issue in cold weather, with freezing and thawing, corrosion and exposure to de-icing salts being the most common examples. Freezing and thawing is directly related to the change in temperature below and above the freezing point. The mechanism of deterioration may be explained by the change in volume of water, which increases by 9% when it transitions from the liquid phase to its solid phase. This volume change creates tension within the cementitious

matrix, resulting in scaling and spalling, as seen in Figure 2.2. The effect of freezing and thawing is particularly visible on surfaces where the concrete or grout are more likely to be saturated (Kosmatka et al. 2002).

(a) (b)

Figure 2.2 Effect of freezing and thawing in concrete: (a) Scaling, and (b) Spalling

Cold weather practices present logistical and planning challenges. Among other factors, protection, heating, and extra labor, all increase the cost of constructing in cold weather. For small projects, these extra costs may not be justified, and construction projects may stop for months in some regions.

Another problem, not limited to cementitious materials, has been reported in the literature (Havers 1972), which is related to the efficiency of workers, materials and equipment in cold weather. The report reviews the psychological and physiological effects of cold weather on men and their productivity. The major psychological issue is the same as that encountered by working in any other extreme condition, including becoming irritable, undisciplined, depressed, losing sleep, quick fatigue, and distraction, among others. The physiological effects were split into categories: tissue damage related issues such as frost bite, immersion foot, chilling of the lungs, and blister of the skin; and non-tissue damage issues such as dehydration, shock, hypothermia, arterial pressure, respiration, and caloric requirements. The report discusses the weather effects on cementitious materials among other construction materials and compares different civil and military codes and practices in various cold region countries.

2.3 Current Cold Weather Standards and Practices for Concrete and Masonry in North America

The previous section described the main problems related to cold weather construction using cementitious materials. Many codes and specifications exist all over the world to ensure that

minimum requirements are met to prevent those problems from happening and/or to reduce their effects. In this section, the Canadian and American regulations are reviewed.

2.3.1 Canadian Regulations

2.3.1.1 CAN/CSA A23.1-14 Concrete Materials and Methods of Concrete Construction

This standard (CSA 2014) relates to the use of concrete as a construction material, and contains a section on cold weather concreting (Cl. 7.1.2). It requires protection of fresh concrete for the entire curing period when the air temperature is expected to drop below +5°C. Acceptable means of protection include the use of heated enclosures, coverings, insulations, or a combination. A note in Section 7.1.2.1 leaves the door open for the use of non-chloride, non-corrosive accelerating admixtures to allow concrete placement at temperatures as low as -5°C, provided sufficient information is available for past performance. Near the end of the curing period, it recommends anticipating a period of gradual cooling to prevent thermal cracking.

2.3.1.2 CAN/CSA A371-04 Masonry Construction for Building

Cold weather provisions for masonry construction are treated in Section 6.7 of the Canadian standard for masonry construction (CSA 2004a), and are divided into three main sections:

- General requirements: guidelines for storage, handling of materials, and protection of the construction when work is not in progress are given in this section.
- During construction requirements: four levels of increasing requirements are defined in tabular form as the temperature decreases (Table 2.1). The temperature of the mortar, when placed, should not exceed 50°C, and for the grout, it should be between 20°C and 50°C.
- Protection requirements: as specified in tabular form (Table 2.1), protection increases as the mean daily temperature decreases. All protection periods are required to last a minimum of 48 hours, except when high-early-strength portland cement or Type S hydrated lime is used, in which case the protection time is then reduced to 24 hours.
- This edition of the standard does not address the use of antifreeze admixtures.

Table 2.1 Requirement during and after construction (CSA 2004a)

Temperature	During Construction	Protection after Construction
4 to 0	Sand or mixing water shall be heated to a minimum of 20°C and a maximum of 70°C.	Masonry shall be protected from rain or snow for 48 h.
0 to -4	Sand and mixing water shall be heated to a minimum of 20°C and a maximum of 70°C.	Masonry shall be completely covered for 48 h.
-4 to -7	(1) Sand and mixing water shall be heated to a minimum of 20°C and a maximum of 70°C. (2) Source heat shall be provided on both sides of the walls under construction. (3) Windbreaks shall be employed when the wind speed exceeds 25 km/h.	Masonry shall be completely covered with insulating blankets for 48 h.
-7 and below	(1) Sand and mixing water shall be heated to a minimum of 20°C and a maximum of 70°C. (2) Enclosures and supplementary heat shall be provided to maintain an air temperature above 0°C. (3) The temperature of the unit when laid shall be not less than 7°C.	The masonry temperature shall be maintained above 0°C for 48 h by enclosure and supplementary heat.

2.3.1.3 CSA A179-04 Mortar and Grout for Unit Masonry

This standard (CSA 2004b) gives specifications for mortar and grout for unit masonry construction. In the section about admixtures, the code is very restrictive on the usage of antifreeze agents. It is stated that substances used for lowering the freezing point shall not be added to mortar or grout.

2.3.1.4 CMDC, Masonry Made EZ, Cold Weather Construction

This bulletin (CMDC 2002) is intended to give a more detailed interpretation of the Canadian standard requirements for cold weather masonry construction. Its purpose is to help the masonry construction community better understand and apply the provisions found in the code. It is a complementary document giving more practical recommendations about the materials, the handling, and the protection. The bulletin recommends not using antifreeze compounds, especially those based on alcohols as they reduce the compressive and bond strengths. The antifreeze compounds based on calcium chloride, salts or other similar substances are banned due to their corrosive effect on metals.

2.3.2 American Regulations

2.3.2.1 ACI 306.1-90, Standard Specification for Cold Weather Concreting and ACI 306R-10 Guide to Cold Weather Concreting

ACI 306.1-90 (ACI 1990) is the standard specification giving minimal requirements for preparation and protection of concrete. ACI 306R-10 (ACI 2010a) is a comprehensive document giving general requirements and methods to satisfy these requirements. These two references are the most cited in the literature related to cold weather concreting.

The objectives of the ACI 306R report are mainly to prevent damage at an early age, assure strength development, maintain curing conditions, and limit rapid temperature change. The main principle stated in this document is that concrete that reaches a compressive strength of 3.5 MPa can resist one cycle of freezing. For more than one cycle, protection should be provided until concrete reaches a minimum compressive strength of 24 MPa.

2.3.2.2 MSJC. TMS602-11/ACI 530.1-11/ASCE 6-11, Specification for Masonry Structures

The American specification for masonry construction (MSJC 2011) is the analog regulation to the Canadian standard CSA A371. The sections discussing cold weather masonry construction (i.e., 1.8 B and 1.8 C) are similar in many respects to the Canadian standard. The Canadian standard is better organized and easier to read, but specifies more stringent requirements in terms of mortar protection times: 48 hours for CSA A371 versus 24 hours for MSJC-11.

2.3.2.3 ACI 212.3R-10, Report on Chemical Admixtures for Concrete

The 2010 edition of ACI 212.3 (ACI 2010b) is the first ACI document to report on the use of cold weather admixture systems (CWAS) as one of the thirteen classified chemical admixtures used in concrete. CWASs are described as accelerators, water freeze depressants and sometimes water reducers. The document refers to ASTM C1622 for standard test methods to be followed to evaluate the admixtures. The common practice described in the document is to mix up to five commercial products (water reducers, accelerators, retarders, corrosion inhibitors and shrinkage reducers) and evaluate their effect on fresh and hardened properties of concrete at cold temperatures. The compressive strength for hardened concrete cured in laboratory conditions at -5°C is expected to develop at a rate equal or higher than that of a control concrete maintained at +5°C. In the field, where cooling may take a few days, strength gain is generally much faster. In terms of freeze-thaw durability, it seems that the air entrained concrete with antifreeze

admixture behaves better than the air entrained control concrete. The document frequently references the experimental work of Korhonen et al. (2004a) on developing and testing CWAS from available off-the-shelf admixtures.

2.3.2.4 ASTM C1622/1622M, Standard Specification for Cold-Weather Admixture Systems

ASTM Standard C1622 (ASTM 2010a) is the first standard document in North America providing minimum requirements on the use of CWASs in concrete construction. The first version of this document was approved in 2005 and edited in 2006. The purpose of this standard is to provide the minimum requirements specifications for concrete with CWAS when its temperature is as low as -5°C before the time of initial set. These specifications include: the time of initial setting limited to twice that of control specimen, the compressive strength at least 40%, 80% and 90% that of control specimen at 7, 28 and 90 days respectively, the maximum shrinkage limited to 135% that of control, and the relative durability factor at least 80% that of control.

2.3.2.5 ASTM C494/C494M-11, C260/C260M-10 and C1384-06

ASTM Standard C494 (ASTM 2010b), entitled Chemical Admixtures for Concrete, gives specifications for eight types of admixtures based on three primitives: water reducers, accelerators, and retarders. The ASTM C260 standard (ASTM 2010c) gives specifications for air entraining admixtures. Finally, the ASTM C1384 standard (ASTM 2006) gives specifications for admixtures for masonry mortar, which are classified into five types: bond enhancer, workability enhancer, set accelerator, set retarder, and water repellent.

2.3.3 Current Practices

Recommendations to deal with cold weather construction have been adopted since the early 1930's (Korhonen et al. 1997b). These provisions are often short and concise, and many other references can be found in the literature explaining and simplifying their practical meaning. One of the most practical for concrete is "Practitioner's Guide to Cold Weather Concreting" (Kurtz 1997), which is a collection of more than thirty papers published between 1988 and 1997, mostly from Concrete International and Concrete Construction. A second example is a reference text for masonry construction, called "Hot & Cold Weather Masonry Construction" edited by Masonry Industry Council (MIC 1999).

The provisions and recommendations pertain to three main phases for both concrete and masonry: preparation before the job starts, provisions during construction, and protection after the job is finished.

2.3.3.1 Preparation

The first recommendation usually given is to plan ahead so that everything is ready 24 hours before the job starts. Meteorological information is useful for planning. The construction materials on the site should be stored and protected from rain, snow, ice, and any contaminant. Any surface in contact with fresh concrete or mortar has to be cleaned from ice and snow. Embedded steel acts as a cooling conductor. Hence, it is usually recommended to heat and insulate embedded metals before pouring (Kurtz 1997).

It is recommended to keep masonry units dry, which will save the time and energy required to clean them if they freeze. Frozen masonry units drain heat from mortar and have their moisture absorption rate reduced due to pore obstruction by ice. Units with a high initial rate of absorption (IRA) are usually a preferable choice. When required by the weather conditions, shelters and enclosures should be prepared in advance (Woodham and Schuller 2005).

2.3.3.2 Construction

The most common practice in cold weather construction is the heating of materials, with water being the easiest ingredient to heat; it is also common to heat other ingredients or even heat the mix as a whole (Krylov 1997). For concrete, the recommended mix temperature is between 7°C and 21°C when no special precautions are taken (ACI 2010a). For masonry, it is between 5°C and 50°C (CSA 2004a). However, extra heating is not considered a good practice, because it is often accompanied by many negative side effects, such as rapid heat loss, higher water demand, higher rate of slump loss, as well as the possibility of thermal and plastic shrinkage (Scanlon and Ryan 1989). It is also highly recommended to maintain the same temperature for consecutive batches (MIC 1999).

Another common practice in cold weather is the use of shelters or heated enclosures. Even though their use increases the project cost, it is claimed by numerous authors (Davison 1970, Krylov 1997, CMDC 2002, IMI 2010) that they positively contribute to improving construction quality and workers' productivity.

A third practice is concerned with the use of special mixes which may involve increasing the cement dosage, using a Type HE cement, or using accelerating admixtures (Kurtz 1997). In the case of masonry construction, a good proportion between cement and lime for mortar is a good practice (Davison 1970). For durability purposes, the use of air entraining agents is recommended.

2.3.3.3 Protection

Curing is a key parameter for the development of the long-term concrete strength and its durability. Curing is mainly influenced by moisture and heat. The use of a heated enclosure is the ideal solution for cold weather concreting; it can approximate laboratory conditions. The main problem with this solution is its prohibitive cost. The use of steam as a curing solution is particularly effective because it provides heat and moisture at the same time. Many other procedures are found in the literature; Krylov (1998) cites thermos curing, electric contact heating, electrode heating, and induction heating. The use of admixtures such as antifreeze agents and accelerators may reduce and, in the best case, eliminate the need for special arrangements for external curing.

Before the end of curing, the temperature has to be lowered gradually to prevent thermal cracking. In addition, prior to form removal, concrete strength needs to be evaluated (Kurtz 1997). The maturity method ASTM C1074 (ASTM 2010d), non-destructive testing ASTM C803 (ASTM 2003), and specimen cured in field conditions ASTM C31 (ASTM 2009) are the most used methods for that purpose (Scanlon 1997).

For masonry construction, hoarding an individual portion of the structure as illustrated in Figure 2.3 (a), is found to be less costly than heating the whole structure. Also, when work is not in progress, it is recommended to cover the top and lateral faces of a masonry wall to prevent intrusion of precipitation (Figure 2.3 (b)) (MIC 1999).

(a)

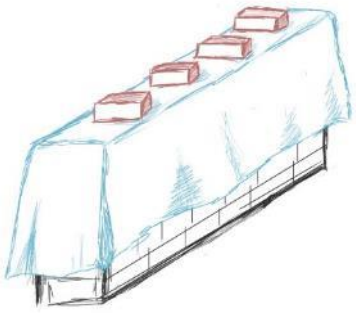

(b)

Figure 2.3 Masonry construction protection:
(a) Hoarding, and (b) Sketch showing covered top and sides of a wall

2.4 Cold Weather Admixture Systems for Concrete

In this section, "antifreeze admixtures" or "cold weather admixture systems (CWASs)" are defined. The two expressions are used interchangeably in this manuscript. A short historical background on the origin and more recent developments with respect to their use in concrete is presented. The effect of CWASs on the most important properties of concrete at various stages of its life are reviewed. Most of the work referenced herein on CWAS is concrete oriented; very little has been done related to masonry mortar. In fact, most of the recent publications (e.g., Jaffe 2003, CSA 2004b, Woodham and Schuller 2005) still do not permit the use of antifreeze admixtures in masonry construction, and an extensive bibliographic search in the most common publication databases identified only one explicit reference dealing with the use of CWASs in masonry (Korhonen et al. 1997d). For this reason, the focus of this section is centered on concrete.

2.4.1 Definition

Antifreeze admixtures are relatively new products in North America. Many names are given to this family of admixtures; low temperature, cold weather, freezing protection and antifreeze are the more common ones. Most authors prefer the name "antifreeze admixtures" because it is more specific and expresses the fact that the admixture is used for temperatures below the water freezing point.

Antifreeze admixtures are chemical compounds that, when added to cementitious products, depress the freezing point of the mixing water and accelerate the hydration reactions (ASTM 2010a). According to this definition, the antifreeze admixture must achieve two functions:

a) depressing the freezing point of the pore solution, and b) accelerating the setting time and strength gain of concrete at low temperatures, as compared to a control specimen at the lowest acceptable temperature without protection. In many cases, water reducers are added to the CWAS to lower the water content of the mix without losing the required workability, and to reduce the required antifreeze dosage since there is less water that is available to freeze.

Three groups of antifreeze admixtures have been defined (Rixom and Mailvaganam 1999):

- Primary, which contain only a freeze depressant; they are weak electrolytes (e.g., solution of ammonia) and non-electrolytes (e.g., alcohols and carbamide);
- Binary and ternary, which contain a combination of freezing depressants and hydration accelerators (e.g., calcium chloride, sodium chloride, sodium nitrite); and
- Other, which contain water reducers and superplasticizers (e.g., sulfonated naphthalene formaldehyde, sulfonated melamine formaldehyde)

A good antifreeze admixture system should also meet some other requirements, such as maintaining the workability, achieving a reasonable setting time, not reducing the strength at normal temperatures, not reducing the freeze-thaw durability, not promoting the silica aggregate nor the corrosion reactions, and being cost effective (Korhonen et al. 1997a).

2.4.2 Historical Background

The use of antifreeze admixtures in concrete started in the early 1950's in the former Soviet Union, where calcium chloride and sodium chloride were used for their high capacity to lower the water freezing point. They discovered later that these two chemical species also promote the corrosion of reinforcing steel (Korhonen 1990). Many other chloride-free admixtures were then effectively tested, such as sodium nitrite, calcium nitrate and calcium nitrite-nitrate. An extensive literature review about the work undertaken in Russia was carried out by Ratinov and Rozenberg (1995). In the late 1970's, Finland and China presented their first work on the subject (reported in Korhonen 1990). In 1985, Finland commercialized its first ready-mix antifreeze concrete. In China, most of the recent developments are focused on the testing of fly ash as a mineral addition to evaluate its effect on freezing protection (Huo and Wang 2013, Zhang et al. 2014). In the USA, extensive research studies on antifreeze admixtures started in the late 1980's (Brook et al. 1988, Korhonen and Cortez 1991, Scanlon 1992). Finally Japan produced its antifreeze containing polyglycolester derivative and calcium nitrite-nitrate in 1991 (Sakai et al. 1991). Although the use

of antifreeze admixtures is not new, research is still being conducted to enhance the performance and durability of antifreeze-added concrete, especially in countries with severe winter conditions such as Canada, Turkey, China, USA, and Serbia (Korhonen 2006, Vasović et al. 2008, Damle 2009, Arslan et al. 2011, Barna et al. 2011, Wang et al. 2011, Çullu and Arslan 2013, Dong et al. 2013, Karagöl et al. 2013, 2015, Saha et al. 2015a, Kazempour et al. 2017).

The Cold Region Research and Engineering Laboratory (CRREL), a branch of the US Army Corps of Engineers, has conducted intensive work since 1990 on developing and testing CWASs for the concrete industry. Charles J. Korhonen, one of the world leaders in this field, conducted most of the CRREL projects related to antifreeze admixtures. The work at CRREL started with a literature review in 1990 (Korhonen 1990). It was followed by the development and testing of new admixtures in 1994, 1996 and 1997 (e.g., Korhonen et al. 1994b, 1997a, Korhonen and Brook 1996). The lack of acceptance by standards, and the wariness of being the first to try a new product by the industry, changed the research orientation. Between 1999 and 2006, the research was oriented towards combining commercially available off-the-shelf admixtures to develop acceptable antifreeze compounds. The authors at CRREL (Korhonen 1999, 2006) determined that one of the most important parameters contributing to the effectiveness of a CWAS was the freezing point. They tested 40 mortar mixes with water to cement ratio ranging from 0.3 to 0.47 and admixture dosage ranging from 1% to 24% by weight of cement. The authors related the freezing point to the percent dissolved solid in the solution through a linear regression model in the form of the equation below:

$$FP = -0.3 \times (\%\, solid) - 1.3 \tag{2.1}$$

where

$FP =$ Freezing point in °C

$\%solid =$ Percent of dissolved solid in the solution

The validity of this model is questionable in the sense that it does not include the types of chemicals used in the mixture, and its use must be limited to a small range of temperatures since most of the solution phase diagrams are not linear in nature. Regardless, in 2006, a report was published discussing the beneficial use of high dose antifreeze chemicals on the freeze-thaw durability (Korhonen 2006).

Many field tests were satisfactorily conducted between 1997 and 2010. The persistent efforts deployed at CRREL ended up with the adoption of one important standard: "Standard Specification for Cold-Weather Admixture Systems, ASTM C1622-10" (ASTM 2010a) and the inclusion of a dedicated section on the CWASs in the ACI report "ACI 212.3R-10 Report on Chemical Admixtures for Concrete" (ACI 2010b).

2.4.3 Effects of Antifreeze Admixtures on Concrete Properties

The most important properties studied in the literature related to the influence of CWASs on concrete can be classified into four categories: preparation and mixing, fresh state, hardened state, and durability.

2.4.3.1 Mixing and Proportioning

No special skills are required for the use of antifreeze admixtures (Korhonen et al. 1997a); however, some recommendations are given on the appropriate timing for adding the admixtures. Three approaches have been tested, as shown in Figure 2.4: adding all of the five admixture types at the mixing plant, adding some at the mixing plant and some at the jobsite, and adding all at the jobsite; each method has its advantages and disadvantages (Korhonen et al. 2004a). It is also advised to use a good cement at a convenient dosage. ACI 306R-10 (ACI 2010a) recommends using a Type HE cement or an increase of the cement dosage by 60 kg/m^3. High alite and low and average aluminates are preferred, because aluminates tend to convert admixtures to salt, reducing the amount of antifreeze in the liquid phase (Ratinov and Rozenberg 1995). It is desirable to minimize the use of mineral admixtures as they act as diluents, but this is not in conformance with the current trend in China for using and testing the effect of fly ash as antifreeze addition (Liu et al. 2007, Yingzi and Hengjing 2007, Huo and Wang 2013, Zhang et al. 2014). Very little explanation is typically given in the literature regarding the rationale behind the selection of individual chemical compounds to form the antifreeze admixture.

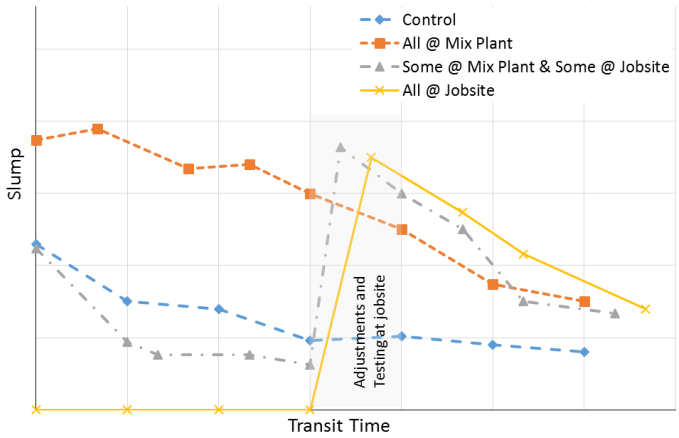

Figure 2.4 Slump as function of transit time corresponding to different scenarios for when the antifreeze admixture is added based on Korhonen et al. (2004a)

2.4.3.2 Fresh Concrete

Regarding workability, most chloride-based admixtures act as weak plasticizers and hence lead to a reduction in water demand. Some other salts do not show any plasticizing effect, and therefore end up being combined with plasticizers or superplasticizers. Figure 2.4 shows the variation of slump as a function of the transit time for cases when a chloride-based admixture was added at various stages (Korhonen et al. 2004a).

It has been shown that some antifreeze admixtures accelerate the setting time, others retard it and some do not change it at all (Ratinov and Rozenberg 1995, Korhonen 2002a, Korhonen et al. 2004a).

The effectiveness of an antifreeze admixture may be ascertained by noting its effect on the freezing temperature. Specimens equipped with a thermocouple are usually used to determine the initial freezing point, which is defined as the point where the slope of the cooling curve, with respect to time, changes, as shown in Figure 2.5 for a typical case. The freezing point provides an indication of when the pore solution in the cementitious mix will start freezing, hence giving an indication about the availability of liquid water needed by the hydration reactions at different temperatures.

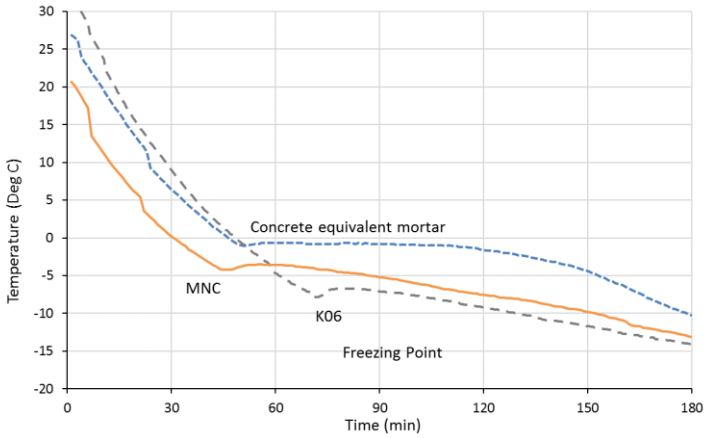

Figure 2.5 Typical cooling curves for control and antifreeze concretes, in which the labels refer to different antifreeze admixtures

Many models that attempt to explain the mechanism of ice formation can be found in the literature. They vary from simple empirical models (Korhonen et al. 2004a) to more complex thermodynamic models (Ratinov and Rozenberg 1995, Penttala 1998, Schulson 1998).

The experiments in the study done by Korhonen (2004b) showed that antifreeze admixtures do not prevent air from being entrained in the concrete; in some cases with continued mixing, air content can even increase. Most admixtures, particularly accelerators, do not promote bleeding (ACI 2010b). However, retarders, weak accelerators and plasticizers may increase risk of bleeding (Ratinov and Rozenberg 1995). Some extra shrinkage relative to control, in the range of 10–40%, was noticed when admixtures containing calcium or when high dosages were used (Ratinov and Rozenberg 1995, Korhonen et al. 1997b). Experience showed that some admixtures tended to be sticky, and required more time to be finished.

2.4.3.3 Hardened Concrete

The effect of antifreeze admixtures on the microstructure and the interfacial transition zone has been shown to improve the physical and mechanical properties of concrete. Many tabular results showing the strength gain can be found in the published literature for different admixtures, dosages, and curing methods (Ratinov and Rozenberg 1995). Most of them show acceptable to good strength gain, especially in the long term.

Typical compressive strengths reported by various researchers, including those presented in Ratinov and Rozenberg (1995), are shown in Table 2.2. The compiled table from multiple references includes the authors of the data, the admixtures used in their experimental program, the

curing schemes adopted, and the range of compressive strengths obtained. One can see the wide spectrum of admixtures and the curing schemes used by the various authors. In some cases, such as Arslan et al. (2011), the strength was relatively low at 18.5 MPa even though the curing scheme was 2 days at -5°C followed by 26 days at 20°C. However, in most other cases, the compressive strength results show the effectiveness of using antifreeze admixtures.

Table 2.2 Compressive strength performance of CWASs reported in the literature

Authors	**Admixtures used**	**Curing Scheme (°C)**	**Strength (MPa or % of control)**
Ratinov and Rozenberg (1995)	SN+CC[1] 10% water	28d -20° + 28d 22°	36 MPa
	CCNN[2] 10%	28d -20° + 28d 22°	38 MPa
	CCNNU[3] 10%	28d -20° + 28d 22°	40 MPa
	SN+0.4%SNF[4]	-5, -10, -15°	90, 70, 50%
Korhonen et al. (1996, 1997, 2001, 2002b)	EY11[5]	28d -5°	24−33 MPa
	KC1[5] (3SN+1S.sulf)	28d -5°, 28d -10°	33, 27 MPa
	DP[5], DPTC[5]	28d -5°	33 MPa
	ASTM C+E+F	14d -5° + 21d 20°	76%, 128%
		14d -10° + 21d 20°	47%, 112%
	ASTM A, F, C, E, Corr, Shrink, cement dose	14d -5° +42d 20°	117%−124%
		14d -10° +42d 20°	82%−120%
Brook et al. (1988)	Pozzutec20[6]	3d -6.7° + 25d 10°	32−37 MPa
Scanlon (1992)	NaSCN[7]	-7°	34 MPa
Sakai et al. (1991)	Polyglycolester + CNN[8]	-5°	16−22 MPa
Wang et al. (2011)	5 no-name compounds	7d -20° + 28d 20°	28−30 MPa
Vasović et al. (2008)	Reobet Antiled T-25[6]	7d -10° + 28d 20°	53 MPa
Arslan et al. (2011)	CN, H.E.Amine, P.H.Amine[9]	2d -5°−-20° + 26d 20°	18.5−14.7 MPa
Damle (2009)	Accel., HRWR, Waterproofing	-7°	12 MPa
Karagöl et al. (2013)	$CaNO_3$ 6%	7d − 28d -5°−-20° + 28d 22°	33 – 57 MPa

[1] Sodium nitrite + calcium chloride
[2] Calcium chloride-nitrite-nitrate
[3] Calcium chloride-nitrite-nitrate + Urea
[4] Sulfonated naphthalene formaldehyde
[5] Code names
[6] Commercial names
[7] Sodium thiocyanate
[8] Calcium nitrite nitrate
[9] Calcium nitrate, hydroxy ethoxy amine, polyhydroxy amine

Figure 2.6 shows qualitative compressive strength curves comparing control concrete cured at the normal temperature (25°C) and at the lowest allowable temperature (+5°C), with concrete

having the best and worst performing antifreeze cured at a temperature of -5°C (Korhonen et al. 2004b). It is clear that in the long term, strength gain at the low temperature is higher than that at higher temperature. The antifreeze-added concrete performs better than normal concrete at the lowest allowable temperature.

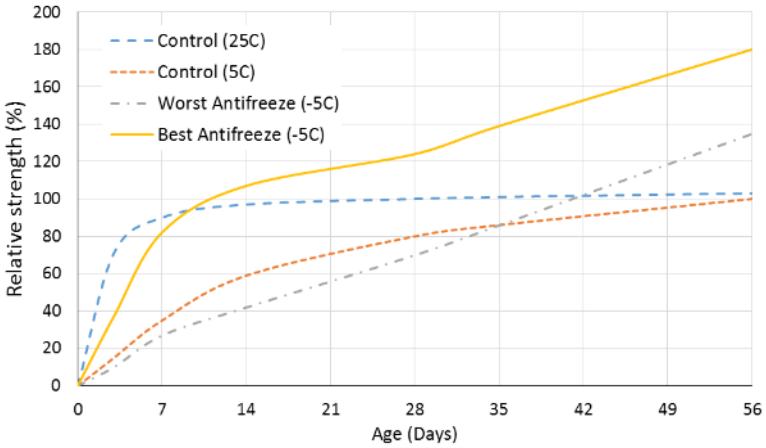

Figure 2.6 Relative compressive strength of control concrete and antifreeze added concrete based on Korhonen et al. (2004b)

Most antifreeze admixtures have been shown to improve the dynamic elastic modulus, except for potash and urea (Ratinov and Rozenberg 1995). Whereas the pore structure was affected variably, depending on its structure size, the overall porosity remained unchanged (Ratinov and Rozenberg 1995, Korhonen et al. 1997a). It seems that antifreeze admixtures improve the density of the paste-aggregate transition zone (Ratinov and Rozenberg 1995).

2.4.3.4 Durability

Two main hypotheses have been proposed to explain concrete failure when subjected to freeze-thaw cycles. The first is a local failure mechanism due to tensile stresses exceeding the material's tensile strength, caused by water-to-ice transformation (Davison 1970). The second is caused by the hydraulic pressure developing in the liquid pore solution when it is squeezed out by ice expansion (Setzer 2001). Most antifreeze admixtures improve the freeze-thaw resistance, some better than others, with complex ones being particularly effective. After a long period under saturated conditions, a partial washout of the species associated with the admixtures, due to dilution, tend to render the freeze-thaw resistance of antifreeze-added concrete similar to normal concrete (Ratinov and Rozenberg 1995). The effect of urea and calcium nitrate on the freeze-thaw durability was investigated for up to 28 cycles (Polat 2016). Samples with the antifreeze agents

showed strength reductions of 53% and 28%, respectively, compared to 72% for control sample. In a more recent study, Liu et al. (2019) used the NMR technique for the first time to check the mechanical and pore size properties of a cement mortar subjected to up to 100 freeze-thaw cycles and found good correlation between the NMR relaxation time and the pore size distribution. The NMR relaxation time is an indicator of the time required to dissipate the effect of an externally induced nuclear magnetization. Li et al. (2016) found that the sodium sulfate and sodium nitrite additives reduced the foaming power of the air entraining agents, shown by a decrease in the pore size, but the salts did not affect the foam stability. In another study, Korhonen (2002b, 2006) investigated the effect of high dose admixtures on the freeze-thaw durability. It was noticed that air entraining agents only slowed down the freeze-thaw process but did not actually prevent it. The optimal concentration of salts in the pore water can have a beneficial effect on long term freeze-thaw durability. The results of a typical freeze-thaw test according to ASTM C666 are shown in Figure 2.7. The decline of the relative dynamic modulus of elasticity indicates a loss of integrity of the concrete samples and the development of micro-cracks. The minimum requirement of the ASTM C666, to consider a concrete to be durable, is that the relative dynamic modulus of elasticity remains above 60% after a minimum of 300 freeze-thaw cycles.

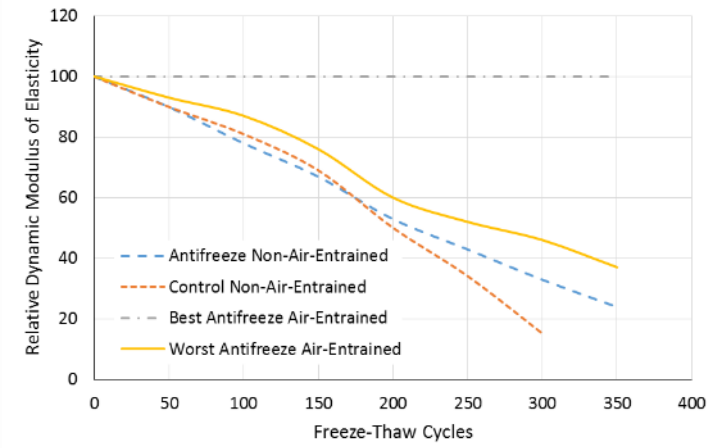

Figure 2.7 Typical freeze-thaw test, based on Korhonen et al. (2004b)

Three groups of antifreeze admixtures can be categorized according to the promotion of steel corrosion: inhibitors (e.g., sodium nitrite, calcium nitrite nitrate), inert (e.g., potash, calcium nitrate, urea), aggressive (e.g., calcium chloride, sodium chloride). The corrosion test conducted by Korhonen et al. (1997d) on two antifreeze prototypes resulted in no increase of the corrosion rate, as the antifreeze agents used were chloride free.

Sodium nitrite and potash are generally prohibited if alkali silica reaction is of concern. Calcium salts, however, do not cause alkali-silica expansion. Antifreeze admixtures promote tightness of the transition zone and microporosity; hence, concrete with antifreeze seems to be more resistant to carbonation. The phenomenon of efflorescence is explained by the migration of liquid salt solution to the surface and the subsequent evaporation of water. Sodium nitrate and sodium chloride are the main admixtures causing this phenomenon (Ratinov and Rozenberg 1995).

2.5 Summary

A review of the effects of the cold weather on cement-based materials has been presented. Two major effects have been highlighted: slower hydration reaction as the temperature drops, and irreversible damage to the cement paste if liquid water freezes before the cement paste gains enough strength. Two possible solutions are available: providing heat to the materials or environment for a sufficient curing period, or using a cold weather admixture system (CWAS), allowing the cement to hydrate at low temperature.

Canadian and American standards for cold weather practices were reviewed. Most of these regulations are still very restrictive regarding the use of antifreeze admixtures, due to the historic experience of using calcium chloride and alcohol as freeze depressants, given their deleterious effect on reinforcing steel and strength gain of concrete. However, thanks in large part to the progressive and sustained work done at CRREL, two regulating standards have been adopted: ASTM C1622-10, stating the minimum fresh and hardened performance requirements of a cold weather admixture system for concrete; and ACI 212.3R-10, report of the ACI committee on chemical admixtures for concrete, which, for the first time, included a section on cold weather admixture systems.

The effects of antifreeze admixtures on the fresh and hardened properties of concrete were summarized, as well as their effect on durability. It appears that most of the antifreeze admixtures proposed are binary or ternary mixtures composed of a freeze depressant, accelerator and, in some cases, water reducer. They present a good solution to cold weather concreting. However, more investigations are needed for many of them to ensure they do not have an adverse effect in the long-term, and to find new compounds or combinations acting effectively at lower concentrations. Compared to concrete, very little work has been done specifically related to masonry. Possible

reasons include the similarities between the two materials, the stricter regulations for mortar, and the relatively short curing period for masonry. The success of a testing program of antifreeze admixtures on masonry mortar, and the economic benefit related to the reduction of the thermal protection costs, will almost certainly lead to a relaxation of the masonry code requirements.

In summary, several gaps were identified in this literature review. These included a lack of experimental data on the use of antifreeze admixtures in masonry mortar, inadequate rationale behind selecting individual compounds in an antifreeze admixture system, the restrictive regulations in North America with regard to the use of CWASs in masonry construction, and the extended protection time required by the regulations.

3 PRELIMINARY REPLICATE TESTING

3.1 Introduction

As follow-up to the literature review, an attempt was made to replicate some of the experiments reported in the literature. It was deemed important, as an introductory step, to compare published data with what could be achieved in the laboratory conditions at the University of Saskatchewan, and to ensure a consistency in the techniques used to prepare and perform the tests. Even though the material of interest in this preliminary step was concrete, both the published and the replicated compression tests were carried out on concrete equivalent mortar samples, for which the composition was formulated on the basis of the target concrete composition, using the concrete equivalent mortar (CEM) method. A worksheet calculating the required ingredients for a specific composition and target volume was prepared; it was improved for later use to include admixture proportioning and multiple combination calculations. The control samples consisted of plain mortar without any additives, prepared and cured at room temperature, and then tested in compression at various ages. The strengths of the control samples were then compared with those of similar samples cured at +5°C without protection, which is the lowest acceptable temperature according to the ACI 306R recommendation. The final preliminary tests were focused on replicating the results of depressing the freezing point of antifreeze-added mortar and water solutions.

3.2 Concrete Equivalent Mortar and Proportioning

The basic idea behind the concrete equivalent mortar (CEM) is to correlate the concrete behavior with a mortar not containing coarse aggregate. Assaad et al. (2009) studied the possibility of predicting several concrete properties through the testing of CEM. They used Type I cement and varied the dosage between 300 and 450 kg/m^3 with an increment of 50 kg/m^3, and varied the water to cement ratio between 0.4 and 0.6 with 0.05 increment. They found that the CEM approach adequately predicted the slump, air content, setting time, and compressive strength of concrete with coefficients of correlation (R^2) greater than 0.86. For example, the compressive strength prediction model for concrete was 1.05 times its corresponding CEM with a coefficient of correlation of 0.94. On the other hand, they found moderate relationships between the concrete

and the CEM for the flexural strength and length change parameters. The CEM is designed to match the mortar fraction of the equivalent concrete; it must contain enough cement paste to fill the interstitial voids and to coat the sand aggregate (Korhonen and Orchino 2001). The cement proportion of the CEM is much higher than that of its concrete counterpart because of the big difference in the specific surface of sand compared to coarse aggregate.

Due to the need to produce many different CEM mixes, an Excel spreadsheet along with a Visual Basic script were developed and used to facilitate the proportioning task (Figure 3.1). The input parameters required for the worksheet were the batch target volume (ml), the water to cement ratio (w/c), the aggregate to cement ratio (a/c), and the relative dosage of the admixtures (%). The output parameters of the worksheet were: the weight of cement, sand, and water (grams), and the quantity of admixtures (ml). The relative admixture dosage was defined as the fraction (in percent) of the maximum recommended dosage given by the manufacturer. The spreadsheet was used extensively in Chapter 4, where the calculation details involved are further described.

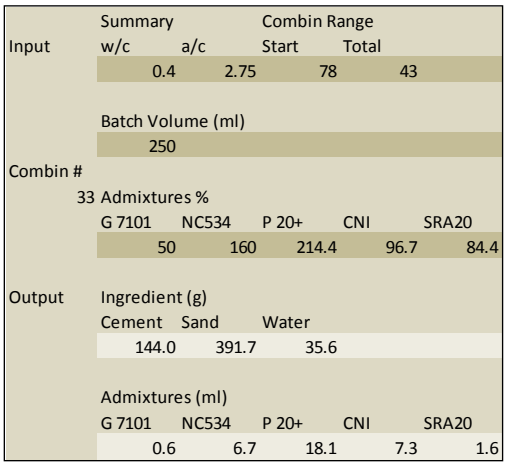

	Summary		Combin Range			
Input	w/c	a/c	Start	Total		
	0.4	2.75	78	43		
	Batch Volume (ml)					
	250					
Combin #						
33	Admixtures %					
	G 7101	NC534	P 20+	CNI	SRA20	
	50	160	214.4	96.7	84.4	
Output	Ingredient (g)					
	Cement	Sand	Water			
	144.0	391.7	35.6			
	Admixtures (ml)					
	G 7101	NC534	P 20+	CNI	SRA20	
	0.6	6.7	18.1	7.3	1.6	

Figure 3.1 Input and Output section of the CEM proportioning Microsoft Excel spreadsheet

3.3 Compression Tests of the Control Samples

The sand used for the replication tests was selected and adjusted to conform to the ASTM C144-11 standard in terms of gradation. A correction to the available sand found in the laboratory was made by removing the aggregate not passing the 4.75 mm sieve, which represented a very low percentage. No other adjustments were required to achieve an acceptable gradation. Figure 3.2 shows that the gradation of the corrected sand used in the CEM mixes fell between the high and low limits stipulated in the standard.

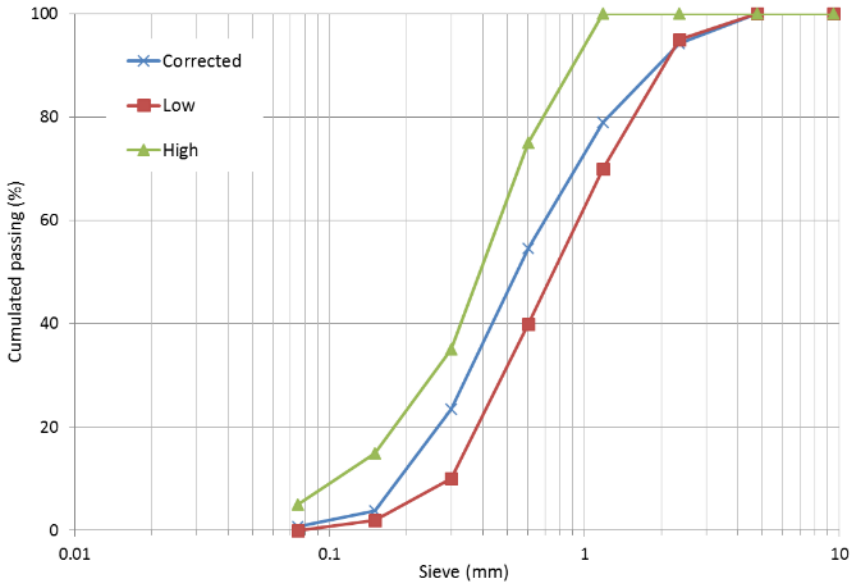

Figure 3.2 Gradation of the sand used in CEM mortar mixes

The mix selected for replication was taken from Korhonen (2006). It is listed in Table 4 of the reference as mix number 8. The mix corresponds to a typical concrete composition containing 474 kg/m^3 cement, with w/c = 0.40, sand/cement = 1.52, and coarse aggregate/cement = 2.27. The CEM counterpart of this composition is a mortar containing 783 kg/m^3 cement, with w/c = 0.36, and sand/cement = 1.59. The effective content of the batch was calculated to fill a total volume of 6 L and included 4.80 kg of cement, 1.77 L of water and 7.66 kg of sand. The purpose of Korhonen's (2006) study was to evaluate the effect of high dose antifreeze admixtures on the freezing point, the compressive strength, the freeze-thaw durability, and the change in length. Korhonen, in an earlier work (Korhonen and Orchino 2001), justified the use of the CEM method by the need of reducing the material waste and by more convenient sample sizes.

A mixing procedure similar to that described in ASTM C305-12 (ASTM 2012a) was followed. It consisted of putting all the water then the cement into the bowl, and running a 10 L Hobart mixer at low speed for 30 sec. The mixer was stopped and the bowl sides were scraped within 15 sec, then all the sand was added at once. A protection grid placed on top of the bowl did not allow a gradual addition of the sand. The mixer was run at low speed for about 45 sec, until the mix looked homogeneous. The mixing procedure was then stopped for 90 sec and then restarted at medium speed for a final 60 sec.

The confectioned mortar was cast in 50 mm diameter x 100 mm long plastic cylinder molds in two layers, and tamped 25 times each with a brass rod. Samples were vibrated for an additional 15 seconds on the shaking table to achieve a better compaction of the relatively stiff mortar in the cylinders. All specimens were capped with plastic sheets held with rubber bands and stored in their respective curing condition. The total mixing, casting, and transferring process took approximately 50 minutes.

Two curing temperatures were selected for this preliminary test: (a) room temperature, and (b) 5°C, also defined as the lowest allowable temperature without protection. The actual temperature and relative humidity (RH) conditions were measured using a humidity thermometer (Omega, model HH311), and found to be 23.7°C and 87% RH for the curing room, and 6.15°C (varying between 7.8°C and 4.5°C) and 22% RH for the cold chamber.

A total of 30 cylinders were prepared for 10 testing conditions, as summarized in Table 3.1. Twelve cylinders were stored in the curing room, and 18 cylinders were stored in the cold chamber. After 14 days, two sets of three cylinders stored in the cold chamber were transferred to the curing room for the remaining period. Two to twenty-four hours ahead of the compression testing time, designated samples for the specific testing age were demolded and capped with sulfur to reduce the effect of uneven surfaces of the hardened mortar cylinders.

Table 3.1 Summary of compressive strength test results in (%)

Curing scheme	**7d**	**14d**	**28d**	**56d**
Curing chamber 22°C full time	63.3	92.8	100.0	107.7
Coef. Var. (%)	13.5	12.6	5.5	10.1
5°C for 14 days, then move to 22°C	53.8	54.8	90.0	103.8
Coef. Var. (%)	3.4	9.4	13.5	12.1
5°C for 28 days, then move to 22°C	-	-	79.1	108.0
Coef. Var. (%)			9.5	4.6

The workability of the CEM mix was evaluated using the flow table test according to ASTM C1437-07 (ASTM 2007) and ASTM C230-08 (ASTM 2008). The flow rate was found to be 93, indicating that the mortar was relatively stiff, as compared to a flow rate of 120 reported by Korhonen (2006). It was observed after demolding the cylinders that a relatively high air pocket ratio existed in most of the samples. The relatively high stiffness of the mortar is likely one reason,

and insufficient compaction energy may have been used to achieve good consolidation. This observation was taken into consideration for the next testing phases. Samples cured in the curing room also seemed much dryer than the ones cured in the cold chamber, even though the relative humidity of the former was higher. In addition, a powdery layer appeared on the surface of the samples as if some of the cement had not reacted.

Table 3.1 shows the mean relative compressive strength obtained for each set of three samples for each curing scheme and testing age. The same results are represented in graph form in Figure 3.3. The relative strength is defined as the ratio of the strength of the specific sample set to the mean strength of the set cured at room temperature for 28 days, which was measured to be 41.4 MPa. For the sake of comparison, Figure 3.3 shows also the results of relative compressive strength of samples cured at 5°C and 20°C reported by Korhonen (1999).

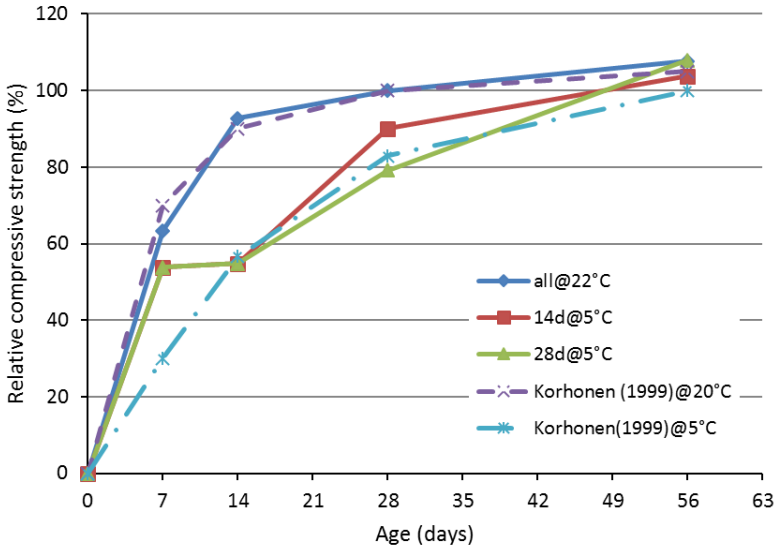

Figure 3.3 Relative compressive strength results for tests replicating Korhonen (1999)

It can be seen that there was a very close match between the results obtained in the laboratory and those reported by Korhonen (1999), except for the data point of 7 days at 5°C, which had a higher strength than expected. Samples cured in cold temperature also demonstrated a higher rate of strength gain at later ages compared to those cured in room temperature.

3.4 Mortar and Water Solution Freezing Point

For the mortar and water solution freezing point replication experiment, the freezing chamber was set to a temperature of -20°C. Type T thermocouples were used to monitor the interior temperature of samples. This type of thermocouple has a validity range between -270°C and 370°C, which is much broader than the current experimental requirements. A thermometer reader (Mastech, model MS 6514 dual channel) equipped with an adjustable time step data logger was used to record the temperature evolution with time, which was required to determine the freezing point of the materials.

3.4.1 Water and Water Solution Freezing Point

The first set of freezing point tests was conducted using simple water solutions in order to test the equipment and procedures. Three solutions were tested: tap water, a calcium chloride solution at a concentration of 15% by weight, and a sodium nitrite solution at a concentration of 16.0% by weight. The solutions were mixed in a test tube and transferred to the freezing chamber with the thermocouple inserted inside. The temperature was recorded at 60 s intervals, and the time evolution of temperature was plotted similar to that shown in Figure 2.5, from which the FP was determined. The measured freezing points are listed in Table 3.2 and plotted in Figure 3.4 along with values reported in the literature. It can be seen that close agreement was achieved between the measured and the reported freezing points. The reference values from the literature were extracted from graphs, which may explain the slight differences observed for the calcium chloride and sodium nitrite solutions.

Table 3.2 Freezing point of water solution

Solution	Measured FP (°C)	Referenced FP (°C)
Tap Water	0.0	0.0
Calcium Chloride (15.0%)	-12.6	-12.0 [1]
Sodium Nitrite (16.0%)	-10.5	-10.0 [2]

[1] (Engineering ToolBox 2007)
[2] (Montoya 2012)

Figure 3.4 shows the freezing point curves of the water, masonry mortar, and salt solutions. Water shows a freezing point equal to zero, as expected. Masonry, on the other hand, showed a

freezing point of -0.2°C which is above -3°C reported in some references (e.g., Korhonen 1990). The sodium nitrite and calcium chloride solutions showed freezing points of -13°C and -12.9°C, respectively, which is very close to results found in the literature of -12°C for sodium nitrite at 18.3 wt% concentration (Montoya 2012) and -12°C for calcium chloride at 15 wt% concentration (Engineering ToolBox 2007).

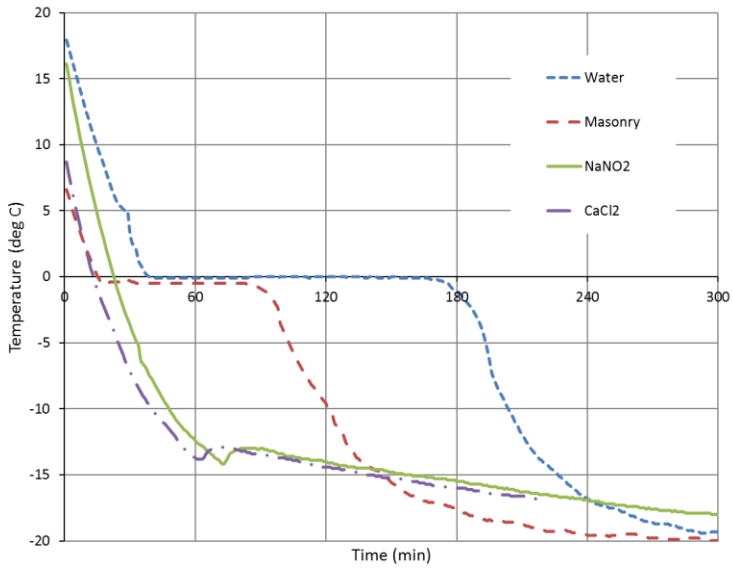

Figure 3.4 Water, masonry mortar and salt solutions freezing points

The thermocouple-thermometer reader was compared with a classic alcohol thermometer and with another thermocouple-thermometer reader in a varying water temperature setup between +40°C and -20°C. The differences were always within ±0.3°C at the 95% confidence interval.

3.4.2 Freezing Point of Mortar and Antifreeze-Added Mortar

The second freezing point replication experiment consisted of measuring the freezing point of mortar and antifreeze-added mortar combinations to compare them with data from the literature. Four mortar mixes were selected: a plain mortar similar to the control mortar prepared in the previous section (a-Plain), a mortar replicated from Korhonen (2002a) (b-K02), a mortar replicated from Korhonen (2006) (c-K06), and a mortar mixed with the commercial antifreeze admixture NMC-C15 (d-MNC).

The water, cement, and sand used in this experiment were identical to those used for the compressive strength experiment described in Section 3.3. A total of six admixtures were used:

Glenium 7101, a high range water reducer (1-HRWR); Pozzolith NC 534, an accelerating admixture (2-Accel.); Pozzutec 20+, an accelerator and a water reducer (3-Accel+WR); Rheocrete CNI, a corrosion inhibitor (4-Corr. Inhib); Masterlife SRA 20, a shrinkage reducer (5-Shrink. Reduc.); and MNC C-15, an antifreeze admixture (6-Antifreeze). All six admixtures were donated, the first five by BASF Canada, and the sixth by Muhu China.

Four different combinations of ingredients were used, as described below. The mix design worksheet described in Section 3.2 was used to calculate the ingredient amounts required for each combination. The mixing procedure was similar to the procedure described in Section 3.3 with the following two adjustments: (1) all admixtures except the HRWR were added with the water before the mixing started, and (2) the HRWR was added to the mix within the first 10 seconds of the last 60 seconds of medium speed mixing. Two cylinders for each of the four replicated experiments were cast and stored in the freezing chamber with an embedded thermocouple to monitor the freezing point (Figure 3.5). The average of the two readings was used to represent the freezing point. Figure 3.6 shows the temperature curve versus time, where the hump characterizes the freezing point of the corresponding mortar mix.

Figure 3.5 Two cylinders with the hand-made bracket to hold the thermocouple centered

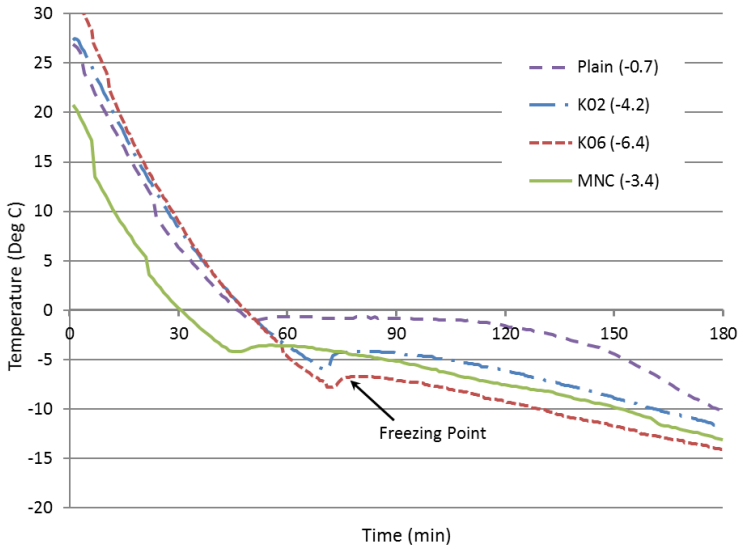

Figure 3.6 Cooling curves and freezing points of replicated mortars

The details of the four mix proportions and the resulting freezing points are shown in Table 3.3, in which w/c designates the water to cement ratio, a/c the aggregate to cement ratio, and the dosage of all admixtures are given as a percentage of the maximum manufacturer recommended dosage. The measured FP in °C represents the high and low values from between two and five repeated attempts.

Table 3.3 Replicated mortar combinations and their freezing points

Mortar Mix	Reference	w/c	a/c	HRWR	Accel.	Accel. + WR	Corr. Inhib	Shrink. Reduc.	Anti-freeze	Measured FP (°C)	Ref. FP (°C)
(a) Plain	(Korhonen 2002a)	0.36	1.59	-	-	-	-	-	-	-0.3 to -0.7	-1.4
(b) K02	(Korhonen 2002a)	0.34	1.59	40	100	60	100	75	-	-4.2 to -5.0	-10.1
(c) K06	(Korhonen 2006)	0.47	2.35	-	-	214	214	-	-	-5.0 to -6.4	-8.3
(d) MNC		0.47	2.35	-	-	-	-	-	100	-3.4 to -4.4	NA

The replicated plain mortar had a very high cement content and resulted in a freezing point of -0.7°C, which differed from the -1.4°C value reported in the literature for the same composition. More conventional mortars were also tested, and their freezing point was measured to be approximately -0.3°C. The second mortar replicate (K02) achieved freezing points between -4.2°C and -5.0°C in the laboratory, whereas the referenced mortar reached -10.1°C, which is a substantial

difference. This discrepancy may have been the result of the admixtures used in the laboratory being different from the one used in the referenced work, since the reference used the Type names (ASTM C494) instead of the commercial names. The third mortar replicate (K06), also referred to in the report as mix 5/24, was an exact replicate, since the names of the admixtures used were revealed. The gap between the freezing points was smaller for this mix but still substantial. The fourth mix was not a replicate, but was similar to the third one in terms of the basic ingredients; however, the admixture used in this case was a commercial antifreeze for concrete instead of a combination of accelerator, water reducer, corrosion inhibitor. The prospectus for this product claimed a usability down to -15°C with the maximum recommended dosage of 4% by cement weight. The resulting mortar was very sloppy and had a large number of small air bubbles with a thin brownish layer in the top surface. The freezing point reached for this mix, between -3.4°C and -4.4°C, was far from the expected -15°C.

Three factors were suspected as possible causes for the large discrepancies between the FP replicated in the laboratory and the FP reported in the literature. These included the volume of the samples, the associated rate of freezing, and the thermocouple placement. To test these hypotheses, an additional set of tests was conducted. A 75 mm diameter x 150 mm long plastic cylinder was used for these samples, the same third mix (K06) was prepared, and the thermocouple was placed in the center of the cylinder in a colloidal cage as described in Korhonen et al. (2004a). The freezing time required for this larger cylinder was almost twice the time required for the small cylinder; however, the freezing point of the mortar mix did not improve, reaching -5.6°C, which leaves the question open.

3.5 Replication of Compression Tests of Antifreeze-Added Concrete Samples

For comparison purposes, another mix was prepared using the same ingredients as reported in the previous section, except that the antifreeze admixture was replaced by calcium nitrite. This set of tests was intended to replicate the work of Korhonen (1999) and Karagöl et al. (2013), who used calcium nitrate and calcium nitrite. The calcium nitrite was the BASF Rheocrete CNI admixture used at a level of 269% of the manufacturer recommended dosage to match the proportion of 6% by cement weight reported in the two cited references. It should be noted that all compression test results presented by Karagöl et al. (2013) were obtained after 24 hours of post-curing at room

temperature, whereas Korhonen's results were obtained from compression tests performed without post-curing, except for the time required for samples to thaw, which was approximately 1 hour.

A partial set of result is shown in Table 3.4 which is an excerpt from a larger compilation of results that can be found in Appendix A. The compressive strengths are expressed as a percentage of the reference concrete moist cured for 28 days at room temperature, and the selected curing temperature for this comparison is -10°C.

Table 3.4 Percent of 28-day compressive strength of replicated antifreeze-added concrete cured at -10°C

Curing time	Kara3	Kor3	Kor2	Saha2
-7d	35.5	3.1	4.4	5.0
-14d	47.1	3.1	9.1	8.3
-28d	20.9	2.1	16.5	7.6

Kara3: Karagöl et al. 2013 $Ca(NiO_3)_2$, Kor3: Korhonen 1999 $Ca(NiO_3)_2$, Kor2: Korhonen 1999 $Ca(NiO_2)_2$, Saha2: Saha $Ca(NiO_2)_2$

The data show acceptable agreement between Kor2, Kor3 and Saha2. The strength gain at -10°C was insignificant, which implies that calcium nitrite and calcium nitrate, when used alone, are not very good antifreeze admixtures, at least not at -10°C. Much higher compressive strengths were reported by Karagöl et al. (2013) compared to the other authors, which is very likely attributable to the 24 h post-curing scheme used by Karagöl. Little to no evolution of the strength gain was noticed in some cases between 14 and 28 days, even showing substantial drop in the case of Karagöl, with no provided explanation. Another unexplained result in the work of Karagöl is the very low strength gain between the ages of 7 and 28 days when control samples were cured in lime water.

3.6 Summary

In the process of preparing the literature review, some preliminary control tests and experimental replications were conducted. Instead of using plain concrete, concrete equivalent mortar samples were used, which have similar overall properties. For this purpose, a mix design spreadsheet was created to calculate the proportion of the mix ingredients including any admixture

combinations to be used in subsequent experiments. A script was added to the spreadsheet to facilitate the creation of multiple mixes at once.

The results obtained for the compressive strength tests at room temperature (23°C) and at the lowest allowable temperature without protection (5°C), compared well with results published in the literature (Korhonen 1999). However, the freezing points of antifreeze-added mortar samples did not show the same agreement with the results obtained by the same authors.

The results of the replicate compression tests conducted at below-freezing temperatures using concrete samples with various admixtures were largely in accordance with those reported in the literature, except for the results obtained by Karagöl (2013), which is likely due to the post-curing used by Karagöl. The results obtained in this chapter demonstrated that the techniques used to prepare and perform the experiments in the laboratory conditions at the University of Saskatchewan were generally consistent with those reported in the literature.

4 DEVELOPING ANTIFREEZE ADMIXTURES FOR MORTAR FROM AVAILABLE OFF-THE-SHELF ADMIXTURES[1]

4.1 Abstract

As a result of the harsh weather conditions and a long winter season, the construction industry in parts of North America faces the problem of the low-rate and even the complete halt of the hydration reaction at low-temperatures. Two solution strategies can be taken; the first is the one adopted by the current regulations and codes, which specifies a certain number of protective measures to take, if the work has to carry on in low-temperature conditions. These measures range from heating individual ingredients to the use of a heated enclosure to protect the whole structure. The second approach, which is explored in this work, is the use of chemical additives to improve the fresh and hardened state of the cementitious materials cured at low temperatures. This paper presents a short literature review on the use of antifreeze admixtures in concrete construction, showing the lack of data related to masonry construction. Initial results of an experimental program are also presented, which consisted of combining a total of six off-the-shelf concrete admixtures, up to five at a time with three concentration levels each using an incomplete response surface design method, due to the large number of possible combinations. The target function of the system was the freezing point of the mortar, which was measured using an embedded thermocouple in the center of the cylinder. The results obtained are relatively good in terms of lowering the freezing point of the mortar mix; however, the attainment of a satisfactory compressive strength was not directly related to the freezing temperature of the mortar. This work demonstrates that it is possible to achieve substantial compressive strengths in masonry mortars cured at sub-freezing temperatures with the use of antifreeze admixtures, but the ability of an admixture to lower the freezing point does not necessarily mean an acceptable compressive strength will be achieved.

Keywords: Masonry mortar; Antifreeze admixtures; Freezing point depression; Statistic design

[1] This chapter was published as "Saha, O., Boulfiza, M., and Wegner, L.D. 2015a. Developing antifreeze admixtures for mortar from available off-the-shelf admixtures. In 12NAMC. Denver, CO. USA". It has been reformatted to conform to a consistent standard throughout the thesis, and a number of grammatical errors in the original manuscript have been corrected. The copyright is assigned to The Masonry Society www.masonrysociety.org

4.2 Introduction

The long winter season in certain parts of North America, as in several other northern regions in the world, with temperatures well below the water freezing point, forces the construction industry to adopt non-conventional construction procedures, centered mainly on protecting the freshly mixed and placed cementitious material for a sufficient period of curing time. This regulation requirement is justified by the fact that masonry mortar, like other cementitious materials, is made of aggregates and a cement paste, which may not react properly under low-temperatures. In general, and under normal conditions, several chemical reactions take place when cement and water are mixed together, collectively known as "the hydration reaction". Like most chemical reactions, lowering the temperature has the effect of lowering the rate of the hydration and even stopping it completely when there is no water left in liquid form. The low strength gain associated with the low-hydration rate is the first problem in cold weather. Another problem related to temperatures below the water freezing point is of physical nature, that is, the volume-increase of water during its transition from liquid to solid, which creates a risk of damaging the microstructure of the cement paste. These are the two major problems for masonry construction in cold weather (Davison 1970, Ratinov and Rozenberg 1995, Woodham and Schuller 2005). Few answers are given to the low-temperature related problems. One is to simply stop construction when the thermal conditions are not favorable and the cost of protection is too high. Another solution is to provide sufficient thermal protection to the materials and construction to ensure that the freshly made cementitious materials have reached an acceptable strength and can withstand the cold weather conditions on its own. The preparation and protection measures range from heating the individual ingredients and covering the finished work at moderately cold temperatures to a complete heated enclosure at much lower temperatures. The Canadian Standard, "Masonry Construction for Building" (CAN/CSA A371-04) as well as the American standard MSJC, "Specification for Masonry Structures" (TMS602-11/ACI 530.1-11/ASCE 6-11) give the requirements on how to protect materials and masonry structures in cold weather conditions. They divide the protection during construction and protection of finished work into four increasing levels as the external temperature decreases.

The other possible answer to the low-temperature problems could be the use of antifreeze admixtures to reduce the requirement for protection and ultimately eliminate it completely for reasonably low temperatures. The idea of using antifreeze additives is not new; it goes back to the

early fifty's in former USSR. Their use in North America in masonry construction is almost nonexistent and prohibited by the current regulation (CSA 2004b, Woodham and Schuller 2005). The main reason for this restrictive approach is that the popular compounds known for their antifreeze effect are calcium chloride and alcohol; unfortunately, both are also known for their detrimental effects of promoting steel reinforcement and anchorage corrosion and lowering concrete strength.

A short literature review is presented in this paper showing the use of antifreeze admixtures in concrete construction and the scarce data related to masonry construction, perhaps due to the fact that many similarities exist between concrete and mortar, since both are based on cementitious materials. However, many differences exist between the two materials, such as their initial water content, initial rate of absorption of the masonry units, aggregate size and distribution, and the possible presence of lime, justifying the need for a separate study to be conducted specifically for antifreeze admixtures applied to masonry construction.

Under the starting hypothesis that a low freezing point will promote the hydration reaction at low temperatures, and hence will provide a better strength gain of the cementitious material, the initial results of a specific experimental program focusing on lowering the freezing point of different combinations of mortar mixes containing various off-the-shelf commercial admixtures are presented. A statistical approach based on the incomplete response surface method is used with five factors at a time and three concentration levels each to design a reduced number of experiments among the large number of possible combinations. A few additional experiments were designed with two and three factors to examine the effect of a smaller number of admixtures and higher dosages. A selection of several candidates was tested for compressive strength at ages of 7 and 14 days. To reduce the total time of the experimental program subsequently, the best samples were subjected to compressive strength tests at the standard 28-day testing age.

4.3 Literature Review

4.3.1 Historical Background

The use of antifreeze admixtures in concrete started in the former Soviet Union in the early 1950's. The idea was to add chemical compounds, mainly salts, to depress the freezing point of water. The first chemicals used were calcium chloride and sodium chloride, until their adverse

effect of promoting steel corrosion was discovered. Many other chloride-free admixtures were then efficiently tested, such as sodium nitrite, calcium nitrate and calcium nitrite-nitrate. An extensive literature review of antifreeze admixtures has been done by Ratinov and Rozenberg (1995), mostly related to the work carried out in Russia.

In the late 1970's, Finland and China presented their first work on developing antifreeze admixtures, and in 1985, Finland commercialized its first ready-mix antifreeze concrete. In China, most of the recent developments are focused on the use of fly ash as a mineral additive to help in freeze protection. In the USA, research on antifreeze admixtures started in the late 1980's (Brook et al. 1988, Korhonen and Cortez 1991, Scanlon 1992). Japan produced its antifreeze containing polyglycolester derivative and calcium nitrite-nitrate in 1991 (Sakai et al. 1991). More recently, some other countries, such as Turkey and Croatia (Vasović et al. 2008, Arslan et al. 2011, Karagöl et al. 2013), have shown an interest in developing cold weather admixture systems (CWAS).

The Cold Region Research and Engineering Laboratory (CRREL), a branch of the US Army Corps of Engineers, has conducted intensive work since the 1990's on developing and experimenting with the use of CWASs in concrete construction. Charles J. Korhonen led most of the CRREL projects related to antifreeze admixtures. The lack of acceptance by standards and the wariness of being the first to try a new product by the industry changed the research orientation from developing new admixtures to combining available products to reach the same goal. This was done between 1999 and 2004. Many field tests were satisfactorily conducted between 1997 and 2010. The persistent efforts deployed at CRREL ended up with the adoption of one important standard: "Standard Specification for Cold-Weather Admixture Systems" (ASTM C1622-10) and the inclusion of a dedicated section in the ACI report "Report on Chemical Admixtures for Concrete" (ACI 212.3R-10).

4.3.2 Current Status of Masonry Design Codes Vis-à-vis Cold Weather Construction

Most of the current building codes opt for the thermal protection solution and do not recommend the use of antifreeze admixtures. Some reasons are objective, such as the lack of convincing experimental data, and some are subjective such as the limitation of antifreeze admixtures to calcium chloride and alcohols, even though many other antifreeze admixtures have been developed since, and their effect on concrete has been demonstrated to be beneficial. The

Canadian code "Mortar and Grout for Unit Masonry" (CAN/CSA A179-04), for example, specifies that antifreeze admixtures and accelerators shall not be used in mortar or grout.

The Canadian Standard, "Masonry Construction for Buildings" (CAN/CSA A371-04) as well as the American standard MSJC, "Specification for Masonry Structures" (TMS602-11/ACI 530.1-11/ASCE 6-11) give the requirements on how to protect materials and masonry structures in cold weather conditions. They divide the requirements into three sections: preparation and material protection, protection during construction, and protection of finished work. The two last sections are divided into four gradually increasing requirements as the external temperature decreases; they start with heating the mixing water and covering the finished walls at moderately cold temperatures and increase to a complete heated enclosure at colder temperatures. Many other documents exist to explain the code requirements and provide additional recommendations. The most popular ones are "Cold Weather Construction, Masonry Made EZ" edited by Canada Masonry Design Centre (CMDC 2002) and "Hot & Cold Weather Masonry Construction" edited by Masonry Industry Council (MIC 1999), among many others.

Unlike the ASTM C1622 "Standard Specification for Cold-Weather Admixture Systems", which gives specifications for testing antifreeze admixtures when the temperature of concrete is as low as -5°C before time of initial set, there is no update to the ASTM C1384 "Standard Specification for Admixtures for Masonry Mortars" with respect to antifreeze admixtures; the only five admixture types specified are: bond enhancer, workability enhancer, set accelerator, set retarder, and water repellent.

4.3.3 Current Developments in CWAS

Antifreeze admixtures or cold weather admixture systems (CWAS) are defined as chemical compounds which, when added to a cementitious product, depress the freezing point of mixing water and accelerate the hydration reaction (ASTM 2010a). According to this definition, CWAS must achieve two principal functions: depressing the freezing point of the pore solution and accelerating the setting time and strength gain of concrete or mortar at low temperature compared to control specimens at the lowest acceptable temperature without protection. In many cases, water reducers are added to the CWAS to lower water content of the mix without losing the workability and to reduce the antifreeze dosage, since there is less water available to freeze.

Developing a CWAS is mostly based on the empirical approach; researchers select some chemical additives and blend them with the mix to see their effect on concrete at low temperatures. This approach is sufficient for a composition made of one or two chemicals but cannot achieve the optimization of complex combinations. More recently, researchers are combining multiple chemicals to reach a desirable result, and statistical design of experiments and optimization techniques, such as the Response Surface Method (Damle 2009, Arslan et al. 2011), are more and more used to give a stronger scientific validation of the optimal combination. Many other research studies have been conducted (Liu and Liu 2008, Vasović et al. 2008, Karagöl et al. 2013) or are still in progress to develop and test new products and procedures. Their recent experimental results have shown that it is possible to use chemical admixtures in concrete construction to a certain extent in relatively low-temperature conditions.

In masonry construction, however, the only explicit reference found in the literature, to the authors' knowledge, was done by Korhonen (1997d). The report focused on three aspects: the evaluation of the cold weather performance of ordinary masonry by following the water content and absorption at the time of freezing, the evaluation of a proprietary concrete admixture applied to masonry mortar, and the elaboration of a new standard for freeze-thaw testing of concrete masonry units. The admixture test section included the compressive and bond strength, the setting time, and the freeze-thaw resistance of the mortar. The author concluded that the antifreeze tested is a viable solution, it has negligible effect on the freeze-thaw durability, it decreases the setting time to an acceptable level, and it substantially increases the compressive and bond strengths.

4.4 Materials and Methods

The first step in the experimental program was to select some admixtures from the literature and some from those that are commercially available. There was a total of six admixtures identified; five were inspired by Korhonen et al. (2004a) and consisted of a high range water reducer (HRWR), an accelerator (PNC 534), an accelerator plus water reducer (P20+), a corrosion inhibitor (CNI), and a shrinkage reducer (SRA20). The sixth was a product commercialized as concrete antifreeze admixture (MNC C15). The stage that preceded the tests on masonry mortar was the replication of some promising experiments done on concrete conducted by Korhonen (2006), as described in Section 3.3. This oriented the choice of the cement used at the beginning of this experimental program to Type GU cement, the water to cement ratio was 0.4 in most cases,

and the sand used was a graded sand of diameter less than 4.75 mm with a sand to cement ratio of 2.75.

The mixing procedure was adopted from the ASTM C305 standard (ASTM 2014). According to this procedure the water plus the admixtures, except the HRWR, were placed first in the bowl, the Hobart mixer was started at low speed and all the cement was added within the first 10 seconds of the 30 second mixing period. The mixer was then stopped and the bowl sides were scraped. After that, the mixer was started again at low speed for 45 seconds while adding all the sand in the first 15 seconds. Next, the mixer was stopped for 90 seconds, any collected mortar on the bowl sides was scraped, and the mortar was left to rest. The final step was to run the mixer at medium speed for 60 seconds while adding the HRWR in the first 10 seconds. The mortar was then cast in 50 mm diameter x 100 mm long plastic cylinders in two layers, each tamped 25 times with a brass rod.

A thermocouple of type T was inserted in the center of the cylinder and maintained in position by a hand-made bracket as shown in Figure 4.1. The assemblage was transferred promptly to the freezer, which was set to a temperature low enough to ensure the freezing point was reached within one to two hours. The thermocouple was connected to a thermometer reader and data logger, set at 1-minute sampling frequency, to allow the identification of the freezing point. A typical temperature-time graph is shown in Figure 4.2. The jump in the curve at about -6.5°C is defined as the freezing point.

Figure 4.1 Cylinder, bracket and thermocouple in the freezer

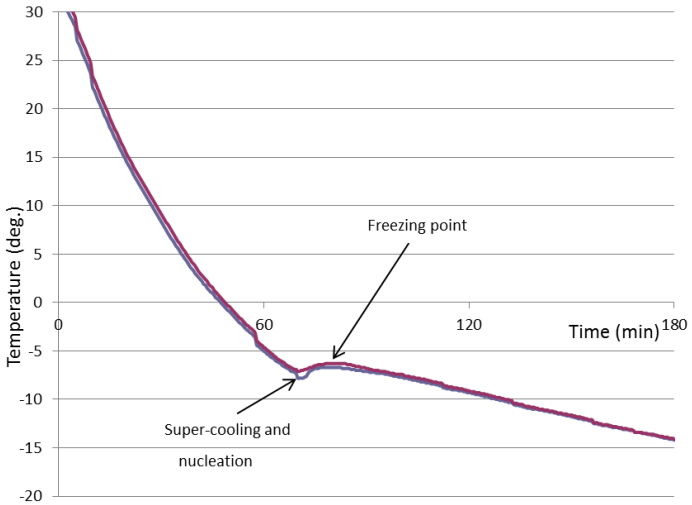

Figure 4.2 Typical temperature-time curve

Two statistical design approaches were adopted in this study, the response surface design and the factorial design. The first was used twice, with five admixtures each time, and the second was used at a later stage with a reduced number of the most effective admixtures. The response surface design was used to minimize one function, which was selected to be the freezing point. For this purpose, the software package Minitab (v15.1 Minitab) was utilized. The response surface design was run with the parameters corresponding to the central composite type with five factors and three central points at alpha=1 (face centered) giving 29 runs in total with the half design option. Once the freezing point was determined for each run, the gradient of the surface was calculated through a linear regression and the steepest descent was followed to the nearest minimum. A second response surface experiment was performed around the local minimum and the regression was applied again to find the next minimum. In the vicinity of the last found minimum freezing point, a factorial design with three factors was implemented to be more precise and to test the effect of a wider range of dosages. By the end of this phase, a total of more than one hundred mixes had been tested. Appendix B shows the calculation details of the mix design spreadsheet, along with the three main statistical experimental designs in tabular form.

Among the many samples prepared and tested for the freezing point, only a few of them were selected to be tested for their compressive strength based on some essential observations, such as having a freezing point around -10°C, a good visual workability, and a reasonable admixture dosage (even though it was higher than the manufacturer recommended dosage). Seven mixes were selected for testing, in addition to one extra sample containing only the concrete antifreeze (MNC-

C15). The selected combinations were prepared in a similar way as was used for the previous phase with a slight modification, consisting of premixing the mortar sand and cement in their dry state, at the same proportion of 2.75 to 1, before introducing them in the mixer. Immediately after mixing, the samples were cast in 50 mm diameter x 100 mm long plastic cylinders and transferred to the freezer set to -10°C to be cured. Quick compressive strength tests were performed on one cylindrical sample each at 7 and 14 days using a universal testing machine and fiberboard capping, in a non-standard form. The use of a single sample shortened the testing period and reduced the material waste. The main objective of this pre-test was to gain a preliminary order of magnitude of the compressive strength of the most promising combinations.

A more complete set of tests was then conducted on three mixes that were selected based on the results of the pre-test. The same procedure was followed in preparing and curing the samples; however, the curing period was extended to 28 days, and the test was performed on three replicas for each age. Prior to subjecting the specimens to a low temperature of -15°C, a pre-curing period of 6 hours at the laboratory ambient temperature (about 23°C) was applied. This was done for two main reasons: first, the mason cannot lay mortar at -15°C without a temporary shelter, which plays the role of pre-curing; second, the relatively low compressive strength obtained by the samples cured at -10°C suggested that a pre-curing would be required when a curing temperature of -15°C is used. In all cases, samples were allowed two hours of post-curing at room temperature to let the temperature at the center of the cylinders reach at least +5°C.

4.5 Results and Discussion

The first response surface design was run with five admixtures originating from the same manufacturer and limited in the mixture composition to their maximum recommended dosage as shown in Table 4.1. The freezing points obtained for this first test were between -0.7°C and -4.7°C.

Table 4.1 Ranges of the admixtures used in the first design, as a percentage of their maximum recommended dosages

Admixtures	**HRWR** (G 7101)	**Accelerator** (P NC 534)	**Accel+WR** (P20+)	**Corr. Inhib.** (CNI)	**Shrink. Red.** (SRA20)
Range (%)	0-100	0-100	0-100	0-100	0-100

Three regression models were tried: linear, linear + partial quadratic, and linear + interaction. Only the first method was retained because the quadratic and interaction factors were not statistically significant. The regression equation for the linear model is given below:

$$FP = -0.3847 - 0.0000x_1 - 0.0110x_2 - 0.01644x_3 - 0.0047x_4 - 0.0034x_5 \qquad (4.1)$$

where x_i corresponds to the admixture dosages of the compounds shown in Table 4.1 in their respective order. The analysis of variance showed negligible effect of the first factor (G 7101) and a relatively important contribution of the second and third factors (PNC534, P10+). The contribution of the fourth and fifth factors (CNI, SRA 20) was not well pronounced and needed more testing, as shown in Figure 4.3.

Equation 4.1 was used to define the gradient of the steepest descent, which was used to find the first local minimum. Starting from the central point, corresponding to a dosage of 50% of each compound, six data points in the gradient direction were experimentally tested and the local minimum was reached at the dosage of (rounded numbers) 50, 225, 300, 125, and 100 (%) for the five selected admixtures, respectively, with a freezing point attaining -9.5°C.

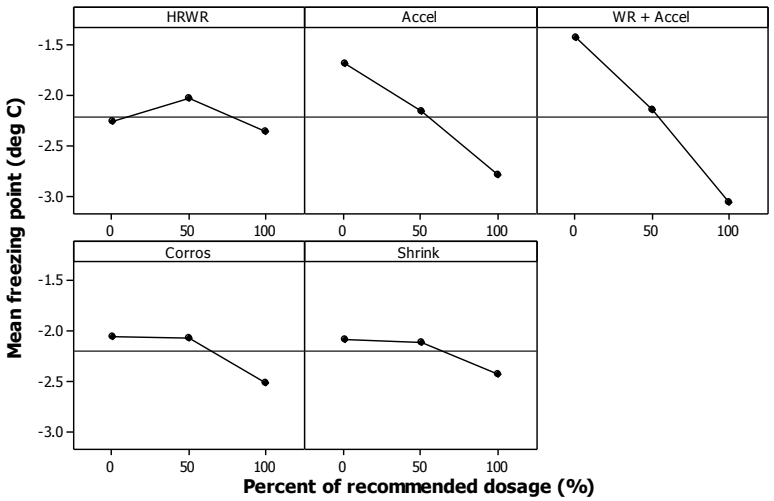

Figure 4.3 Main effect of the first response surface

From the result of the first response design, the first admixture (HRWR) was found to be ineffective in lowering the freezing point; thus, it was removed and replaced by another product (MNC C15) provided by a different manufacturer. The list of admixtures used in the second response surface design is given in Table 4.2, along with the dosage range. The results obtained

for this test varied between -8.9 and -15.3°C, and the main effect of the linear regression is shown in Figure 4.4. The two admixtures MNC C15 and P20+ appear to have the most significant effect on the freezing point, the two compounds PNC534 and SRA20 were insignificant in their effect, and the last factor CNI had a low effect, as seen in Equation 4.2.

Table 4.2 Admixture ranges for the second design, as a percentage of their maximum recommended dosages

Admixtures	**MNC C15**	**P NC 534**	**P20+**	**CNI**	**SRA20**
Range (%)	0-100	200-250	280-320	100-150	75-125

$$FP = -1.18659 - 0.05289x_1 - 0.01806x_3 - 0.00800x_4 \quad (4.2)$$

It was observed that when the antifreeze admixture MNC C15 was used the workability and entrapped air were much higher than the other cases, which means that it acted as a plasticizer and a frothing agent. In the presence of both MNC C15 and P20+ the mortar was sticky and had a very slow rate of hardening both at low and at room temperatures. This indicates a probable incompatibility between these two compounds. A later observation indicated that there is a gum-like formation when they are mixed together.

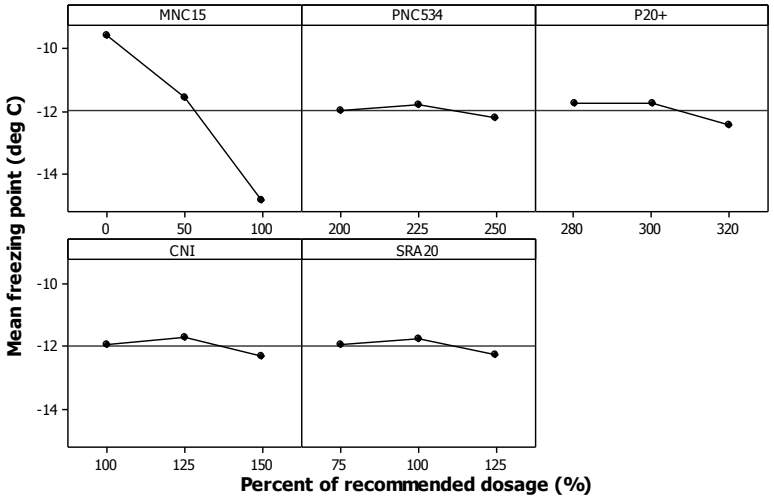

Figure 4.4 Main effect of the second response surface

According to Equation 4.2, a second gradient was calculated, and several data points were experimentally tested in that direction. It should be noted that even though PNC534 (x_2) was

optimum at a dosage of 225%, it was eliminated from the steepest descent due to its very high accelerating effect, rendering mortar unworkable in less time than was required for casting. The SRA20 (x_5) admixture was also eliminated due to its low effect and to simplify the regression equation. The result obtained in this test started at -8.8°C and continued dropping down to -25.6°C where the test was stopped for practical reasons. In fact, the FP did not show a minimum at this stage, but the high sloppiness and very high admixture doses made pursuing the test meaningless.

In the light of these observations, two more designs were tested. The first was a factorial design with three admixtures at two, two, and three levels respectively: MNC C15 (50, 100%), PNC534 (100, 200%), and P20+ (100, 200, 300%), giving twelve mixes. The second design involved only the two most effective admixtures in terms of depressing the freezing point, namely MNC C15 and P20+. They were used individually at extreme doses of 200 and 300% and combined at equal doses of 50, 100, 150, and 200%. The full data analysis of the two response surface designs, the two steepest descent analysis, and the factorial design are presented in Appendix C.

From the long list of admixture combinations, seven were selected for the quick compressive strength test based on their freezing point performance, their visual workability and the admixture dosage. The eighth candidate did not satisfy the freezing point criteria, but it was tested to confirm the claim of being a concrete antifreeze admixture. Table 4.3 shows the retained candidates along with their dosage, freezing point, and compressive strength. The first four candidates were selected from the first and the second steepest descent, the next two were selected from the factorial design, the seventh was selected from the two compounds equally dosed, and the last was the antifreeze alone at the manufacturer's recommended dosage.

The first sample did not show any significant strength gain, and the second was too stiff to be cast. Both were discarded from further analysis. The third and fourth samples, originating from the second steepest descent, showed better compressive strengths, but given their high admixture contents and the comparable or lower strength relative to other candidates, they were also discarded. The samples originating from the factorial design showed a better result at an early age (7 days), but the visual inspection of the crushed cylinder showed a dry condition indicating that no more hydration had taken place afterward. This was confirmed in the test at 14 days. The seventh sample showed a very low strength at an early age, but the strength at 14 days was acceptable. A possible explanation is that the single sample at early age was not representative.

The last sample, containing the concrete antifreeze MNC-C15 alone at the manufacturer's recommended dosage, produced a surprising result by giving the highest compressive strength, even though its freezing point was only -4.4°C. This gave rise to questions about the importance of the freezing point in the hydration and strength gain processes, and the quantity and effect of water in liquid form at below freezing temperatures. This observation, and the lower effectiveness of high admixture doses, led to a reconsideration of the starting hypothesis of prioritizing lowering the freezing point and using complex admixtures at high doses instead of simple admixture combinations.

Table 4.3 Admixture combinations and their resulting compressive strengths, based on single samples

Label	G 7101	MN C 15	NC 534	P 20+	CNI	SRA 20	FP (°C)	-7d+1h (MPa)	-14d+2h (MPa)
L1-16K	50		226	313	125	105	-9.8	1.73	3.12
L1-19K	50		259	362	139	115	-9.5	NA	NA
L2-2K		156		336	141		-13.5	5.2	12.8
L2-3K		209		354	149		-14.9	3.2	7.7
Fact9		100	100	300			-10.5	9.0	9.0
Fact12		100	200	300			-11.8	10.1	6.6
PM200		200		200			-10.2	1.0	11.4
M100		100					-4.4	12.4	15.5

A more complete set of compression tests was conducted on three simpler compositions containing the two most effective admixtures, P20+ and MNC C15, at their maximum recommended dosages, at two subfreezing temperatures of -10 and -15°C. Table 4.4 and Figure 4.5 show the compressive strength results up to the age of 28 days. The first mix, M100, showed an acceptable workability with a possible need for a little more water. The other two were quite stiff which required the addition of a certain amount of water to reach, by visual inspection, a good workability. This water adjustment modified the w/c ratio from 0.4 to 0.443. The P100 mix became relatively stiff at the end of the casting, and it was dropped from the test at -15°C because, in addition to the fast hardening, it did not achieve an acceptable compressive strength.

Table 4.4 Compressive strength (MPa) of three mixes at -10 and -15°C

Label	-7d+2h	-14d+2h	-28d+2h	+6h-7d+2h	+6h-14d+2h	+6h-28d+2h
	@-10°C (MPa)			@-15°C (MPa)		
M100	5.83	8.56	9.00	6.15	8.23	8.99
95% confid.	1.05	1.69	1.72	0.59	1.54	1.56
PM100	3.93	5.10	7.14	4.91	5.55	5.74
95% confid.	0.58	1.60	0.59	0.68	1.33	1.61
P100	1.30	1.72	2.73	NA	NA	NA
95% confid.	0.90	0.88	1.21	NA	NA	NA

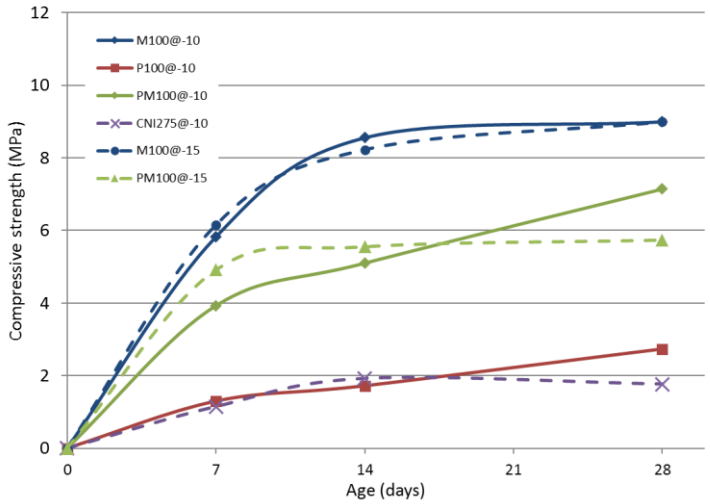

Figure 4.5 Compressive strength of the best candidates

Another parameter was modified in this last experiment, in that Type S mortar cement was used instead of Type GU cement, in order to have a basis for comparison with the next experimental phase of testing masonry mortar. This explains the relative decrease of the compressive strength compared to the previous test for the same admixture composition. The compressive strength shows an acceptable agreement with the results obtained by Korhonen (1997d), given the very low water to cement ratio and the Type M masonry cement used by that author.

The examination of the crushed M100 cylinder revealed the presence of reflecting crystals visible with the naked eye. The identification of this phase is under exploration, and it is suspected to be one of the reasons explaining the strength gain at low-temperatures. The crystal-like phase remains visible many days after the test. It can be seen that the use of MNC C15 alone has a better effect on the strength gain, up to the testing age of 28 days, than P20+ or a combination of the two. Given the fact that the test was done on cylindrical samples, the compressive strength can be

considered to be very close to the acceptable limit specified by the standard (ASTM C270) for Type S mortar, knowing that a correction factor of 1/0.85 (ASTM C780) has to be applied to convert the compressive strength of a cylindrical specimen to that of a cubic specimen.

4.6 Conclusion

An experimental program has been conducted to develop and test antifreeze admixtures for mortar in masonry construction. The major outcomes of this work can be classified into two categories, lowering the freezing point and assessing the compressive strength.

The use of combinations of non-dedicated admixtures at their maximum recommended dosage rates was shown to be ineffective in depressing the freezing point. A freezing point of around -10°C was achieved using three effective compounds at dosages that exceeded the manufacturer recommendation. Very low freezing points were reached with some combinations, but the dosages were extremely high and the mixes were impractical.

The starting hypothesis of there being a direct relationship between depressing the freezing point and increasing the strength gain at low curing temperatures was not proven. In fact, mixes having higher freezing points showed higher compressive strengths than mixes having lower freezing points. The combination of multiple admixtures with high doses did not result in higher strengths than simpler mixes. With some adjustments to the dosages and the pre-curing time, it is expected that an acceptable mortar strength can be reached at low temperatures.

The entrapped air observed in the antifreeze-added samples was not very detrimental to the compressive strength up to the age of 28 days, but could have a different effect in the long term. Mixing the two compounds most effective in depressing the freezing point, namely MNC C15 and P20+, should be avoided as they showed an incompatibility reaction and a negative effect on the strength gain. The crystals observed on some samples may be a key to the hydration reaction happening at low temperatures and a separate study should be conducted to this end. A few other questions are raised by this study, such as: what is happening for the M100 mix to gain enough strength at -10°C even though its FP is only -4.4°C? Why do mixes with freezing points less than -10°C not gain enough strength? How much water is available in liquid form at below freezing temperatures, and is it responsible for the strength gain? What is the effect of the antifreeze on the other important mortar properties such as workability, setting time, and board life?

5 BEHAVIOR OF MASONRY MORTAR CONTAINING A NON-HARMFUL ANTIFREEZE ADMIXTURE[2]

5.1 Abstract

One of the major hurdles to a wider adoption of antifreeze admixtures in cold weather concreting applications is a lack of performance data for the increasing number of products currently available on the market. This paper assesses the performance of an existing non-harmful commercial antifreeze admixture (MNC-C15) in masonry mortar. The performance was evaluated in terms of strength gain at 7 days, 28 days and 56 days at two different temperatures (-10°C and -15°C). The potential need for heat protection before exposure to subfreezing temperatures was also evaluated. The results showed that the control mortar gained little to no strength during the curing period in subfreezing conditions. The mortar with the antifreeze admixture, on the other hand, showed appreciable strength gain even without an initial period of protection from freezing, suggesting that the admixture allowed the hydration reactions to proceed at temperatures of -10°C and -15°C. However, a freezing prevention period between 6 and 12 hours was necessary for the mortar to reach an acceptable compressive strength at those temperatures.

Keywords: Masonry mortar; antifreeze admixtures; compressive strength; pre-curing; post-curing.

5.2 Introduction

In many northern regions, the use of cementitious materials for construction during cold seasons requires special procedures. Canada, the USA, the Scandinavian region, Russia, China, and Japan are all affected by the problem of cold weather concreting. Each country has its own regulations and practices, with some being more restrictive than others. For example, newly completed masonry must be maintained above 0°C for 24 hours in the United States (MSJC 2011) and 48 hours in Canada (CSA 2004a).

[2] This chapter was submitted as "Saha, O., Boulfiza, M., and Wegner, L.D. (accepted-2019). Behavior of masonry mortar containing an antifreeze admixture. TMS Journal". It was accepted in 2019. It has been reformatted to conform to a consistent standard throughout the thesis. The copyright is assigned to The Masonry Society www.masonrysociety.org

The low temperatures that are experienced during cold seasons generate diverse challenges for the construction industry in many northern countries. Cementitious materials, in particular, suffer from low rates of hydration at low temperatures and are susceptible to damage caused by the formation of ice at temperatures below freezing (Davison 1970). The most common solution to this problem is to heat and protect the ingredients and the finished material until it reaches an acceptable strength (ACI 2010a). Another possible solution, still under investigation by many researchers, is to use chemical admixtures to reduce the temperature below which protection is required (Ratinov and Rozenberg 1995).

Masonry mortar, like other cementitious materials, consists of aggregate that are bonded together by cement paste. In most cases, the paste is formed by a mixture of water and portland cement. Under normal conditions, the mixing of these two materials results in several chemical reactions, collectively known as the hydration reactions, which cause the cement paste to harden and gain strength over time. When the temperature drops, the hydration reactions slow down, and may even stop completely if the temperature is low enough to convert the available liquid water into ice. When this happens, strength gain becomes very slow and irreversible damage to the cement paste may occur, due mainly to the expansion of water upon freezing. These are two major problems for concrete and masonry construction in cold weather that have been identified by many authors (e.g., Davison 1970, Ratinov and Rozenberg 1995, Woodham and Schuller 2005).

To address this problem, many codes and standards (e.g., ACI 1990, CSA 2004a, MSJC 2011), specify the heating of ingredients, beginning with water, and extending to sand and aggregate if heating the water alone is insufficient. Some standards also recommend increasing the cement dosage, using Type HE cement, or using accelerating admixtures (ACI 2010a). In extreme cases, an entire area of a construction project must be protected from freezing by heating and hoarding. This solution is costly, and the cost may not be justified for small projects (Davison 1970).

Antifreeze admixtures are an attractive alternative to more traditional cold weather concreting practices. Although they were used in the former Soviet Union as early as the 1950’s, their use in parts of North America is still very limited and is restricted by current codes (Korhonen 1990, 2002a, CSA 2004b). The main reason for the restrictive approach is that the most common compounds that could be used in antifreeze admixtures are calcium chloride and alcohols, both of which are known to have detrimental effects on concrete, grout, and masonry mortar by promoting

the corrosion of steel reinforcement and lowering concrete strength (CSA 2004b, Woodham and Schuller 2005).

Many research studies have been conducted in North America since the late 1980's, particularly by the U.S. Army Cold Region Research and Engineering Laboratory (CRREL), whose objectives include developing and testing new admixtures, making results widely available, and contributing to updates in construction standards (Korhonen 1990, 1999, 2002a, 2006, Korhonen et al. 1994a, 1997a, Korhonen and Brook 1996, Barna et al. 2010). Many other research studies have been conducted in other countries, including China, Turkey, and Serbia, and are still in progress to develop and test new products and procedures (Vasović et al. 2008, Arslan et al. 2011, Wang et al. 2011, Dong et al. 2013, Karagöl et al. 2013).

Some recent experimental studies (Arslan et al. 2011, Wang et al. 2011, Dong et al. 2013, Karagöl et al. 2013) have shown that it is possible, to a certain extent, to use chemical admixtures to permit concrete construction in relatively low temperature conditions. Arslan et al. (2011) tested three compounds, including calcium nitrate, hydroxy ethoxy amine, and polyhydroxy amine at four dosages and five low temperatures, using a curing pattern of two days at subfreezing temperatures followed by twenty-six days at room temperature. They achieved strengths between 15 and 28 MPa using a Type I cement and water to cement ratio of 0.52. Curing temperatures between -5 and -20°C did not have a significant effect on the strength. Wang et al. (2011) tested five un-named compounds at three dosages under curing conditions of seven days at -20°C and 28 days at +20°C and reached a compressive strength around 30 MPa. They used Type I cement and a water to cement ratio between 0.54 and 0.68. Karagöl et al. (2013) used calcium nitrate at a dosage of 6% by cement weight as an antifreeze admixture. The Type I cement dosage was 400 kg/m^3 and a superplasticizer was added to the mix, which was prepared with a water to cement ratio of 0.4. They adopted a full factorial experiment design that included four subfreezing temperatures (-5, -10, -15, -20°C), three curing ages (7, 14, 28 days) and four post-curing ages (0, 7, 14, 28 days). Before compressive strength testing, the samples were cured at room temperature for 24 hours, allowing some strength recovery. The results showed a significant strength gain, in the order of 24 MPa for 28 day curing at -10°C; however, some unexplained strength drop was also observed.

Although non-harmful antifreeze admixtures have been successfully tested over the past two decades, the historic ban on the use of any antifreeze admixture is still governing the masonry construction codes, making them more restrictive than those pertaining to concrete. For this reason, it is important that studies specifically addressing the use of antifreeze admixtures in masonry mortar be conducted. The only reference available in the literature explicitly related to masonry, to the authors' knowledge, is that of Korhonen et al. (1997d), who found that the U.S.-Army-patented antifreeze named "KC1" was able to appreciably promote strength gain in mortar, to decrease the setting time, to substantially increase the bond between the masonry and the units, and had negligible effect on the freeze-thaw durability; the longer term durability was under investigation.

This paper presents the results of an investigation into the effect of using a non-harmful antifreeze admixture in masonry mortars on the development of compressive strength when subjected to curing temperatures of -10 and -15°C, with room temperature pre-curing times ranging from 0 to 24 hours. The use of a pre-curing period is justified for two main reasons: first, without pre-curing, the compressive strength may not reach the acceptable value defined by ASTM Standard C270 (2010e), so a protection period may be required; and second, below a certain temperature, the masons will need a shelter to do their work and thus a pre-curing period will generally be provided.

5.3 Scope and Objectives

Despite the apparent benefits of antifreeze admixtures in terms of their ability to reduce or eliminate the need for thermal protection of freshly placed concrete in cold weather, along with the resulting cost savings, their use by the construction industry has fallen short of expectations. One of the major hurdles to their wider adoption is a lack of performance data for the products currently available in the published literature. This paper assesses the performance of an existing commercial concrete antifreeze admixture (MNC-C15) applied to masonry mortar. The choice of this particular admixture was guided by an indication of its potential performance in a previous study (Saha et al. 2015a). The performance was evaluated in terms of strength gain at 7 days, 28 days and 56 days at two different freezing temperatures (-10°C and -15°C). The curing temperatures were selected after consultation with the local masonry community on the practicality for masons to work in cold conditions without protection. The potential need for heat protection

before exposure to the freezing temperatures was also evaluated. In other words, the time required to protect the mortar from freezing (the pre-curing time) in order for it to reach an acceptable compressive strength was determined. The curing scheme consisted of four pre-curing times (0, 6, 12, and 24 hours) at room temperature, followed by the remainder of the 28-day curing period in a freezing chamber at -10°C and -15°C. Samples were then post-cured at room temperature for an additional 28 days. This experimental work identifies practical conditions under which the antifreeze admixture can be used to permit the development of compressive strength of masonry mortar cured under freezing conditions, as well as its effectiveness to promote post-freezing strength recovery.

5.4 Materials and Methods

In this study, a Type S mortar cement (with lime content) was used, due to its regular use in cold areas, in conjunction with fine aggregate passing the 2.36 mm sieve, which met the requirements for the sand used in masonry mortar. The admixture used was a commercial product known as MNC-C15 (manufactured by Muhu), which comes in powder form and is marketed as a dedicated antifreeze additive for concrete. According to the manufacturer, this product is non-corrosive with no chloride content, possesses accelerating and plasticizing properties, and can reduce the need to protect fresh concrete from freezing at temperatures as low as -15°C. No reports on the use of the admixture in masonry mortar are available in the open literature. Its main ingredient is sodium nitrate, which is not known to cause damage to either cement-based materials or steel reinforcement. The manufacturer's test data sheet indicates that the chloride content is approximately 0.08%. Considering that the maximum recommended dosage is 4% per weight of cement, the chloride added to the mortar will be at most 0.0032%, which is well below the acceptable limit of 0.2% given by MSJC (2011) or 0.0065% given by ASTM C1384 (2006).

The mortar was prepared using a water to cement (w/c) ratio of 0.443 for the control mortar and 0.4 for the mortar containing the antifreeze admixture. The additional water was required to improve the workability of the control mixture to an acceptable level, while the plasticizing properties of the admixture allowed the use of the lower w/c ratio in that mortar. The aggregate to cement ratio was 2.75 by weight, as per the ASTM C109 recommendation (ASTM 2011). The admixture was used at the manufacturer's maximum recommended proportion of 4% by cement weight.

The mortar was prepared in either a large or small Hobart mixer, depending on the amount of material required for each batch. The mixing procedure was adopted from the Text Book of Canadian Masonry (CMCA 2010). As specified by this procedure, three-quarters of the water was first added to the mixing bowl, the mixer was started at low speed, half of the sand was added, and the total quantity of cement was then progressively added. The mixing was conducted for two more minutes, after which the mixer was stopped, and the bowl sides were scraped. Upon restarting the mixer, half of the remaining water was added before and half after the addition of the remaining sand. Mixing continued for at least three more minutes at medium speed, resulting in a total mixing time of approximately 10 minutes for the small mixer and 15 minutes for the larger mixer, the longer mixing time being due to the inability to add material to the mixer while it was running. For the samples containing the admixture, the powder was added with the first portion of water and mixed for a few minutes prior to adding any other material.

Once ready, the mortar was cast into 50 mm diameter by 100 mm long plastic cylindrical molds, and then immediately transferred either to the curing room or to the freezing chamber, depending on the curing scheme, summarized in Table 5.1. The cast cylinders were covered with plastic sheets to reduce the water evaporation.

Table 5.1 Summary of the curing schemes and strength testing ages

Sample	Pre-curing time at 23°C (Hours)	Curing temperature (°C)	Testing ages (Days)	Post-curing temperature (°C)	Testing age (Days)
Control	-	+23	7, 28	+23	-
	0	-10	7, 28	+23	35,56
	6	-10	7, 28	+23	35,56
Antifreeze	0	-10	7, 28	+23	56
	6	-10	7, 28	+23	56
	12	-10	7, 28	+23	56
	24	-10	7, 28	+23	56
Antifreeze	0	-15	7, 28	+23	56
	6	-15	7, 28	+23	56
	12	-15	7, 28	+23	56
	24	-15	7, 28	+23	56

As shown in Table 5.1, three curing schemes were followed for the control mortar, the first being in the curing room (23°C and 80% RH) to serve as a reference, the second in the freezing

chamber at -10°C without pre-curing, and the third in the freezing chamber at -10°C after six hours of pre-curing in the curing room.

A total of eight different curing schemes were followed for the antifreeze-added mortar, including combinations of two different subfreezing temperatures (-10°C and -15°C) and four different pre-curing times (0, 6, 12, and 24 hours). For each subfreezing temperature, one of the four sets was transferred to the freezing chamber immediately after casting, while the other three sets were transferred to the freezing chamber after the specified pre-curing period. The pre-curing scheme consisted of transferring the samples immediately after casting to a curing room set to a temperature of 23°C and a relative humidity (RH) of approximately 80% for the specified pre-curing time. The samples were then transferred to the freezing chamber for the remainder of the 28-day curing time.

The pre-curing period was added when it became clear that samples without pre-curing did not meet the ASTM C270 standard requirement that the average compressive strength at 28 days be a minimum of 12.4 MPa (Section 4.5). However, the pre-curing time can be justified by considering the fact that the mason will need a temporary heated shelter while laying the bricks or blocks at these temperatures, inevitably providing the pre-curing condition for a certain period of time.

The compressive strength of the anti-freeze added samples was measured at 7, 28, and 56 days, measured from the time of mixing. The strength of control samples was also measured at an additional age of 35 days. Each set consisted of three replicate cylinders. In all cases, the frozen samples were moved from the freezing chamber to the curing room at 28 days of age, following the common practice adopted by the research community working on antifreeze admixtures. Thus, the samples tested at 56 days were exposed to a 28-day post-freezing period at 23°C and 80% relative humidity prior to testing, while those tested at 7 and 28 days had no post-freezing period of curing. Before conducting the compression tests, the frozen samples were transferred from the freezing chamber to the curing room until the center of the sample had reached a temperature of at least 5°C, thereby ensuring that no ice was present at the time of testing. The time required for thawing was approximately one hour and the temperature was measured on a dummy sample using a thermocouple embedded in its center. The samples were removed from their molds and left for one additional hour to let the condensed water on the sides of the samples evaporate, as seen in

Figure 5.1. A longer post-freezing period such as one day adopted by other authors (Karagöl et al. 2013) could not be justified since strength recovery begins even during this short period of time.

Figure 5.1 Close up view of a cylinder after de-molding, showing a crow-foot pattern indicative of early-age freezing

Compression testing was performed using an Instron 600 DX universal testing machine controlled by a software module called Partner (v8.4a Instron), which was configured for compression testing of concrete cylinders under load-controlled conditions. The testing speed was 8 MPa/min for most of the samples, except that the speed was reduced to 1 MPa/min for the control mortar samples tested after 7 or 28 days of curing under freezing conditions because of the very low compressive strengths. The samples were centered and capped with fiberboard to reduce the effects of surface irregularities, as seen in Figure 5.2.

Figure 5.2 Broken sample after compression testing

5.5 Results and Discussion

Compressive strength test results of the control mortar samples are summarized in Table 5.2. The mean 7 and 28 day compressive strengths of the control mortar cured in curing room conditions were 18.6 and 23.1 MPa, respectively, with a 95% confidence interval at 28 days of approximately ±1.5 MPa based on five samples. One can see that the compressive strength at 7 days was approximately 80% of that at 28 days. The measured compressive strength was almost twice as high as a regular masonry Type S mortar, which is required to have a minimum average strength of 12.4 MPa at 28 days (ASTM C270). This may be attributed to the low w/c ratio used for this study compared to the 0.55 to 0.70 ratio typically used in regular masonry mortar. The low w/c ratio was used to achieve comparable strengths in control and admixture-added mortars.

The compressive strengths obtained for the control mortar exposed to a curing temperature of -10°C are also shown in Table 5.2 and represented in Figure 5.3. Also listed in Table 5.2 are the ratio of the mean compressive strengths to the 28-day strength of the control samples (23.1 MPa), and the coefficients of variation. The samples transferred to the freezing chamber right after mixing (0-hour pre-curing) could not be tested at 7 and 28 days because they were damaged during the unmolding process as a result of the mortar being too soft. The samples pre-cured for 6 hours were de-molded successfully, but their compressive strengths were very low and did not even reach 1 MPa at 28 days. The remaining samples of this set were transferred to the curing room and tested at 35 and 56 days. The results showed an increasing strength gain and a partial compressive strength recovery, reaching 73% and 87% of the reference compressive strength for the 0 h and 6 h pre-curing periods, respectively, after the 28 additional days of curing. The overall coefficients of variation were less than 6% for all test groups, except for those tested at 7 days due to the very low mean compressive strength.

Table 5.2 Compressive strength of control samples cured under freezing conditions for 28 days

Temp (°C)	Pre-curing time		Age at Testing 7 d	28 d	35 d	56 d
+23	0 h	Comp. Strength (MPa)	**18.6**	**23.1**		
		Ratio to Ctrl (%)	80.5	100		
		Coef. Var (%)	4.1	5.1		
-10	0 h	Comp. Strength (MPa)	**NA**	**NA**	**8.30**	**16.8**
		Ratio to Ctrl (%)	NA	NA	35.9	72.6
		Coef. Var (%)	NA	NA	5.7	5.5
	6 h	Comp. Strength (MPa)	**0.55**	**0.92**	**11.9**	**20.1**
		Ratio to Ctrl (%)	2.4	4.0	51.5	86.8
		Coef. Var (%)	9.2	5.3	5.0	5.9

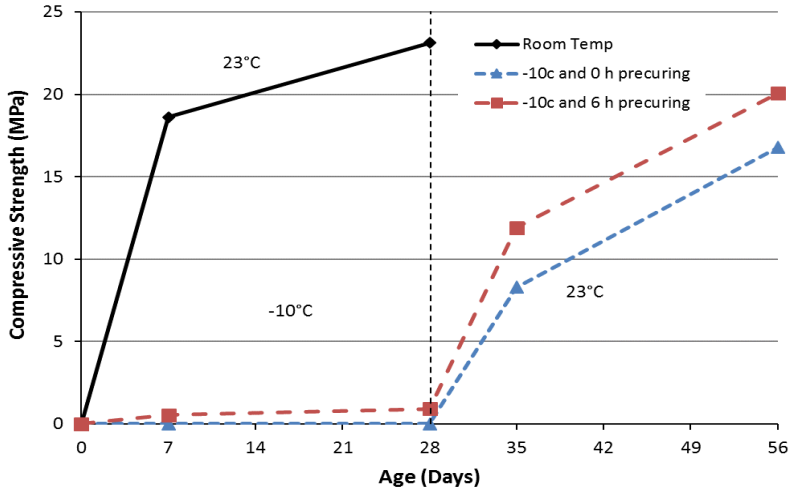

Figure 5.3 Compressive strength of control samples with and without pre-curing

The results of the compressive strength tests for the admixture-added mortar cured for 28 days under freezing conditions of -10 and -15°C are shown in Table 5.3 and represented in Figure 5.4.

The compressive strength of the mortar samples cured at -10°C without pre-curing was approximately 10 MPa at 28 days. A correction factor of 1/0.85 can be applied according to ASTM C780 (2012b) to account for the fact that tests were performed on cylinders rather than cubes, resulting in an equivalent compressive strength of 11.6 MPa, which is quite close to the minimum acceptable limit of 12.4 MPa. At -15°C, the compressive strength at 28 days did not reach an acceptable level (6.6 MPa). For the pre-cured samples, the compressive strengths at 28 days exceeded the 12.4 MPa threshold for all pre-curing times at both temperatures. Increasing the pre-

curing time from 6 to 12 to 24 hours led to a consistent increase in compressive strength, the only exception being the decrease in strength from 6 to 12 hours at -10°C, which may be attributed to a w/c ratio mistakenly taken slightly higher for the batch pre-cured for 12 hours. The coefficients of variation were no more than 11% for sets pre-cured for at least 6 hours, which is considered an acceptable level of statistical variability (ACI 2002), particularly since only three samples were tested for each data point.

The effect of the first 6 hours of pre-curing is noticeable compared to 6 or even 18 additional hours. Samples that were pre-cured for 6 hours had 28-day compressive strengths that were 72% and 80% higher than those that were not pre-cured, for curing temperatures of -10 and -15ºC, respectively, and reached 86% and 64% of the strengths achieved with 24 hours of pre-curing, respectively. This means that providing heated protection for 6 to 8 hours can improve considerably the strength performance of the mortar when the antifreeze admixture is used. The 24-hour protection time required by the United States MSJC-11 code, or the 48 hours required by the Canadian CSA A371 standard, could be relaxed to a much shorter period, provided additional testing is done.

Table 5.3 Compressive strength of antifreeze-added mortar samples cured under freezing conditions for 28 days, with and without a pre-curing period

Temp (°C)	Pre-curing time		Age at Testing		
			7 d	28 d	56 d
-10°C	0 h	Comp. Strength (MPa)	**6.7**	**9.9**	**20.5**
		Ratio to Ctrl (%)	29.1	42.8	88.6
		Coef. Var (%)	6.7	10.1	11.9
	6 h	Comp. Strength (MPa)	**8.6**	**17.0**	**27.5**
		Ratio to Ctrl (%)	37.4	73.5	119
		Coef. Var (%)	4.0	5.7	9.7
	12 h	Comp. Strength (MPa)	**9.0**	**15.3**	**30.4**
		Ratio to Ctrl (%)	38.8	66.0	131
		Coef. Var (%)	1.2	10.5	2.6
	24 h	Comp. Strength (MPa)	**14.9**	**19.7**	**31.9**
		Ratio to Ctrl (%)	64.3	85.3	138
		Coef. Var (%)	3.9	8.2	6.4
-15°C	0 h	Comp. Strength (MPa)	**3.8**	**6.6**	**17.1**
		Ratio to Ctrl (%)	16.5	28.6	73.9
		Coef. Var (%)	1.4	9.2	13.0
	6 h	Comp. Strength (MPa)	**7.9**	**11.9**	**28.8**
		Ratio to Ctrl (%)	34.0	51.5	124
		Coef. Var (%)	3.7	6.5	7.8
	12 h	Comp. Strength (MPa)	**11.8**	**15.0**	**24.8**
		Ratio to Ctrl (%)	50.9	65.0	107
		Coef. Var (%)	1.8	2.2	8.7
	24 h	Comp. Strength (MPa)	**15.8**	**18.5**	**26.5**
		Ratio to Ctrl (%)	68.3	80.1	114
		Coef. Var (%)	10.6	8.7	8.9

The reference compressive strength = 23.1 MPa

Samples experienced substantial strength recovery after being moved from the freezing chamber to the curing room at 28 days. In the case of the samples without pre-curing, the compressive strength at 56 days was more than double that at 28 days; however, it did not fully recover, and reached only 89% and 74% of the strength of the control specimens, for samples cured at -10 and -15°C, respectively. For all the pre-cured samples, the compressive strength at 56 days fully recovered and even exceeded the reference strength. The effect of pre-curing time in the long term is not well pronounced, and additional data points may be required to better describe the behavior at intermediate and later ages.

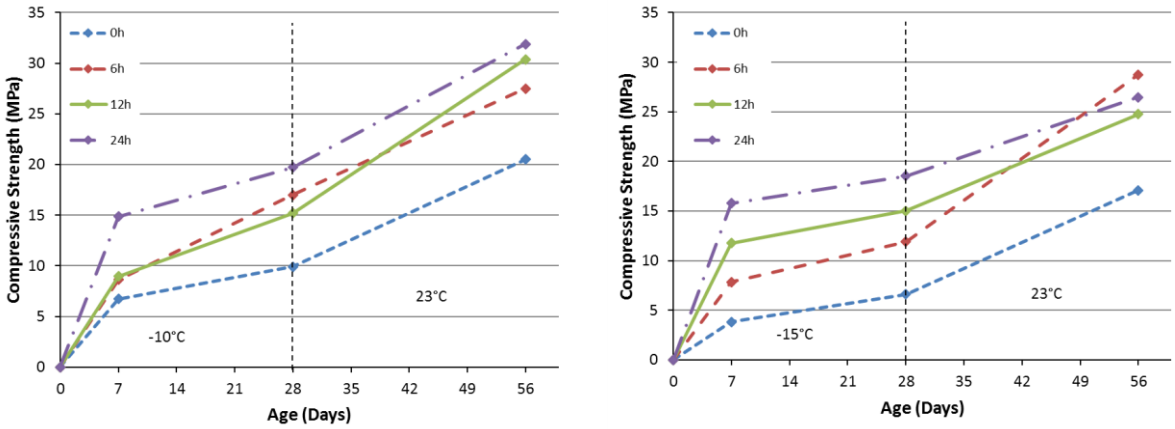

(a) (b)

Figure 5.4 Compressive strength of antifreeze-added mortar samples cured at (a) -10ºC and (b) -15ºC after various pre-curing periods

At below freezing temperatures, by the age of 28 days, the control mortar did not show any significant strength gain, even with a pre-curing time of 6 hours. On the other hand, the antifreeze-added mortar showed strength gains of 9.9 MPa and 6.6 MPa at -10 and -15°C, respectively, without any pre-curing, and an acceptable compressive strength above 12.4 MPa was observed starting from 6 hours of pre-curing. The results obtained for the admixture-added mortar cured at -10°C compare very well with results reported by Korhonen et al. (1997d) under the same conditions and displaying relative compressive strengths of 26, 56, and 77% for ages of 7, 28 and 56 days respectively. The observed strength gain must be attributed to the ability of the antifreeze admixture to permit the hydration reactions to proceed, even at temperatures considerably below freezing. The mechanism by which this occurs is the subject of a future article. The strength recovery of control samples at -10°C did not reach that of the antifreeze-added mortar at -15°C let alone the one cured at -10°C. The good performance of the antifreeze admixture suggests that at milder temperatures (e.g., near -5°C), no pre-curing time will likely be required to reach an acceptable compressive strength. Future studies will address this hypothesis.

5.6 Conclusion

The performance of an off-the shelf antifreeze admixture for concrete was evaluated as an antifreeze admixture in masonry mortar. The admixture was tested on a masonry mortar using curing temperatures of -10°C and -15°C in the laboratory. The following conclusions can be drawn:

- The control mortar gained almost no compressive strength during the subfreezing curing period. Substantial strength gain occurred only after the samples were returned to a favorable curing condition, at room temperature.
- The chemical admixture has been shown to meet the ASTM C270 strength requirement provided that a heat protection period of 6 hours is used for temperatures in the range of -10°C and -15°C.
- The strength gains at -10°C, without heat protection, were slightly below the ASTM C270 requirement. However, they were so close that it is believed that temperatures around -5°C and higher would not need any heat protection for strength development, if the admixture is used.
- The admixture cannot be used at temperatures -10°C and lower without a heat protection period during the first curing hours.
- The pre-curing period had a beneficial effect on the strength recovery, as the pre-cured samples recovered approximately 20% more strength than the non-pre-cured samples.
- These results suggest that the protection time of 24 to 48 hours required by current regulations may be relaxed, although additional testing, such as testing other mortar cement types, testing the bond strength, testing the masonry block assembly, and testing a more representative number of samples, is required to confirm this.

The results obtained in this experimental work identify the conditions under which the tested antifreeze admixture can be used effectively to permit the development of compressive strength of masonry mortar cured under freezing conditions, as well as its effectiveness to promote post-freezing strength recovery. The strength gain observed under freezing conditions indicates that the admixture is capable of causing the hydration reactions to proceed even under these conditions, which is not the case in the control mortar. The nature and exact mechanism by which the admixture works is the subject of an ongoing investigation. However, initial indications are that a certain amount of water remains unfrozen, thus allowing the hydration reactions to take place, even below the usual pore solution freezing point.

6 EFFECT OF SODIUM NITRITE-BASED ANTIFREEZE ADMIXTURES ON THE HYDRATION OF MASONRY MORTAR[3]

6.1 Abstract

The negative effects of subfreezing temperatures on cement hydration are well documented. One possible approach for mitigating these effects is the use of chemical admixtures. As their use is becoming more common in cold weather construction, there has been a renewed interest in understanding the impact of non-detrimental salts on the hydration of masonry mortar and cement-based materials, in general. In an earlier study, a commercial proprietary admixture was shown to be effective at allowing the hydration reactions to proceed in a masonry mortar at temperatures as low as -15ºC. In this paper, the resulting hydration products of sodium nitrite-based antifreeze admixtures in masonry mortar are characterized, and the dosage required to maximize the compressive strength of the mortar is determined. Elemental and mineral characterization of the admixture revealed a high concentration of sodium nitrite with some mullite, in addition to an unidentified amorphous phase. A semi-quantitative approach was used to track the evolution of the mineral phases within the hydration products of cement pastes containing no additive, the proprietary admixture, or sodium nitrite alone, cured at ambient and subfreezing temperatures. The absence of any uncommon hydration products suggests that the strength gain observed in the treated pastes was mainly due to the presence of a certain amount of unfrozen water that allowed for the development of C-S-H. Compressive strength tests on masonry mortars cured at -10ºC confirmed the effectiveness of sodium nitrite as an antifreeze agent, achieving an acceptable 28-day compressive strength according to masonry standards. The optimal dosage of sodium nitrite was found to be around 5% by cement weight to maximize strength gain.

Keywords: Cement hydration, masonry mortar, antifreeze admixtures, cold weather masonry, compressive strength, pre-curing, post-curing, elemental and mineral characterization.

[3] This chapter was submitted under reference id M-2019-168 as "Saha, O., Boulfiza, M., and Wegner, L.D. (under review-a). Effect of sodium nitrite-based antifreeze admixtures on the hydration of masonry mortar. ACI Materials Journal". It has been reformatted to conform to a consistent standard throughout the thesis.

6.2 Introduction

The cold weather placement of cementitious materials such as concrete and masonry mortar has long been known to be problematic for two main reasons: 1) the hydration reactions occur very slowly or not at all when the temperature falls below freezing, leading to very low strength gain; and 2) the expansion of water upon freezing leads to internal cracking and spalling. These two phenomena and others are well described in the literature (Davison 1970, Korhonen 1990, Schulson 1998, Kaufmann 2004, Ortiz et al. 2005, Grant et al. 2006). The most common approaches to address the problem have been to provide heat and protection or to wait for milder weather, both of which may be costly. An alternative approach is to use chemical admixtures to depress the freezing point and accelerate the hydration reactions.

Incorporating admixtures into concrete and mortar mixes to improve certain properties has become commonplace. Aïtcin (2000) referred to the classification of chemical admixtures into four types on the basis of the actions they produced: dispersants, hydration kinetics modifiers, reactants with hydration subproducts, and those that have only a physical action. Antifreeze admixtures demonstrate the second and fourth types, and to a lesser extent the first type. They may act as a freeze depressant, an accelerator, and, in some cases, a plasticizer (ASTM 2010a). The development of a better understanding of the effects of different chemical admixtures on the hydration and microstructure of cement and concrete continues to be an important field of research, strongly reflected in two recent international conferences (Cheung et al. 2011, Plank et al. 2015). Significant research interest has been shown in accelerators and superplasticizers and, to a lesser extent, retarders (Puertas et al. 2005, Jupe et al. 2007, Sandberg et al. 2007, Riding et al. 2010, Yamada 2011, Liu et al. 2015b).

Several characterization techniques are available for researchers in laboratories and in-situ (Taylor 1997, Ramachandran and Beaudoin 2001, Bensted and Barnes 2002) including chemical, optical, thermal, electromagnetic, and electrical methods, to list only a few. They have been proven to be effective and to complement each other in terms of their effect on studying the hydration processes. Research to understand cement hydration under low temperature conditions is relatively scarce in the literature due to the limited geographic area in the world affected by these conditions. In a recent investigation (Liu et al. 2017a, 2017c, 2017b), several characterization techniques including electrical resistivity, degree of hydration, maturity, thermodynamic calculation, X-ray

diffraction (XRD), and scanning electron microscopy (SEM) were used to study portland cement hydration at low temperatures in the range of +20°C to -5°C. They found that the hydration rate was significantly delayed at lower temperatures but did not completely stop. However, the research did not include the use of antifreeze admixtures. The formation of ettringite was analyzed at low temperature down to 0°C using XRD and ESEM (Xu et al. 2012). The authors found that the setting time was reduced as the temperature increased, and compared the effect of anhydrite versus hemihydrate. Silica fume was used with portland cement to enhance the properties of the binary system at low temperatures between +5°C and -10°C (Liu et al. 2015a), while mechanical testing, thermo gravimetry, scanning electron microscopy, and mercury intrusion porosimetry were used as characterization techniques. The research showed mixed results regarding strength development, heat of hydration, compactness, and porosity. Low temperatures seemed to hinder the effect of the silica fume.

On the other hand, the mechanical properties of cementitious materials treated with antifreeze admixtures seem to be well covered in the literature (Kivekas and Leivo 1985, Lee et al. 1988, Korhonen 1990, Sakai et al. 1991, Karagöl et al. 2013, 2015, Qiao et al. 2016). These studies tend to agree that the use of an antifreeze admixture is a viable solution to improve the mechanical properties of the cementitious material when cured at low temperatures.

Due to historical reasons, antifreeze compounds are still not recommended for use in masonry mortar or grout. This is mainly due to the fact that many of the antifreeze compounds that were initially investigated were typically made with alcohols or mixtures of salts, for which it was practically impossible to depress the freezing point low enough (typically in the range of -5ºC and -10ºC) without inducing a significant reduction in the compressive strength and flexural bond capacity. Moreover, calcium chloride-based antifreeze admixtures and other similar substances were clearly shown to cause efflorescence and premature corrosion of metals, when present. Over the last few years, however, there has been a renewed interest in the use of non-detrimental salts, such as sodium nitrate and calcium nitrate, in cement-based materials, due to their many advantages compared to traditional heat protection methods.

In a previous study (Saha et al. accepted-2019, 2015b, 2015a), a commercial concrete antifreeze admixture was shown to allow the hydration reactions in a masonry mortar to proceed at temperatures as low as -10°C and -15ºC, such that acceptable compressive strengths were

achieved. However, the mechanism by which the admixture worked was not identified. In the current study, the major phases in the admixture were identified, and the evolution of the hydration products was tracked in an effort to understand the influence of the admixture on phase development at low temperatures. In addition, the dosage of the active compound in the admixture was optimized in order to maximize the strength gain.

6.3 Overview of Experimental Program

The experimental program was divided into three major phases: 1) characterization of the initial ingredients; 2) characterization of the hydration products; and 3) dosage optimization of the active antifreeze ingredient to achieve an acceptable compressive strength of the masonry mortar.

Characterization of the initial solid ingredients, namely the cement and the admixture powder, was performed using a combination of elemental and mineral identification techniques, including combustion (CHNS), inductively coupled plasma mass spectrometry (ICP-MS), X-ray fluorescence (XRF) and X-ray diffraction (XRD).

Characterization of the hydration products was performed using the XRF and XRD techniques on treated and untreated cement pastes cured at room and subfreezing temperatures after the hydration process had been arrested at specific ages, following the methodology described by Ramachandran and Beaudoin (2001). A simplified semi-quantitative analysis, inspired by Talero et al. (2011) and Liu et al. (2014), was applied to the XRD diffractograms to follow the dissolution and formation of the various phases during the hydration process.

Finally, the active compound identified in the admixture was isolated and tested on masonry mortar at subfreezing temperatures to confirm its action. The dosage of the active compound was optimized, within the practical range of 2% to 6% by weight of cement, to achieve an acceptable strength.

Table 6.1 provides a summary of the experimental program, identifying batch labels for subsequent reference, mix proportions, curing conditions, and the types of tests performed in each phase of the experimental program. Detailed test procedures are provided in the following section.

Table 6.1 Summary of the experimental program

Experimental Phase	Batch Label	Number of replicates	Ingredients	Proportions (wt. %)	Curing Temperature (°C)	Curing Duration (Days)	Tests performed
1		2	Cement Type GU	100			XRF, XRD
		2 to 4	Proprietary admixture	100			CHNS, ICP-MS, XRF, XRD
2	C	2	Cement Type GU	100			
			Al_2O_3	10			
			Water	50	-10°C and +23°C	1, 3, 7, 14, 28	XRF, XRD
	A	2	C + Proprietary admixture	4			
	Na	2	C + $NaNO_2$	4			
3	Ctrl	5	Mortar Cement Type S	100	+23°C	7, 28	
			Mortar Sand	275			
			Water	40			
	M100	3	Ctrl + Proprietary admixture	4	-10°C then +23°C	7, 28, 56	Compressive strength
	SN	3	Ctrl + $NaNO_2$	4	-10°C then +23°C	7, 14, 28, 35, 56	
	SN+SP	3	SN + Sodium Lignosulfonate	0.5	-10°C then +23°C	7, 14, 28, 35, 56	
	SN	5	Ctrl + $NaNO_2$, w/c=0.5	2 to 6	-10°C then +23°C	28, 56	

6.4 Characterization of the Initial Products (Phase 1)

6.4.1 Sample Preparation and Experimental Methods

The two materials characterized in the first phase of the study included ordinary portland cement Type GU, equivalent to ASTM Type I, and the commercial antifreeze admixture (MNC-C15, MUHU, China). The admixture was advertised as a chloride free superplasticizer admixture for cold weather concreting based on naphthalene, with minor nitrate and sulfate contents.

Among a wide range of characterization techniques available for the analysis of cement and concrete (Ramachandran and Beaudoin 2001), the four most relevant and readily available were used in this work. For the elemental or oxide composition analyses, CHNS, ICP-MS, and XRF were used, whereas XRD was used for the mineral characterization.

Carbon, hydrogen, nitrogen, and sulfur analysis (CHNS) is a technique used to determine the elemental composition of a sample by combustion in an enriched oxygen atmosphere at about 1000°C. The four main oxides (CO_2, H_2O, NO_2, SO_2), found in most organic compounds, are collected, separated, and quantified.

Inductively coupled plasma mass spectrometry (ICP-MS) is a technique used to detect metals, even at very low concentrations. The inductively coupled plasma is responsible for ionizing the elements, and the mass spectrometry is responsible for separating and detecting the particles based on their mass-to-charge ratio. Sample preparation consisted of a lengthy concentrated acid digestion process, followed by the ICP-MS experiment on the digested solution. The CHNS and ICP-MS techniques were used only for the characterization of the antifreeze admixture.

X-ray fluorescence (XRF) is based on the detection of a characteristic secondary X-ray specific to each atom. The principle consists of exposing an atom to a primary high energy X-ray capable of knocking off an electron from the inner orbitals, so that the atom is in an excited unstable state. To return to a stable state, an electron from the higher orbital fills the gap left behind, and by doing so releases the secondary X-ray, which is detected as fluorescence. Samples were analyzed as loose powder in a helium atmosphere using a special cup equipped with a thin Mylar window, 6 µm thick.

X-Ray diffraction (XRD) is based on the angle by which an incident X-ray is diffracted due to the orientation, interplanar distances, and crystal structure of the material under investigation. The

XRF-XRD techniques are commonly used together to characterize and sometimes quantify the constituents of a compound. The diffraction scan was performed with a Cu Kα radiation, corresponding to a wavelength λ=1.54056Å. The scan was taken between 5° and 70° (Two-Theta) angle with a step angle=0.02°, taking about 20 minutes for each sample. Both initial and hydrated products, in powder form, were the subject of the XRF and/or XRD tests. The XRD experiments were performed in two different laboratories: SRC Advanced Microanalysis Centre (Lab X) in Saskatoon, and Catalysis and Chemical Engineering Laboratory (Lab Y) at the University of Saskatchewan. The XRF experiments were performed in Lab X.

In order to identify the mineral content of the initial compounds, a compilation of the most common crystallographic information files (CIF) was prepared based on the work of well recognized authors (Taylor 1997, Bensted and Barnes 2002, Kocaba 2009, Aranda et al. 2012). Bruker EVA software, associated with a recent version of the International Centre for Diffraction Data (ICDD) data base, was instrumental in the background subtraction and the search/match processing of the XRD diffractograms. Equivalent CIF cards from the Crystallography Open Database (COD) were also used to simulate the diffractogram peaks using the free software Mercury – Cambridge Crystallographic Data Centre (v3.6 CCDC). The full list of the potential crystalline phases structural details is presented in Appendix D.

6.4.2 Results and Analysis

From the XRF analysis, the most relevant oxides found in the Type GU cement are listed in Table 6.2. The magnesium oxide content was at the high end, whereas the calcium and silicon oxides were at the low end of a typical range. The remaining elements were in the intermediate level of the typical ranges. The diffractogram shown in Figure 6.1, without background subtraction, presents the result of the XRD analysis of the cement. The major peaks are labeled and were found to reflect a typical mineral content of portland cements. No reliable quantitative analysis was possible for the XRD analysis.

Table 6.2 XRF phase analysis of the cement Type GU (weight percent)

Oxide	Measured (wt%)	Typical Low (wt%)	Typical High (wt%)
MgO	4.59	1.5	5.0
Al_2O_3	4.85	2.5	6.0
SiO_2	19.36	19.0	23.0
SO_3	3.05	1.5	4.5
CaO	61.05	61.0	67.0
Fe_2O_3	3.15	0.0	6.0

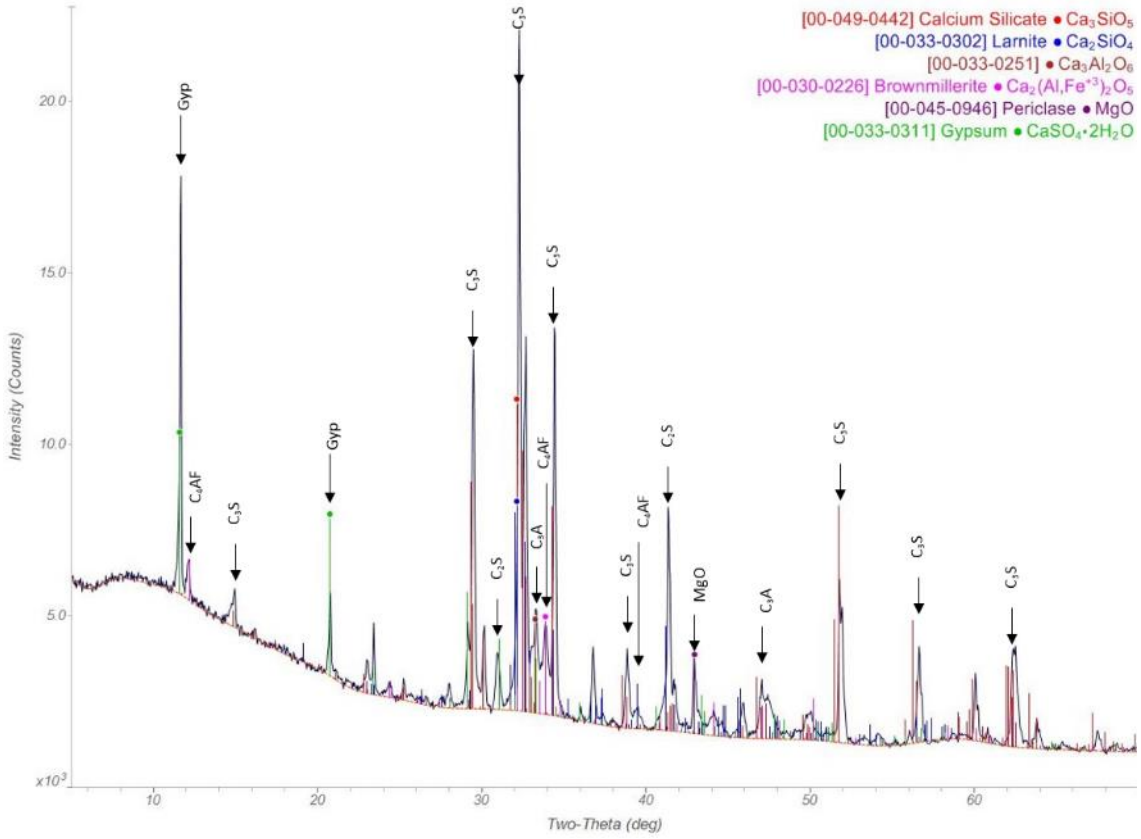

Figure 6.1 Diffractogram of the cement Type GU obtained from XRD analysis

Results of the CHNS analysis for the admixture are provided in Table 6.3, which shows a content of about 14% nitrogen. The carbon, not detectable by the other techniques, is very likely part of the amorphous phases in the admixture, along with sulfur. High coefficients of variation were noted for the carbon and sulfur contents.

Table 6.3 CHNS elemental analysis of the antifreeze admixture

Sample	Weight (g)	N (%)	C (%)	S (%)	H (%)
Average	**5.12**	**13.74**	**10.93**	**0.74**	**1.15**
Std. Dev.		0.910	1.876	0.220	0.089
95% conf.		1.448	2.985	0.349	0.142
Coef. Var.		**6.63**	**17.17**	**29.52**	**7.78**

The ICP-MS analysis of the admixture showed a content of 27.32% Na, 1.19% Al, 0.18% Ca, and 0.14 Fe, with all other metal elements being less than 0.1%. The full ICP-MS results are presented in Appendix E. This technique and the XRF (Table 6.4) are the two most reliable techniques in terms of accuracy, capable of reaching very low limits of detection. In addition to the metal elements detectable by the ICP-MS technique, the XRF had the advantage of detecting other important elements, including silicon and sulfur. It is noted that the sodium content detected by the ICP-MS was higher than that detected by the XRF, whereas the calcium and iron contents were lower, likely due to sampling issues. The complete XRF results are reported in Appendix F.

Table 6.4 XRF phase analysis of the antifreeze admixture

Oxide	Avg (wt%)	Main Element (wt%)	Oxygen (wt%)
Na_2O	29.33	21.76	7.57
MgO	0.02	0.01	0.01
Al_2O_3	2.26	1.20	1.07
SiO_2	3.73	1.74	1.99
P_2O_5	0.06	0.02	0.03
S	5.93	5.93	0.00
K_2O	0.00	0.00	0.00
CaO	0.68	0.50	0.18
TiO_2	0.20	0.12	0.08
MnO	0.03	0.03	0.01
Fe_2O_3	0.51	0.35	0.15

The XRD analysis (Figure 6.2) shows a near perfect match between the peaks of the antifreeze admixture diffractogram and the sodium nitrite card. Most of the remaining peaks match the mullite card. Two very small peaks at about 19.0° and 33.8° match the cesanite card, not shown in the legend. A quantitative analysis was provided by the laboratory and the results are discussed in the next paragraph. The "Total" line of Table 6.5 shows the quantity of the minerals, in which the elemental break-down of each "pure" phase is also shown for comparison purposes with the previous tests.

The reported 87.2% of sodium nitrite corresponds to 29.1% sodium, which is higher than what was found by the ICP-MS, and much higher than the XRF results in Table 6.4. It is very likely that the actual sodium nitrite content is between 75 and 80%, corresponding to a sodium content of 25 to 27%, and a nitrogen content of 15 to 16%, both fairly consistent with what was found by the ICP-MS and CHNS tests, respectively. The mullite, reported as 5.1%, corresponds to an aluminum content of 2%, which again is higher than the 1.2% found by both the ICP-MS and XRF analyses. To match the aforementioned contents, a 3.2% mullite content would be more appropriate. Finally, traces of cesanite with very low amounts of calcium, sulfur, and sodium was suspected at a rate of 1%.

The remaining portion of the total content that was not detected in the mineral composition is believed to be one or more amorphous phases. It is safe to consider that the amorphous phases, based essentially on sulfur and carbon, constitute the superplasticizer. The advertised naphthalene compound was not detected, at least not in a crystalline form.

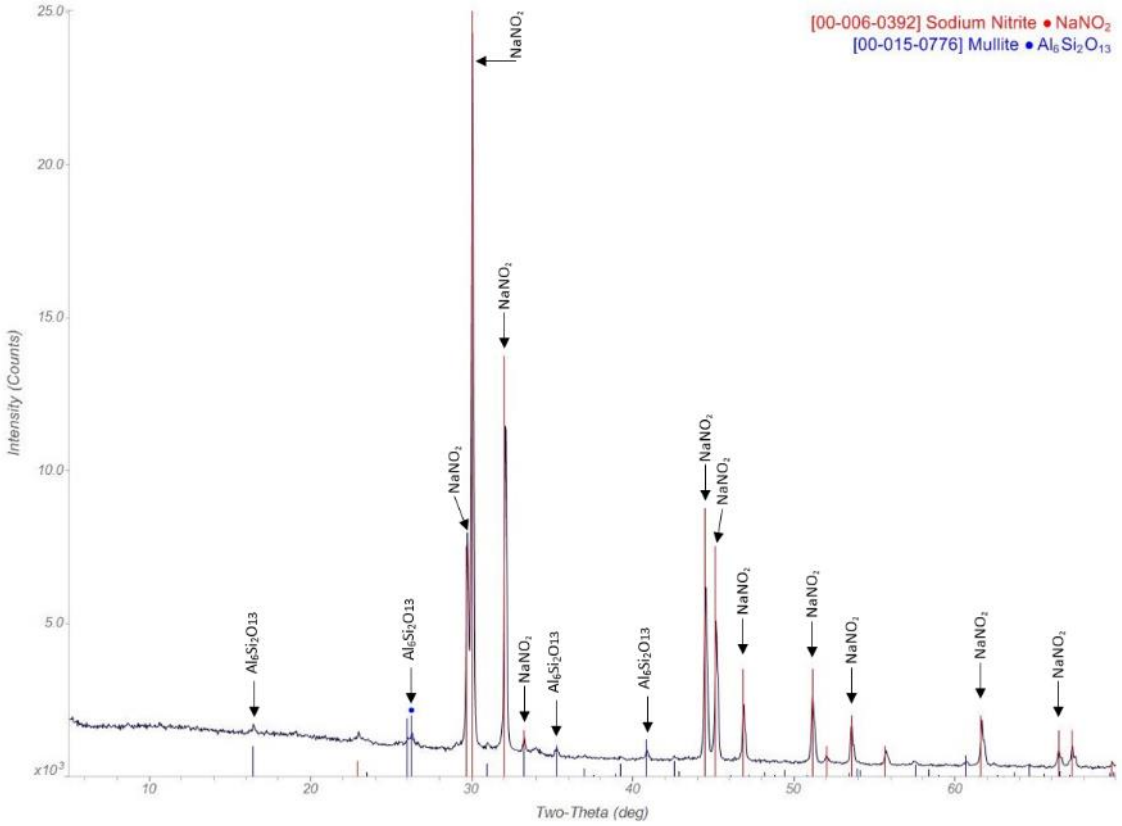

Figure 6.2 Diffractogram of the antifreeze admixture with sodium nitrite and mullite peaks

Table 6.5 Elemental composition of the admixture based on the mineral phases (%)

Elements	**Sodium Nitrite ($NaNO_2$)**	**Mullite ($Al_6Si_2O_{13}$)**	**Cesanite ($Ca_2Na_3(SO_4)_3(OH)$)**
N	17.7		
O	40.4	2.5	0.5
Na	29.1		0.2
Al		2.0	
Si		0.7	
S			0.2
Ca			0.2
Total	87.2	5.1	1.1
Std. Dev.	0.60	0.67	-
95% conf.	1.50	1.65	-

6.5 Characterization of the Hydration Products (Phase 2)

The beneficial effect of the commercial antifreeze admixture on the compressive strength of the masonry mortar was demonstrated in an earlier work (Saha et al. 2015a, 2015b), while the main compound constituting this admixture was shown in the previous section to be sodium nitrite. The aim of the second phase of this work, described in this section, was to track the development of the crystalline phases in the hydration products over time, with the expectation of identifying the phase or phases responsible for the strength gain at subfreezing temperatures.

6.5.1 Sample Preparation and Experimental Methods

6.5.1.1 Mixing and Curing

Five ingredients were used for the preparation of samples for this phase of the work: 1) ordinary portland cement Type GU; 2) the commercial antifreeze admixture; 3) sodium nitrite powder; 4) tap water; and 5) aluminum oxide (Al_2O_3) powder, used as an internal standard for an amorphous-phase quantitative analysis. As summarized in Table 6.1, three different types of cement paste samples were prepared as part of the second experimental phase: control samples were prepared using only the portland cement, aluminum oxide and water, while treated samples contained either the antifreeze admixture or sodium nitrite as additional ingredients. The mix proportions are also provided in Table 6.1. The cement and antifreeze admixture were individually characterized as described in the previous section. In this section, the hydration products of the treated and untreated cement pastes were characterized and compared.

Cement paste samples were prepared by first dry mixing the cement and aluminum oxide powder at a mass ratio of Al_2O_3/Cement = 10%, with a total of 150 g of cement used for each batch. In the case of the treated batches, the antifreeze or the sodium nitrite powder was mixed with the other dry ingredients at a dosage of 4% by weight of cement. This dosage was selected to match the maximum manufacturer recommended dosage. The dry ingredients were mixed by hand shaking them in a closed container for 3 minutes. The mixed powder was then transferred to a ceramic bowl and mixed again with a hand beater for 2 more minutes. Three quarters of the mixing water was added to the dry powder and mixed in the bowl until a homogeneous paste was reached. The remainder of the water was then added and mixed for an additional 3 minutes. The wet mixing was performed by hand. A water to cement ratio (w/c) of 0.5 was selected for two reasons: 1) it resulted in an acceptable plasticity for both the control and the admixture-added cement pastes;

and 2) a consistent water content allowed a direct comparison of the hydration products among the different batches. For this w/c ratio, the control and sodium nitrite pastes reached an acceptable workability, whereas the cement paste with the antifreeze admixture was very sloppy, almost certainly due to the superplasticizer contained in the admixture.

Six batches were prepared, comprising the three types of pastes identified above, each cured at two different temperatures: room (+23°C), and subfreezing (-10°C). The hydration products were characterized at five curing durations: 1, 3, 7, 14, and 28 days. Two replicate samples were prepared for each testing condition, resulting in a total of sixty samples. Each sample consisted of approximately 10 grams of the prepared paste cast in a sealed plastic cylindrical vial, 80 mm deep x 27 mm in diameter.

For subsequent reference, samples are labeled as C, A or Na for control, admixture added or sodium nitrite added, respectively, followed by '+' or '-' for curing at room or subfreezing temperature, followed by a number (1, 3, 7, 14, or 28) specifying the curing duration in days. For example, A–7 refers to the antifreeze-added sample cured at -10°C for 7 days.

6.5.1.2 Hydration Interruption

In order to perform an XRD characterization on the reacted cement paste, it was necessary to arrest the hydration at the specified age and grind the paste to powder. For this purpose, a solvent exchange technique was used, as described by Ramachandran and Beaudoin (2001) and summarized here. The freeze-drying arresting technique was also attempted; however, the technique was limited to samples with ages of less than three days. The gravimetry results for the freeze-drying are presented in Appendix G.

The solvent exchange technique consisted of immersing a thin layer (wafer 4 mm thick x 25 mm diameter) of the hydrated cement paste in isopropyl alcohol for two hours and exchanging the alcohol every two hours three times. The samples were then wet crushed while immersed in isopropanol (Figure 6.3), using a ceramic mortar and pestle. Crushing continued until most of the powder passed a 200-micron sieve. During this grinding process, reflective crystals were observed that became the subject of a separate investigation (Saha et al. 2015b). The powder was then washed twice with diethyl ether before it was stored in a sealed vial in a desiccator. The desiccator contained silica gel and soda lime to reduce the humidity and carbon dioxide, respectively.

Figure 6.3 Cement paste samples immersed in isopropanol ready for wet-crushing

6.5.1.3 Characterization Techniques

The main characterization technique used for the hydrated cement was the XRD, where the same procedure and parameters described in the previous section were applied. In a few cases, the XRF technique was used to support a quantitative analysis. However, the attempt to perform a full quantitative analysis was not successful for multiple reasons, including the number of phases (more than 12), the complexity of the hydration products, and in some cases the quality of the diffractograms. This led to the use of a semi-quantitative approach (Talero et al. 2011, Liu et al. 2014).

The semi-quantitative approach comprised three steps: 1) normalizing the diffractogram by considering the average background intensity between $2\theta = 20°$ and 22° (where there were virtually no peaks) as 100%, 2) subtracting the background fitting from the diffractogram, and 3) taking the intensity of the most prominent peak for each phase as the quantitative indicator of that specific phase. As opposed to an alternative approach based on normalization of the highest peak (Barnes et al. 2000), this approach offers the advantage of allowing the comparison of the relative peak intensity of each phase at various ages.

Although a total of sixty samples were prepared for this phase of the work, a subset of only fourteen samples was subjected to XRD characterization. The results of the XRD tests were compiled in a spreadsheet, but they were difficult to analyze in this form. A more convenient way to display the results was to create a meta-table capable of extracting the results of only one phase at a time by selecting the name of the phase from a drop-down selection box, as seen in Figure 6.4.

In this figure, ‘Lab X’ and ‘Lab Y’ denote the two laboratories where the XRD tests were performed.

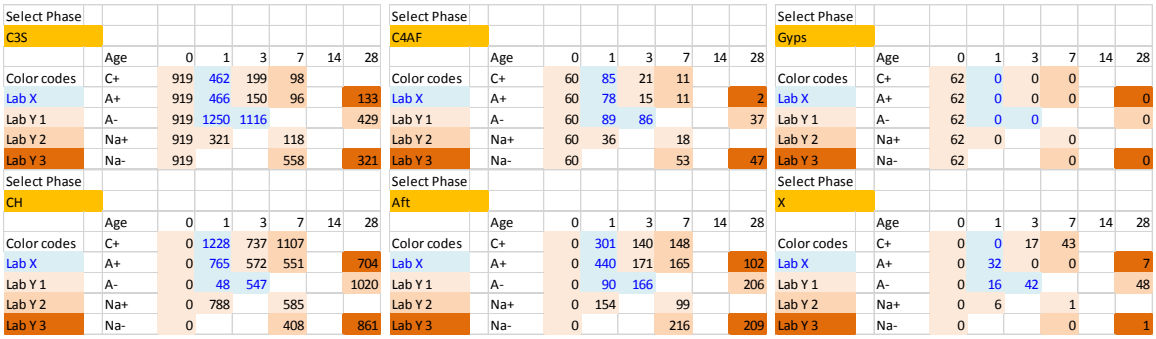

Select Phase							
C3S							
	Age	0	1	3	7	14	28
Color codes	C+	919	462	199	98		
Lab X	A+	919	466	150	96		133
Lab Y 1	A-	919	1250	1116			429
Lab Y 2	Na+	919	321		118		
Lab Y 3	Na-	919			558		321

Select Phase							
C4AF							
	Age	0	1	3	7	14	28
Color codes	C+	60	85	21	11		
Lab X	A+	60	78	15	11		2
Lab Y 1	A-	60	89	86			37
Lab Y 2	Na+	60	36		18		
Lab Y 3	Na-	60			53		47

Select Phase							
Gyps							
	Age	0	1	3	7	14	28
Color codes	C+	62	0	0	0		
Lab X	A+	62	0	0	0		0
Lab Y 1	A-	62	0	0			0
Lab Y 2	Na+	62	0		0		
Lab Y 3	Na-	62			0		0

Select Phase							
CH							
	Age	0	1	3	7	14	28
Color codes	C+	0	1228	737	1107		
Lab X	A+	0	765	572	551		704
Lab Y 1	A-	0	48	547			1020
Lab Y 2	Na+	0	788		585		
Lab Y 3	Na-	0			408		861

Select Phase							
Aft							
	Age	0	1	3	7	14	28
Color codes	C+	0	301	140	148		
Lab X	A+	0	440	171	165		102
Lab Y 1	A-	0	90	166			206
Lab Y 2	Na+	0	154		99		
Lab Y 3	Na-	0			216		209

Select Phase							
X							
	Age	0	1	3	7	14	28
Color codes	C+	0	0	17	43		
Lab X	A+	0	32	0	0		7
Lab Y 1	A-	0	16	42			48
Lab Y 2	Na+	0	6		1		
Lab Y 3	Na-	0			0		1

Figure 6.4 Screenshots of the meta-table showing relative content of each phase

6.5.2 Results and Analysis

In Figure 6.5, five main diffractograms between 2θ = 15° and 45° for plain and treated cement pastes cured for 7 and 28 days are stacked in the same graph to allow a clearer view of the peaks and easier comparison. The major peaks of each phase are identified and labeled. Note that in Figure 6.4, no XRD data were available for the control samples (C-) cured at subfreezing temperature due to the lack of hydration. In fact, the C- samples turned into powder as soon as they were immersed in the isopropyl alcohol during the hydration interruption procedure. Figure 6.6 shows the highest peak intensities, after normalization by background noise removal, of two representative unhydrated cement phases, alite (C_3S) and brownmillerite (C_4AF), and two cement hydration product phases, portlandite (CH) and ettringite (Aft). The diffractograms obtained from all XRD experiments performed can be found in Appendix H.

The major constituent of the Type GU cement is alite (C_3S), which also has the most complex crystal structure, making the quantification analysis a difficult exercise. Its major peaks lie between 29° and 35°, which is also the diffraction zone for belite (C_2S) and brownmillerite (C_4AF), not shown in Figure 6.5. It is evident that the alite had a higher dissolution and consumption at room temperature than at subfreezing temperature. The same remark is valid for the periclase (MgO), with peaks at 42.86° and 36.89°. Gypsum ($C\hat{S}H$), on the other hand, did not show any peak regardless of the curing temperature, shown also in Figure 6.4, suggesting a total dissolution and consumption during the first 24 hours.

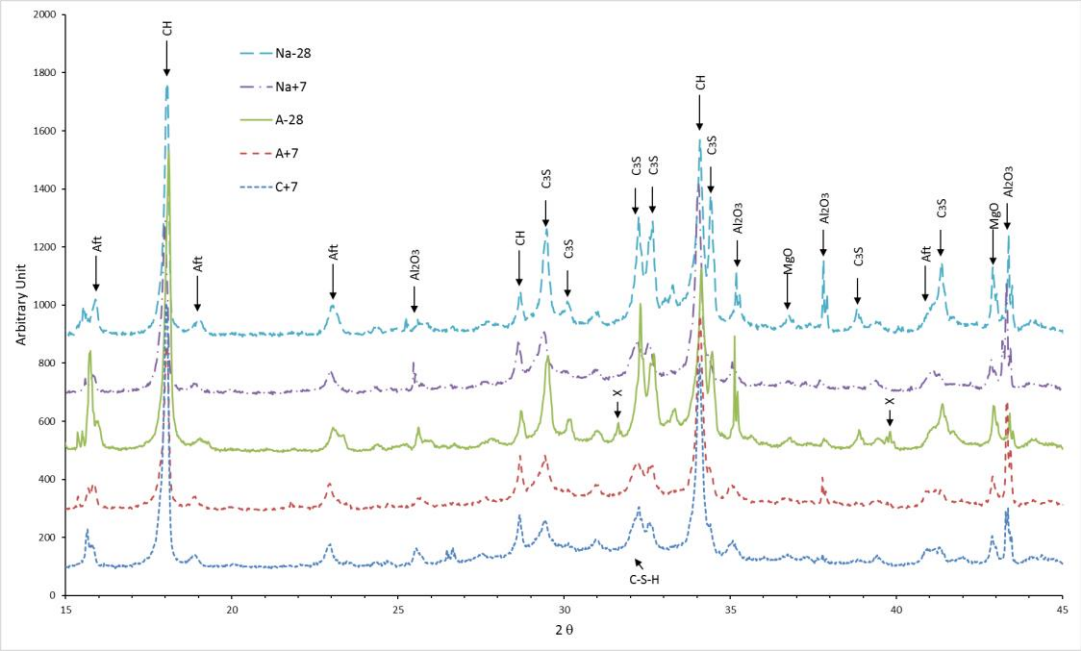

Figure 6.5 Stacked XRD diffractograms of select hydrated cement paste samples

The same observations for alite and brownmillerite are confirmed in Figure 6.6 (a) and (b), where the data points of the samples cured at subfreezing temperature lie above those cured at room temperature. In addition, and more importantly, the trend shows that there is a consumption of C_3S and C_4AF over time, even at subfreezing temperature, which is a major indicator of ongoing hydration of antifreeze and sodium nitrite treated samples. Moreover, the C_3S consumption rates of sodium nitrite treated samples (Na-) are fairly similar to those of commercial antifreeze treated samples (A-) with slightly higher, yet not conclusively so, consumption rates apparent in the $NaNO_2$ treated samples.

Portlandite (CH) and ettringite (Aft) are the two major crystalline hydration products and they can easily be seen in Figure 6.5, with their characteristic peaks at approximately 34.2°, 18.1°, and 28.7° for CH and 15.8° and 22.9° for Aft. The major hydration product and binding phase primarily responsible for the mechanical strength of the cement paste is the calcium silicate hydrate (C-S-H), which is an amorphous phase commonly referenced in the literature (e.g., Kocaba, 2009) as the "hump" between 26° and 38°, shown in Figure 6.5 for the C+7 sample as the curved black line. Its quantification requires the use of an internal standard to compensate for the unknown phases. Corundum (Al_2O_3) was initially used as an internal standard for a potential amorphous-phase quantification, but despite using a high-quality powder, the diffractograms showed a non-

consistent peak location and intensity. This was very likely caused by a non-uniform particle distribution (Skibsted and Hall 2008, De Schepper et al. 2014).

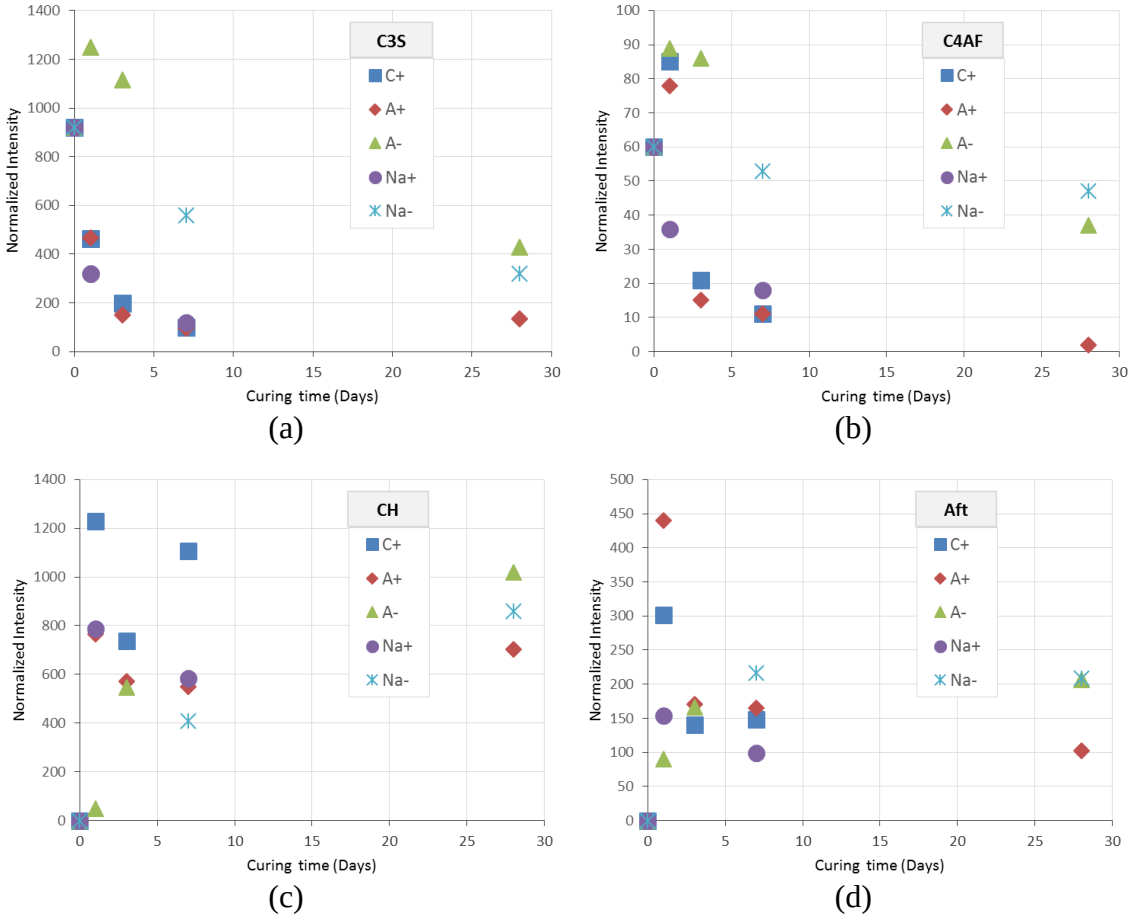

Figure 6.6 Most prominent peak intensity evolution over time of four hydration phases, in which intensities have been normalized by background noise removal

The evolution over time of the normalized most prominent peak of the two major hydration product phases, CH and Aft, are presented in Figure 6.6 (c) and (d). The data points of samples cured at room temperature do not show a steady increasing trend, which can partially be attributed to the variation of the quality of data issued from Lab X compared to Lab Y, in particular for day 1. After that the peaks tend to stabilize. The low Aft value of the A+28 sample might be attributed to the conversion of ettringite into monosulfoaluminate (Afm). For the samples cured at subfreezing temperature, the trend seems to be a steady increase of both CH and Aft up to the age of 28 days. This, again, is a strong indication that the sodium nitrite, whose effect was comparable

to the commercial admixture, is responsible for the ongoing of the hydration reactions at subfreezing temperature.

Two unidentified peaks, labeled X in Figure 6.5, were observed at about 31.6° and 39.9° for the commercial antifreeze treated sample cured at subfreezing temperature. They may belong to the same reflective phase observed when crushing the samples into powder (see p. 53) (Saha et al. 2015b). However, due to non-consistency, low intensity, and there being only two peaks, it was not possible to identify the crystalline phase. It is unlikely that the unidentified phase contributed to the strength gain at subfreezing temperatures, since it had fairly low-peaks and did not appear in the sodium nitrite treated samples.

6.6 Confirmation of Active Ingredient and Dosage Optimization (Phase 3)

The characterization of the commercial admixture in Phase 1 showed that it contained a high proportion of sodium nitrite and Phase 2 showed that there was a close similarity between the hydration products in the cement pastes produced using the commercial admixture and the sodium nitrite. In the third phase, the sodium nitrite was first evaluated as an additive to masonry mortar to confirm its antifreeze action on strength gain, and then its content was varied within a practical range to maximize the compressive strength.

6.6.1 Sample Preparation and Experimental Methods

Mortar cement Type S (containing lime), mortar sand, tap water, the commercial admixture, sodium nitrite, and sodium lignosulfonate superplasticizer were used in the preparation of the masonry mortar samples used for the third phase of the work. As summarized in Table 6.1, four batches were prepared and tested to confirm the action of the sodium nitrite. These included 1) a control batch containing only mortar cement, mortar sand, and water, in proportions indicated in the table; 2) the control mix plus 4% of the admixture (labeled M100); 3) the control mix plus 4% sodium nitrite (labeled SN); and 4) the control mix plus 4% sodium nitrite and 0.5% sodium lignosulfonate (labeled SN+SP), with all dosages given by weight of cement. The sample labeling in this phase was slightly different than for the previous phase to differentiate mortar from cement paste samples. The water to cement ratio (w/c) was 0.4 and sand to cement was 2.75. A Hobart mixer was used, and a mixing procedure similar to the one described in Saha et al. (2015a) was followed. The mortar was cast in 50 mm diameter x 100 mm long plastic cylindrical molds and

stored in the freezing chamber set at -10°C until their testing ages. At 7, 14, and 28 days, three cylinders of each batch were tested for compressive strength. The remaining samples were transferred from the freezing chamber to the curing room (set at 23°C) to be tested at ages of 35 and 56 days.

For the dosage optimization experiment, five batches of 10 samples each were prepared containing only sodium nitrite as an additive, with dosages varying from 2% to 6% at 1% intervals. All samples from each batch were cured at -10°C, then five of them were tested at 28 days, after which the remaining five samples were transferred to the curing room set at +23°C and 80% relative humidity and tested at 56 days. The water to cement ratio used for these samples was 0.5 in order to meet the minimum workability requirements of the fresh masonry mortar (ASTM 2007). The same testing machine and testing procedures as described in Saha et al. (2015a) were followed. The number of replicates for each batch in this phase was constrained by the size of the freezing chamber and the number of testing dates.

6.6.2 Results and Analysis

Table 6.6 shows the compressive strength test results for the masonry mortar cylinders treated with the commercial antifreeze admixture (M100), the sodium nitrite alone (SN), and the sodium nitrite plus superplasticizer (SN+SP), respectively. The same results are presented in graphical form in Figure 6.7, along with compressive strengths for the control batch, which was cured at +23ºC for 28 days and reached a strength of 23.1 MPa at that age. All three of the treated batches showed substantial strength gains while being cured at -10ºC, reaching between 44% and 57% of the strength of the control batch at 28 days. The strength gain of the treated samples at 7 days was found to be between 55% and 70% of their respective 28-day strengths. The sodium nitrite samples had the highest 28-day strength of 13.1 MPa, satisfying the masonry code minimum strength requirement of 12.4 MPa (ASTM 2010e). This was not the case for the commercial admixture samples, which reached only 9.9 MPa. One possible reason for this difference is that the same dosage of 4% was used for both additives, even though the commercial admixture contained only 85% sodium nitrite, resulting in an effective sodium nitrite dosage of only 3.4% compared to the effective 4% used in the SN and SN+SP samples.

Since the characterization results presented in Section 6.4.2 revealed an unidentified amorphous phase in the commercial admixture based on sulfur and very likely carbon, an attempt to replicate

the plasticizing effect was made by adding 0.5% sodium lignosulfonate to a batch otherwise containing only sodium nitrite as an additive. The mixing process showed that there was a substantial mismatch in the color and also in the workability between the M100 and the SN+SP mortars, which suggested that sodium lignosulfonate was not the compound used in the commercial admixture. The strength results and observed workability suggest that other superplasticizers should be tested in future experiments.

The strength recovery observed after the additional 28 days of curing at room temperature was substantial and ranged from 147% to 207% times the strength at 28 days. The commercial antifreeze showed the highest recovery, reaching 20.5 MPa at 56 days, slightly exceeding the strength of the sodium nitrite samples but with an insignificant margin. Most of the coefficients of variation within a batch were around 10%, which is an acceptable indicator of statistical repeatability for masonry mortar compression tests.

Table 6.6 Compressive strength of commercial and sodium nitrite treated mortars

Temp.	Mixture		7 d	14 d	28 d	56 d
-10°C	**M100**	Comp. Strength (MPa)	**6.7**	**NA**	**9.9**	**20.5**
		Coef. Var (%)	6.7	NA	10.1	11.9
	SN	Comp. Strength (MPa)	**7.9**	**10.5**	**13.1**	**20.3**
		Coef. Var (%)	8.7	3.8	8.7	11.3
	SN+SP	Comp. Strength (MPa)	**6.8**	**11.1**	**12.8**	**18.8**
		Coef. Var (%)	1.7	9.4	13.3	2.6

The reference compressive strength = 23.1 MPa

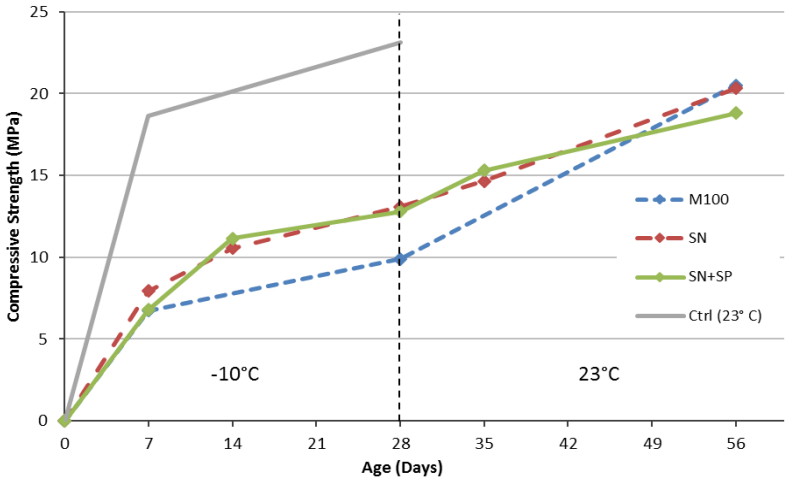

Figure 6.7 Compressive strength of antifreeze-added mortar samples

The results of compression strength tests for batches cast as part of the optimization stage are reported in Table 6.7 along with the coefficients of variation, and in Figure 6.8 along with quadratic fitting functions. Similar to the previous strength tests, the strength recovery at 56 days after the initial 28 days in subfreezing temperature was between 170 and 210%.

The strengths achieved in this stage were lower than those observed for the previous stage, which can be attributed to the higher w/c ratio of 0.5 used for the optimization batches compared to 0.4 used in the previous stage. The w/c ratio was increased to meet the flow table requirement according to ASTM C1437 (2007). Also, by increasing the w/c ratio and maintaining the sodium nitrite dosage calculation based on the cement content, the concentration of the sodium nitrite in the pore solution becomes lower, which may additionally explain the reduction of the antifreeze effect on the compressive strength.

Figure 6.8 indicates that the optimal sodium nitrite dosage was around 5% by cement weight, which is slightly higher than the 4% recommended by the manufacturer for the commercial admixture. Even though the overall variation of the 56-day regression function was high, indicated by the relatively low R^2, the within-batch variations obtained in this stage were smaller than the previous stage, which is almost certainly due to using five samples for each data point instead of the usual three samples.

Table 6.7 Compressive strength of mortar batches with different sodium nitrite dosages

Temp.	**Age**		**2%**	**3%**	**4%**	**5%**	**6%**
-10°C	**-28d**	Comp. Strength (MPa)	**5.1**	**6.7**	**6.8**	**7.3**	**7.6**
		Coef. Var (%)	6.4	2.1	8.0	8.6	4.9
+23°C	**-28d+28d**	Comp. Strength (MPa)	**10.7**	**12.2**	**11.8**	**14.1**	**13.0**
		Coef. Var (%)	3.1	7.9	7.7	8.0	2.9

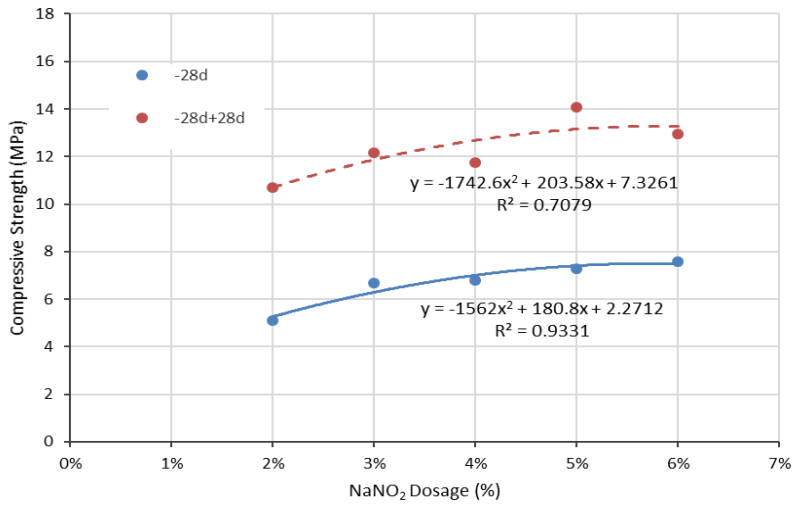

Figure 6.8 Variation of compressive strength with sodium nitrite dosage

6.7 Summary and Conclusion

The use of antifreeze admixtures to improve the hydration of cementitious materials in cold weather has been shown in previous work to be a viable solution when compared to the current regulations and practices of using heat and protection. In this work, the effectiveness of sodium nitrite-based antifreeze admixtures on the hydration of masonry mortar was investigated and the optimum dosage identified. The experimental program produced several conclusions, summarized in the following paragraphs.

The elemental and mineral characterization techniques confirmed that the Type GU cement used was a regular cement with slightly higher magnesium content and slightly lower calcium and silicon, but still in the range of ordinary cement. The commercial antifreeze product that was considered in this study was initially intended for concrete applications and was found to be composed primarily of sodium nitrite ($NaNO_2$) and a lower quantity of mullite. Elemental characterization also identified some sulfur content, which did not appear in the crystalline phases, and is believed to be part of an amorphous phase constituting the superplasticizer contained in the admixture as advertised by the manufacturer.

A semi-quantitative approach to track the crystalline phases present within treated and untreated cement pastes at various stages of hydration when cured at both room and subfreezing temperatures revealed similar results for samples containing either the antifreeze admixture or pure sodium nitrite and suggested that the hydration reactions proceeded at -10°C. The absence of any

unusual minerals in the XRD diffractograms indicates that the strength gain can very likely be attributed to the formation of the amorphous C-S-H phase. Although the exact mechanism of strength development has yet to be determined, it can be reasonably hypothesized that the presence of sodium nitrite prevents the pore water solution from freezing at -10ºC, making water available for the hydration reactions to proceed at subfreezing temperatures.

Compressive strength tests on masonry mortars prepared with either the commercial antifreeze admixture or sodium nitrite and cured at -10ºC confirmed the effectiveness of sodium nitrite as an antifreeze agent, with the sodium nitrite treated batch reaching a compressive strength of 13.1 MPa at 28 days. An additional 28 days of curing at room temperature brought the compressive strength to greater than 20 MPa. Subsequently varying the dosages of sodium nitrite between 2% and 6% showed that the optimal dosage was approximately 5% by weight of cement for the particular mix design tested when cured at -10ºC. However, the optimum dosage is likely dependent on the w/c ratio as it has a strong influence on final pore water solution concentration.

7 TRACKING THE HYDRATION OF ANTIFREEZE TREATED CEMENT PASTE AT SUBFREEZING TEMPERATURES USING THE TDR TECHNIQUE[4]

7.1 Abstract

Portland-cement based materials are the most used materials in construction. However, in cold seasons at below freezing temperatures, their usage requires extra thermal protection measures to ensure adequate strength is reached before unprotected exposure is allowed. Another method of mitigating the effect of low temperatures is the use of antifreeze admixtures capable of accelerating the hydration and depressing the freezing point of the pore water solution to reduce or eliminate the thermal protection requirements. In a previous work, a non-harmful antifreeze admixture was shown to effectively promote hydration at subfreezing temperatures. Characterization of the hydration products did not reveal anything unusual in the chemical composition, so it was postulated that the mechanism of antifreeze action was physical in nature; investigation of that hypothesis is the subject of this paper. The non-destructive time domain reflectometry (TDR) technique was used to track the evolution of the volumetric water content together with hydrated and unhydrated cement in control and antifreeze-added cement pastes from the mixing time to an age of three weeks when cured at -10ºC. The Lichtenecker-Rother mixing model was used to estimate the volumetric content of the individual constituents of the cement paste, considering their individual dielectric constants. The results showed clear evidence of the existence of liquid water in the antifreeze treated samples, and that the amount of water and unreacted cement decreased with time at subfreezing temperatures, confirming the presence of ongoing hydration. Modelling results also suggest that the liquid water available for the hydration reactions is in the form of adsorbed water at subfreezing temperatures and as free water above freezing.

Keywords: Cement hydration; Antifreeze admixtures; Low temperature; Tracking water content; TDR; mechanistic mixing model.

[4] This chapter was submitted under reference id Conbuildmat-D-19-06144 as "Saha, O., Boulfiza, M., and Wegner, L.D. (under review-b). Tracking the hydration of antifreeze treated cement paste at subfreezing temperatures using the TDR technique. Construction and Building Materials". It has been reformatted to conform to a consistent standard throughout the thesis.

7.2 Introduction

Portland cement is the main ingredient of concrete and other cementitious materials, which are the most used construction materials in the world. Water being an essential component in the hydration reactions, its availability in liquid form is a key factor in determining the short- and long-term properties of the final product. Subjecting freshly mixed cement paste to subfreezing temperatures at an early age gradually reduces the amount of liquid water available for hydration as it freezes, bringing the hydration reactions, and therefore strength gain, to a halt. Thus, thermal protection is generally used to ensure proper curing and strength development when concrete or masonry construction is undertaken at subfreezing temperatures.

An alternative approach would be to prevent the water from freezing through the use of antifreeze admixtures. In a previous study (Saha et al. accepted-2019), a commercial admixture with a primary ingredient of sodium nitrite was used in masonry mortar and resulted in acceptable compressive strength development at temperatures as low as -10°C with minimal thermal protection. Semi-quantitative characterization of the initial and hydration products of the antifreeze treated cement, as reported by Saha et al. (under review-a), did not identify any differences in chemical composition compared to ordinary untreated hydrated cement cured at room temperature. It was therefore hypothesized that liquid water was available for the hydration reactions to proceed at -10ºC.

Tracking the liquid water content is crucial in determining the evolution of the hydration during the curing process. Although the individual initial ingredients of the composite cementitious material are relatively easy to identify, it is a challenge to identify their volume fraction as the hydration proceeds due to their irregular nature over time (Lee 2010). Knowing the physical status of water molecules (free versus bound) can help inferring the hydration rate and, eventually, the curing and strength development of the cementitious material.

Multiple destructive and non-destructive techniques can be used to track the transient moisture content profile of porous building materials, including gravimetry, oven drying, nuclear magnetic resonance (NMR), capacitance, X-ray projection, and time domain reflectometry (TDR) (Roels et al. 2004). Among these, TDR is considered a non-destructive technique and has been applied to porous media by modelling them as mixtures of three phases (solid, water, and air) using a simplified mixing model (Tinga et al. 1973). Initially developed as a cable testing technique, the

applicability of TDR widened to the domain of water quantification in soil and other porous materials (Davis and Chudobiak 1975, Topp et al. 1980, Korhonen et al. 1997c). The possibility of using TDR to quantify the water content in porous media is essentially due to the fact that water has a much higher dielectric constant (79~81) than any other component of the composite material. A more comprehensive literature review of the use of TDR in tracking water content in porous building materials is available in Černý (2009) and Lee (2010).

In the presence of highly conductive media, the applicability of the TDR technique is limited due to the high attenuation of the electromagnetic signal, rendering the detection of the end of probe reflection virtually impossible (Mojid et al. 1998). To overcome this limitation, the use of insulated probes was proposed to reduce the signal attenuation (Kelly et al. 1995). However, this comes at the price of probe sensitivity reduction and the requirement of probe re-calibration (Yoon et al. 1994, Mojid et al. 1998, Entus 2000, Staub et al. 2008, McIsaac 2010). Analytical and numerical models have been developed and used to simulate the effect of the coatings and gaps on the dielectric permittivity measurement of a two-rod probe (Knight et al. 1997, Fujiyasu et al. 2004)

The unfrozen water content of soils was investigated using TDR by Smith and Tice (1988) and Hivon and Sego (1990), where the technique showed promising results. Fabbri et al. (2006, 2009) studied the water-to-ice phase change in clay, glass beads, and hardened cement paste. They used a semi-empirical method based on the Lichtenecker-Rother mixing model and found accurate estimation of the liquid water content versus temperature in freezing cement paste. The dielectric spectra in the frequency domain have also been examined for fresh cement paste at subfreezing temperatures (Yoon et al. 1994). The bulk dielectric constant was derived from the complex spectra and found to be much lower than that at room temperature due to the reduced ionic mobility at subzero temperatures.

Adsorbed water and temperature are other factors affecting the dielectric constant of water, which enables the evaluation of the water volume fraction based on the bulk dielectric constant (Skierucha 2011, Luong et al. 2015). In another study, Olson et al. (1995) used a computer modelling approach to confirm the dielectric amplification coming from the capillary pores. They noticed a large drop of the dielectric constant upon freezing of the capillary pores. Ford et al. (1997) confirmed the observation of dielectric amplification of fresh cement paste ($K_{app} > 80$) in

the frequency domain, and showed evidence that it is inversely proportional to barrier thickness, meaning that as the pore structure forms, the bulk dielectric constant decreases. They also noticed a slight residual amplification of the dielectric constant of the C-S-H gel and suggested a pore solution dielectric constant of $K_r \approx 50$.

In this paper, the TDR technique was used to infer the presence of liquid water and its consumption by hydration reactions in antifreeze treated and sodium nitrite treated cement paste when cured at subfreezing temperatures. It was motivated by a desire to explain the previously observed strength gain in masonry mortars that had been treated with the same admixtures.

7.3 The TDR Technique and the Dielectric Constant

The TDR technique was introduced in the early 1930's as a cable testing technique. It is based on the principle that a change in the impedance of the transmission line would affect the reflection of an electromagnetic wave propagating through the line. By measuring the time between the launching of the wave and its reflection, the spatial location of an impedance change can be located, provided that the propagation velocity is known. Due to the homogeneous nature of liquids, TDR was widely used by researchers in the fields of physics and chemistry of liquids (Černý 2009). In the late 1970's and early 1980's, measurement of moisture content in porous materials using TDR became one of the fast growing applications (Davis and Chudobiak 1975, Topp et al. 1980, Smith and Tice 1988, Camp and Bilotta 1989). The interest in this technique kept growing until the early 2010's, by which time it had become widely established in scientific laboratories, and the number of international publications stabilized at 120-130 references per year (Černý 2009).

Dielectric materials, as opposed to conductive materials, are insulators that do not conduct electricity but can sustain an electric field. Therefore, the dielectric constant is a measure of the ability of a material to store an electric charge from an applied field and then transmit that energy. This constant, also called the relative complex permittivity, is defined as the ratio of the electrical permittivity of a particular material to the electrical permittivity of free space (Ledieu et al. 1986). The magnitude of the dielectric constant can also be determined by the electrical dipole moment per unit volume of the material (Sun 2008). Many construction materials such as soil, cement, and wood are solid dielectrics that contain liquid water in their porous network. Table 7.1 shows the

dielectric constants of a few typical materials commonly used in construction. Clearly, water has the highest dielectric constant, due to its high molecular polarity, which is the main reason for using the TDR technique to estimate the volumetric water content of a composite material.

Table 7.1 Typical dielectric constants of construction materials and cement paste constituents

Material	Dielectric constant	Material	Dielectric constant
Water	79-81	Ice	3-4
Sand	3-6	Limestone	4-8
Unreacted cement	3-4	Hydrated cement	4-7
Air	1	In-pore solution	225-275

The TDR equipment, as represented in Figure 7.1, consists of a system capable of emitting an electromagnetic pulse along a waveguide, then recording the reflected waveform. A more detailed review of the principle of the TDR operation can be found in Černý (2009). The velocity of the wave is influenced by the dielectric constant of the media surrounding the probe, and its amplitude is influenced by the conductivity of the media. Relative reflection usually varies between +1 and -1, depending on the degree of open and short circuitry, respectively. Based on this principle, a relative amplitude reflection trace as a function of time, or apparent distance, is generated. Three main points in the trace are of particular interest for sample characterization, identified as points ①, ②, and ③ in Figure 7.2. Point ① corresponds to the end of the coaxial cable and the connection to the probe handle, point ② represents the end of the probe handle and beginning of the sample, and point ③ shows the final rise of the TDR trace and marks the probe open end. The apparent length of the probe can be derived from the difference along the horizontal axis between points ③ and ②. Various methods can be found in the literature to determine the three key points of the TDR trace, the most common being the dual tangent and the flat tangent plus offset methods (Klemunes 1995, McIsaac 2010).

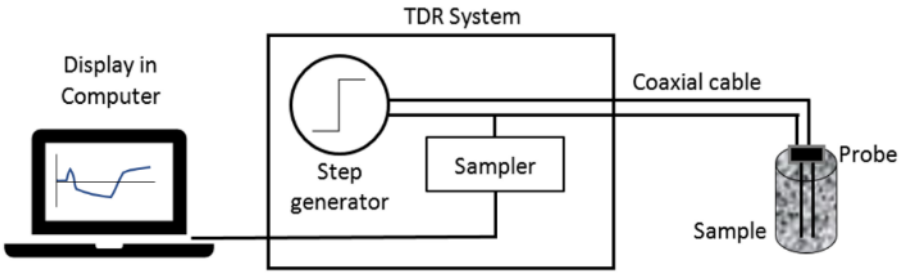

Figure 7.1 Schematic of a typical TDR system

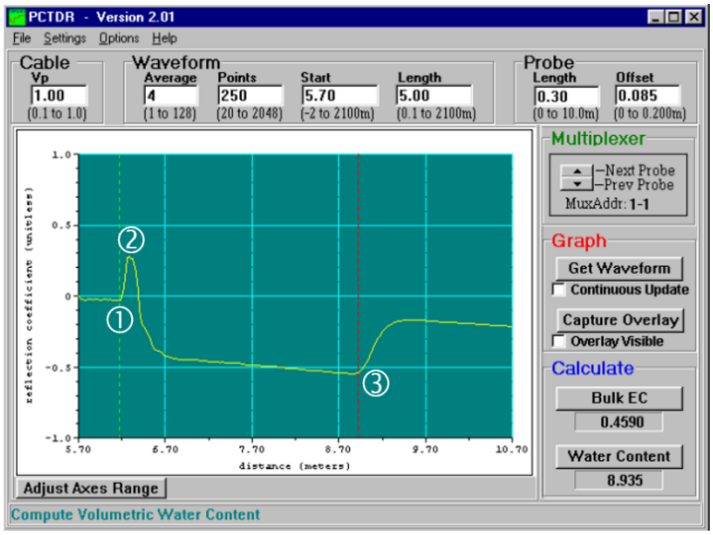

Figure 7.2 Typical display of a TDR trace using PCTDR software (v2.08, Campbell Scientific)

From a physical standpoint, the equation governing the TDR signal can be expressed as the simplest solution of Maxwell's equation for electromagnetic wave propagation in an absorbing medium. The full development of these equations is beyond the scope of this paper. However, the apparent dielectric constant (K_{app}) can be calculated as follows (Mojid et al. 1998, Lee et al. 2008):

$$\sqrt{K_{app}} = \frac{L_{app}}{L_p v_p} \tag{7.1}$$

where

K_{app} = apparent dielectric constant (measured)

L_{app} = apparent length (m) of probe distance between point ③ and ②

L_p = probe length (m)

v_p = relative velocity of electromagnetic wave (usually 0.99)

In most related literature, v_p is taken equal to 1, which leads to the following simplified form of the equation:

$$\sqrt{K_{app}} = \frac{L_{app}}{L_p} \tag{7.2}$$

Three main approaches can be used to estimate the water content of a porous medium from the apparent dielectric constant. The first is based on the use of empirically pre-calibrated curves valid for certain classes of materials. Figure 7.3 shows a compilation of pre-calibrated curves of water content as a function of the measured dielectric constant for various soils and concrete (Topp et al. 1980, Smith and Tice 1988, Hivon and Sego 1990, Korhonen et al. 1997c, McIsaac 2010, Yu and Liu 2010, Li 2014). Here, a solid line is used to represent the water content calibration curves for concrete, the long-dashed line is used for soils, and the short-dashed line is used for peat soils. These curves were plotted based on their reported fitting functions, and a few have been extended beyond their valid range. The second approach is based on the calibration of the material of interest using a reference method, such as the gravimetric method; this is the most reliable method. The curves shown in Figure 7.3 are based on this approach.

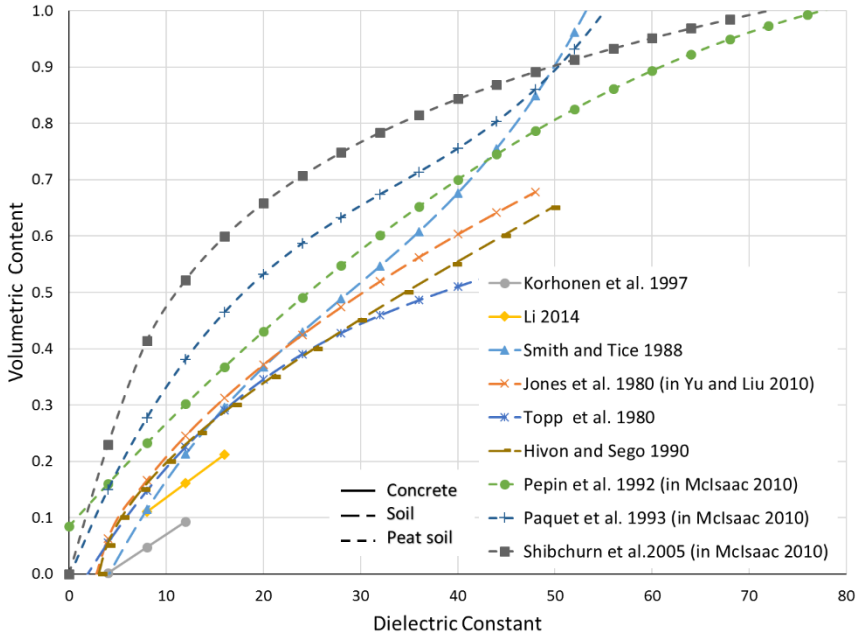

Figure 7.3 Calibrated water content curves for concrete and soils from multiple authors

The third approach is referred to as the mechanistic approach or the mixing model approach for multiphase materials. This approach is based on incorporating the physical properties, the geometric distribution, and the volume fractions of the individual components of the multiphase material into an expression to calculate the apparent bulk physical property of the composite material. It is used mostly when the volume fraction of the composing phases is difficult to measure. Various models can be found in the literature (Entus 2000, Fabbri et al. 2006, Černý 2009, Lee 2010).

In the case of cementitious materials, a schematic representation of the volumetric content of the major phases during the hydration process is shown in Figure 7.4. To simplify the schematic, the various forms of water, i.e., bound, adsorbed, or ice, in the case of frozen samples, are not explicitly shown. The bulk dielectric constant of the material will change over the course of the hydration process as the volumetric content of each phase changes, and the mixing model can be used to infer the volumetric content of each phase, including the different forms of water, at various stages based on the measured dielectric constant.

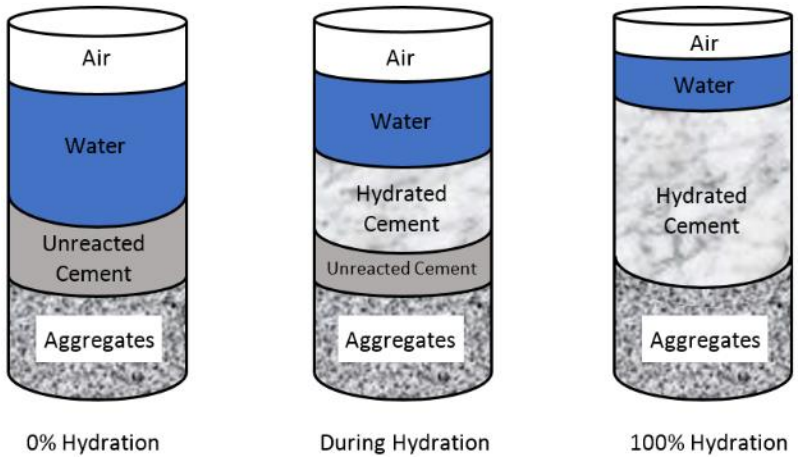

Figure 7.4 Volumetric and constituent change of concrete during hydration

In the current work, the Lichtenecker-Rother model was applied (Lichtenecker and Rother 1931). This model is widely used in practice. It is applicable to multiphase materials and takes into account the geometric arrangement of the constituents (Zakri et al. 1998, Černý 2009). The relationship between the bulk apparent dielectric constant and the volume fractions and dielectric constants of the constituents is described by

$$K_{app}^{\alpha} = \sum_{i=1}^{n} f_i K_i^{\alpha} \tag{7.3}$$

where

$K_{app} =$ bulk apparent dielectric constant

$K_i =$ dielectric constant of the individual constituents, $i = 1..n$

$f_i =$ volume fraction of the individual constituents, $i = 1..n$, and $\sum f_i = 1$

$\alpha =$ geometric arrangement factor. $-1 \leq \alpha \leq +1$

The geometric arrangement factor accounts for the relationship between the direction of the applied field and the orientation of the material layering, where $\alpha = +1$ when the field and the layers are parallel, and $\alpha = -1$ when the field and the layers are perpendicular. Theoretically, for an isotropic material α has been found to be 0.5 (Birchak et al. 1974, Roth et al. 1992).

Experimental data for moist mineral soils showed that α can vary from 0.4 to 0.8 (Jacobsen and Schjonning 1995). In the particular case where $\alpha = 0.5$, the model is referred to as the complex refractive index model (CRIM) and the governing equation becomes

$$\sqrt{K_{app}} = \sum_{i=1}^{n} f_i \sqrt{K_i} \tag{7.4}$$

Details of how this model was applied are presented in Section 6.5.

7.4 Materials and Experimental Methods

7.4.1 Sample Preparation and Gravimetry

The materials used for the TDR and associated experiments consisted of regular portland cement Type GU, tap water, a commercial MNC-C15 admixture (from Muhu China), and sodium nitrite. Three cement paste types were prepared, including plain, with MNC C-15 and with sodium nitrite. The water to cement ratio was w/c=0.5 and the admixture proportion, when used, was 4% by cement weight. A Hobart mixer was used to combine the ingredients, operated at medium speed for five minutes and interrupted twice to scrape the sides of the bowl. The mixed cement paste was then poured into 50 mm diameter x 100 mm long plastic cylindrical molds, with a single cylinder prepared for each cement paste type. The TDR and thermocouple probes were inserted in the center

of the sample and the whole setup was transferred to a freezing chamber set to -10°C. The custom-made TDR probe was held in a vertical centered position in the cement paste cylinder using a lab clamp on the side, and the thermocouple probe was inserted approximately 50 mm deep slightly aside from the center to reduce its electromagnetic interference with the TDR probe.

Three samples of approximately 30 g of each cement paste were stored in sealed plastic vials for gravimetric measurement of water content. The samples were weighed before starting the curing, then measurements were taken at three discrete ages of one, two and three weeks. Each set of measurements at a particular age consisted of four individual measurements of sample weight. One was taken right after the vial was taken from the freezer, to confirm that the weight had not changed since the start of the experiment. The sample was then transferred to an oven set to 150°C for fast drying, and the next readings were taken at 1, 2.5, and 24 hours, respectively, with samples returned to the oven after the first two measurements. The weight measurements were taken using a digital scale with a precision of 0.01 g. The purpose of these measurements was to compare the water content obtained by the gravimetric method to that obtained from the TDR-calculated volumetric results at the end of the curing period.

7.4.2 Insulated Probes and Data Collection

The TDR probe was made in-house and consisted of a 1.5 m length of coaxial cable (RG 58A/U), a BNC connector at one end, and two stainless steel rods at the other end (Figure 7.5). The rods were 90 mm long, 1.56 mm in diameter, and separated by 15 mm. The rods were attached to a connector strip to keep them parallel and preserve their embedded length after insertion in the cement paste. The connector strip was also used as a handle to keep the TDR probe at the center of the cement paste cylinder as it was supported by the edges of the plastic cylinder. Due to signal attenuation in the highly conductive fresh cement paste, one of the rods was covered with a heat-shrink polyolefin tube (final diameter 2.21 mm) and connected to the shield (sensor) of the coaxial cable, whereas the bare rod was connected to the center (feeder) of the coaxial cable. Only one rod was insulated to reduce the sensitivity loss of the probe due to the effect of the polyolefin (Fujiyasu et al. 2004, McIsaac 2010).

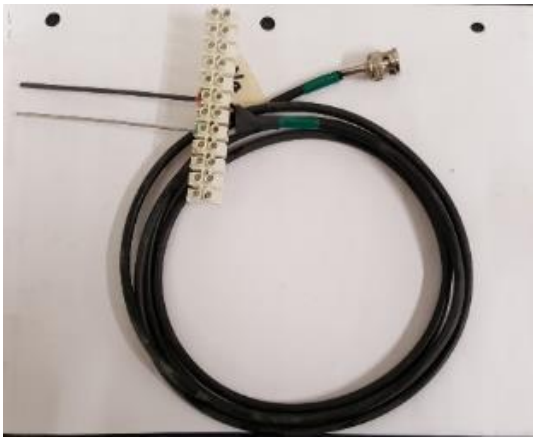

Figure 7.5 TDR coaxial cable with 2-rod probe, one rod being coated

A Campbell TDR100 (operating at 6.25 GHz frequency) was used to generate the electromagnetic pulse and to collect the reflected waveform. It was connected, through a USB cable, to a computer running the PCTDR software (v2.08, Campbell Scientific) in combination with a personalized macro-command responsible for triggering the TDR impulse signal and recording the reflected wave at specific time intervals for post treatment. Readings were taken as soon as the sample was transferred to the freezer, then every 5 minutes for the first 6 hours. The interval increased to 30 minutes for the remainder of the first day. Due to very little change between readings, one reading per day was taken for the remaining three weeks of the experiment. A thermometer reader (Mastech, model MS 6514 dual channel) equipped with a built-in data logger connected to the inserted thermocouple was used to record temperature at the center of the cement paste at fixed intervals.

Figure 7.6 shows some typical TDR readings for plain cement paste with non-insulated stainless-steel probes. Fresh cement at positive temperatures (blue curve) was too conductive, making the open end reflection position undetectable. This highlights the necessity of using insulated or coated probes. Some interference was also noticed (orange and grey curves) early in the experimental program and was eliminated by removing the AC-DC converter used for the thermometer logger. At very low temperatures (around -30°C), when most liquid water was converted into ice, multiple TDR readings were taken and were practically identical, indicating that there was no change in the position of the open end reflection.

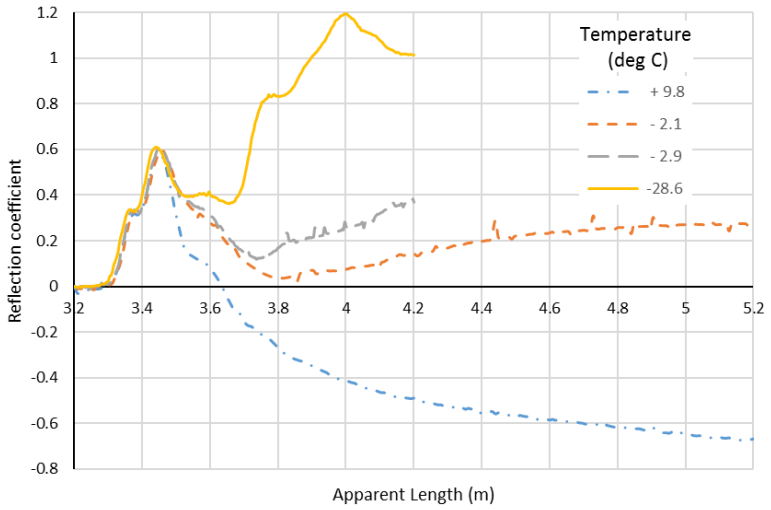

Figure 7.6 Typical TDR reflections of fresh cement paste at various temperatures with bare stainless-steel probes

7.4.3 TDR Probe Calibration

One method of calibration that was used to quantify the volumetric liquid water content was the air-water immersion method (McIsaac 2010). It consisted of progressively immersing the probe in a water container and measuring the dielectric constant at various depths, from no contact with water to full immersion depth. The setup for this procedure is shown in Figure 7.7. The probe length used in this experiment was 90 mm, and the depth increment was 10 mm for each reading. For one set of tests, the shielded rod (sensor) was covered with heat shrink polyolefin to match the experiment performed on the cement paste. Figure 7.8 shows the TDR readings for the air-water immersion experiment for both coated and uncoated probes, where it can be seen that for shallow depths the curve was too wavy due to signal reflections and the short length of the probe, preventing a good localization of the second reflection corresponding to the open end of the probe. The full set of data for the air-water calibration can be found in Appendix I.

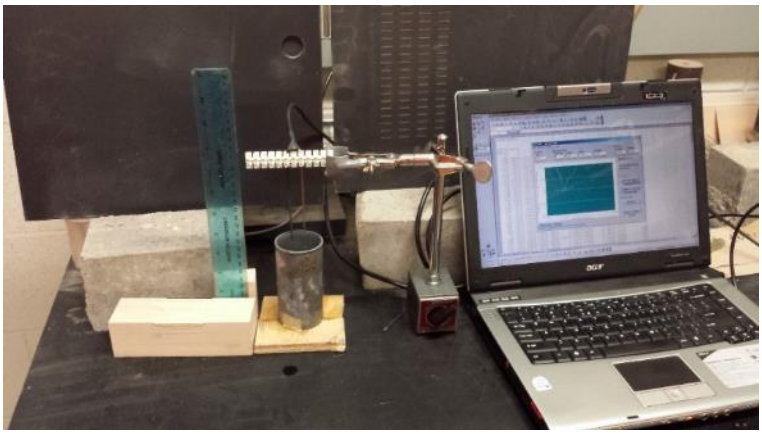

Figure 7.7 Air-Water immersion calibration setup

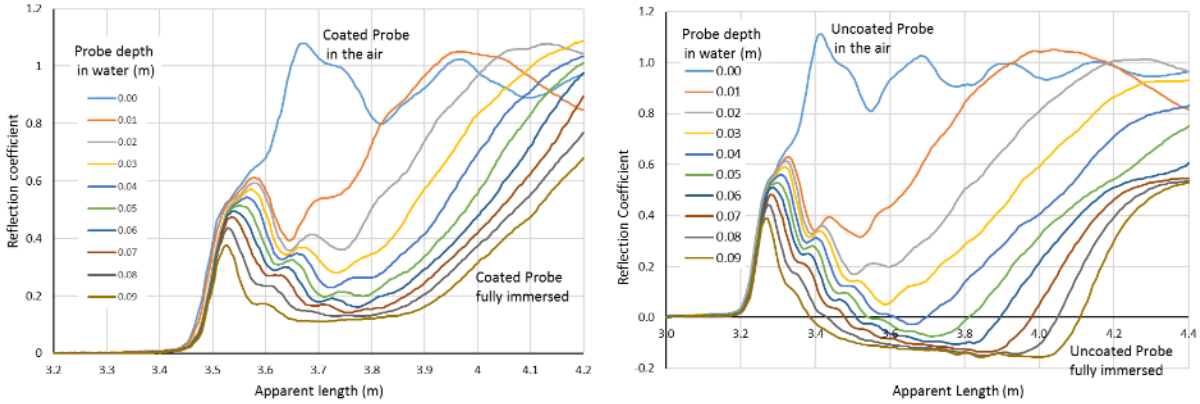

Figure 7.8 Typical TDR traces of coated and uncoated probes during air/water calibration

This method has been successfully used to emulate a dry layer of soil on a wet layer (Robinson et al. 2003), and can provide very accurate estimates of volumetric water content, but it leads to complex responses that would be very difficult to interpret without the use of advanced analysis techniques. The problem is exacerbated in the case of insulated probes where the effect of the coating needs to be accounted for. The complexity of the response, which is a manifestation of the various signal reflections occurring at the discontinuities along the TDR cable and probe, highlights the importance of the common practice that probes should be tightly immersed (without air gaps) in the media for which the dielectric constant is being measured.

A second calibration method, which consisted of taking multiple measurements under the same conditions of homogeneous moisture distribution using fully immersed probes, was also applied. It was used to calibrate the system consisting of a combination of the coated probe with the regular uncoated probe. The procedure consisted of measuring the dielectric constant of homogeneously mixed sand with water, starting from totally dry sand and ending with fully saturated sand in five

increments. The measurements were taken using the same probes that were used to measure the dielectric constant of the cement paste samples. The last data point was obtained for 100% immersion in a container full of tap water.

7.4.4 Conversion of TDR Traces to Dielectric Constants

The evaluation of the dielectric constant K_{app} according to equation 7.2 is governed by the determination of the apparent length l_{app} of the probe inserted in the studied media, and the physical length of the probe l_p. The objective of this section was to present the two methods used in this work to derive the apparent length from the TDR traces. Essentially the methods consist of determining points ② and ③ defined in Section 7.3 and shown in Figure 7.2.

The two methods of interest were the dual tangent and the flat tangent plus offset methods. The method of dual tangent is illustrated in Figure 7.9 (a), where point ② is defined by the intersection of the two tangents at the inflection points on both sides of the initial maximum, and point ③ is defined by the intersection at the final minimum. The method of flat tangent plus offset is illustrated in Figure 7.9 (b), where point ① is located at the intersection of the horizontal tangent of the coaxial cable and the tangent of the first rise at the inflection point. Point ② is an offset from point ① measured by a distance representing the probe handle. Point ③ is determined from the intersection of the flat tangent at the final minimum and the tangent of the last rise at the inflection of the TDR trace. The apparent length is the distance between points ② and ③.

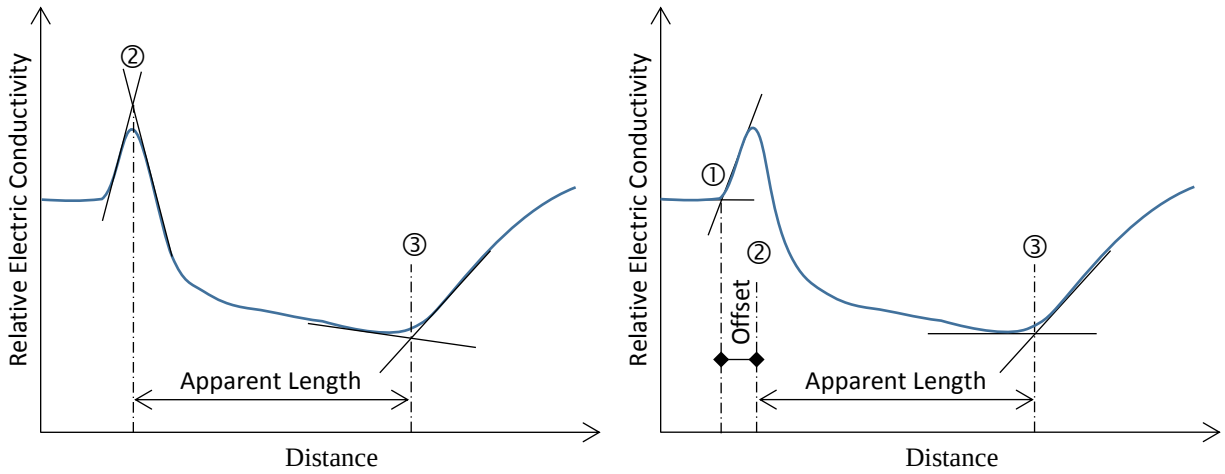

Figure 7.9 Illustration of dual tangent and flat tangent plus offset apparent length determination

Due to the amount of data collected through the TDR testing (about 900 readings), and the difficulty of determining the dielectric constant manually, a semi-automatic method of evaluating the dielectric constant from each TDR reading curve was prepared using an Excel spreadsheet, which is described in Appendix J.

7.5 Results and Discussion

7.5.1 Drying Gravimetry

Table 7.2 shows the results of the gravimetric water content measurements after one, two, and three weeks of curing at -10°C for the three types of cement paste. The weight of samples taken after the curing period but before commencement of the drying procedure confirmed that there had been no total weight reduction since the start of curing. During the fast-drying process, which was a non-standardized method, the samples were weighed several times and showed no significant change in mass after 150 min; however, the drying process was maintained for 24 hours to ensure that all the free water had evaporated. The results shown in Table 7.2 correspond to the 24-hour weights. At the beginning of the drying process, the temperature of the samples increased rapidly from -10°C to +150°C; this undoubtedly induced the hydration of a small amount of cement. Assuming that no hydration had occurred in the control sample before the start of fast-drying, which is supported by the absence of any strength development (Saha et al. accepted-2019), the amount of water retained (bound) in the sample after drying was in the range of 4% to 5.5% relative to the initial water content. For the antifreeze treated sample, the retained water increased from approximately 10% after one week to approximately 14.5% after three weeks, indicating that some of the water had been consumed by the hydration reactions and was retained in the hydration products. For the sodium nitrite treated sample, the change was not as pronounced, increasing from approximately 9% after the first week to approximately 10% after the third week. These values are only qualitative indicators of the rate of hydration. More information, such as the amount of water required for a full hydration, is necessary to infer any quantitative conclusions. Nevertheless, the evidence shows that there was a clear difference in water consumption between the plain cement paste and the treated cement pastes.

Table 7.2 Gravimetry measurements of the water content in the cement paste samples

Sample	Age (Weeks)	Retained water to initial water (%)	Retained water to total weight (%)	Water loss to total weight (%)
Control	1	5.44	1.81	31.52
	2	4.13	1.38	31.96
	3	5.57	1.92	31.42
MNC-C15	1	9.88	3.21	29.26
	2	12.19	3.96	28.51
	3	14.46	4.69	27.77
$NaNO_2$	1	8.91	2.89	29.58
	2	10.11	3.28	29.19
	3	10.14	3.29	29.17

7.5.2 Probes Calibration

As shown by the typical TDR trace of fresh cement paste in Figure 7.6, the signal attenuation due to the conductive media prevented any valid estimation of the dielectric constant at an early age. The use of coated probes was suggested in the literature (Yoon et al. 1994, Mojid et al. 1998, Entus 2000, Staub et al. 2008, McIsaac 2010). The coating layer of the probe rod has the effect of reducing the sensitivity and underestimating the bulk dielectric constant of the analyzed material (Mojid et al. 1998). In this case, it is necessary to calibrate the coated probe to reflect dielectric constant values of a regular uncoated probe.

As presented earlier, Figure 7.8 shows two sets of typical TDR traces for the air-water immersion calibration method, one for the coated probe and the second for the uncoated probe. The wavy form of the TDR traces, especially for shallow probe immersions, prevented locating the open-end reflection point accurately, more so for the coated probe than the uncoated probe. The traces were analyzed using the Excel procedure described and summarized in Appendix J, to determine the corresponding dielectric constants. A visual correction was made in some cases to better locate the position of the inflection points. The rising segment of the coated TDR traces was not steep enough, and this reduced the precision of the open-end reflection point determination. Figure 7.10 displays three calibration curves, one each for the bare and insulated probes, respectively, and limited to the data points where the open-end reflection points were localized

with acceptable accuracy, and a third curve representing the CRIM mixing model governed by Equation 7.4, which can be rewritten as:

$$\sqrt{K_{app}} = f_w\sqrt{K_w} + (1 - f_w)\sqrt{K_{air}} \tag{7.5}$$

There is a good match between the bare probe calibration curve and the CRIM mixing model curve. The small number of acceptable data points from the insulated probes did not allow a good mapping between the coated and uncoated probes. This result is in line with the finding of McIsaac (2010), who concluded that the air-water immersion method could not be used as a surrogate for other mediums. The incorporation of the polyolefin coating in the mixing model equation requires a more involved theoretical effort, as the near field effect of the polyolefin coating layer is more complex to include in the model.

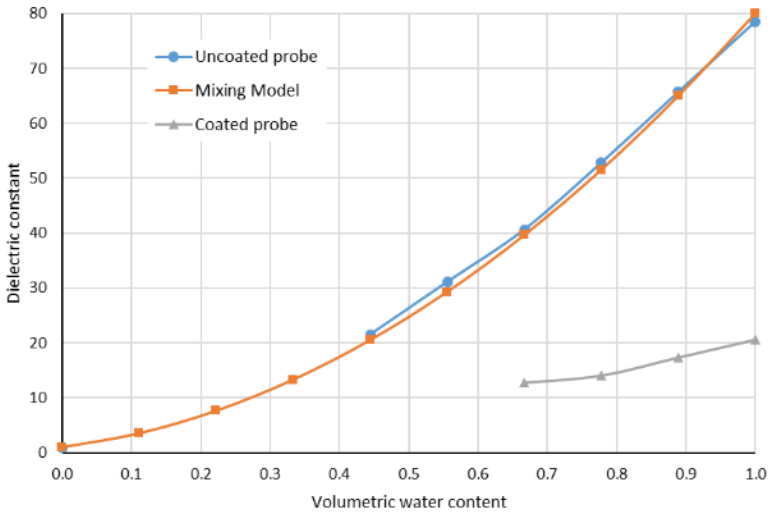

Figure 7.10 Calibration curves for the uncoated and incomplete curve for the coated probes

The results of the second calibration procedure, using coated and uncoated probes in the same condition of sand saturation, are shown in Figure 7.11. The figure also includes the analytical curve representing the effect of a non-concentric coating on a double parallel rod probe (Annan 1977, Knight et al. 1997, Fujiyasu et al. 2004). The analytical solution is governed by the following equation:

$$K_{app} = \frac{K_{coat}\cosh^{-1}(s_0/r_0)}{K_{soil}\{\cosh^{-1}(s_0/r_0) - \cosh^{-1}(s_1/r_1)\} + K_{coat}\cosh^{-1}(s_1/r_1)}K_{soil} \tag{7.6}$$

where

$s_0, r_0 =$ half center to center spacing and radius of the rods, respectively

$s_1, r_1 =$ half center to center spacing and radius of the rods with coating, respectively

$K_{app} =$ apparent dielectric constant

$K_{soil} =$ dielectric constant of soil

$K_{coat} =$ coating material, or gap dielectric constant

Figure 7.11 shows that, up to the level of the fully saturated sand, the regression was linear with a slope of 1.33 for the coated probe; in this case, the intercept was forced to be zero. Beyond the fully saturated point, the curve has a much higher gradient, shown by the dashed line. Due to the lack of additional data points in the last segment, and to the pronounced curvature shown by the analytical solution, it is expected that the assumed linear interpolation will have a reduced accuracy. Despite the reduction in accuracy in this restricted interval, the methodology leading to the determination of the water content will not be affected.

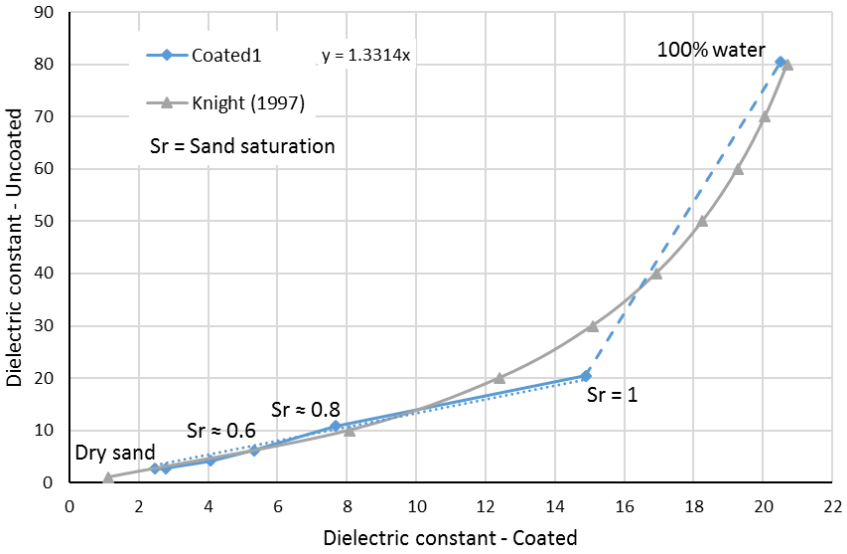

Figure 7.11 Mapping of dielectric constants of the coated probe to that of the uncoated probe using the second calibration procedure

7.5.3 Dielectric Constants

The measured sample temperatures from the embedded thermocouple and the apparent bulk dielectric constants determined from the TDR traces for the three samples are presented in Figure 7.12 in the top and bottom graphs, respectively. The horizontal axis represents the time in days. The graphs are divided into three distinct time periods. The left-most portion of each graph shows

a finer time scale to capture the freezing point transition and the corresponding dielectric constant evolution immediately after the transfer of the specimens to the freezing chamber. The center portion of the graphs shows an expanded time scale, due to the slow variation of both temperature and dielectric constants. The right-most portion shows the variation of temperature and dielectric constants as the samples thawed at the end of the three-week curing period.

The dielectric constant curves show a good and synchronized match with the temperature curves. There is, however, a little lag of the dielectric constant behind the temperature, very likely due to the off-center position of the thermocouple and the corresponding faster response time to the outside temperature of the freezing chamber. The dielectric constants of all samples display a slight rise at the beginning of the cooling process caused by the increase of the dielectric constant of water as temperature drops (Kaatze 1997), from ~80 at 22°C to ~92 at -10°C. The dielectric constant of water continues to increase as the temperature drops below freezing; however, the overall bulk dielectric constant decreases due to the transformation of water-to-ice.

The slope of the monotonic portion of the three dielectric constant curves between one and 21 days was found to be -0.006, -0.193, and -0.063 per day for the control, MNC-C15 and $NaNO_2$ samples, respectively. The negligible slope for the control sample reflects a negligible change in the phase composition of the mixture. On the other hand, the MNC-C15 sample has the highest slope, indicating a reduction of the liquid water content. The $NaNO_2$ sample also demonstrates a reduction in liquid water content, but at a less pronounced rate. This result gives a strong indication of ongoing hydration, even at subfreezing temperatures. However, the apparent rate of hydration does not fully correlate to compressive strength measurements of the associated masonry mortars (Saha et al. under review-a), for which the $NaNO_2$ treated mortar had a higher compressive strength in the first three weeks than the MNC-C15 treated mortar.

Considering the near zero slope of the control curve and its intercept at approximately 5.6, and assuming that all the water in this sample has turned into ice, it is apparent that both the MNC-C15 and the $NaNO_2$ samples have higher overall dielectric constants, implying that there is still water in liquid form in the treated samples. The decrease of the overall dielectric constant can be attributed to water evaporation, conversion of free water to bound water, and conversion of liquid water-to-ice (Sun 2008). The degree to which each mechanism was present must yet be determined.

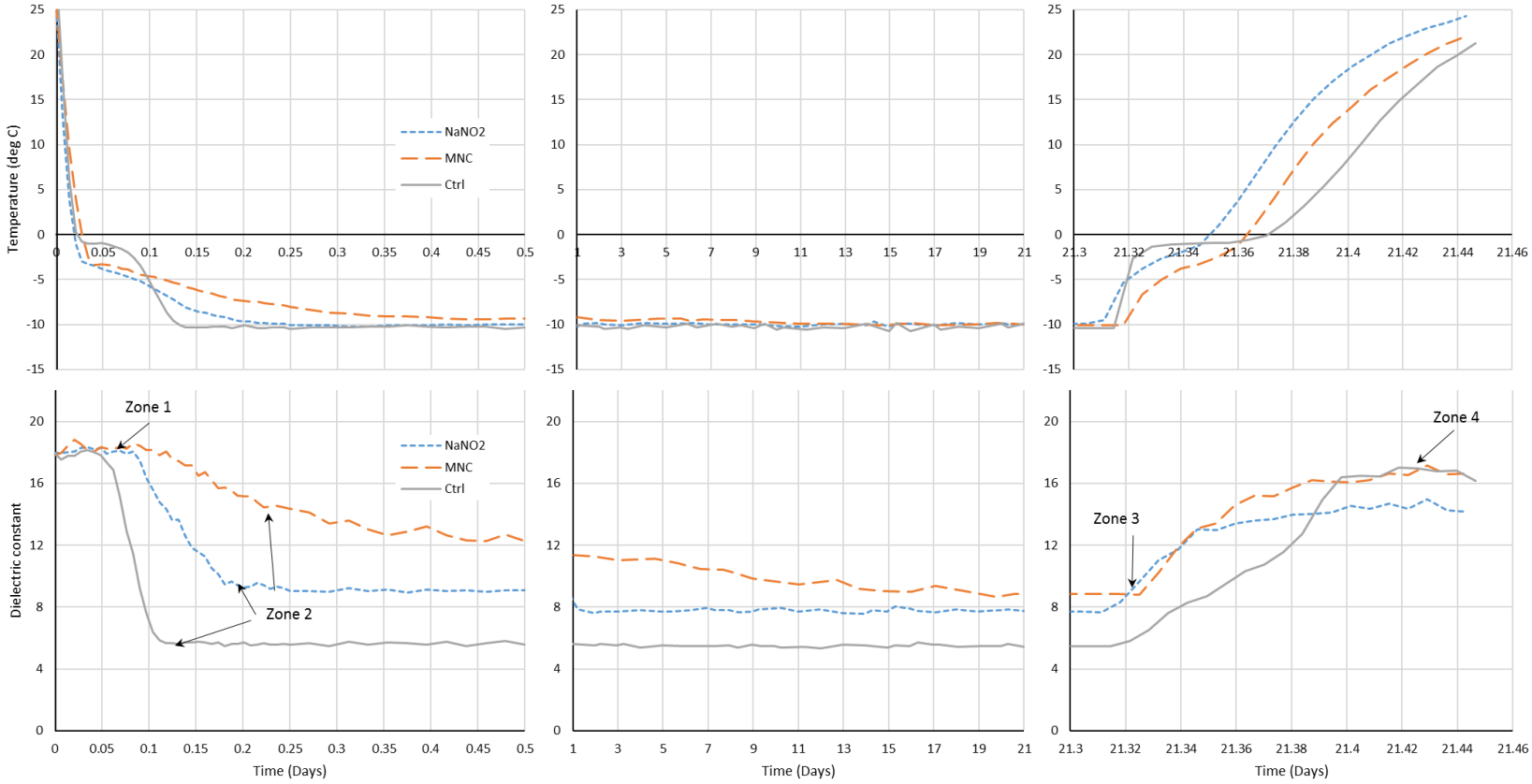

Figure 7.12 Evolution of the dielectric constants (with insulated probes) and temperature over time for the three samples

7.5.4 Volume Fraction

From the dielectric constant curves in Figure 7.12, four key points were selected to describe the water content and the hydration evolution, labeled as Zones 1 to 4. These zones represent the start of sample curing, the point where the rapid cooling period ends and slow cooling begins, the end of curing and start of thawing, and the end of thawing, respectively. The measured dielectric constants at these key points are reported in Table 7.3 in the column labeled "Coated Dielectric Constant". In order to use the CRIM mixing model described in Section 7.3, the measured dielectric constant was converted to the uncoated dielectric constant using the bi-linear calibration curve shown in Figure 7.11. Results are reported in the right-most column in Table 7.3.

Table 7.3 Measured coated and equivalent uncoated dielectric constants of the three samples

Sample	Age	Coated Dielectric Constant	Equivalent Uncoated Dielectric Constant
Control	Mixing	17.02	35.83
	Freezing	5.59	7.45
	End curing	5.57	7.41
	Thawing	16.97	35.39
MNC-C15	Mixing	18.30	48.87
	Freezing	11.40	15.18
	End curing	8.82	11.74
	Thawing	16.22	29.35
$NaNO_2$	Mixing	18.10	46.60
	Freezing	9.27	12.34
	End curing	7.65	10.19
	Thawing	14.97	21.46

A more detailed version of the cement-paste phases model shown in Figure 7.4 was developed and consisted of six phases, including air, free water, adsorbed pore water, ice, unreacted cement and hydrated cement. The complex refractive index model (CRIM) was used, as represented by the following equation:

$$\sqrt{\boldsymbol{K_{app}}} = \boldsymbol{f_{air}}\sqrt{\boldsymbol{K_{air}}} + \boldsymbol{f_w}\sqrt{\boldsymbol{K_w}} + \boldsymbol{f_{pore}}\sqrt{\boldsymbol{K_{pore}}} + \boldsymbol{f_{ice}}\sqrt{\boldsymbol{K_{ice}}} + \boldsymbol{f_{uc}}\sqrt{\boldsymbol{K_{uc}}} + \boldsymbol{f_{hc}}\sqrt{\boldsymbol{K_{hc}}} \qquad (7.7)$$

where

$K_{app} =$ equivalent bulk apparent dielectric constant

$K_i =$ dielectric constant of the individual constituents, $i = 1..6$

$f_i =$ volume fraction of the individual constituents, $i = 1..6$

The total volume fraction and the total specific gravity of the mixture are given by equations:

$$\mathbf{1} = \boldsymbol{f_{air}} + \boldsymbol{f_w} + \boldsymbol{f_{pore}} + \boldsymbol{f_{ice}} + \boldsymbol{f_{uc}} + \boldsymbol{f_{hc}} \qquad (7.8)$$

$$\boldsymbol{\gamma_{total}} = \boldsymbol{f_w}\boldsymbol{\gamma_w} + \boldsymbol{f_{pore}}\boldsymbol{\gamma_{pore}} + \boldsymbol{f_{ice}}\boldsymbol{\gamma_{ice}} + \boldsymbol{f_{uc}}\boldsymbol{\gamma_{uc}} + \boldsymbol{f_{hc}}\boldsymbol{\gamma_{hc}} \qquad (7.9)$$

where

$\gamma_i =$ specific gravity of constituent i, $i = 1..6$

In ideal situations, a linear system of n independent equations with n unknowns is formulated and the solution is derived using any of the conventional solving methods. In certain cases, however, a system may not be well conditioned, in which case a solution may be obtained using an optimization approach. Equations 7.7 to 7.9 constitute three equations with six unknowns f_i. Depending on the initial and final conditions of each selected interval, additional assumptions need to be made to better condition (constrain) the system. In this work, the linear programming algorithm named simplex was used as a method to optimize equation 7.7 for the calibrated apparent dielectric constant $\sqrt{\boldsymbol{K_{app}}}$.

The simplex optimization method (Frontline Systems, 2010), implemented using Excel's "LP Simplex" solver, was used to calculate the volume fractions of the individual constituents. Equation 7.7 was used as the objective function, and Equations 7.8 and 7.9 as constraints. In addition, the following assumptions for each of the four key points were made to ensure that a solution was obtained:

- At the start of the curing (Zone 1), no ice nor hydrated cement were present, and the freezable water was related to the total water and adsorbed water.

- At the end of rapid cooling (Zone 2), the volume fraction of air was reduced by the amount of water-to-ice expansion rate, the freezable water was fully transformed into ice, and hydration was considered not to have started.
- At the end of curing (Zone 3), the volume fraction of air was assumed to be unchanged from its Zone 2 value, and the volume fraction of the hydrated cement was linked to the reduction in volume fraction of the unhydrated cement using the Powers-Brownyard ratio of ~1.4 (Taylor 1997). The Powers-Brownyard ratio is defined as the additional space required by the hydrated cement after consuming a unit volume of unhydrated cement. In addition, the volume fraction of freezable water was assumed to be zero. This assumption is consistent with the freezing response of a pore water solution that was extracted from samples containing antifreeze admixtures, as described in 0.
- At the end of thawing (Zone 4), all the ice was converted to water, and up to 3% consumption of the unreacted cement was allowed to better condition the solver.

The solution at each key point was taken as the initial condition when solving for the next point. Since the LP Simplex method can be used only for linear equations, the square root of the equivalent bulk dielectric constant was set as the objective function. The volume fractions of the six major constituents of the cement paste resulting from the solution procedure are reported in Table 7.4.

As seen in the table, the air contents of the three samples follow a similar trend, starting at approximately 6%, then falling to approximately 2% due to freezing, and finally increasing back to between 6% and 10% after thawing. The ice, on the other hand, follows the opposite trend, starting and ending at 0% and occupying the highest volume fraction in all samples at the subfreezing temperature during the curing process. The ice in the control and the MNC-C15 sample stays almost unchanged at about 55% and 46%, respectively, during the entire curing period, whereas it decreases slightly from 48% to 46% in the case of the $NaNO_2$ sample.

Water was represented in the mixing model as two phases, free water and adsorbed pore water. This distinction was necessary since the two have significantly different dielectric constants, as seen in Table 7.1. The distinctive values can be explained by the release of some polar species during the hydration, which are responsible for the dielectric amplification (Ford et al. 1997, Fabbri et al. 2006). The total starting water (free and adsorbed) of the three samples at mixing time was

the same, but differences appeared in the ratio of adsorbed to free water, with values of 2.3%, 38.0%, and 30.5% for control, MNC-C15 and $NaNO_2$, respectively. The extra ionic content of the admixtures and the superplasticizer incorporated in the MNC-C15 can explain the higher apparent dielectric constant.

While the free water content during the subfreezing curing period was equal to zero for all samples (as assumed), the adsorbed pore water content was significantly higher, by a factor of 1.5 to 2.3, in the antifreeze treated samples as compared to the control sample. Moreover, the relative consumption of the adsorbed pore water was 3%, 24%, and 21% for control, MNC-C15, and $NaNO_2$ samples, respectively, from the beginning to the end of the subfreezing period. This constitutes clear evidence of the existence and consumption of liquid water even at subfreezing temperatures for antifreeze treated samples, in contrast to control cement paste samples.

Comparing the ratio of total water consumption (retained) between the gravimetric results in Table 7.2 in the third week (5.6%, 14.5%, 10.1%) and the TDR results in Table 7.4 (5.6%, 22.0%, 17.8%), there is reasonably good agreement in the trend.

The volume fraction of hydrated cement was linked to that of the unreacted cement using the Powers-Brownyard ratio and achieved values of 3.6%, 12.2%, and 17.6% for the control, MNC-C15, and $NaNO_2$ samples, respectively. This provides additional evidence of the ongoing hydration reactions at subfreezing temperatures in the antifreeze treated cement paste samples. The volumetric calculation details are presented in Appendix L.

Table 7.4 Volume fractions of the cement paste constituents at key stages of curing

Sample	Age	Air	Free Water	Adsorbed pore water	Ice	Unreacted cement	Hydrated cement
Control	Mixing	0.057	0.564	0.013	0.000	0.366	0.000
	Freezing	0.016	0.000	0.067	0.548	0.370	0.000
	End curing	0.016	0.000	0.065	0.549	0.370	0.000
	Thawing	0.065	0.504	0.040	0.000	0.355	0.036
MNC-C15	Mixing	0.057	0.418	0.159	0.000	0.366	0.000
	Freezing	0.020	0.000	0.150	0.455	0.366	0.000
	End curing	0.016	0.000	0.114	0.461	0.335	0.074
	Thawing	0.095	0.388	0.061	0.000	0.333	0.122
$NaNO_2$	Mixing	0.057	0.442	0.135	0.000	0.366	0.000
	Freezing	0.017	0.000	0.123	0.482	0.366	0.000
	End curing	0.016	0.000	0.097	0.461	0.323	0.104
	Thawing	0.057	0.161	0.313	0.000	0.293	0.176

It is well-known that pore water can exist either as free water or as adsorbed water. Table 7.4 shows that hydration was taking place for the samples containing the admixtures by consumption of adsorbed water. For the control cement paste, however, there was no hydration taking place despite the apparent existence of some adsorbed water after all freezable water was converted into ice. The control cement paste contained substantially less adsorbed water than the antifreeze treated cement pastes, and the absence of new hydration products below the freezing point may suggest the presence of thinner layers of adsorbed water that are more tightly bound to the surface of solid particles when antifreeze admixtures are not used. In this case, the adsorbed water may not be available to promote the hydration reactions. Antifreeze treated cement pastes, on the other hand, may have thicker layers of adsorbed water, with the outer layers being less tightly bound to the surface of particles than the inner layers, thus making them more accessible to the hydration reactions.

7.6 Conclusions

The impact of two antifreeze admixtures, one commercially available and the second consisting of sodium nitrite, on the hydration of cement paste when cured at subfreezing temperatures was

investigated. Time domain reflectometry (TDR) was used as a non-destructive technique to track the evolution of the volumetric water content together with hydrated and unhydrated cement of the control and antifreeze-added cement pastes from the time of mixing to an age of three weeks. A short background of the TDR technique as applied to porous materials was provided, describing the use of coated probes to reduce the effect of conductive solutions, probe calibration, amplification effects of fresh cement and the application of mechanistic mixing models to evaluate volumetric content of composite materials. An easily applied calibration procedure was developed to match uncoated and coated probes from the beginning to the end of the experimental tests.

The higher dielectric constant of the antifreeze treated cement pastes compared to that of the control cement paste, as determined using the TDR traces, indicates that there is still water in liquid form in the antifreeze treated samples at -10ºC. The decreasing values over time suggest that the hydration reaction is occurring at this temperature. The dielectric constants at four key points in the TDR traces were selected and used to estimate the volumetric content of the six phases of the cement paste using the CRIM mixing model. The following conclusions can be drawn.

- More ice was detected in the control sample than in the antifreeze treated cement pastes at subfreezing temperatures.
- Most of the water available for hydration in the samples containing the admixtures was in the form of adsorbed water at subfreezing temperatures.
- Although the control samples did contain adsorbed water at subfreezing temperatures, according to modelling results, its volume fraction was lower than that of the antifreeze treated cement pastes and did not seem to lead to further hydration of the cement particles after the free water had completely frozen. It is postulated that this could be caused by thinner layers of adsorbed water that are more tightly bound to the surface of solid particles, and hence, effectively not available to promote the hydration reactions.

The volumetric content of the adsorbed pore water can be considered as clear evidence of the existence of liquid water even at subfreezing temperatures for the antifreeze treated samples. The consumption of the liquid water and unreacted cement in the antifreeze treated samples, as determined using the mixing model, can be considered as clear evidence of ongoing hydration, in contrast to the control sample that did not show similar consumption. This result was confirmed by gravimetric measurements of the retained water.

8 CONCLUSIONS AND RECOMMENDATIONS

8.1 Summary

The work presented in this thesis was motivated by the need to mitigate the thermal protection requirements for masonry construction in the long winter season in Canada. The main objectives of the project were to develop and evaluate a cold weather admixture system (CWAS) for masonry mortars from commercially available admixtures, and to identify the active ingredients responsible for promoting the strength development and the mechanism by which they act at temperatures below freezing.

A review of the literature on cold weather practices for construction with cementitious materials was presented, and showed that, despite investigation into the use of antifreeze additives going back to the 1950's, very limited use of antifreeze admixtures for concrete, and no use at all for masonry, still governs the common practices in North America. The lack of experimental data for masonry construction was striking, highlighting the need to test and produce data on using antifreeze admixtures for mortar in masonry. In the first stage of the experimental program, related to the development of a CWAS, a statistical combinatory approach was used to evaluate the effectiveness of different combinations of commercially available admixtures in masonry mortar. This differed from the more commonly used empirical approach to minimize the freezing point of the combined mixture. The best mortar mix candidates from this stage were selected for further testing to measure their compressive strength development at temperatures between -10°C and -15°C. The results revealed the necessity of an initial pre-curing period of protection from freezing to reach the minimum compressive strength specified by the relevant ASTM standards. The next stage consisted of applying various pre- and post-curing schemes to identify the minimum protection time required to reach acceptable compressive strengths.

The second main objective of this research was to identify the active ingredients in the antifreeze admixture and their mechanism of action. Several characterization techniques, including XRF and XRD, were used and found to be instrumental in identifying the active compound of the antifreeze admixture. This compound was then isolated, tested, and its dosage optimized vis-à-vis compressive strength. The absence of any unusual phases in the hydration products directed the investigation toward tracking the water content, which was believed to be responsible for the

C-S-H phase formation at subfreezing temperatures. For this investigation, the time domain reflectometry (TDR) technique was used to measure the dielectric constant of plain and treated cement pastes during the curing process. A mixing model was also formulated to quantitatively track the individual constituents of the cement paste, with a particular interest in the available liquid water at subfreezing temperatures.

8.2 Conclusions

The following conclusions address the specific objectives defined in Chapter 1:

1. The evaluation of the combined admixtures for their ability to lower the freezing point of the masonry mortar to a level between -10°C and -15°C was achieved after two cycles of applying the steepest descent regression of the incomplete surface design experiment. Freezing points as low as -20°C were reached; however, unreasonably high dosages, in some cases almost three times the maximum recommended manufacturer dosage, were required to reach this level. In a case where two particular admixtures from two different manufacturers were combined, the freezing point of the mixed mortar met the experimental program requirements, but the mortar did not harden even after three days at room temperature, which indicated possible incompatibilities between various admixtures such that the hydration reactions could not proceed. Preliminary tests to measure compressive strength development after curing at temperatures of -10°C and -15°C when the freezing point was lowered did not indicate a good correlation between the two properties. In fact, the best performing admixture in terms of strength development had a moderate freezing point around -4°C.

2. Curing the mortar samples at temperatures of -10°C and -15°C without an initial period of protection from freezing resulted in strength development at both temperatures for the antifreeze treated samples, but no strength development for the untreated control mortar. The compressive strength reached after 28 days of curing at the subfreezing temperatures was not sufficient to meet the minimum ASTM standard requirements for any of the samples tested. This led to the addition of a protection period before exposing the fresh mortar to the low temperature conditions. Three pre-curing times of 6, 12 and 24 hours were adopted, and the results showed that as little as 6 hours of pre-curing were adequate for the treated mortar

to meet the ASTM minimum requirement when cured at -10°C and approximately 8 hours when cured at -15°C. Further testing showed that all the samples, including the control samples, experienced major strength recovery after an additional 28 days of curing at room temperature. The strength reached as high as 140% for the treated samples and 87% for the control samples, compared to the strength of the control samples cured for 28 days at room temperature. The strength development observed in this phase of the experimental program strongly indicated an ongoing hydration reaction. Crushed fragments of the antifreeze treated samples displayed a reflective phase when cured at subfreezing temperatures. This observation became the subject of a separate investigation (Saha et al. 2015b), in which the reflective phase was not fully characterized and its content was not significant enough to explain the strength gain.

3. The Canadian CSA A179 (2004b) should be reviewed for potential relaxation of its restrictions on the use of any freeze depressants to allow the use of antifreeze admixtures not containing alcohols or chlorides. In addition, CSA A371 (2004a) should be reviewed to reduce the freezing protection time from 48 hours to a more reasonable time, between 6 and 12 hours depending on the temperature, when an effective antifreeze admixture is used. Given the number of samples used in the current project, additional testing for a better statistical reliability, and complementary testing for other important mortar properties are required.

4. The XRF and XRD techniques used to characterize the active ingredients in the antifreeze admixture successfully identified, with a very high level of certainty, that the major phase in the effective admixture was sodium nitrite. Two other crystalline phases were present in the admixture: mullite and possibly cesanite. The XRF tests revealed the presence of sulfur, which was not detected by the XRD, indicating the existence of an amorphous phase, very likely a sulfur-based superplasticizer. The primary action of the sodium nitrite was confirmed by a compressive strength test of masonry mortar treated with 4% of laboratory grade sodium nitrite. A parametric study in which the dosage of sodium nitrite was varied between 2% and 6% in masonry mortar showed that 5% sodium nitrite by cement weight was the optimal dosage for the development of compressive strength at -10°C.

5. A semi-quantitative XRD approach to track the crystalline hydrated phases for samples containing either the antifreeze admixture or sodium nitrite additives showed that the two samples had similar content and suggested, based on tracking the calcium hydroxide and the ettringite, that the hydration reactions proceeded at below freezing temperatures. The absence of any unusual minerals in the XRD diffractograms indicated that the strength gain can very likely be attributed to the formation of the amorphous C-S-H phase. Due to the lack of evidence of the contribution of a crystalline phase to the strength development, it is concluded that the sodium nitrite lowers the freezing point and allows liquid water to exist and be available for hydration at subfreezing temperatures.
6. The TDR traces showed a clear slope of the dielectric curve for the treated cement pastes, supporting the hypothesis of ongoing hydration. The volumetric content of the cement paste constituent was derived from the apparent dielectric constant using a mixing model and suggested that pore water and unreacted cement were being consumed, further supporting the hypothesis of ongoing hydration reactions. Gravimetric measurements before mixing and after curing and oven drying produced additional evidence of water consumption by hydration.

8.3 Recommendations

1. Because of the weak correlation between the freezing point and the strength of mortar samples, it is recommended that a quick strength test be performed at an early age instead of only measuring the freezing point when evaluating the effectiveness of antifreeze admixtures.
2. The observation of air bubbles in the antifreeze treated mortar did not have a significant effect on the tested strength but may have an effect on the durability and freeze-thaw resistance. It is highly recommended that additional testing be performed to measure other masonry mortar properties, including setting time, board life, flexural and bond strength, and efflorescence. It is recommended also that tests be performed on other mortar cement types, cubic mortar samples, initial rate of absorption of masonry units, and assemblage of blocks. The effect of the admixture on grout is also worth studying, as it has a high initial water content.

3. Two temperatures were tested in this work, -10°C and -15°C, and the observed trends led to inferring that there would be no protection time required for temperatures around -5°C. It is recommended that tests be performed at this temperature and other temperature patterns commonly encountered in field conditions.
4. Some samples were observed to reach very low freezing points with very little corresponding strength development. Investigating this topic merits consideration.
5. The relative variation of the peaks' intensity from sample to sample in the XRD measurements, especially for the Al_2O_3 used as internal standard, was partially attributed to the variation of particle size. It would be interesting to redo the XRD tests with a finer powder size and to conduct a more precise XRD scan to attempt the quantitative analysis of amorphous phase again.
6. Several improvements to the experimental work using the TDR technique can be suggested. These include controlling the thickness and material of the probe coating, increasing the length of the probe to reduce the wavy form of the dielectric trace and improve the resolution, using a three-rod probe to reduce the noise in the signal, and reducing the spacing between the rods. Other improvements for the analytical work may include establishing a parametric relation between the liquid water and ice based on the pore solution concentration, including the variability of the water dielectric constant in terms of temperature and ionic concentration, improving the mixing model calculation to include the cement hydration in the first few hours before freezing, and trying other mixing models and other geometric factors.
7. The current study was limited to cement paste. It would be interesting to evaluate the water content using the same TDR method on concrete and mortar at below freezing temperatures.
8. Two potential improvements to the calibration procedure include using other known materials or mixes of materials to refine the mapping in the calibration gap area and using the nuclear magnetic resonance (NMR) technique to evaluate the water content.

REFERENCES

ACI. 1990. Standard specification for cold weather concreting (Reapproved 2002). ACI 306.1-90. American Concrete Institute, Detroit, MI, USA.

ACI. 2002. Evaluation of strength test results of concrete. ACI 214R-02. American Concrete Institute, Farmington Hills, MI, USA.

ACI. 2010a. Guide to cold weather concreting. ACI 306R-10. American Concrete Institute, Farmington Hills, MI, USA.

ACI. 2010b. Report on chemical admixtures for concrete. ACI 212R-10. American Concrete Institute, Detroit, MI, USA.

Aïtcin, P.C. 2000. Cements of yesterday and today: concrete of tomorrow. Cement and Concrete Research, **30**(9): 1349–1359.

Annan, A.P. 1977. Time-domain reflectometry-Air-gap problem for parallel wire transmission lines. Geological Survey of Canada, **77**–**1B**: 59–62.

Aranda, M.A.G., Ángeles, G., and León-Reina, L. 2012. Rietveld quantitative phase analysis of OPC clinkers, cements and hydration products. Reviews in Mineralogy and Geochemistry, **74**(1): 169–209.

Arslan, M., Çullu, M., and Durmuş, G. 2011. The effect of antifreeze admixtures on compressive strength of concretes subjected to frost action. Gazi University Journal of Science, **24**(2): 299–307.

Assaad, J.J., Harb, J., and Chakar, E. 2009. Relationships between key ASTM test methods determined on concrete and concrete-equivalent-mortar mixtures. Journal of ASTM International, **6**(3): 1–13.

ASTM. 2003. Standard test method for penetration resistance of hardened concrete. ASTM C803-03/C803M. American Society for Testing and Materials, West Conshohocken, PA, USA.

ASTM. 2006. Standard specification for admixtures for masonry mortars. ASTM C1384-06a. American Society for Testing and Materials, West Conshohocken, PA, USA.

ASTM. 2007. Standard test method for flow of hydraulic cement mortar. ASTM C1437-07. American Society for Testing and Materials, West Conshohocken, PA, USA.

ASTM. 2008. Standard specification for flow table for use in tests of hydraulic cement. ASTM C230/C230M-08. American Society for Testing and Materials, West Conshohocken, PA, USA.

ASTM. 2009. Standard practice for making and curing concrete test specimens in the field. ASTM C31/C31M-09. American Society for Testing and Materials, West Conshohocken, PA, USA.

ASTM. 2010a. Standard specification for cold-weather admixture systems. ASTM C1622-10/1622M. American Society for Testing and Materials, West Conshohocken, PA, USA.

ASTM. 2010b. Standard Specification for Chemical Admixtures for Concrete. ASTM C494/494M-10. American Society for Testing and Materials, West Conshohocken, PA, USA.

ASTM. 2010c. Standard specification for air-entraining admixtures for concrete. ASTM C260/260M-10. American Society for Testing and Materials, West Conshohocken, PA, USA.

ASTM. 2010d. Standard practice for estimating concrete strength by the maturity method. ASTM C1074-10. American Society for Testing and Materials, West Conshohocken, PA, USA.

ASTM. 2010e. Standard Specification for Mortar for Unit Masonry. ASTM C270-10. American Society for Testing and Materials, West Conshohocken, PA, USA.

ASTM. 2011. Standard test method for compressive strength of hydraulic cement mortars (using 2-in. cube specimens). ASTM C109/M109-11. American Society for Testing and Materials, West Conshohocken, PA, USA.

ASTM. 2012a. Standard practice for mechanical mixing of hydraulic cement pastes and mortars of plastic consistency. ASTM C305-12. American Society for Testing and Materials, West Conshohocken, PA, USA.

ASTM. 2012b. Standard Test Method for Preconstruction and Construction Evaluation of Mortars for Plain and Reinforced Unit Masonry. ASTM C780-12. American Society for Testing and Materials, West Conshohocken, PA, USA.

ASTM. 2014. Standard Practice for Mechanical Mixing of Hydraulic Cement Pastes and Mortars of Plastic Consistency. ASTM C305-14. American Society for Testing and Materials, West Conshohocken, PA, USA.

Barna, L.A., Seman, P.M., and Korhonen, C.J. 2010. Cold Weather Admixture Systems Demonstration at Fort Wainwright , Alaska. U.S. Army Cold Regions Research and Engineering Laboratory, Hanover, NH, USA.

Barna, L.A., Seman, P.M., and Korhonen, C.J. 2011. Energy-efficient approach to cold-weather concreting. Journal of Materials in Civil Engineering, **23**(11): 1544–1551.

Barnes, P., Colston, S., Craster, B., Hall, C., Jupe, A.C., Jacques, S., Cockcroft, J., Morgan, S., Johnson, M., O'Connor, D., and Belloto, M. 2000. Time-and space-resolved dynamic studies on ceramic and cementitious materials. Journal of Synchrotron Radiation, **7**(3): 167–177.

Basham, K.D. 2005. Cold-weather concrete construction. Concrete International, **27**(11): 31–34.

Bensted, J., and Barnes, P. 2002. Structure and performance of cements. Spon Press, London.

Birchak, J.R., Gardner, C.G., Hipp, J.E., and Victor, J.M. 1974. High dielectric constant microwave probes for sensing soil moisture. Proceedings of the IEEE, **62**(1): 93–98.

Brook, J.W., Factor, D.F., Kinney, F.D., and Sarkar, A.K. 1988. Cold weather admixtures. Concrete International, **10**(10): 44–49.

Camp, P.R., and Bilotta, S. 1989. Dielectric properties of portland cement paste as a function of

time since mixing. Journal of Applied Physics, **66**(12): 6007–6013.

Černý, R. 2009. Time-domain reflectometry method and its application for measuring moisture content in porous materials: A review. Measurement, **42**(3): 329–336.

Cheung, J., Jeknavorian, A.A., Roberts, L., and Silva, D.A. 2011. Impact of admixtures on the hydration kinetics of portland cement. *In* Conferences Special: Cement Hydration Kinetics and Modeling, Quebec City, 2009 & CONMOD10, Lausanne, 2010. pp. 1289–1309.

CMCA. 2010. Text Book of Canadian Masonry. Canadian Masonry Contractors Association, Mississauga, ON, Canada.

CMDC. 2002. Masonry made EZ, cold weather construction. Bulletin CMDC No. 1. Canada Masonry Design Center, Mississauga, ON, Canada.

CSA. 2004a. Masonry construction for building. Standard CAN/CSA A371-04. Canadian Standards Association, Mississauga, ON, Canada.

CSA. 2004b. Mortar and grout for unit masonry. Standard CAN/CSA A179-04. Canadian Standards Association, Mississauga, ON, Canada.

CSA. 2014. Concrete materials and methods of concrete construction: Test methods and standard practices for concrete. Standard CAN/CSA A23.1-14/A23.2-14. Canadian Standards Association, Mississauga, ON, Canada.

Çullu, M., and Arslan, M. 2013. The effects of antifreeze use on physical and mechanical properties of concrete produced in cold weather. Composites Part B: Engineering, **50**(0): 202–209.

Damle, S. 2009. Optimization of antifreeze admixture formulations. The Pennsylvania State University.

Davis, J.L., and Chudobiak, W.J. 1975. In situ meter for measuring relative permittivity of soils. Geological Survey of Canada, **75**(1): 75–79.

Davison, J.I. 1970. Cold weather masonry construction. *In* Canadian Building Digests 101-150.

National Research Council of Canada, Ottawa, ON, Canada.

Dong, S., Feng, D., Jiang, S., and Zhu, W. 2013. Effect of a new type antifreeze agent on the mechanical behavior of negative temperature concrete. *In* Fourth International Conference on Transportation Engineering. *Edited by* P. Qiyuan and W.C.P. Kelvin. Chengdu, China. pp. 3027–3032.

Engineering ToolBox. 2007. Calcium Chloride and Water. Available from http://www.engineeringtoolbox.com/calcium-chloride-water-d_1186.html [accessed 12 April 2019].

Entus, J. 2000. Use of Time Domain Reflectometry to Monitor Water Content and Electrical Conductivity of Saline Soil. McGill University Libraries.

Fabbri, A., Fen-Chong, T., Azouni, A., and Thimus, J.-F. 2009. Investigation of water to ice phase change in porous media by ultrasonic and dielectric measurements. Journal of Cold Regions Engineering, **23**(2): 69–90.

Fabbri, A., Fen-Chong, T., and Coussy, O. 2006. Dielectric capacity, liquid water content, and pore structure of thawing–freezing materials. Cold Regions Science and Technology, **44**(1): 52–66.

Ford, S.J., Hwang, J.-H., Shane, J.D., Olson, R.A., Moss, G.M., Jennings, H.M., and Mason, T.O. 1997. Dielectric amplification in cement pastes. Advanced Cement Based Materials, **5**(2): 41–48.

Fujiyasu, Y., Pierce, C.E., Fan, L., and Wong, C.P. 2004. High dielectric insulation coating for time domain reflectometry soil moisture sensor. Water resources research, **40**(4): 1–7.

Grant, S.A., Boitnott, G.E., Korhonen, C.J., and Sletten, R.S. 2006. Effect of temperature on hydration kinetics and polymerization of tricalcium silicate in stirred suspensions of CaO-saturated solutions. Cement and Concrete Research, **36**(4): 671–677.

Havers, J.A. 1972. Literature survey of cold weather construction practices. U.S. Army Cold Regions Research and Engineering Laboratory, Hanover, NH, USA.

Hivon, E., and Sego, D.C. 1990. Determination of the unfrozen water content of saline permafrost using time-domain reflectometry (TDR). *In* Proceedings of the 5th Canadian Permafrost Conference. Univ. Laval, Quebec City, QC, Canada. pp. 257–262.

Hover, K. 2002. Avoiding injury in cold weather: For humans and for recently-cast concrete. Concrete International, **24**(11): 31–36.

Huo, J., and Wang, T. 2013. Study of mixed mineral admixtures on microstructure in frost resistance of mixed aggregate concrete. Ready-mixed Concrete, **8**: 65.

IMI. 2010. Cold Weather Masonry Construction. International Masonry Institute, Annapolis, MD, USA.

IMIAWC. 1988. Recommended practices & guide specifications for cold weather masonry construction. International Masonry Industry All-Weather Council, Washington, DC, USA.

Jacobsen, O.H., and Schjonning, P. 1995. Comparison of TDR calibration functions for soil water determination. *In* Proceedings of the Symposium: Time-Domain Reflectometry Applications in Soil Science. Danish Institute of Plant and Soil Science, Lyngby, Denmark. pp. 25–33.

Jaffe, R.C. 2003. Masonry instant answers. McGraw Hill Professional.

Jupe, A.C., Wilkinson, A.P., Luke, K., and Funkhouser, G.P. 2007. Slurry consistency and in situ synchrotron X-Ray diffraction during the early hydration of portland cements with calcium chloride. Journal of the American Ceramic Society, **90**(8): 2595–2602.

Kaatze, U. 1997. The dielectric properties of water in its different states of interaction. Journal of solution chemistry, **26**(11): 1049–1112.

Karagöl, F., Demirboğa, R., Kaygusuz, M.A., Yadollahi, M.M., and Polat, R. 2013. The influence of calcium nitrate as antifreeze admixture on the compressive strength of concrete exposed to low temperatures. Cold Regions Science and Technology, **89**: 30–35.

Karagöl, F., Demirboğa, R., and Khushefati, W.H. 2015. Behavior of fresh and hardened

concretes with antifreeze admixtures in deep-freeze low temperatures and exterior winter conditions. Construction and Building Materials, **76**: 388–395.

Kaufmann, J.P. 2004. Experimental identification of ice formation in small concrete pores. Cement and Concrete Research, **34**(8): 1421–1427.

Kazempour, H., Bassuoni, M.T., and Hashemian, F. 2017. Masonry mortar with nanoparticles at a low temperature. *In* Proceedings of the Institution of Civil Engineers-Construction Materials. pp. 297–308.

Kelly, S.F., Selker, J.S., and Green, J.L. 1995. Using short soil moisture probes with high-bandwidth time domain reflectometry instruments. Soil Science Society of America Journal, **59**(1): 97–102.

Kivekas, L., and Leivo, M. 1985. Research and Use of Antifreeze Admixtures in Finland. *In* The Third International RILEM Symposium on Winter Concreting. Espoo, Finland. pp. 208–222.

Klemunes, J.A. 1995. Determining volumetric moisture using the time domain reflectometry response. University of Maryland.

Knight, J.H., Ferré, P.A., Rudolph, D.L., and Kachanoski, R.G. 1997. A numerical analysis of the effects of coatings and gaps upon relative dielectric permittivity measurement with time domain reflectometry. Water resources research, **33**(6): 1455–1460.

Kocaba, V. 2009. Development and evaluation of methods to follow microstructural development of cementitious systems including slags. Ecole Polytechnique Federale de Lausanne.

Korhonen, C.J. 1990. Antifreeze admixtures for cold regions concreting: A literature review. U.S. Army Cold Regions Research and Engineering Laboratory, Hanover, NH, USA.

Korhonen, C.J. 1999. Expedient low-temperature concrete admixtures for the Army. U.S. Army Cold Regions Research and Engineering Laboratory, Hanover, NH, USA.

Korhonen, C.J. 2002a. Off-the-shelf antifreeze admixtures. U.S. Army Cold Regions Research and Engineering Laboratory, Hanover, NH, USA.

Korhonen, C.J. 2002b. Effect of high doses of chemical admixtures on the freeze–thaw durability of portland cement concrete. U.S. Army Cold Regions Research and Engineering Laboratory, Hanover, NH, USA.

Korhonen, C.J. 2006. Extending the season for concrete construction and repair. Phase II - Defining engineering parameters. U.S. Army Cold Regions Research and Engineering Laboratory, Hanover, NH, USA.

Korhonen, C.J., and Brook, J.W. 1996. Freezing temperature protection admixture for portland cement concrete. U.S. Army Cold Regions Research and Engineering Laboratory, Hanover, NH, USA.

Korhonen, C.J., Chartes, B.A., and Cortez, E.R. 1994a. Pushing the winter concreting envelope. Military Engineer, **86**(565): 8–10.

Korhonen, C.J., Chartes, B.A., and Romisch, K. 1997a. Developing new low-temperature admixtures for concrete. A field evaluation. U.S. Army Cold Regions Research and Engineering Laboratory, Hanover, NH, USA.

Korhonen, C.J., and Cortez, E.R. 1991. Antifreeze admixtures for cold weather concreting. Concrete International, **13**(3): 38–41.

Korhonen, C.J., Cortez, E.R., Chartes, B.A., and Smith, J.C.E. 1994b. Low-temperature admixtures for concrete. *In* 7th International Cold Regions Engineering Specialty Conference. Reston, Virginia: American Society of Civil Engineers, Edmonton, Alberta, Canada.

Korhonen, C.J., Cortez, E.R., Durning, T.A., and Jeknavorian, A.A. 1997b. Antifreeze admixtures for concrete. U.S. Army Cold Regions Research and Engineering Laboratory, Hanover, NH, USA.

Korhonen, C.J., Janoo, V.C., and Berini, C.M. 1997c. Time-domain reflectometry of water

content in portland cement concrete. U.S. Army Cold Regions Research and Engineering Laboratory, Hanover, NH, USA.

Korhonen, C.J., and Orchino, S.A. 2001. Off-the-Shelf Antifreeze Admixture for Concrete Initial Laboratory Investigation. U.S. Army Cold Regions Research and Engineering Laboratory, Hanover, NH, USA.

Korhonen, C.J., Semen, P.M., and Barna, L.A. 2004a. Extending the season for concrete construction and repair. Phase I-Establishing the technology. U.S. Army Cold Regions Research and Engineering Laboratory, Hanover, NH, USA.

Korhonen, C.J., Semen, P.M., and Barna, L.A. 2004b. An off-the-shelf approach to winter concreting. *In* Proceedings, 12th International Specialty Conference on Cold Regions Engineering.

Korhonen, C.J., Thomas, R.D., and Cortez, E.R. 1997d. Increasing cold weather masonry construction productivity. U.S. Army Cold Regions Research and Engineering Laboratory, Hanover, NH, USA.

Kosmatka, S.H., Kerkhoff, B., and Panarese, W.C. 2002. Design and control of concrete mixtures. Portland Cement Association, Skokie, IL.

Krylov, B.A. 1997. Cold weather concreting. CRC Press, Boca Raton, FL.

Kurtz, F.S. 1997. Practitioner's guide to cold weather concreting. ACI International.

Ledieu, J., De Ridder, P., De Clerck, P., and Dautrebande, S. 1986. A method of measuring soil moisture by time-domain reflectometry. Journal of Hydrology, **88**(3–4): 319–328.

Lee, G.C., Shih, T.S., and Chang, K.-C. 1988. Mechanical properties of concrete at low temperature. Journal of cold regions engineering, **2**(1): 13–24.

Lee, S., Zollinger, D., and Lytton, R. 2008. Determining moisture content of soil layers with time domain reflectometry and micromechanics. Transportation Research Record: Journal of the Transportation Research Board, (2053): 30–38.

Lee, S.I. 2010. Development of approach to estimate volume fraction of multiphase material using dielectrics. Texas A&M University.

Li, G. 2014. Effect of Cracks on the Transport Characteristics of Cracked Concrete. University of Saskatchewan.

Li, Q., Ge, Y., and Yang, W. 2016. Effect of sodium sulfate and sodium nitrite on air-void system in air-entrained concrete. Magazine of Concrete Research, **68**(23): 1200–1209.

Lichtenecker, K., and Rother, K. 1931. Die Herleitung des logarithmischen Mischungsgesetzes aus allgemeinen Prinzipien der stationaren Stromung. phys. Z, **32**: 255–260.

Liu, J., Li, Y., Ouyang, P., and Yang, Y. 2015a. Hydration of the silica fume-portland cement binary system at lower temperature. Construction and Building Materials, **93**: 919–925.

Liu, J., Li, Y., Yang, Y., and Cui, Y. 2014. Effect of low temperature on hydration performance of the complex binder of silica fume-portland cement. Journal of Wuhan University of Technology (Mater.Sci.Ed.), **29**(1): 75–81.

Liu, J., and Liu, R. 2008. Prediction of antifreeze critical strength of infant age concrete. Journal of Wuhan University of Technology (Mater.Sci.Ed.), **23(**2): 272–275.

Liu, J., Tian, Y., and Liu, Z. 2007. Study on porosity of low-temperature concrete with mineral admixture. Journal of Shenyang Jianzhu University (Natural Science), **23**(4): 597–601.

Liu, M., Lei, J., Guo, L., Du, X., and Li, J. 2015b. The application of thermal analysis, XRD and SEM to study the hydration behavior of tricalcium silicate in the presence of a polycarboxylate superplasticizer. Thermochimica Acta, **613**: 54–60.

Liu, T., Wang, Y., Zhou, K., Gao, F., and Xie, S. 2019. Research on the Mechanical Properties and NMR Characteristics of Cement Mortar during Freeze-Thaw Cycles. Advances in Civil Engineering, **2019**: 1–7.

Liu, Z., Jiao, W., Sha, A., Gao, J., Han, Z., and Xu, W. 2017a. Portland cement hydration behavior at low temperatures: views from calculation and experimental study. Advances in

Materials Science and Engineering, **2017**.

Liu, Z., Sha, A., Hu, L., Lu, Y., Jiao, W., Tong, Z., and Gao, J. 2017b. Kinetic and thermodynamic modeling of portland cement hydration at low temperatures. Chemical Papers, **71**(4): 741–751.

Liu, Z., Sha, A., Hu, L., and Zou, X. 2017c. A laboratory study of portland cement hydration under low temperatures. Road Materials and Pavement Design, **18**(sup3): 12–22.

Luong, D., Sephton, M.A., and Watson, J.S. 2015. Subcritical water extraction of organic matter from sedimentary rocks. Analytica chimica acta, **879**: 48–57.

McIsaac, G.R. 2010. Time domain reflectometry measurement of water content and electrical conductivity using a polyolefin coated TDR probe. University of Waterloo.

MIC. 1999. Hot & cold weather masonry construction. Masonry Industry Council, Lombard, IL.

Mojid, M.A., Wyseure, G.C.L., and Rose, D.A. 1998. The use of insulated time-domain reflectometry sensors to measure water content in highly saline soils. Irrigation science, **18**(2): 55–61.

Montoya, A. 2012. Sodium nitrate and nitrite. Available from https://www.scribd.com/doc/118061111/30122669-Sodium-Nitrate-and-Nitrite [accessed 12 April 2019].

MSJC. 2011. Specification for masonry structures. TMS 602-11/ACI 530.1-11/ASCE 6-11. Masonry Standards Joint Committee, Boulder, CO., Farmington Hills, MI., Reston, VA., USA.

Olson, R.A., Christensen, B.J., Coverdale, R.T., Ford, S.J., Moss, G.M., Jennings, H.M., Mason, T.O., and Garboczi, E.J. 1995. Interpretation of the impedance spectroscopy of cement paste via computer modelling. Journal of Materials Science, **30**(20): 5078–5086.

Ortiz, J., Aguado, A., Agulló, L., and García, T. 2005. Influence of environmental temperatures on the concrete compressive strength: Simulation of hot and cold weather conditions.

Cement and concrete research, **35**(10): 1970–1979.

Penttala, V. 1998. Freezing-induced strains and pressures in wet porous materials and especially in concrete mortars. Advanced Cement Based Materials, **7**(1): 8–19.

Plank, J., Sakai, E., Miao, C.W., Yu, C., and Hong, J.X. 2015. Chemical admixtures - Chemistry, applications and their impact on concrete microstructure and durability. Cement and Concrete Research, **78**: 81–99.

Polat, R. 2016. The effect of antifreeze additives on fresh concrete subjected to freezing and thawing cycles. Cold Regions Science and Technology, **127**: 10–17.

Puertas, F., Santos, H., Palacios, M., and Martínez-Ramírez, S. 2005. Polycarboxylate superplasticiser admixtures: effect on hydration, microstructure and rheological behaviour in cement pastes. Advances in Cement Research, **17**(2): 77–89.

Qiao, Y., Wang, H., Cai, L., Zhang, W., and Yang, B. 2016. Influence of low temperature on dynamic behavior of concrete. Construction and Building Materials, **115**: 214–220.

Ramachandran, V.S., and Beaudoin, J.J. 2001. Handbook of analytical techniques in concrete science and technology: principles, techniques and applications. Noyes Publication, Park Ridge, NJ.

Ratinov, V.B., and Rozenberg, T.I. 1995. Antifreezing admixtures. *In* Concrete Admixtures Handbook, Propeties Science and Technology. *Edited by* V.S. Ramachandran. Noyes Publication, Park Ridge, NJ. pp. 740–799.

Riding, K., Silva, D.A., and Scrivener, K.L. 2010. Early age strength enhancement of blended cement systems by CaCl2 and diethanol-isopropanolamine. Cement and Concrete Research, **40**(6): 935–946.

Rixom, M.R., and Mailvaganam, N.P. 1999. Chap. 6. Special purpose admixtures. & Chap.7 Application of admixtures. *In* Chemical admixtures for concrete. E&FN Spon, New Fetter Lane, London.

Robinson, D.A., Schaap, M., Jones, S.B., Friedman, S.P., and Gardner, C.M.K. 2003. Considerations for improving the accuracy of permittivity measurement using time domain reflectometry: air-water calibration, effects of cable length. Soil Science Society of America Journal, **67**(1): 62–70.

Roels, S., Carmeliet, J., Hens, H., Adan, O., Brocken, H., Cerny, R., Pavlik, Z., Ellis, A.T., Hall, C., and Kumaran, K. 2004. A comparison of different techniques to quantify moisture content profiles in porous building materials. Journal of Thermal Envelope and Building Science, **27**(4): 261–276.

Roth, C.H., Malicki, M.A., and Plagge, R. 1992. Empirical evaluation of the relationship between soil dielectric constant and volumetric water content as the basis for calibrating soil moisture measurements by TDR. Journal of Soil Science, **43**(1): 1–13.

Saha, O., Boulfiza, M., and Wegner, L.D. accepted-2019. Behavior of masonry mortar containing a non-harmful antifreeze admixture. TMS Journal,.

Saha, O., Boulfiza, M., and Wegner, L.D. under review-a Effect of sodium nitrite-based antifreeze admixtures on the hydration of masonry mortar. ACI Materials Journal,.

Saha, O., Boulfiza, M., and Wegner, L.D. 2015a. Developing antifreeze admixtures for mortar from available off-the-shelf admixtures. *In* 12th North American Masonry Conference. Denver, CO. USA.

Saha, O., Boulfiza, M., and Wegner, L.D. 2015b. Characterization of the hydration products of an antifreeze treated cement paste. *In* CONMAT15. Whistler, BC, Canada.

Sakai, K., Watanabe, H., Nomachi, H., and Hamabe, K. 1991. Antifreeze admixture developed in Japan. Concrete International, **13**(3): 26–30.

Sandberg, P., Porteneuve, C., Serafin, F., Boomer, J., LoConte, N., Gupta, V., Dragovic, B., Doncaster, F., Alioto, L., and Vogt, T. 2007. Effect of admixture on cement hydration kinetics by synchrotron XRD and isothermal calorimetry. *In* Proceedings of the 12th International Congress on the Chemistry of Cement. Montreal, QC, Canada. pp. 663–666.

Scanlon, J.M. 1992. Admixtures - What's new on the market. Concrete International, **14**(10): 28–31.

Scanlon, J.M. 1997. Controlling concrete during hot and cold weather. Concrete International, **19**(6): 52–58.

Scanlon, J.M., and Ryan, R.J. 1989. Placing cold weather concrete. Construction Specifier, **42**(12): 58–65.

De Schepper, M., De Buysser, K., Van Driessche, I., and De Belie, N. 2014. A hydration study by XRD/Rietveld analysis of cement regenerated from completely recyclable concrete. *In* Non-Traditional Cement and Concrete V. NTCC, Brno, Czech Republic.

Schulson, E.M. 1998. Ice damage to concrete. U.S. Army Cold Regions Research and Engineering Laboratory, Hanover, NH, USA.

Senbetta, E., and Bury, M.A. 1991. Control of plastic shrinkage cracking in cold weather. Concrete International, **13**(3): 49–53.

Setzer, M.J. 2001. Micro-ice-lens formation in porous solid. Journal of colloid and interface science, **243**(1): 193–201.

Skibsted, J., and Hall, C. 2008. Characterization of cement minerals, cements and their reaction products at the atomic and nano scale. Cement and Concrete Research, **38**(2): 205–225.

Skierucha, W. 2011. Time domain reflectometry: temperature-dependent measurements of soil dielectric permittivity. Vitaliy Zhurbenko, IntechOpen. Available from https://www.intechopen.com/books/electromagnetic-waves/time-domain-reflectometry-temperature-dependent-measurements-of-soil-dielectric-permittivity.

Smith, M.W., and Tice, A.R. 1988. Measurement of the unfrozen water content of soils. comparison of NMR (Nuclear Magnetic Resonance) and TDR (Time Domain Reflectometry) methods. U.S. Army Cold Regions Research and Engineering Laboratory, Hanover, NH, USA.

Staub, M., Laurent, J.-P., Morra, C., Stoltz, G., Gourc, J.-P., and Quintard, M. 2008. Calibration of time-domain reflectometry probes to measure moisture content in municipal solid waste in laboratory-scale cells. Geo Environmental Engineering,: 1–7.

Sun, Z.J. 2008. Estimating volume fraction of bound water in portland cement concrete during hydration based on dielectric constant measurement. Magazine of Concrete Research, **60**(3): 205–210.

Suprenant, B.A. 1992. Protecting fresh concrete from freezing weather. Concrete Construction, **37**(2): 126–128.

Talero, R., Trusilewicz, L., Delgado, A., Pedrajas, C., Lannegrand, R., Rahhal, V., Mejía, R., Delvasto, S., and Ramírez, F.A. 2011. Comparative and semi-quantitative XRD analysis of Friedel's salt originating from pozzolan and portland cement. Construction and Building Materials, **25**(5): 2370–2380.

Taylor, H.F.W. 1997. Cement Chemistry. Thomas Telford, Heron Quay, London.

Tinga, W.R., Voss, W.A.G., and Blossey, D.F. 1973. Generalized approach to multiphase dielectric mixture theory. Journal of Applied Physics, **44**(9): 3897–3902.

Topp, G.C., Davis, J.L., and Annan, A.P. 1980. Electromagnetic determination of soil water content: Measurements in coaxial transmission lines. Water resources research, **16**(3): 574–582.

Vasović, D., Folić, R.J., and Vasović, T. 2008. Antifreeze water additives applied to fresh concrete in winter conditions. Materijali i konstrukcije, **51**(3): 24–29.

Wang, B.M., Song, K., and Tu, N. 2011. Experimental research on a new-type concrete antifreeze. Applied Mechanics and Materials, **148**–**149**: 1209–1213.

Woodham, D., and Schuller, M. 2005. Masonry construction in cold weather. Concrete International, **27**(11): 27–30.

Xu, L., Wang, P., and Zhang, G. 2012. Formation of ettringite in portland cement/calcium

aluminate cement/calcium sulfate ternary system hydrates at lower temperatures. Construction and Building Materials, **31**: 347–352.

Yamada, K. 2011. Basics of analytical methods used for the investigation of interaction mechanism between cements and superplasticizers. Cement and Concrete Research, **41**(7): 793–798.

Yingzi, Y., and Hengjing, B. 2007. Interface microstructure and mechanical properties of concrete with antifreezing admixture at subzero temperatures. Journal of the Chinese Ceramic Society, **35**(8): 1125–1130.

Yoon, S.S., Kim, S.Y., and Kim, H.C. 1994. Dielectric spectra of fresh cement paste below freezing point using an insulated electrode. Journal of materials science, **29**(7): 1910–1914.

Yu, X., and Liu, Y. 2010. Development of time domain reflectometry instrument for QA/QC of fresh and early stage concrete. National cooperative highway research program. Ohio Department of Transportation,.

Zakri, T., Laurent, J.P., and Vauclin, M. 1998. Theoretical evidence for "Lichtenecker's mixture formulae" based on the effective medium theory. Journal of Physics D: Applied Physics, **31**(13): 1589.

Zhang, N., Liao, J., Zhang, T., Ji, W.Z., Wang, B.H., and Zhang, D.H. 2014. The effect of mineral admixtures on mechanical properties of high-performance concrete at very Low temperature. Applied Mechanics and Materials, **584**: 1509–1513.

APPENDICES

APPENDIX A – COMPARISON OF REPLICATED EXPERIMENTS

This appendix presents the results of the preliminary tests conducted to replicate other authors' experiments reported in the literature. Table A.1 shows a comparison of the results of compressive strength tests on concrete equivalent mortar from Korhonen (1999) and concrete from Karagöl (2013) using the same additive, namely calcium nitrate. While Korhonen published only strength ratios, Karagöl published the compressive strength values as well. It can be seen that the compressive strengths obtained by Karagöl are much higher than those obtained by Korhonen. One possible reason could be the difference in the curing adopted by the two authors. Karagöl tested the samples after an additional 24 hours of post-curing at room temperature. However, this alone cannot explain the big difference between the two author's results.

Table A.1 Comparison of Korhonen (1999) and Karagöl (2013) compressive strength results using calcium nitrate as antifreeze

Calcium Nitrate $Ca(NiO_3)_2$=6%		**Korhonen curing temperature (°C)**				**Karagöl curing temperature (°C) + 1d**			
		-5	**-10**	**-15**	**-20**	**-5**	**-10**	**-15**	**-20**
-7d	(MPa)					35.9	18.2	16.1	15.5
-14d						26.3	24.2	16.3	6.5
-28d						33.2	10.8	5.4	4.1
-28d+28d						57.5	52.9	51.3	47.0
-7d	(%)	3.2	3.1		1.9	69.8	35.5	31.3	30.2
-14d		8.9	3.1		1.9	51.2	47.1	31.7	12.7
-28d		12.0	2.1		0.7	64.6	20.9	10.4	8.0
-28d+28d		92.2	98.8		84.3	111.9	102.9	99.8	91.4

The effect of calcium nitrite on the compressive strength of concrete equivalent mortar samples cured at subfreezing temperatures was reported by Korhonen (1999). A comparison of replicated tests conducted at -10°C is presented in Table A.2. In this table, only the relative strength results, as compared to the control sample at 28 days, are presented. The results show a good agreement for 7 and 14 days, and a larger discrepancy at 28 days. Comparing the results of Saha for calcium nitrite and Karagöl (2013) for calcium nitrate at -10°C with 24 hours of post curing shows again a significant difference. One reason could be the use of cement Type CEM 42 as compared to mortar cement Type S, and w/c=0.4 as compared to w/c=0.443 for Karagöl and Saha respectively.

Table A.2 Comparison of Korhonen (1999) and Saha compressive strength results using calcium nitrite with and without one day of post-curing

Calcium Nitrite		**Curing Temperature (°C)**				**Curing Temperature (°C) + 1d**			
$Ca(NiO_2)_2$=6%		**-5**	**-10**	**-15**	**-20**	**-5**	**-10**	**-15**	**-20**
			Korhonen				**Karagöl (Sodium Nitrate)**		
-7d	(%)	44.8	4.4		1.1		35.5		
-14d		73.0	9.1		1.5		47.1		
-28d		80.0	16.5		2.0				
-28d+28d		143.5	124.1		118.0				
			Saha				**Saha**		
-7d	(%)		5.0				28.9		
-14d			8.3				28.7		
-28d			7.6						

The main specifications for each experiment were as follow:

- Karagöl: w/c=0.4, cement Type CEM42, curing temperature -5 to -20, samples tested after 24 h of post-curing.
- Korhonen: w/c=0.41, cement Type I, curing temperature -5 to -20, samples tested as they reach +5°C (approximately 2 h).
- Saha: w/c=0.443, mortar cement type S, curing -10, samples tested after 2 h and 24 h of post-curing.
- The admixture concentration was 6% by cement weight for all experiments.
- In all experiments, samples were put in the freezing chamber right after mixing and casting.

APPENDIX B – CONCRETE EQUIVALENT MORTAR MIX DESIGN

Due to the numerous concrete equivalent mortar (CEM) mixes needed in this work, a spreadsheet was developed based on the work of Assaad et al. (2009) and Korhonen (2006). A macro command was also written to automatically calculate the ingredients for the mixes generated by the statistic surface design and to record the results to the side of the percentage proportions. The interface of the spreadsheet is shown in Figure B.1.

The input parameters are in the dark lines of the top section and defined as follow:

w/c	Water to cement ratio
a/c	Aggregate to cement ratio
Batch volume (ml)	Target volume of mortar expected for the mix
Admixtures %	The amount of the five admixtures in the mix relative to the manufacturer maximum recommended dosage
Comb. #	Selection of one set defining a combination of five admixture proportions, used for manual selection
Limits	Used to delimit the range of the mix designs to be generated by the Excel VB macro command
Start	Gives the first line in the spreadsheet where the macro command will start automatically generating the mix designs
Total	Number of lines included in the statistical design (29 combinations in the case of incomplete response surface design with five factors and three level each)

The output parameters are shown in the two lighter lines in the bottom section of the interface and are defined as follow:

Ingredients (g)	Shows the resulting content required for the specified mix design of the three main ingredients in grams, namely Cement, Sand and Water
Admixtures (ml)	Shows the resulting admixtures required for the specified mix design of the five admixtures in milliliters

% solid Shows the total percent dissolved solid in the mix based on the percent solid content of the admixtures

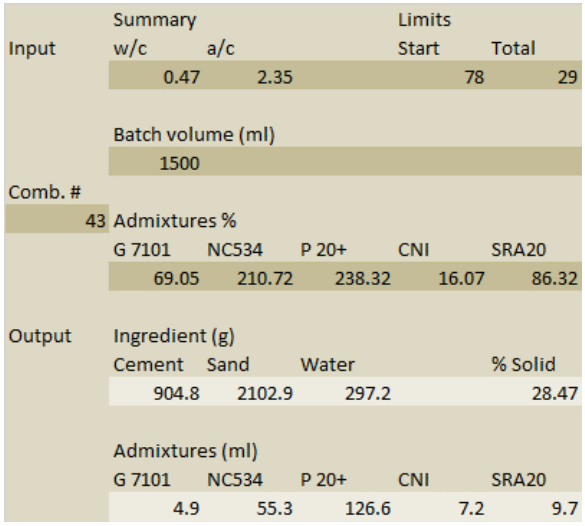

Figure B.1 Input and Output section of the CEM proportioning spreadsheet

The first step in the mix design composition was to determine the weight of the main three ingredients required to make a unit volume of mortar. Detailed calculations are shown in Table B.1. In this case the volume chosen was 1000 ml (1 *l*), and the initial cement dosage used to make 1 m^3 of concrete (including coarse aggregates) was 474 kg/m^3 or 474 g/l.

Table B.1 CEM composition for a unit volume of 1000 *ml*

	Spec. Gravity	**Weight prop.**	**Weight (g)**	**Volume (ml)**	**Norm. Vol. (ml)**	**Weight (g/l)**
cement	3.15	1.00	474.0	150.48	191.49	603.20
w/c	1.0	0.47	222.8	222.78	283.50	283.50
fa/c	2.7	2.35	1113.9	412.56	525.01	1417.52
Total			1810.7	785.8	1000	2304.2

where:

Weight = initial cement dosage (474g) x Weight proportions

Volume = Weight / Specific Gravity

Norm. Vol. = Volume x 1000 / Total Volume

Weight = Normalized Volume x Specific Gravity

The second step was to recalculate the weight of the three ingredients to reach the target volume using the simple rule of three. In this example, the target volume was 1500 ml resulting in Cement = 904.8 g, Total Water = 425.3 g, and Sand = 2126.2 g.

The third step was to calculate the volume (or weight) of the five admixtures based on their respective statistic design ratio (Table B.2)

Table B.2 Admixtures dosage and their water content for a mix design

Admixture Name	**G 7101**	**NC534**	**P 20+**	**CNI**	**SRA20**
Max dosage (ml)	0.78	2.0	5.87	30	7.5
Units	l/100kg	l/100kg	l/100kg	l/m^3	l/m^3
Spec. Gravity	1.059	1.399	1.35	1.295	1.01
Percent solid (%)	0.31	0.51	0.45	0.325	0.01
Water Content (%)	0.73	0.69	0.74	0.87	1.00
Batch design ratio (%)	69.0	210.7	238.3	16.1	86.3
Admix. Vol. (ml)	4.87	55.29	126.58	7.23	9.71
Water in Admix. (ml)	3.56	37.90	93.98	6.32	9.71

where

Max dosage = The maximum recommended dosage, provided by the manufacturer

Units = The units used to measure the admixture dosage in the mix, l/100 kg of cement or l/m^3 of concrete

Specific Gravity = Admixture specific gravity, provided by the manufacturer

Percent solid = Average percent solid in the admixture, provided by the manufacturer

Water content = (Specific Gravity) x (1 – Percent solid)

Batch design ratio = percentage of the admixtures to combine in a mix, based on the statistic experimental design

Admixture Volume = (Max dosage) x (Batch design ratio) x (Cement weight or Batch volume) the formula includes unit adjustment

Water in Admixture = (Admixture volume) x (Water content)

Total percent solid = $\frac{\sum_{Admix} \%Solid_i \times (Specific\_gravity_i \times Volume_i)}{Total\ water}$

The fourth step was to adjust the mixing water and sand by accounting for the water content of the liquid admixtures and the moisture content of the sand. For this purpose, the two following equations were used:

$$\text{Water to add} = (Total\ Water) - \sum(Water\ in\ Admix) + (Water\ Adsorbed\ by\ sand)$$

$$\text{Sand to add} = (Sand) \times \left(1 - \frac{\%Sand\ adsorption - \%Sand\ Moisture\ Content}{100}\right)$$

The last step was to run the Excel VB macro command to loop through all the combinations defined in the cells “Start” and “Total” representing the scope of the statistic experimental design list. The results were recorded in the adjacent columns.

The three main statistical experimental designs are shown in Table B.3 through Table B.5. The last column in each table displays the measured freezing point of that mortar mix.

Table B.3 First response surface design experiment

StdOrder	G 7101	NC534	P 20+	CNI	SRA 20	Cement	Sand	Water	G 7101	NC534	P 20+	CNI	SRA 20	%Solid	FP
1	0	0	0	0	100	144.0	391.7	60.1	0.0	0.0	0.0	0.0	1.9	0.03	-0.9
2	100	0	0	0	0	144.0	391.7	61.1	1.1	0.0	0.0	0.0	0.0	0.64	-0.7
3	0	100	0	0	0	144.0	391.7	59.1	0.0	4.2	0.0	0.0	0.0	5.17	-1.4
4	100	100	0	0	100	144.0	391.7	56.4	1.1	4.2	0.0	0.0	1.9	5.85	-2.0
5	0	0	100	0	0	144.0	391.7	55.7	0.0	0.0	8.5	0.0	0.0	8.92	-2.2
6	100	0	100	0	100	144.0	391.7	53.0	1.1	0.0	8.5	0.0	1.9	9.59	-2.3
7	0	100	100	0	100	144.0	391.7	50.9	0.0	4.2	8.5	0.0	1.9	14.12	-3.6
8	100	100	100	0	0	144.0	391.7	52.0	1.1	4.2	8.5	0.0	0.0	14.73	-3.3
9	0	0	0	100	0	144.0	391.7	55.4	0.0	0.0	0.0	7.5	0.0	5.48	-0.7
10	100	0	0	100	100	144.0	391.7	52.7	1.1	0.0	0.0	7.5	1.9	6.15	-1.3
11	0	100	0	100	100	144.0	391.7	50.7	0.0	4.2	0.0	7.5	1.9	10.69	-2.6
12	100	100	0	100	0	144.0	391.7	51.7	1.1	4.2	0.0	7.5	0.0	11.29	-2.2
13	0	0	100	100	100	144.0	391.7	47.3	0.0	0.0	8.5	7.5	1.9	14.43	-2.9
14	100	0	100	100	0	144.0	391.7	48.3	1.1	0.0	8.5	7.5	0.0	15.03	-2.9
15	0	100	100	100	0	144.0	391.7	46.3	0.0	4.2	8.5	7.5	0.0	19.57	-3.5
16	100	100	100	100	100	144.0	391.7	43.6	1.1	4.2	8.5	7.5	1.9	20.24	-4.1
17	0	50	50	50	50	144.0	391.7	53.2	0.0	2.1	4.2	3.8	0.9	9.80	-2.0
18	100	50	50	50	50	144.0	391.7	52.4	1.1	2.1	4.2	3.8	0.9	10.44	-2.4
19	50	0	50	50	50	144.0	391.7	54.2	0.6	0.0	4.2	3.8	0.9	7.53	-1.3
20	50	100	50	50	50	144.0	391.7	51.3	0.6	4.2	4.2	3.8	0.9	12.71	-2.4
21	50	50	0	50	50	144.0	391.7	55.9	0.6	2.1	0.0	3.8	0.9	5.66	-1.0
22	50	50	100	50	50	144.0	391.7	49.6	0.6	2.1	8.5	3.8	0.9	14.58	-2.8
23	50	50	50	0	50	144.0	391.7	56.0	0.6	2.1	4.2	0.0	0.9	7.38	-2.1
24	50	50	50	100	50	144.0	391.7	49.5	0.6	2.1	4.2	7.5	0.9	12.86	-2.5
25	50	50	50	50	0	144.0	391.7	53.7	0.6	2.1	4.2	3.8	0.0	10.10	-1.9
26	50	50	50	50	100	144.0	391.7	51.8	0.6	2.1	4.2	3.8	1.9	10.14	-2.2
27	50	50	50	50	50	144.0	391.7	52.8	0.6	2.1	4.2	3.8	0.9	10.12	-2.0
28	50	50	50	50	50	144.0	391.7	52.8	0.6	2.1	4.2	3.8	0.9	10.12	-2.0
29	50	50	50	50	50	144.0	391.7	52.8	0.6	2.1	4.2	3.8	0.9	10.12	-4.7

Table B.4 Second response surface design experiment

StdOrder	MNC1	NC534	P 20+	CNI	SRA20	Cement	Sand	Water	MNC15	P NC53	P 20+	CNI	SRA20	%Solid	FP
1	0	200	280	100	125	144.0	391.7	29.8	0.0	8.4	23.7	7.5	2.3	40.8	-9.05
2	100	200	280	100	75	144.0	391.7	30.7	5.8	8.4	23.7	7.5	1.4	50.8	-13.4
3	0	250	280	100	75	144.0	391.7	29.3	0.0	10.4	23.7	7.5	1.4	43.4	-8.9
4	100	250	280	100	125	144.0	391.7	28.3	5.8	10.4	23.7	7.5	2.3	53.4	-14.3
5	0	200	320	100	75	144.0	391.7	28.2	0.0	8.4	27.1	7.5	1.4	44.4	-9.5
6	100	200	320	100	125	144.0	391.7	27.3	5.8	8.4	27.1	7.5	2.3	54.4	-15.35
7	0	250	320	100	125	144.0	391.7	25.8	0.0	10.4	27.1	7.5	2.3	47.0	-10.1
8	100	250	320	100	75	144.0	391.7	26.8	5.8	10.4	27.1	7.5	1.4	57.0	-15.3
9	0	200	280	150	75	144.0	391.7	27.4	0.0	8.4	23.7	11.3	1.4	43.6	-8.9
10	100	200	280	150	125	144.0	391.7	26.5	5.8	8.4	23.7	11.3	2.3	53.6	-15
11	0	250	280	150	125	144.0	391.7	25.1	0.0	10.4	23.7	11.3	2.3	46.2	-9.9
12	100	250	280	150	75	144.0	391.7	26.0	5.8	10.4	23.7	11.3	1.4	56.1	-15
13	0	200	320	150	125	144.0	391.7	24.0	0.0	8.4	27.1	11.3	2.3	47.1	-10.1
14	100	200	320	150	75	144.0	391.7	24.9	5.8	8.4	27.1	11.3	1.4	57.1	-15.2
15	0	250	320	150	75	144.0	391.7	23.5	0.0	10.4	27.1	11.3	1.4	49.7	-9.9
16	100	250	320	150	125	144.0	391.7	22.5	5.8	10.4	27.1	11.3	2.3	59.7	-15.2
17	0	225	300	125	100	144.0	391.7	26.6	0.0	9.4	25.4	9.4	1.9	45.3	-9.8
18	100	225	300	125	100	144.0	391.7	26.6	5.8	9.4	25.4	9.4	1.9	55.3	-15
19	50	200	300	125	100	144.0	391.7	27.3	2.9	8.4	25.4	9.4	1.9	49.0	-11.3
20	50	250	300	125	100	144.0	391.7	25.9	2.9	10.4	25.4	9.4	1.9	51.6	-11.2
21	50	225	280	125	100	144.0	391.7	27.9	2.9	9.4	23.7	9.4	1.9	48.5	-11.3
22	50	225	320	125	100	144.0	391.7	25.4	2.9	9.4	27.1	9.4	1.9	52.0	-11.6
23	50	225	300	100	100	144.0	391.7	28.3	2.9	9.4	25.4	7.5	1.9	48.9	-11.5
24	50	225	300	150	100	144.0	391.7	25.0	2.9	9.4	25.4	11.3	1.9	51.6	-11.8
25	50	225	300	125	75	144.0	391.7	27.1	2.9	9.4	25.4	9.4	1.4	50.3	-11.2
26	50	225	300	125	125	144.0	391.7	26.2	2.9	9.4	25.4	9.4	2.3	50.3	-11.6
27	50	225	300	125	100	144.0	391.7	26.6	2.9	9.4	25.4	9.4	1.9	50.3	-11.85
28	50	225	300	125	100	144.0	391.7	26.6	2.9	9.4	25.4	9.4	1.9	50.3	-12.05
29	50	225	300	125	100	144.0	391.7	26.6	2.9	9.4	25.4	9.4	1.9	50.3	-12.15

Table B.5 Full factorial design

StdOrder	MNC15	NC534	P 20+	Cement	Sand	Water	MNC15 P	NC534	P 20+	%Solid	FP
1	50	100	100	144.0	391.7	52.8	2.9	4.2	8.5	19.1	-5.3
2	50	100	200	144.0	391.7	46.5	2.9	4.2	16.9	28.0	-6.8
3	50	100	300	144.0	391.7	40.3	2.9	4.2	25.4	36.9	-8.3
4	50	200	100	144.0	391.7	50.0	2.9	8.4	8.5	24.3	-6.8
5	50	200	200	144.0	391.7	43.7	2.9	8.4	16.9	33.2	-7.7
6	50	200	300	144.0	391.7	37.4	2.9	8.4	25.4	42.1	-9.2
7	100	100	100	144.0	391.7	52.8	5.8	4.2	8.5	24.1	-6.9
8	100	100	200	144.0	391.7	46.5	5.8	4.2	16.9	33.0	-9.2
9	100	100	300	144.0	391.7	40.3	5.8	4.2	25.4	41.9	-10.5
10	100	200	100	144.0	391.7	50.0	5.8	8.4	8.5	29.3	-8
11	100	200	200	144.0	391.7	43.7	5.8	8.4	16.9	38.2	-9.7
12	100	200	300	144.0	391.7	37.4	5.8	8.4	25.4	47.1	-11.8

APPENDIX C – RESPONSE SURFACE DESIGN – FULL DATA

In Chapter 4, the response surface design method was used to minimize the freezing point of masonry mortar mixtures made with a combination of five admixtures at a time. This appendix presents the full results of two iterations of the incomplete surface design experiment and the associated steepest descent, as well as one factorial design with the three most efficient admixtures.

First Iteration of the Response Surface Design

For the first iteration of the response surface design, the statistical analysis of the linear regression is given in the two tables below. Table C.1 shows the linear regression coefficients with their associated statistical parameters. Table C.2 shows the analysis of variance (ANOVA) table. The main effects of the five admixtures used in the first iteration of the surface design experiment are presented in Figure 4.3. The effects of two factors at a time by fixing the other three factors are presented in Figure C.1.

Table C.1 Estimated regression coefficients for the FP (Iteration 1)

Term	Coef.	SE Coef.	T	P
Constant	-0.3847	0.1305	-2.947	0.007
HRWR	-0.0009	0.0011	-0.807	0.428
Accel	-0.0110	0.0011	-9.988	0
WR + Accel	-0.0164	0.0011	-14.932	0
Corros.	-0.0047	0.0011	-4.237	0
Shrink	-0.0034	0.0011	-3.128	0.005

Adj R^2=92.52%

Table C.2 Analysis of variance for the FP (Iteration 1)

Source	DF	Seq SS	Adj SS	Adj MS	F	P
Regression	5	19.1633	19.1633	3.8327	70.22	0
Linear	5	19.1633	19.1633	3.8327	70.22	0
Residual Error	23	1.2553	1.2553	0.0546		
Lack-of-Fit	21	1.2286	1.2286	0.0585	4.39	0.202
Pure Error	2	0.0267	0.0267	0.0133		
Total	28	20.4186				

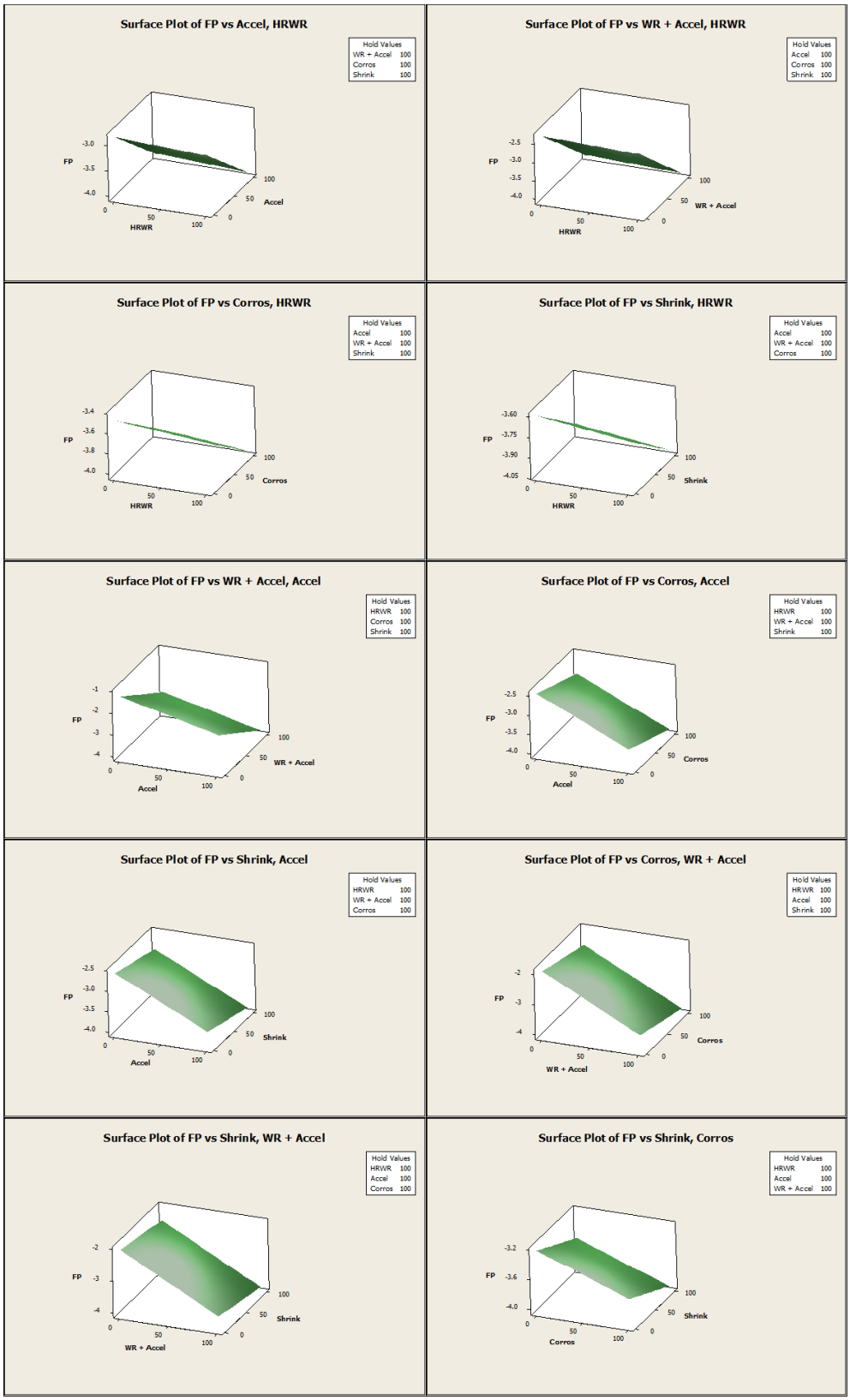

Figure C.1 Surface representation of two factors in each graph (Iteration 1)

The regression equation between the freezing point (FP) and the total percent solid of the combined admixtures is given by the equation below, with the statistical significance of the regression factors and the ANOVA table given in Table C.3 and Table C.4. Figure C.2 shows the main effect of the percent solid on the freezing point, which shows a fairly monotonic decrease as the percent solid increases.

$$FP = -0.506 - 0.168 \times \%solid$$

Table C.3 Regression analysis: FP versus %Solid

Predictor	Coef.	SE Coef.	T	P
Constant	-0.5056	0.1504	-3.36	0.002
%Solid	-0.1681	0.0135	-12.43	0

Adj R^2=84.6%

Table C.4 Analysis of variance: FP versus %Solid

Source	DF	SS	MS	F	P
Regression	1	17.381	17.381	154.47	0
Residual Error	27	3.038	0.113		
Total	28	20.419			

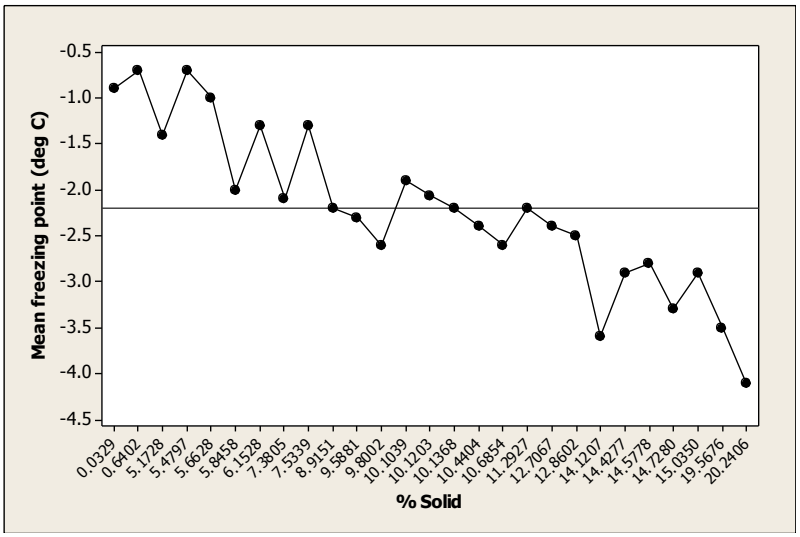

Figure C.2 Freezing point as function of the percent solid (Iteration 1)

First Steepest Descent

The results of the first steepest descent are shown in Table C.5 and graphically in Figure C.3

Table C.5 Freezing point as a function of the gradient factor

Factor	%Solid	Calculated (°C)	FP Measured (°C)
0	10.10	-2.2	-2.6
4000	19.29	-3.9	-4.4
7000	26.16	-5.1	-5.9
10000	33.04	-6.4	-7.5
13000	39.91	-7.7	-8.4
16000	46.79	-9.0	-9.8
19000	53.66	-10.2	-9.5

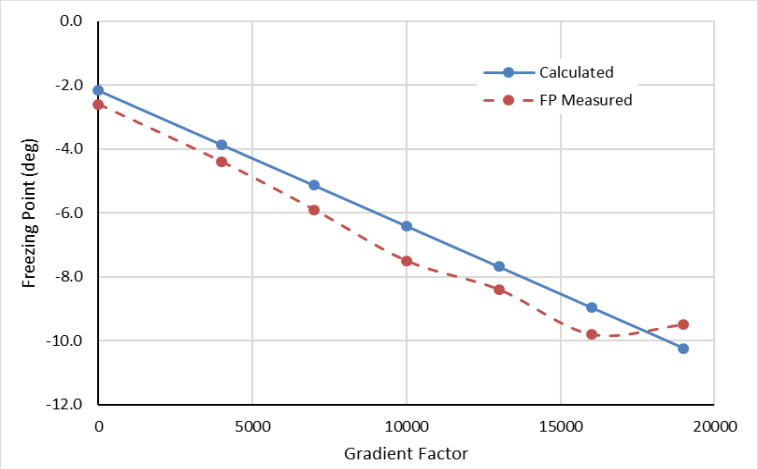

Figure C.3 Calculated and measured freezing points vs. gradient factor (Iteration 1)

Second Iteration of the Response Surface Design

For the second iteration of the response surface design, developed around the minimum identified in the first steepest descent, the statistical analysis of the linear regression is given in the two tables below. Table C.6 shows the linear regression coefficients with their associated statistic parameters. Table C.7 shows the ANOVA table. The main effect of the five admixtures used in the second iteration of the surface design are presented in Figure 4.4. The effect of two factors at a time by fixing the other three factors are presented in Figure C.4.

Table C.6 Estimated regression coefficients for the FP (Iteration 2)

Term	Coef.	SE Coef.	T	P
Constant	-1.1866	2.0585	-0.576	0.570
MNC15	-0.0529	0.0022	-23.986	0.000
Accel	-0.0044	0.0044	-1.008	0.324
WR + Accel	-0.0181	0.0055	-3.275	0.003
Corros.	-0.0080	0.0044	-1.814	0.083
Shrink	-0.0073	0.0044	-1.663	0.110

Adj R^2=95.46%

Table C.7 Analysis of variance for the FP (Iteration 2)

Source	DF	Seq SS	Adj SS	Adj MS	F	P
Regression	5	129.77	129.77	25.954	118.63	0
Linear	5	129.77	129.77	25.954	118.63	0
Residual Error	23	5.032	5.032	0.2188		
Lack-of-Fit	21	4.985	4.985	0.2374	10.17	0.093
Pure Error	2	0.047	0.047	0.0233		
Total	28	134.802				

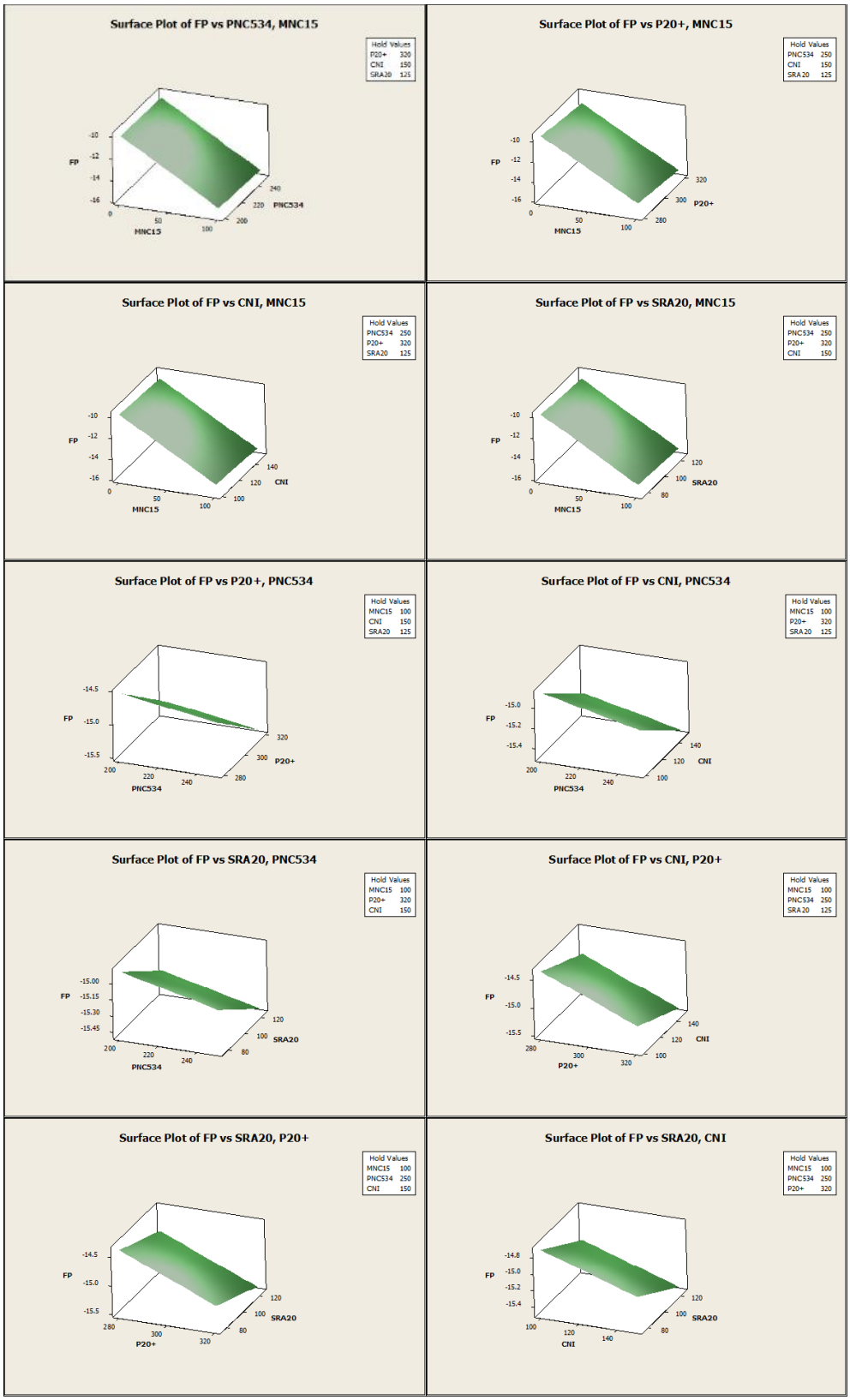

Figure C.4 Surface representation of two factors in each graph (Iteration 2)

The regression equation, for the second iteration, between the freezing point and the total percent solid of the combined admixtures is given by the equation below, with the statistical significance of the regression factors and the ANOVA table given in Table C.8 and Table C.9. Figure C.5 shows the main effect of the percent solid on the freezing point. The intercept of the linear regression equation is positive in this case, however, the slope is almost three times steeper.

$$FP = 10.651 - 0.450 \times \%solid$$

Table C.8 Regression analysis: FP versus %Solid

Predictor	Coef.	SE Coef.	T	P
Constant	10.651	1.773	6.01	0
%Solid	-0.450	0.035	-12.82	0

Adj R^2=85.4%

Table C.9 Analysis of variance: FP versus %Solid

Source	DF	SS	MS	F	P
Regression	1	115.77	115.77	164.26	0
Residual Error	27	19.03	0.70		
Total	28	134.80			

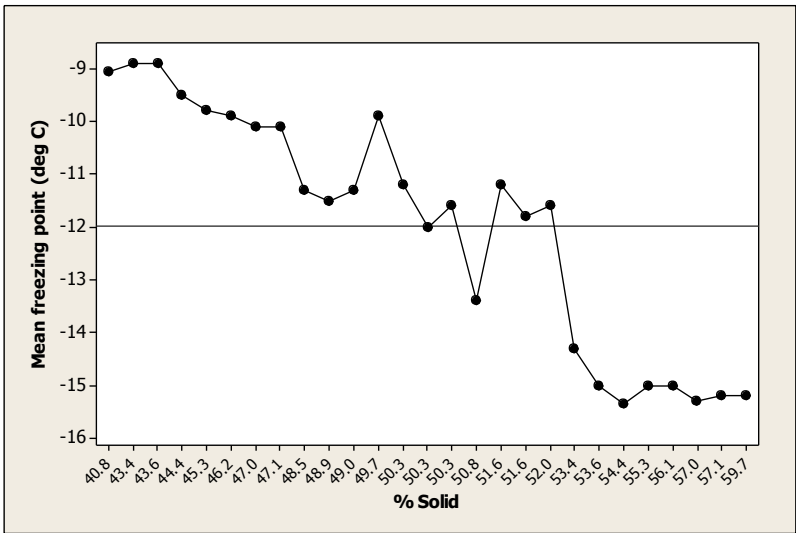

Figure C.5 Freezing point as function of the percent solid (Iteration 2)

Second Steepest Descent

Following the second response surface design, a second steepest descent was performed. The linear regression and the corresponding graph are shown in Table C.10 and Figure C.6. The difference between the calculated and the measured freezing points is more important in this steepest iteration, showing a gap of about 10°C at the highest dosage as opposed to less than 1°C in the first iteration of the steepest descent.

Table C.10 Freezing point as a function of the gradient factor

Factor	%Solid	Calculated (°C)	FP Measured (°C)
0	38.59	-10.2	-8.8
2000	53.27	-16.6	-13.5
3000	60.61	-19.8	-14.9
4000	67.94	-23.0	-17.3
5000	75.28	-26.2	-19.0
6000	82.62	-29.4	-21.8
7000	89.96	-32.6	-22.9

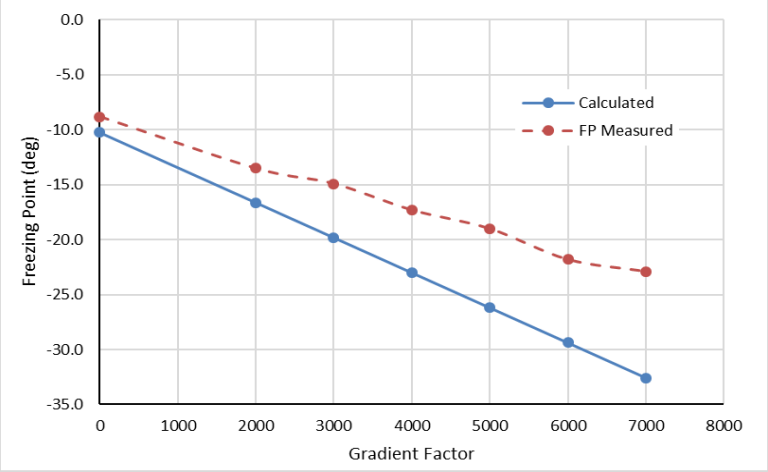

Figure C.6 Calculated and measured freezing points vs. gradient factor (Iteration 2)

Factorial Design

The three more efficient admixtures identified from the previous iterations were used in a full factorial design with two levels for the antifreeze and the accelerator, and three levels for the water reducer + accelerator. The linear regression equation and the statistical significance of the coefficients are given below in Table C.11 and Table C.12. The main effect of each factor alone is shown in Figure C.7.

$$FP = -0.600 - 0.040 \times MNC15 - 0.010 \times PNC534 - 0.016 \times P20+$$

Table C.11 Regression analysis of FP versus MNC15, PNC534, P20+

Term	Coef.	SE Coef.	T	P
Constant	-0.600	0.4751	-1.26	0.242
MNC15	-0.040	0.0038	-10.52	0
Accel	-0.010	0.0019	-5.44	0.001
WR + Accel	-0.016	0.0012	-13.75	0

Adj R^2=96.27%

Table C.12 Analysis of variance for FP

Source	DF	SS	MS	F	P
Regression	3	35.683	11.894	109.79	0
Error	8	0.867	0.108		
Total	11	36.55			

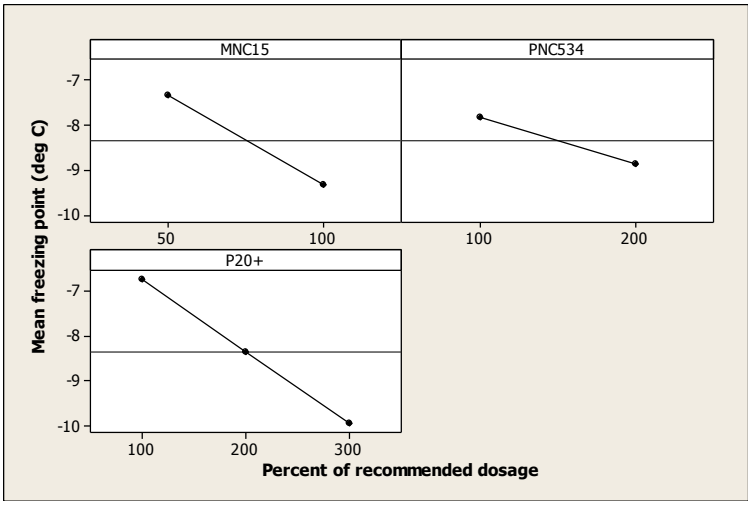

Figure C.7 Main effect of the three most effective admixtures (Factorial Design)

APPENDIX D – XRD CRYSTALLINE REFERENCE DATA USED

Table D.1 through Table D.4 list the most common mineral phases present in the cement and its hydrated products along with the reference to their crystallography identification cards. They were used as the reference cards to identify the phases of interest during the XRD analysis.

Table D.1 Structures of phases potentially present in OPC clinkers

Phase	**Formula**	**Crystal system**	**ICSD codes**	**PDF codes**	**Ref** (Aranda et al. 2012)
Alite	Ca_3SiO_5-Mg,Al	Monoclinic/M3	94742	01-070-8632	De la Torre
				00-055-0740	
				01-073-0599	
	Ca_3SiO_5-Mg	Triclinic/T3	162744	NA	De la Torre
	Ca_3SiO_5	Triclinic/T1	4331	01-070-1846	Golovastikov
	Ca_3SiO_5	Monoclinic		00-049-0442	Mumme
Belite	Ca_2SiO_4	Monoclinic/β	81096	01-086-0398	Mumme
	Ca_2SiO_4	Orthorhombic/α'	81097	01-086-0399	Mumme
	Ca_2SiO_4	Orthorhombic/γ	81095	01-086-0397	Mumme
	Ca_2SiO_4	Monoclinic		00-033-0302	NIST
Aluminate	$Ca_3Al_2O_6$	Cubic	1841	01-070-0839	Mondal, Jeffry
	$Ca_{8.5}NaAl_6O_{18}$	Orthorhombic	100220	01-083-1359	Takeuchi
	$Ca_{8.25}Na_{1.5}Al_6O_{18}$	Monoclinic	100221	01-083-1360	Takeuchi
Ferrite	Ca_2AlFeO_5	Orthorhombic	9197	01-071-0667	Colville, Geller
Lime	CaO	Cubic	52783	01-071-4121	Smith, Leider
Periclase	MgO	Cubic	9863	01-071-1176	Sasaki
Arcanite	K_2SO_4	Orthorhombic	79777	01-083-0681	Ojima
Aphthitalite	$K_3Na(SO_4)_2$	Rhombohedral	26018	01-074-0398	Okada, Ossaka
Thenardite	Na_2SO_4	Orthorhombic	81506	00-037-1465	Rasmussen
Ca-Langbenite	$Ca_2K_2(SO_4)_3$	Orthorhombic	40989	01-074-0404	Speer, Salje
Sulfate-spurrite	$Ca_5(SiO_4)_2(SO_4)$	Orthorhombic	85123	01-088-0812	Irran
Ellesteadite	$Ca_{10}(SiO_4)_3(SO_4)3Cl_2$	Hexagonal	154205	00-041-0479	Saint-Jean, Hansen
Fluorellesteadite	$Ca_{10}(SiO_4)3(SO_4)3F_2$	Hexagonal	97203	01-072-7301	Pajares
Mayenite	$Ca1_2Al_{14}O_{33}$	Cubic	241243	70-2144	Palacios

Table D.2 Structures of additional phases potentially present in OPC (blended) cements

Phase	**Formula**	**Crystal system**	**ICSD codes**	**PDF codes**	**Ref** (Aranda et al. 2012)
Gypsum	$CaSO_4.2H_2O$	Monoclinic	151692	33-0311	De la Torre
Hemihydrate	$CaSO_4.0.5H_2O$	Monoclinic	79528	01-083-0438	Bezou
Anhydrite-III	$CaSO_4$	Hexagonal	24473	01-073-1942	Floerke
Anhydrite-II	$CaSO_4$	Orthorhombic	16382	01-072-0916	Kirfel, Will
Syngenite	$K_2Ca(SO_4)2.H_2O$	Monoclinic	157072	28-0739	Ballirano
Calcite	$CaCO_3$	Rhombohedral	80869	01-086-0174	Maslen
Dolomite	$CaMg(CO_3)_2$	Rhombohedral	31277	01-075-1711	Effenberger
Quartz	SiO_2	Rhombohedral	41414	46-1045	Will
Gehlenite	$Ca_2Al_2SiO_7$	Tetragonal	87144	01-089-5917	Louisnathan
Yeelemite	$Ca_4A1_6SO_{16}$	Orthorhombic	80361	42-1478	Carlos
	$Ca_4A1_6SO_{16}$	Cubic	9560	01-071-0969	Saalfeld, Depmeire
Mullite	Al_4SiO_8	Orthorhombic	23867	01-073-1389	Sandanaga
Yoshiokaite	$Ca_{5.5}Al_{11}Si_5O_{32}$	Rhombohedral	69380	01-080-1547	Steele, Pluth
Hematite	Fe_2O_3	Rhombohedral	82904	01-087-1166	Sawanda
Magnetite	Fe_3O_4	Cubic	49549	01-077-1545	Fleet
Wollastonite	$CaSiO_3$	Monoclinic	30884	00-043-1460	Hesse
Rankinite	$Ca_3Si_2O_7$	Monoclinic	2282	01-070-1138	Saburi
Merwinite	$Ca_3Mg(SiO_4)_2$	Monoclinic	43078	01-089-2432	Yamaguch, Suzuki
Akermanite	$Ca_2Mg(Si_2O_7)$	Tetragonal	158177	00-035-0592	Gemmi
Monticellite	$CaMg(SiO_4)$	Orthorhombic	34591	00-035-0590	Onken

Table D.3 Structures of additional phases potentially present in OPC hydration products

Phase	Formula	Crystal system	ICSD codes	PDF codes	Ref (Aranda et al. 2012)
Gibbsite	$A1(OH)_3$	Monoclinic	6162	01-070-2038	Saalfeld, Wedde
Tobermorite	$Ca_5Si_6O_{16}(OH)_{2.7}H_2O$	Monoclinic	152489	00-029-0331	Bonaccorsi
Jennite	$Ca_9Si_6O_{18}(OH)_{6.8}H_2O$	Triclinic	151413	00-018-1206	Bonaccorsi
Hydrogarnet or C3AH6	$Ca_3Al_2(OH)_{12}$	Cubic	202316	01-084-1354	Lager
Katoite	$Ca_3Al_2(OH)_{7.6}(SiO_4)_{1.1}$	Cubic	172077	00-038-0368	Ferro
AFt					
Ettringite	$Ca_6Al_2(OH)_{12}(SO_4)3.2$ $6H_2O$	Rhombohedral	155395	00-041-1451	Goetz-Neunhoeffer, Neubauer
Ettr-CO3	$Ca_6Al_2(OH)_{12}(CO_3)3.2$ $6H_2O$	Structure not reported		00-036-1465	McMurdie
Thaumasite	$Ca_6Si_2(OH)_{12}(CO_3)_2(SO_4)2$ $.24H_2O$	Hexagonal	31247	01-075-1688	Effenberger
AFm					
Kuzelite or C_4ASH_{12}	$Ca_4Al_2(OH)_{12}[SO_4].6H_2O$	Rhombohedral	100138	01-083-1289	Allmann
Friedel's salt	$Ca_4Al_2(OH)_{12}[Cl]2.4H_2O$	Rhombohedral	88617	01-089-8294	Renaudin & Rousselot
Kuzel's salt	$Ca_4Al_2(OH)_{12}[(SO_4)_{0.5}Cl].$ $5H_2O$	Rhombohedral		00-019-0203	Mesbah
Monocarbo-aluminate	$Ca_4Al_2(OH)_{12}[CO_3].5H_2O$	Triclinic	59327	01-087-0493	Fancois
Hydrocalumite	$Ca_4Al_2(OH)_{12}[Cl(CO_3)_{0.5}].$ $4.8H_2O$	Monoclinic	63250	01-078-2050	Sacerdoti, Passaglia
Hemicarbo-aluminate	$Ca_4Al_2(OH)_{12}[OH(CO_3)_{0.5}]$ $.5.5H_20$	Structure not reported		00-041-0221	
C2AH8	$Ca_4Al_2(OH)_{12}[Al(OH)_4]2.$ $6H_2O$	Structure not reported		00-011-0205	
Stratlingite or C2ASH8	$Ca_4Al_2(OH)_{12}[AlSi(OH)_8]$ $2.2H_2O$	Rhombohedral	69413	01-080-1579	Rinaldi

Table D.4 Structures of phases used as additives in the experimental program

Phase	Formula	Crystal system	PDF codes	Ref
Sodium Nitrite	$NaNO_2$	Monoclinic	00-006-0392	
Corundum	Al_2O_3	Rhombohedral		
Calcium Silicon	$CaSi_2$	Rhombohedral	00-047-1518	Nakano

APPENDIX E – ICP-MS RESULTS

Inductively coupled plasma mass spectrometry (ICP-MS) is a technique used to detect metals, even at very low concentrations. The inductively coupled plasma is responsible for ionizing the elements, and the mass spectrometry is responsible for separating and detecting the particles based on their mass-to-charge ratio. Sample preparation consists of a lengthy concentrated acid digestion process, followed by the ICP-MS experiment on the digested solution.

Table E.1 and Table E.2 show the main elemental contents of the commercial antifreeze admixture MNC-C15 and the treated hydrated cement paste as determined using the ICP-MS analysis technique.

Table E.1 MNC-C15 Antifreeze (ppm)

Name	Li	B	Na	Mg	Al	P	K	Ca
MNC-C15	23.33	14.49	271543.48	272.18	11909.04	95.17	ud	1787.18
MNC-C15R	22.75	14.68	274919.49	263.24	11876.75	93.24	ud	1740.47
% wt.	0.002	0.001	27.323	0.027	1.189	0.009	ud	0.176

Table E.2 Antifreeze treated cement paste (ppm)

Name	Li	Na	Mg	Al	K	Ca	Mn	Fe
A+1	13.15	7839.87	19307.96	24618.12	3719.75	325396.85	222.05	15645.49
A+1R	13.18	7834.72	18952.39	24045.14	3728.29	322082.51	223.01	15571.39
% wt.	0.00	0.78	1.93	2.46	0.37	32.54	0.02	1.56

APPENDIX F – XRF RESULTS

Figure F.1 and Figure F.2 show the results of the XRF analysis for the antifreeze admixture and four of the treated and control cement pastes. Description of the samples is provided in Table F.1.

Client: UofS
Contact: Ouafi Saha
Samples: 2

SRC Advanced Microanalysis Centre
125 - 15 Innovation Blvd, Saskatoon, SK, S7N 2X8
Tel: 306.933.7893 Fax: 306.933.5656 Email: microlab@src.sk.ca

XRF Analysis
40 mm Loose Powder

Samples	Na_2O Wt%	MgO Wt%	Al_2O_3 Wt%	SiO_2 Wt%	P_2O_5 Wt%	K_2O Wt%	CaO Wt%	TiO_2 Wt%	MnO Wt%	Fe_2O_3 Wt%	S Wt%	Sum Wt%
GSP2 Std	2.37	0.900	14.4	65.6	0.280	5.46	1.96	0.599	0.038	4.80	0.038	96.4
Admix	27.9	0.020	2.25	3.75	0.050	<0.01	1.06	0.200	<0.01	0.520	5.38	41.1
Admixdup	28.0	0.010	2.22	3.72	0.060	<0.01	0.480	0.200	<0.01	0.510	5.41	40.6
Admix200	32.1	0.040	2.32	3.72	0.060	<0.01	0.500	0.189	<0.01	0.490	6.99	46.4
LLD	0.01	0.01	0.01	0.03	0.01	0.01	0.01	0.01	0.01	0.01	0.01	

Figure F.1 XRF results of the antifreeze admixture

Client: UofS
Contact: Ouafi Saha
Samples: 4

SRC Advanced Microanalysis Centre
125 - 15 Innovation Blvd, Saskatoon, SK, S7N 2X8
Tel: 306.933.7893 Fax: 306.933.5656 Email: microlab@src.sk.ca

XRF Analysis
40 mm Loose Powder

Samples	Na_2O Wt%	MgO Wt%	Al_2O_3 Wt%	SiO_2 Wt%	P_2O_5 Wt%	K_2O Wt%	CaO Wt%	TiO_2 Wt%	MnO Wt%	Fe_2O_3 Wt%	S Wt%	Sum Wt%
A-3	1.69	2.39	6.91	19.5	0.090	0.640	43.2	0.085	0.011	1.40	1.84	77.8
A-1	1.50	2.59	7.36	19.9	0.100	0.650	43.7	0.088	0.012	1.41	2.00	79.3
A-1dup	1.44	2.55	6.99	19.6	0.110	0.660	43.7	0.087	0.011	1.41	1.96	78.5
A+1	1.17	2.15	5.87	20.4	0.100	0.620	41.9	0.088	0.011	1.38	1.57	75.2
C+1	0.019	2.21	5.60	21.6	0.110	0.650	43.4	0.082	0.011	1.38	1.44	76.4
GSP2 Std	2.68	1.00	15.3	67.2	0.280	5.47	2.01	0.628	0.038	4.82	0.041	99.5
LLD	0.01	0.01	0.01	0.03	0.01	0.01	0.01	0.01	0.01	0.01	0.01	

Figure F.2 XRF results of the hydrated cement pastes

Table F.1 XRF samples description

Sample	Description
Admix	MNC-C15 admixture raw form
AdmixDup	MNC-C15 admixture raw form, duplicated test
Admix200	MNC-C15 admixture lightly crushed and passing 200μm sieve
A-3	Admixture added paste cured at -10°C for 3 days
A-1	Admixture added paste cured at -10°C for 1 day
A-1dup	Admixture added paste cured at -10°C for 1 day, duplicated test
A+1	Admixture added paste cured at +23°C for 1 day
C+1	Control cement paste cured at +23°C for 1 day
GSP2 Std	Reference standard
LLD	Lower limit of detection

APPENDIX G – FREEZE DRYING GRAVIMETRY

One of the techniques used to arrest the hydration was the freeze-drying. The principle of the freeze-drying technique is to cool the material to a very low temperature, -80°C in this case, then to vacuum the air to a very low pressure. This puts the water below the triple point of the phase diagram. As the temperature rises, the frozen water turns into vapor by sublimation without passing through the liquid phase, to prevent any further hydration. Gravimetry measurements were taken before and after the freeze-drying process and the results are represented in Figure G.1 and Figure G.2. Samples labeled "A" are antifreeze treated and samples labeled "C" are control. The signs indicate the curing temperature, where "+" refers to room temperature and "–" refers to -10°C.

There is a clear difference between the room temperature and below freezing temperature curing that can be seen in Figure G.1. Clearly the retained water increases rapidly with time for the room temperature for both the control and the antifreeze treated samples. However, the bound water at below freezing temperature does not show the same clear pattern. Nevertheless, the antifreeze samples "A-" display a slightly higher water retention than the samples "C-". In both cases of curing temperatures, the antifreeze treated paste shows a slightly higher water retention. Conversely, the reverse comments can be stated about the evaporated water shown in Figure G.2.

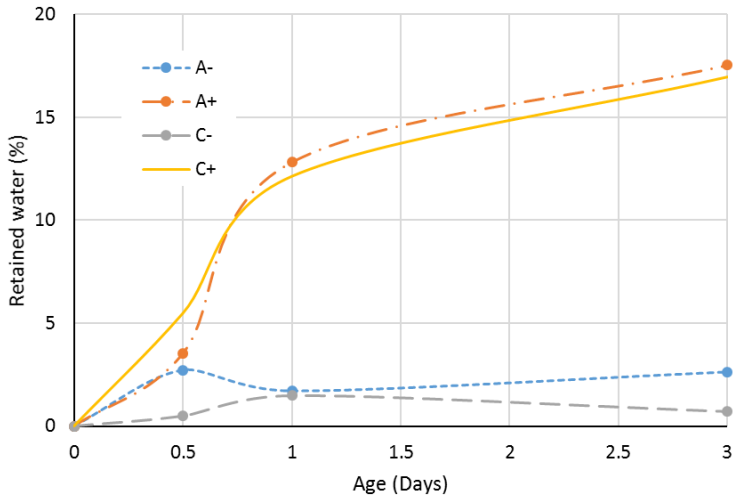

Figure G.1 Retained (bound) water by initial water content

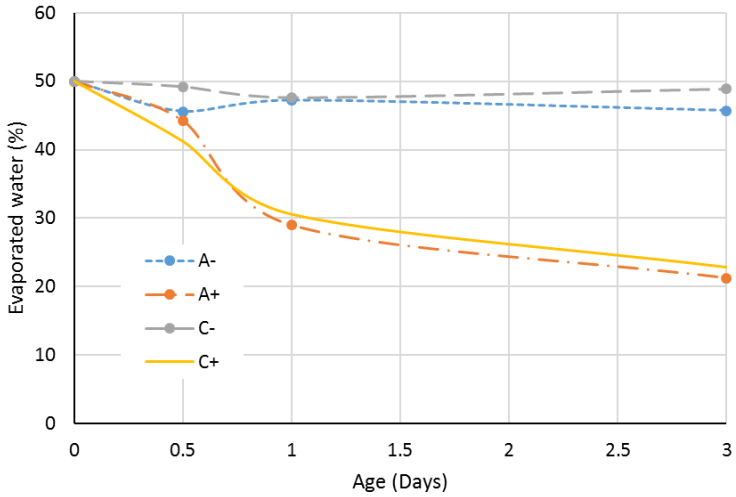

Figure G.2 Evaporated water by cement weight

APPENDIX H – XRD SPECTROGRAMS

This appendix shows all the XRD spectrograms performed during the characterization phase. The horizontal axis represents 2θ (deg) and the vertical represents the count rate (unitless).

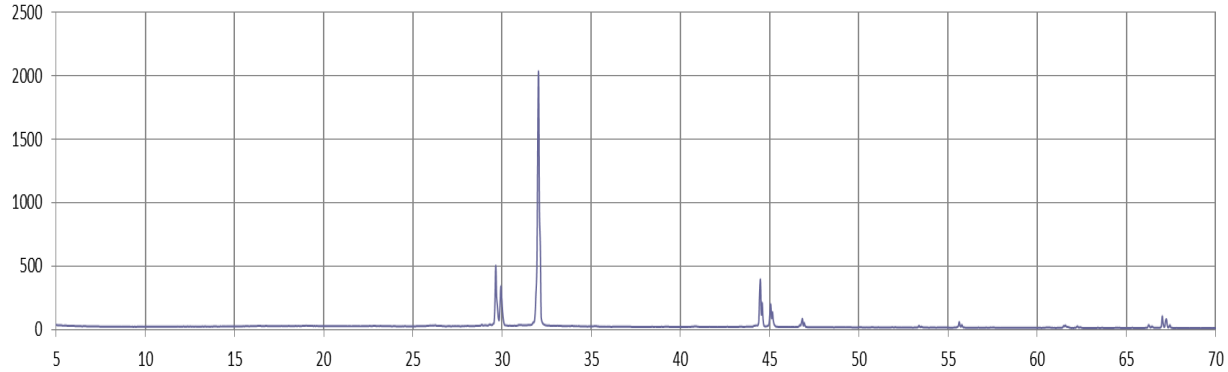

Figure H.1 XRD diffractogram of the admixture MNC-C15

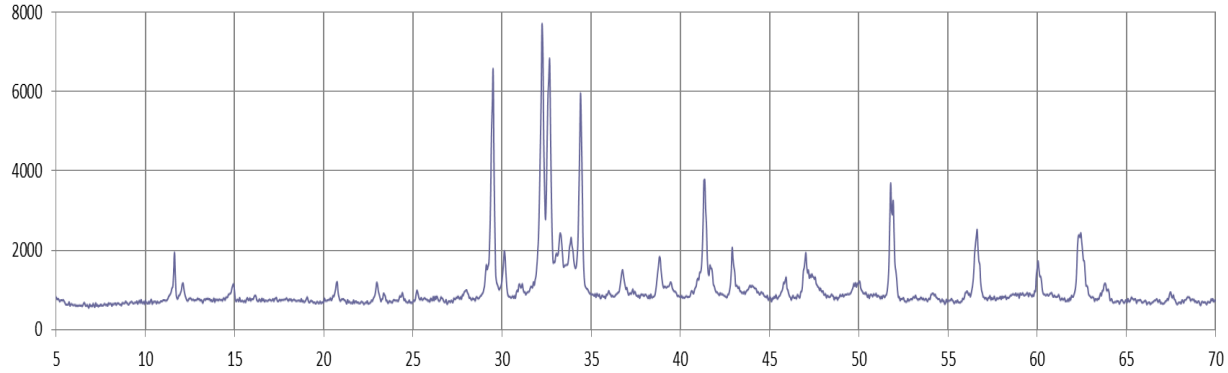

Figure H.2 XRD diffractogram of the cement Type GU

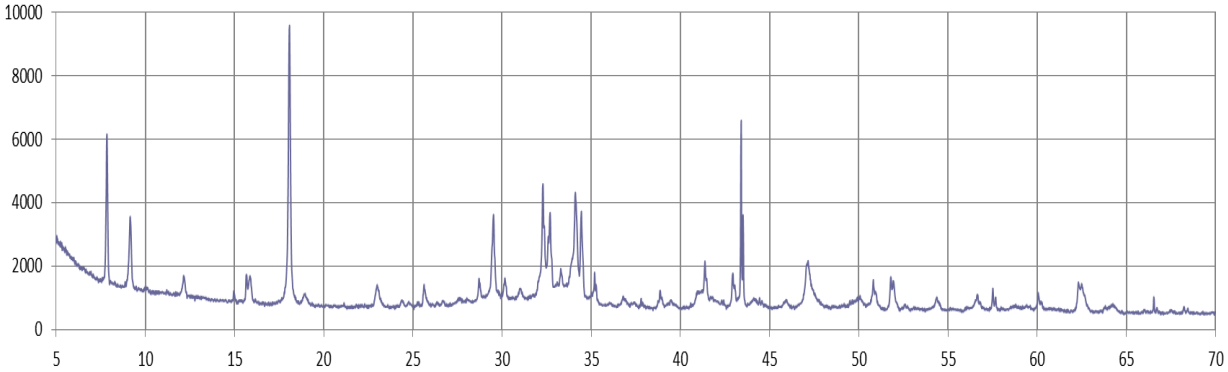

Figure H.3 XRD diffractogram of the sample C+1
(Control paste cured at 23°C for 1 day)

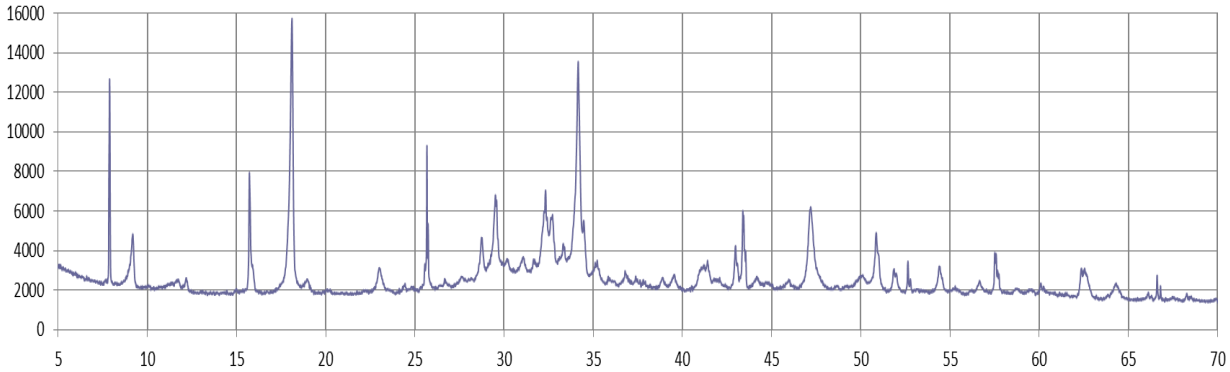

Figure H.4 XRD diffractogram of the sample C+3
(Control paste cured at 23°C for 3 days)

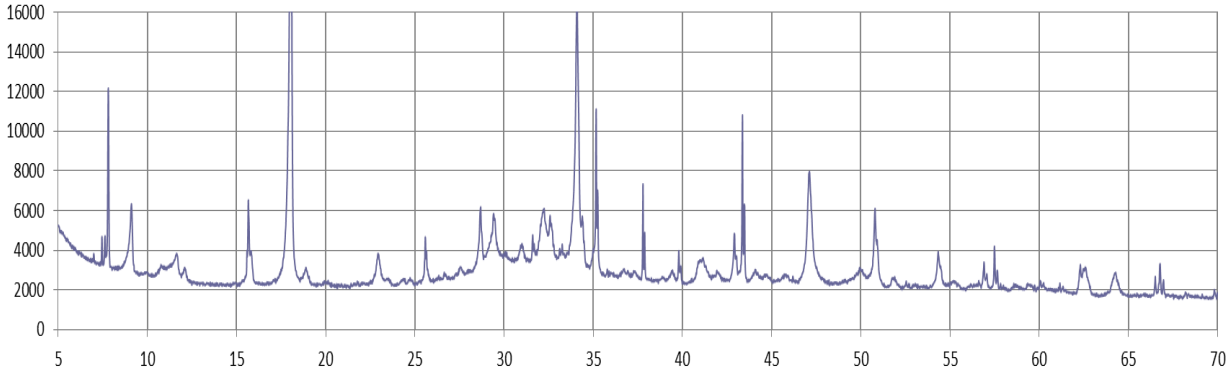

Figure H.5 XRD diffractogram of the sample C+7
(Control paste cured at 23°C for 7 days)

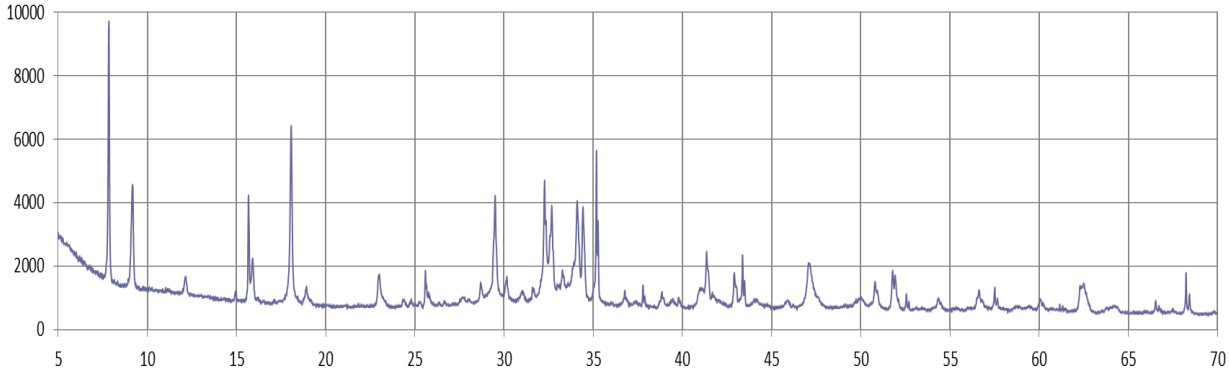

Figure H.6 XRD diffractogram of the sample A+1
(Admixture added paste cured at 23°C for 1 day)

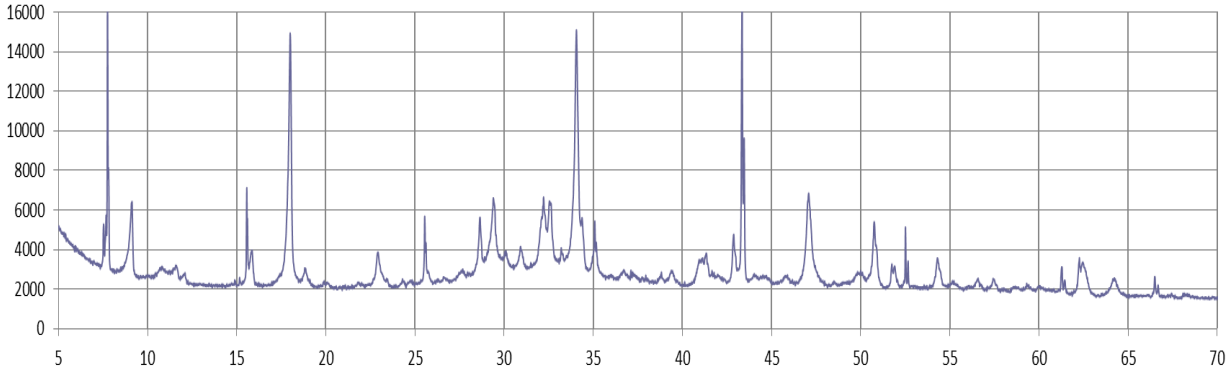

Figure H.7 XRD diffractogram of the sample A+3
(Admixture added paste cured at 23°C for 3 days)

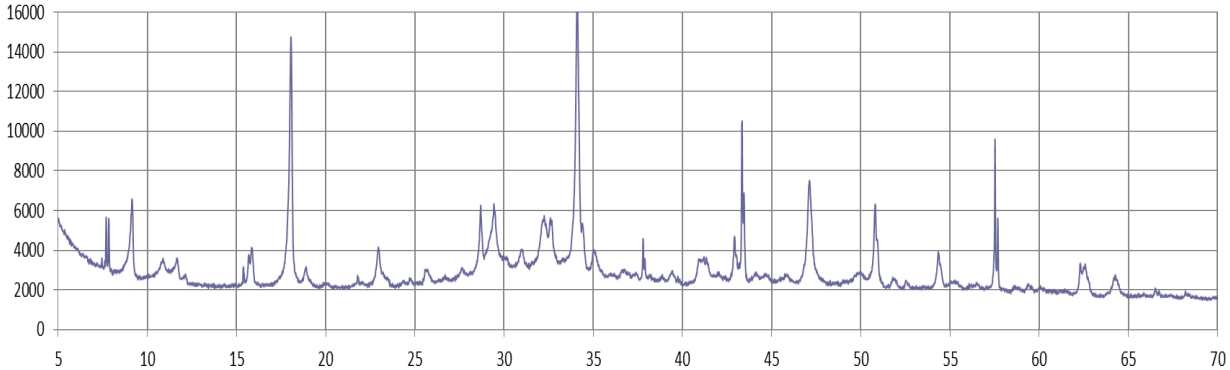

Figure H.8 XRD diffractogram of the sample A+7
(Admixture added paste cured at 23°C for 7 days)

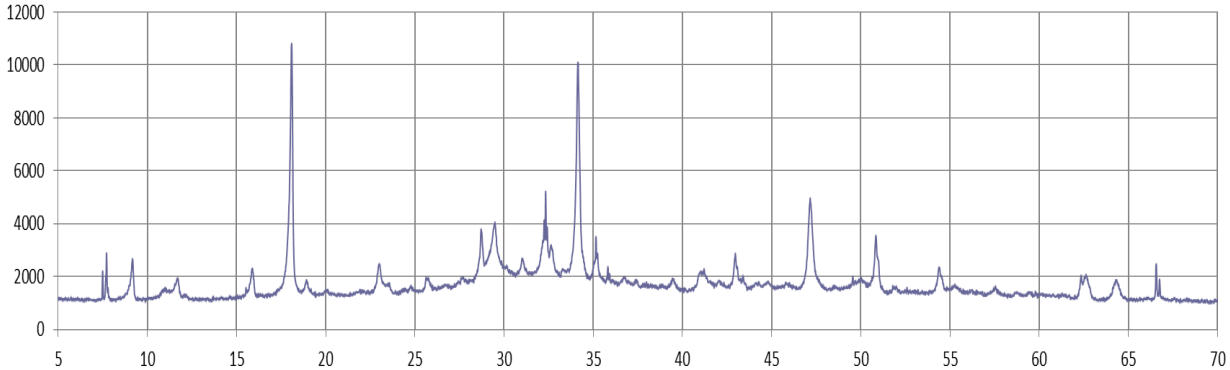

Figure H.9 XRD diffractogram of the sample A+28
(Admixture added paste cured at 23°C for 28 days)

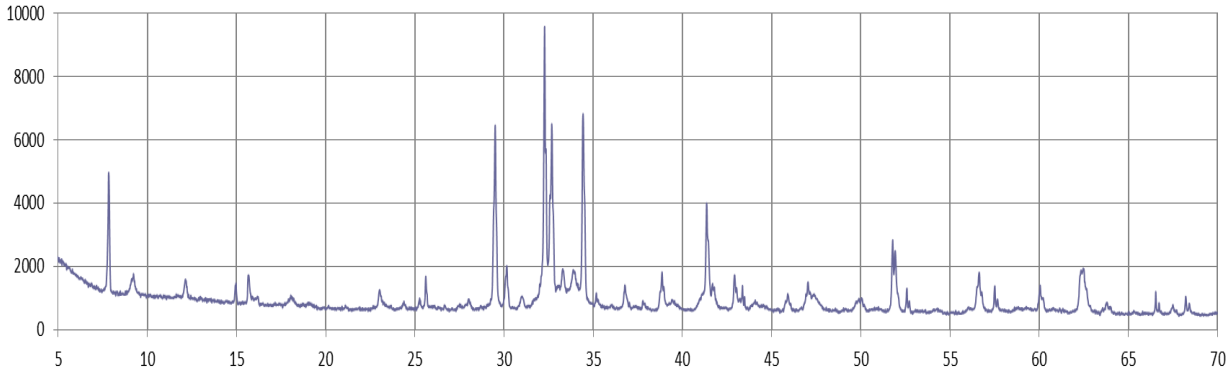

Figure H.10 XRD diffractogram of the sample A-1
(Admixture added paste cured at -10°C for 1 day)

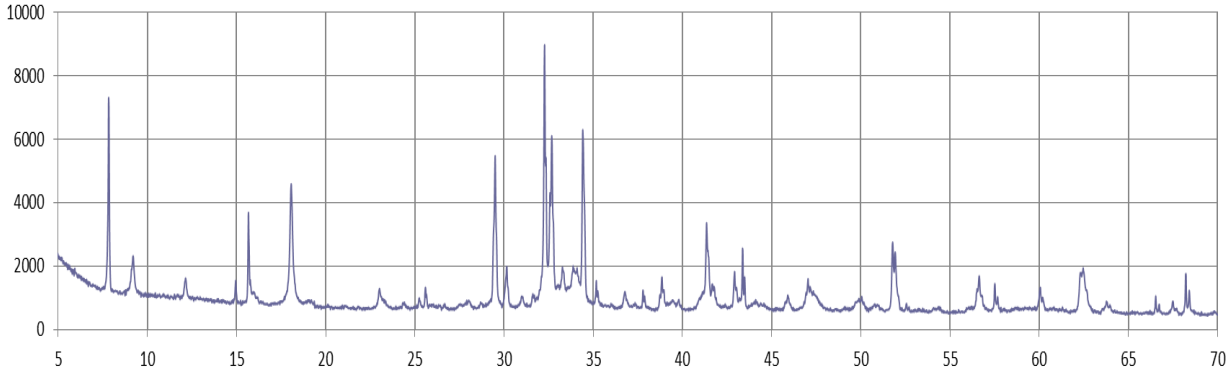

Figure H.11 XRD diffractogram of the sample A-3
(Admixture added paste cured at -10°C for 3 days)

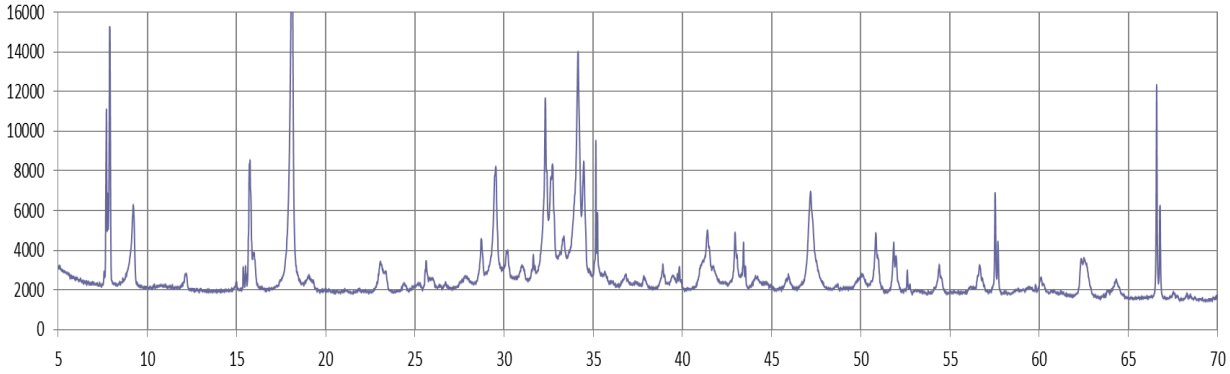

Figure H.12 XRD diffractogram of the sample A-28
(Admixture added paste cured at -10°C for 28 days)

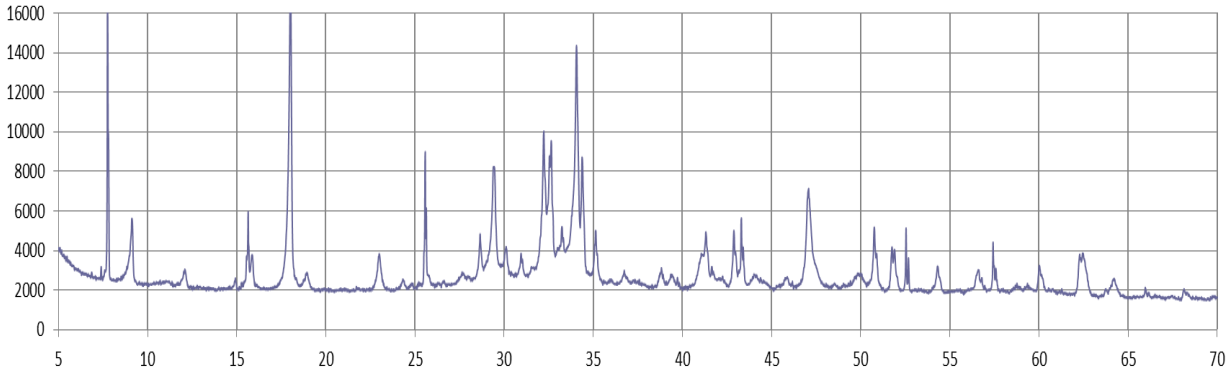

Figure H.13 XRD diffractogram of the sample Na+1
(Sodium nitrite added paste cured at 23°C for 1 day)

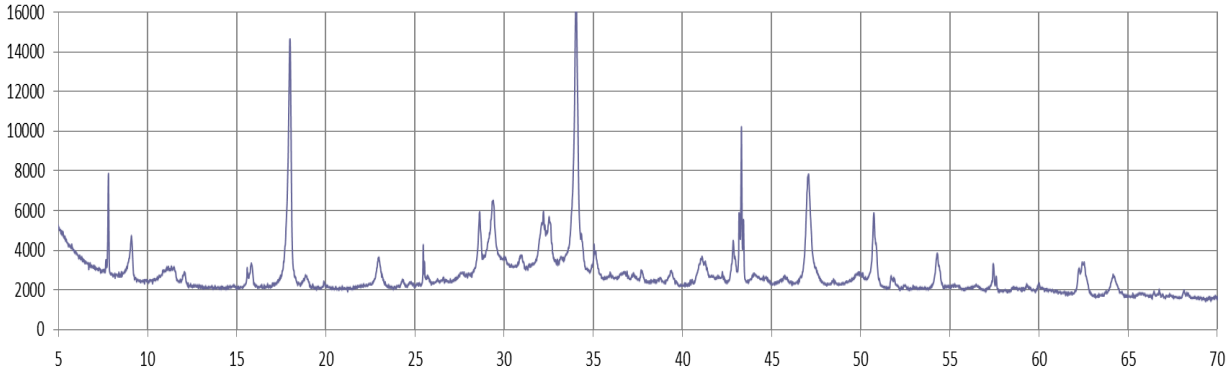

Figure H.14 XRD diffractogram of the sample Na+7
(Sodium nitrite added paste cured at 23°C for 7 days)

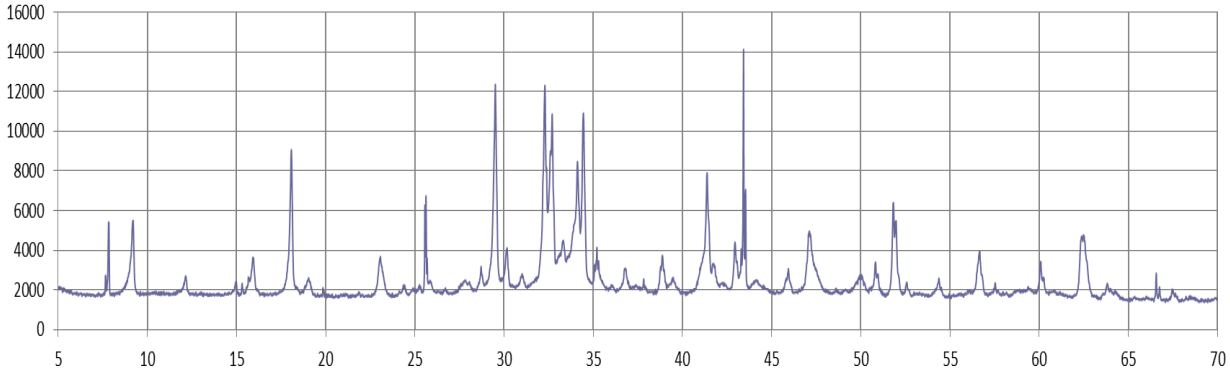

Figure H.15 XRD diffractogram of the sample Na-7
(Sodium nitrite added paste cured at -10°C for 7 days)

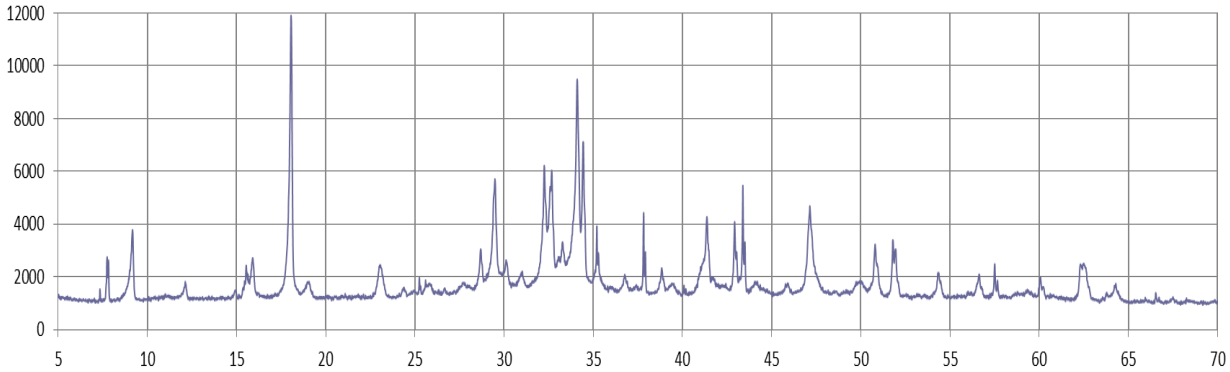

Figure H.16 XRD diffractogram of the sample Na-28
(Sodium nitrite added paste cured at -10°C for 28 days)

APPENDIX I – TDR AIR – WATER CALIBRATION

Prior to curing the various cement paste mixes, an Air-Water calibration was performed, and the raw data collected are represented in Figure I.1 through Figure I.7. The horizontal axis represents the apparent length and the vertical axis represents the relative conductivity (or reflection coefficient).

The simplified formula to calculate the dielectric constant is: $K_{app} = \left(\frac{L_{app}}{L_p}\right)^2$, were L_{app} is the apparent length and L_p is the probe length.

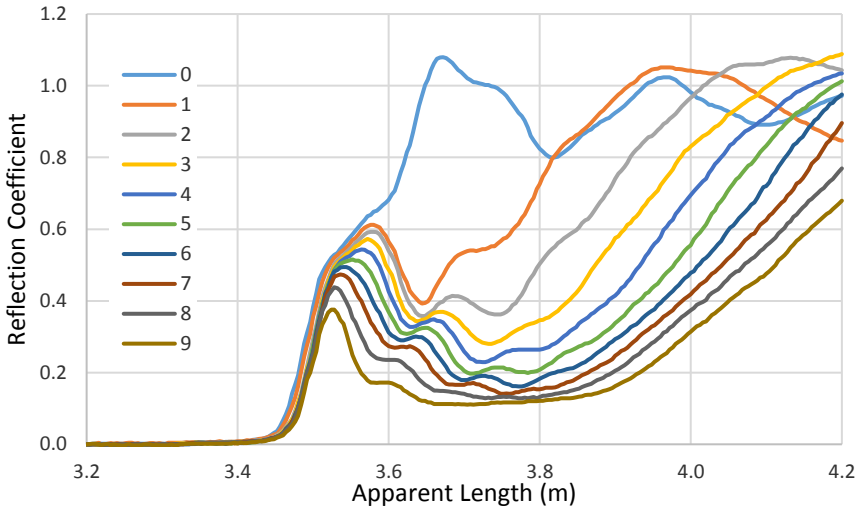

Figure I.1 TDR traces of Control_1

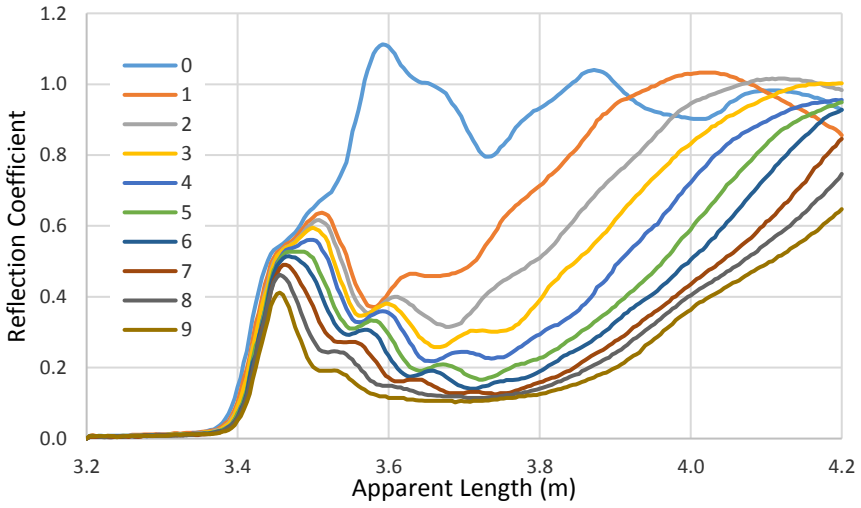

Figure I.2 TDR traces of Control_2

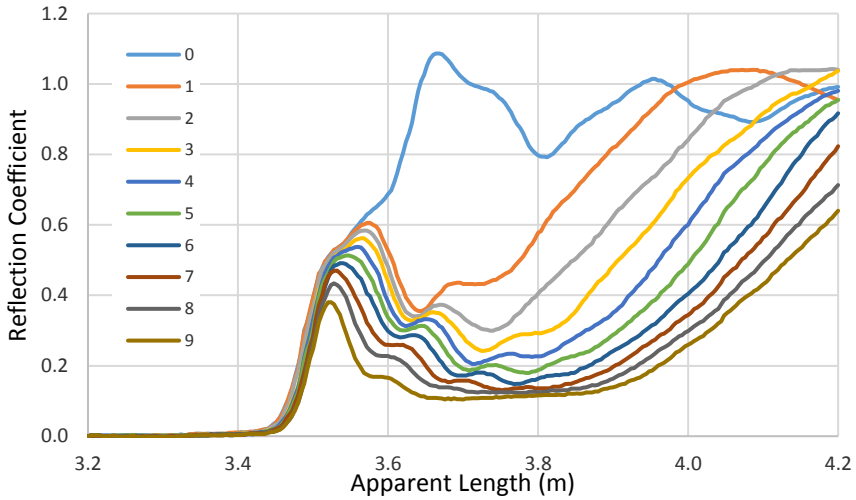

Figure I.3 TDR traces of MNC-C15_1

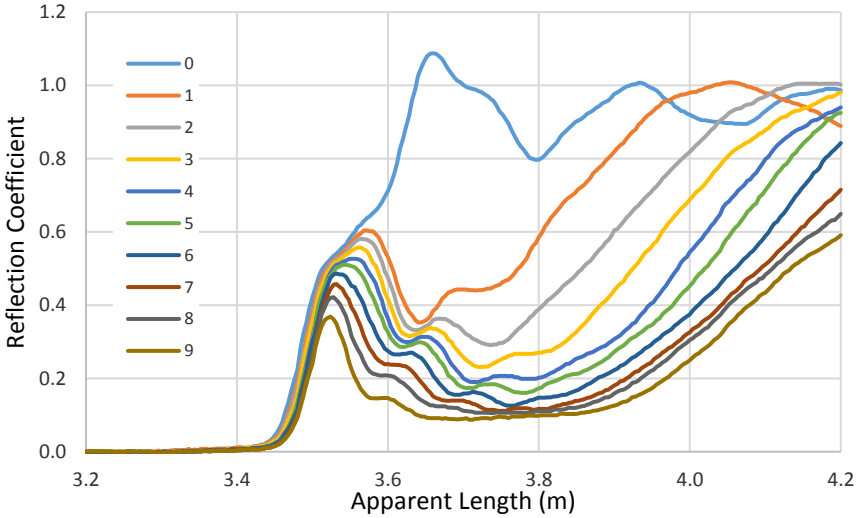

Figure I.4 TDR traces of MNC-C15_2

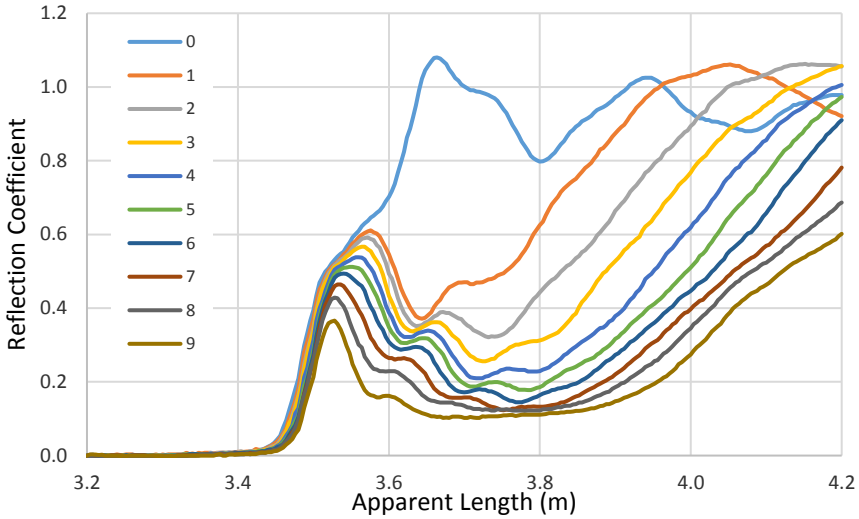

Figure I.5 TDR traces of MNC-C15_3

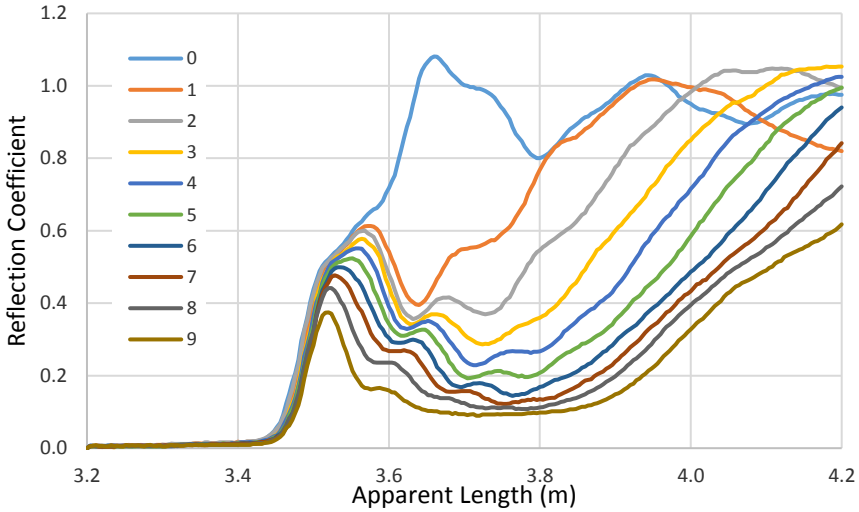

Figure I.6 TDR traces of $NaNO_2$ Cal_1

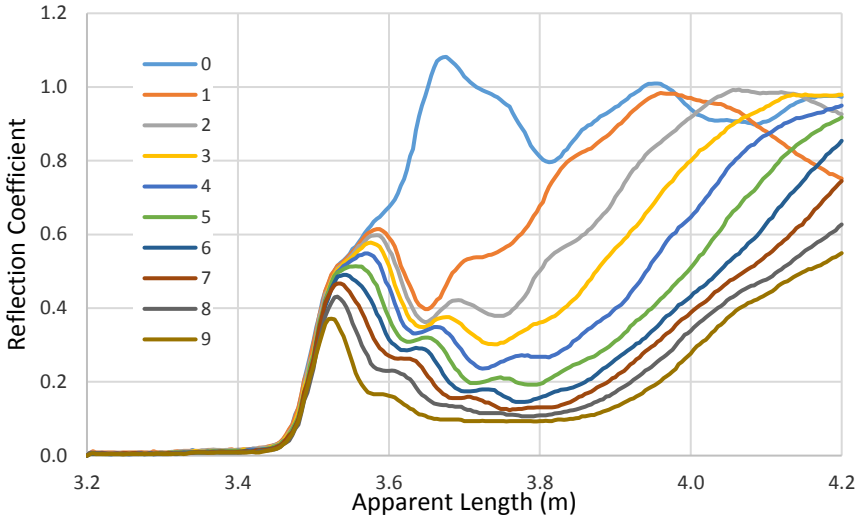

Figure I.7 TDR traces of $NaNO_2$ Cal_2

The semi-automatic Excel treatment spreadsheet was used for the determination of the dielectric constants, one curve at a time, and the partial compilation of K_{app} is shown in Figure I.8. The complex exercise was to determine the open end of probe reflection point when the curve was wavy, resulting in a high variability when estimating the dielectric constants.

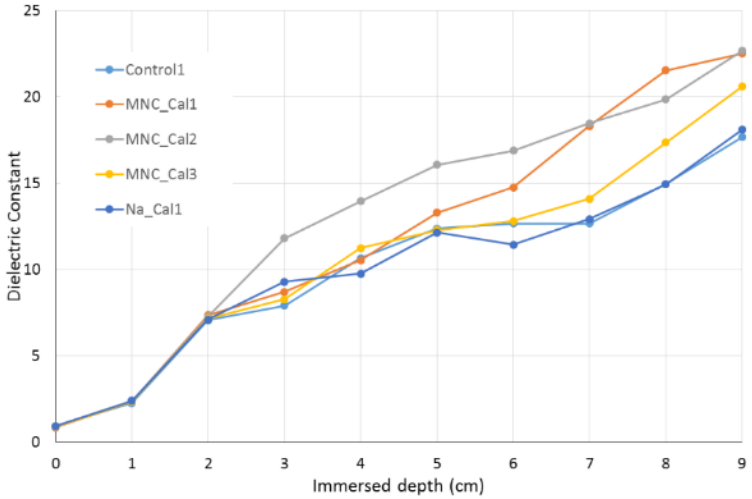

Figure I.8 Air-Water dielectric constants for calibration

A visual determination of the open end of the probe reflection point was attempted using all the probe traces at the same time, and avoiding the shallow immersed probes as shown in Figure I.9. The issue in this case was that curves seem to be more linear than quadratic, as opposed to what they were supposed to be, according to the (CRIM) mixing model given by the following equation:

$$K_{app}^{0.5} = \theta_v K_w^{0.5} + (1 - \theta_v) K_{air}^{0.5}$$

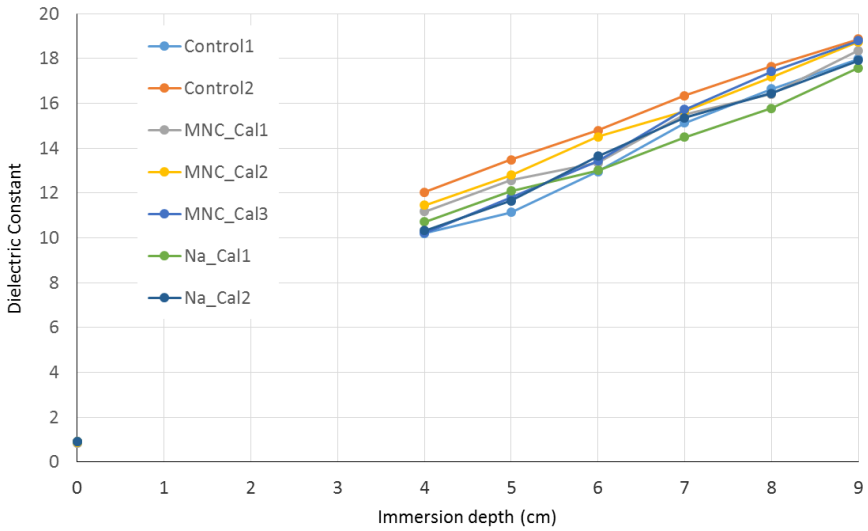

Figure I.9 Air-Water dielectric constants by visual calibration

The air-water calibration using an uncoated probes, as seen in Figure I.10, showed a relatively quadratic (square root) shape comparable to what one would expect from the (CRIM) mixing model.

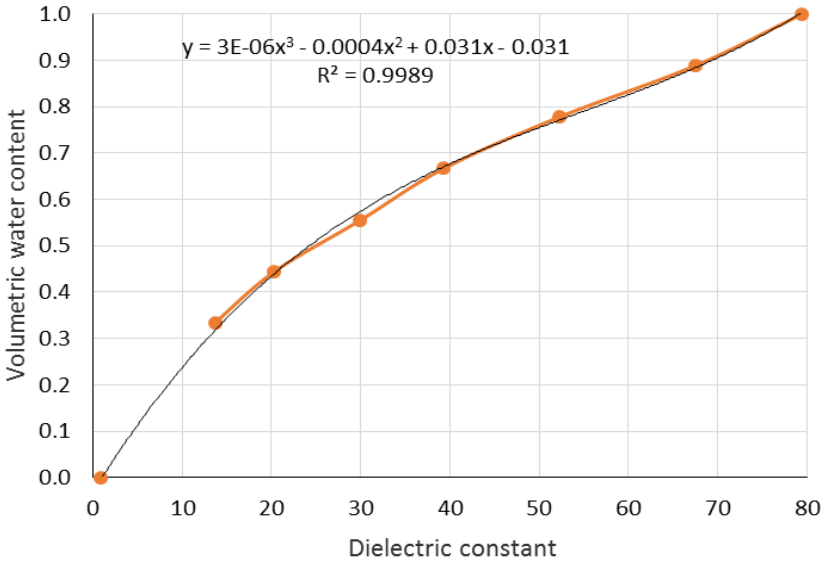

Figure I.10 Air-Water dielectric constants calibration with uncoated probe

APPENDIX J – CONVERSION OF TDR TRACES INTO DIELECTRIC CONSTANTS

This appendix describes the procedure and parameters used in the TDR-to-Dielectric constants conversion spreadsheets shown in Figure J.1 and Figure J.2 utilized for the semi-automatic determination of the dielectric constants from the TDR traces.

After three weeks of data collection for a specific experiment, a script combined all the individual readings into one master Excel file. The data were then processed using the semi-automatic procedure, in which a scroll bar was first used to select the data for treatment (plotted in light grey in the upper graph), and a cubic spline interpolation function was used to smooth the data and reduce signal noise (plotted in the same graph in blue). The first derivative of the cubic spline was then calculated and plotted in the lower graph in green. This derivative was used to determine the inflection points of the smoothed curve, and the slope of the tangent lines at the inflection points. The position of the red lines could be adjusted, using the spin buttons in the top four yellow cells, to approximate the locations of the inflection points. The tangents were then calculated and plotted on the top graph, shown as black dashed lines, and the distance between the intersections of the tangent lines was taken as the apparent length. The dielectric constant was then calculated using Equation 7.2. Finally, the resulting K_{app} was saved to the corresponding data set and the process was repeated for the next reading.

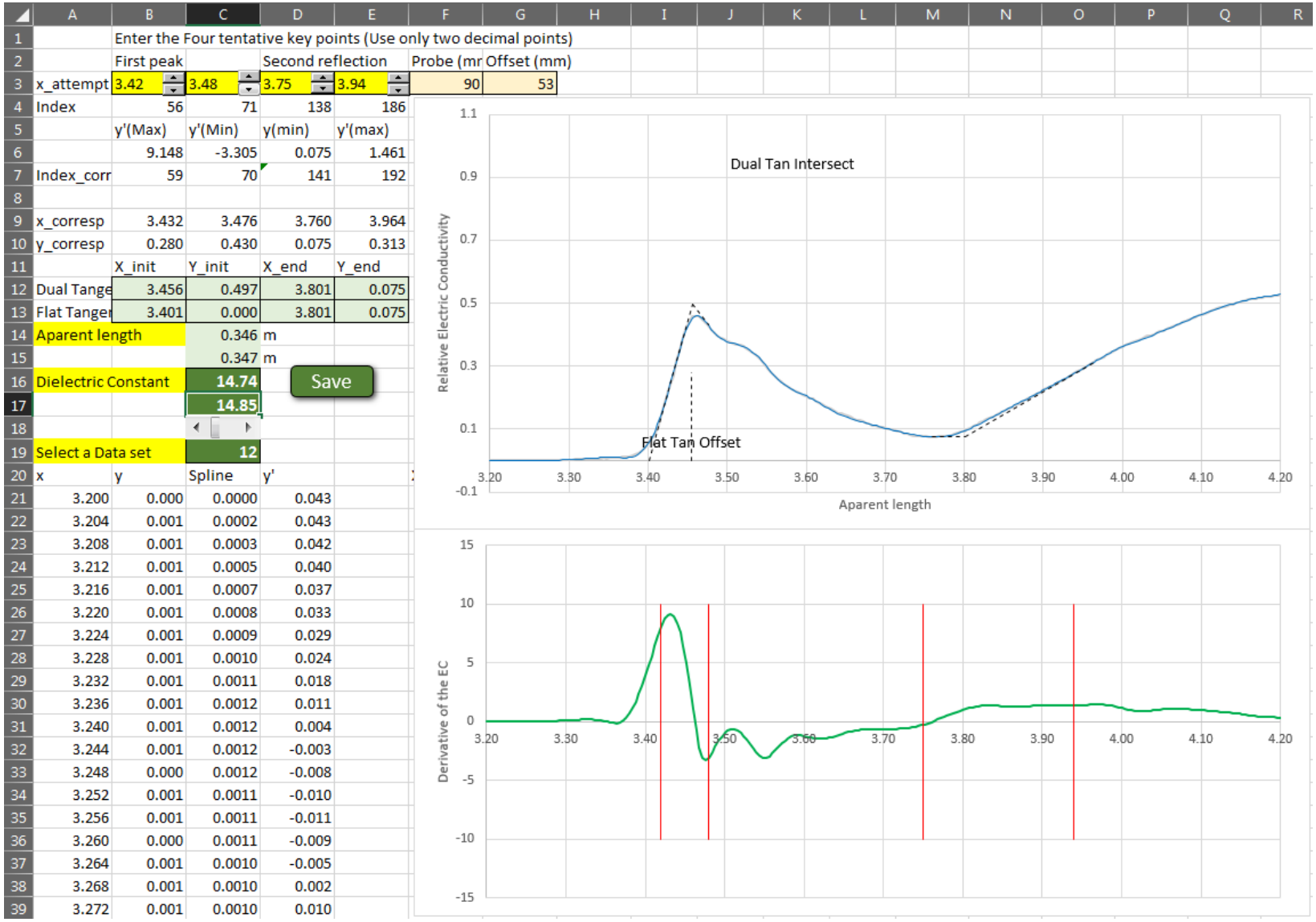

Figure J.1 Screenshot of the TDR to dielectric constants conversion spreadsheet

	A	B	C	D	E	F	G	H	I	J	K	L	M	N	O	P
16	Empty space to align the data with the Treatment sheet															
17																
18	K	K Dual tan												14.7377		
19		K Flat tan												14.8484		
20	Index	x	1	2	3	4	5	6	7	8	9	10	11	12	13	14
21	Data	3.2	0	0	0	0	0	0	0	0	0	0	0	0	0	0
22		3.204	0.001	-0.0031	-0.0013	-0.0042	-0.0005	-0.0014	-0.0012	-0.0012	-0.0039	-0.0015	-0.0008	0.0012	0.0002	0.0021
23		3.208	0.001	-0.0021	-0.0013	-0.002	-0.0005	0.0007	-0.0023	-0.0012	-0.0028	-0.0015	-0.0008	0.0012	0.0002	0.0021
24		3.212	0	0.0001	-0.0003	-0.001	-0.0005	-0.0004	-0.0002	-0.0002	-0.0028	-0.0015	0.0003	0.0012	0.0002	0.0021
25		3.216	0	0.0001	-0.0003	0.0012	-0.0005	0.0017	0.0009	-0.0012	-0.0028	-0.0015	0.0003	0.0012	0.0002	0.0021
26		3.22	-0.0011	0.0043	0.0008	0.0001	0.0005	0.0017	-0.0012	-0.0012	-0.0007	-0.0015	0.0003	0.0012	0.0002	0.0021
27		3.224	0.001	0.0001	-0.0013	0.0012	0.0005	-0.0004	-0.0012	-0.0002	-0.0018	-0.0015	-0.0008	0.0012	0.0002	0.0021
28		3.228	0	0.0001	-0.0013	-0.001	0.0016	-0.0004	-0.0023	0.0009	-0.0018	-0.0015	-0.0008	0.0012	0.0002	0.0021
29		3.232	0.001	0.0001	-0.0003	-0.002	0.0005	-0.0025	-0.0033	0.0009	0.0004	-0.0005	-0.0008	0.0012	0.0002	0.001
30		3.236	0	0.0001	-0.0013	-0.001	0.0005	-0.0025	-0.0012	-0.0012	-0.0018	-0.0015	-0.0008	0.0012	0.0002	0.001
31		3.24	0.001	0.0001	-0.0013	-0.001	0.0005	-0.0014	-0.0012	-0.0002	-0.0018	-0.0005	-0.0008	0.0012	0.0002	0.001
32		3.244	0	0.0001	-0.0003	-0.002	-0.0005	-0.0025	-0.0023	0.0009	-0.0018	-0.0015	0.0003	0.0012	0.0002	0.001
33		3.248	0.0021	0.0001	0.0008	-0.001	0.0005	-0.0014	-0.0023	-0.0002	-0.0018	-0.0015	0.0003	0.0001	0.0002	0.0021
34		3.252	0.0031	0.0001	-0.0013	-0.002	0.0005	-0.0025	-0.0012	-0.0002	0.0004	0.0006	0.0014	0.0012	0.0002	0.0021
35		3.256	0	0.0001	-0.0003	0.0001	0.0005	0.0007	-0.0023	-0.0002	-0.0018	0.0006	0.0003	0.0012	0.0002	0.0021
36		3.26	0.0021	0.0001	-0.0013	0.0001	-0.0005	-0.0004	-0.0012	-0.0012	-0.0007	0.0006	0.0014	0.0001	0.0002	0.0021
37		3.264	0.001	-0.001	-0.0013	-0.001	0.0005	-0.0025	0.0009	0.0009	0.0014	0.0006	-0.0008	0.0012	0.0002	0.0021
38		3.268	0	-0.001	-0.0013	-0.002	0.0026	-0.0014	0.0009	0.0009	0.0014	0.0006	0.0003	0.0012	0.0002	0.001
39		3.272	0.001	0.0001	0.0019	-0.001	-0.0005	-0.0004	-0.0002	0.002	-0.0007	0.0006	-0.0008	0.0012	0.0002	0.0021
40		3.276	0.0021	0.0011	0.0029	-0.001	0.0005	-0.0014	0.0009	0.0009	0.0014	0.0027	0.0003	0.0012	0.0034	0.0021
41		3.28	0.0021	0.0011	0.0029	0.0012	0.0026	-0.0004	0.0009	0.0009	0.0014	0.0027	0.0035	0.0012	0.0024	0.0021
42		3.284	0.0021	0.0011	0.0029	0.0012	0.0037	-0.0004	0.002	0.003	0.0014	0.0027	0.0003	0.0012	0.0024	0.0021
43		3.288	0.0031	0.0001	0.0029	0.0001	0.0005	0.0007	0.002	-0.0002	0.0014	0.0027	0.0035	0.0012	0.0034	0.0021
44		3.292	0.0042	0.0011	0.0019	-0.001	0.0005	0.0017	0.0009	0.0009	0.0014	0.0027	0.0035	0.0012	0.0013	0.0021
45		3.296	0.0021	0.0011	0.0019	0.0022	0.0016	0.0028	0.003	0.003	0.0014	0.0027	0.0035	0.0012	0.0034	0.0021
46		3.3	0.0031	0.0022	-0.0003	0.0022	0.0037	0.0039	0.0051	0.003	0.0014	0.0027	0.0035	0.0012	0.0002	0.0021
47		3.304	0.0031	0.0011	0.0008	0.0022	0.0016	0.0017	0.002	0.003	0.0014	0.0027	0.0035	0.0012	0.0034	0.0032
48		3.308	0.0042	0.0011	0.004	0.0022	0.0016	0.0017	0.0009	0.003	0.0014	0.0027	0.0035	0.0044	0.0045	0.0021
49		3.312	0.0053	0.0032	0.0029	0.0012	0.0016	0.0028	0.0009	0.002	0.0004	0.0027	0.0035	0.0044	0.0045	0.0042
50		3.316	0.0042	0.0043	0.0029	0.0022	0.0016	0.0039	0.003	0.003	0.0025	0.0027	0.0035	0.0054	0.0034	0.0053
51		3.32	0.0053	0.0043	0.0019	0.0033	0.0026	0.0028	0.002	0.003	0.0025	0.0027	0.0035	0.0054	0.0034	0.0053
52		3.324	0.0053	0.0043	0.0029	0.0022	0.0026	0.0028	0.003	0.0041	0.0014	0.0027	0.0045	0.0054	0.0034	0.0053
53		3.328	0.0084	0.0043	0.004	0.0022	0.0037	0.0039	0.003	0.003	0.0014	0.0038	0.0067	0.0054	0.0034	0.0053
54		3.332	0.0084	0.0043	0.0051	0.0033	0.0037	0.0028	0.0051	0.003	0.0014	0.0038	0.0077	0.0054	0.0045	0.0064

Figure J.2 Work sheet containing the TDR trace data and the calculated dielectric constants

Table J.1 shows the definition of the parameters used in the semi-automatic TDR-to-Dielectric constants conversion spreadsheet.

Table J.1 Description of Excel parameters shown in Figure J.1

Cell	Description
B3-E3	Four key points in the X axis defining the location of the vertical red lines in the bottom "derivative" graph. They can be entered manually or changed by the spin buttons. Each point is used to search for a particular value in its vicinity.
B3	Location of the first inflection point of the TDR trace
C3	Location of the second inflection point of the TDR trace
D3	Location of the minimum point characterizing the open end of the probe
E3	Location of the last inflection point of the TDR trace
F3	Probe length (mm)
G3	Probe offset (mm), to account of the probe handle
B6	Search maximum derivative around **B3**
C6	Search minimum derivative around **C3**
D6	Search local "relative electric conductivity" minimum around **D3**
E6	Search maximum derivative around **E3**
B9-E10	Corresponding coordinates of points defined in **B6-E6**, using **INDEX** / **MATCH** functions
B12	X coordinate of the intersection of the two tangent lines defining the start of the probe
D12	X coordinate of the intersection of the two tangent lines defining the end of the probe
B13	X coordinate of the intersection of the rising tangent line and the X axis
D13	Same as D12
C14	Apparent length (m) **= D12-B12**, Using dual tangent method
C15	Apparent length (m) **= D13-B13-(G3/1000)**, Using Flat tangent and offset method
C16	Apparent dielectric constant **= (C14*1000/F3)^2**
C17	Apparent dielectric constant **= (C15*1000/F3)^2**
C19	Defines the serial number of the TDR trace under analysis. Imports data to columns **A** and **B** starting from line 21, and calculates the Spline fitting and the derivatives in columns **C** and **D**.
Save	Button to copy the dielectric constant results to the original datasheet in Figure J.2

APPENDIX K – PORE SOLUTION EXTRACTION AND FREEZING POINT DETERMINATION

To measure the freezing point of the cement paste pore solution, a simple extraction technique was used in the environmental lab located at the University of Saskatchewan. At room temperature, and approximately one hour after mixing the cement at w/c=0.5, and admixture at 4% as applicable, the cement paste was transferred to the vacuum extraction device shown in Figure K.1. The vacuum valve was then opened for 30 minutes to collect the pore solution in a beaker. The extracted pore solution was transferred to a transparent plastic vial and tested for its freezing point using an embedded thermocouple with data logger in a freezer set at -10°C. Visual assessment was done to check for complete solidification of the extracted pore solution, and did not reveal any residual liquid solution at -10°C. Figure K.2 shows the freezing points of the extracted pore solution from control and antifreeze treated cement pastes. Good agreement was observed between the freezing points obtained for mortar of -0.4°C and -0.7°C and for the MNC-C15 of -3.3°C and -3.5°C by using the pore solution extraction and the imbedded measurement in mortar respectively.

A cloudy substance was observed after the frozen pore solution melted, which did not dissolve afterward.

Figure K.1 Pore solution extraction apparatus

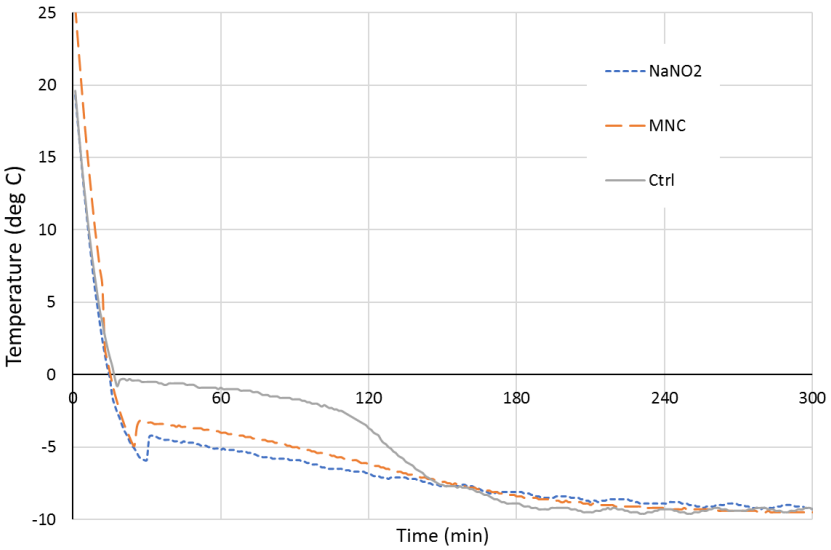

Figure K.2 Freezing points of extracted pore solutions

APPENDIX L – DETAILS OF WATER CONTENT CALCULATIONS

This appendix presents the governing equations of the spreadsheet used to derive the constituents' volumetric content from the apparent calibrated dielectric constant using the complex refractive index model (CRIM). Table L.1 shows the physical parameters used in the mixing model. Column $Sqrt(K)$ was added to linearize the CRIM equation since this is a requirement to use the Simplex LP solver.

Table L.1 Dielectric constants used

Phase	Symbol	Dielectric constant (K)	$Sqrt(K)$	Spec. Gravity
Air	air	1	1.00	0.00
Water	w	80	8.94	1.00
Pore solution	$pore$	250	15.81	1.00
Ice	ice	3.2	1.79	0.91
Unreacted cement	uc	3.5	1.87	3.15
Hydrated cement	hc	4.5	2.12	1.90

As discussed in Section 7.5, four key moments were used to define the change in volumetric phase composition. For each key moment, appropriate assumptions were made to solve for the volumetric content of the unknown phases. The unknown and constraints of each key moment are described in Table L.2 through Table L.5.

Table L.2 Volumetric fraction parameters at the start of curing

Volume fraction	Description
$f_{air}^{(1)}$	Variable, determined by the Solver
$f_{w}^{(1)}$	$= w/c \times \gamma_{uc} \times f_{uc}^{(1)} - f_{pore}^{(1)}$, based on total water to cement ratio
$f_{pore}^{(1)}$	Variable, determined by the Solver
$f_{ice}^{(1)}$	$= 0$, no ice at the start of the experiment
$f_{uc}^{(1)}$	Variable, determined by the Solver
$f_{hc}^{(1)}$	$= 0$, no hydrated cement at the start of the experiment

Table L.3 Volumetric fraction parameters at the first inflexion point

Volume fraction	Description
$f_{air}^{(2)}$	$= f_{air}^{(1)} - 0.09 \times (f_w^{(1)} - f_w^{(2)})$, based on air void occupied by ice
$f_w^{(2)}$	Variable, determined by the Solver
$f_{pore}^{(2)}$	Variable, determined by the Solver
$f_{ice}^{(2)}$	$= 1.09 \times (f_w^{(1)} - f_w^{(2)})$, based on water-to-ice expansion
$f_{uc}^{(2)}$	$= f_{uc}^{(1)}$, no change in unreacted cement
$f_{hc}^{(2)}$	$= 0$, hydration did not start

Table L.4 Volumetric fraction parameters at the end of curing

Volume fraction	Description
$f_{air}^{(3)}$	$= f_{air}^{(2)}$, no change in previous air content
$f_w^{(3)}$	Variable, determined by the Solver
$f_{pore}^{(3)}$	Variable, determined by the Solver
$f_{ice}^{(3)}$	Variable, determined by the Solver
$f_{uc}^{(3)}$	Variable, determined by the Solver
$f_{hc}^{(3)}$	$= (1 + 1.4) \times \left(f_{uc}^{(2)} - f_{uc}^{(3)}\right)$, based on unreacted to reacted cement volume ratio

Table L.5 Volumetric fraction parameters at the end of thawing

Volume fraction	Description
$f_{air}^{(4)}$	Variable, determined by the Solver
$f_w^{(4)}$	Variable, determined by the Solver
$f_{pore}^{(4)}$	Variable, determined by the Solver
$f_{ice}^{(4)}$	$= 0$, all ice converted back to water
$f_{uc}^{(4)}$	$= f_{uc}^{(3)} - 0.03$, to account for reacted cement during thawing
$f_{hc}^{(4)}$	$= f_{hc}^{(3)} + (1 + 1.4) \times (0.03)$, based on extra cement reaction while thawing

In all cases, the total volume fraction was forced to 1 as per Equation 7.8, the overall density was forced to 1.73 as per Equation 7.9, and the square root of the dielectric constant defined in Equation 7.7 was forced to the appropriate values taken from Table 7.3.

Figure L.1 shows the dialog box of the Simplex LP solver in Excel along with a description of the parameters and constraints used.

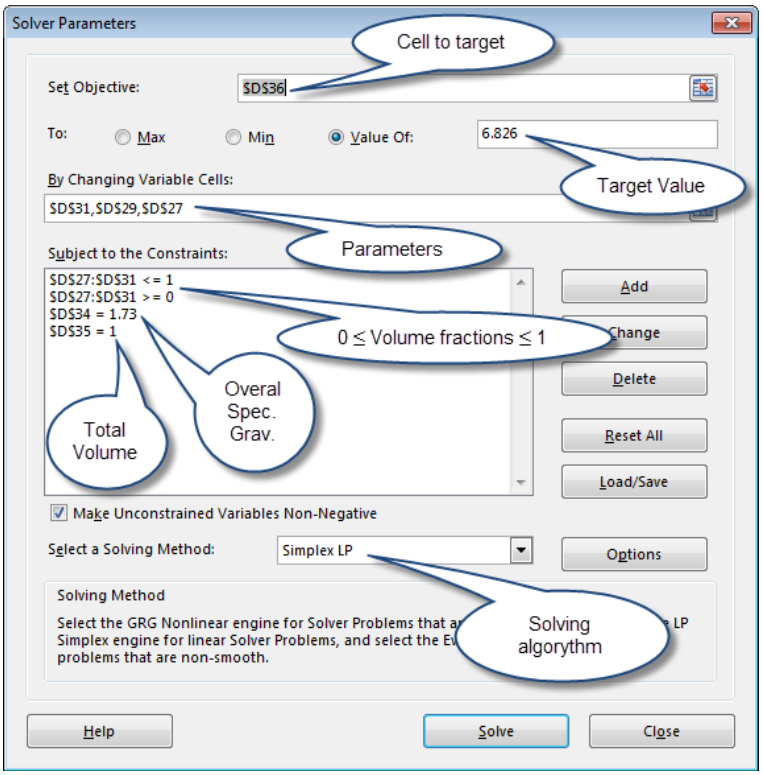

Figure L.1 Dialog box for the Simplex LP solver in Excel

APPENDIX M – COPYRIGHT PERMISSIONS

Chapter 4

TMS Info <info@masonrysociety.org>
Mon 2019-02-04 3:51 PM
Saha, Ouafi

Ouafi,

Our Executive Director is out of town and unable to respond to your email at this time.

Therefore, I am granting the University of Saskatchewan the right to add your 12NAMC paper, published in the Proceedings of the 12 NAMC and which is a portion of your Ph.D. dissertation, to their website and for your use in your PH.D. dissertation.

Please include the full citation as well as a note that the copyright is assigned to The Masonry Society with our website URL included www.masonrysociety.org

> The Masonry Society
>
> The Masonry Society is an international gathering of people interested in the art and science of masonry--we're advancing the knowledge of masonry.
>
> www.masonrysociety.org

.

Thank you.

Susan Scheurer TMS Meeting Planner/Membership Coordinator/Committee Liaison/TMS Journal Managing Editor

THE MASONRY SOCIETY

Chapter 5

Re: Fw: TMS Journal Paper 2019-100

SS

Susan Scheurer <tmsmeetings@masonrysociety.org>

Thu 2019-08-15 2:59 PM

To: Saha, Ouafi

Ouafi,

This email will serve as permission from The Masonry Society (TMS) for you to use the TMS copyrighted article, "Behavior of Masonry Mortar Containing an Antifreeze Admixture" in your dissertation to be presented at the University of Saskatchewan. Furthermore, TMS gives the University permission to retain your dissertation, including the TMS copyrighted article, in any university database of dissertations.

Susan Scheurer
TMS Meeting Planner/Membership Coordinator/Committee Liaison/TMS Journal Managing Editor

Chapter 7

For subscription articles	For open access articles
Authors transfer copyright to the publisher as part of a journal publishing agreement, but have the right to: • Share their article for Personal Use, Internal Institutional Use and Scholarly Sharing purposes, with a DOI link to the version of record on ScienceDirect (and with the Creative Commons CC-BY-NC- ND license for author manuscript versions) • Retain patent, trademark and other intellectual property rights (including research data). • Proper attribution and credit for the published work.	Authors sign an exclusive license agreement, where authors have copyright but license exclusive rights in their article to the publisher**. In this case authors have the right to: • Share their article in the same ways permitted to third parties under the relevant user license (together with Personal Use rights) so long as it contains a CrossMark logo, the end user license, and a DOI link to the version of record on ScienceDirect. • Retain patent, trademark and other intellectual property rights (including research data). • Proper attribution and credit for the published work.

Personal use

Authors can use their articles, in full or in part, for a wide range of scholarly, non-commercial purposes as outlined below:

- Use by an author in the author's classroom teaching (including distribution of copies, paper or electronic)
- Distribution of copies (including through e-mail) to known research colleagues for their personal use (but not for Commercial Use)
- Inclusion in a thesis or dissertation (provided that this is not to be published commercially)
- Use in a subsequent compilation of the author's works
- Extending the Article to book-length form
- Preparation of other derivative works (but not for Commercial Use)
- Otherwise using or re-using portions or excerpts in other works

These rights apply for all Elsevier authors who publish their article as either a subscription article or an open access article. In all cases we require that all Elsevier authors always include a full acknowledgement and, if appropriate, a link to the final published version hosted on Science Direct.